

**SYNTHESIS, MODIFICATION AND CHARACTERIZATION OF
ECONOMICAL, HIGH PERFORMANCE REVERSE OSMOSIS MEMBRANES**

A Dissertation
Presented to
The Academic Faculty

By

Wail S. Falath

In Partial Fulfillment
Of the Requirements for the Degree
Doctor of Philosophy in Polymer, Textile and Fiber Engineering

Georgia Institute of Technology

August 2016

Copyright © Wail S. Falath 2016

**SYNTHESIS, MODIFICATION AND CHARACTERIZATION OF
ECONOMICAL, HIGH PERFORMANCE REVERSE OSMOSIS MEMBRANES**

Approved by:

Dr. Karl Jacob, Advisor
School of Materials Science and
Engineering
Georgia Institute of Technology

Dr. Youjiang Wang
School of Materials Science and
Engineering
Georgia Institute of Technology

Dr. Hamid Garmestani
School of Materials Science and
Engineering
Georgia Institute of Technology

Dr. Kyriaki Kalaitzidou
G. W. Woodruff School of Mechanical
Engineering
Georgia Institute of Technology

Dr. Donggang Yao
School of Materials Science and
Engineering
Georgia Institute of Technology

Date Approved: June 21, 2016

DEDICATED TO

My beloved parents, wife, children, brothers and sister

ACKNOWLEDGEMENTS

All praise and thanks are due to God (Allah), who created the chance, created me and guided me to get the work completed.

Thank you to my advisor, Prof. Karl Jacob, for his sincere advice and guidance, during my graduate studies. Also, thanks to him for showing so much patience and consideration throughout the course of my thesis work. His help to get this work completed will not be forgotten. I would like also to acknowledge my committee members, Dr. Hamid Garmestani, Dr. Donggang Yao, Dr. Youjiang Wang and Dr. Kyriaki Kalaitzidou, for their guidance and encouragement.

I would like to thank Eng. Aneela Sabir for the persistent help and guidance through the experimentation part.

Thanks before all of them to my parents. Their love and prayers gave me a great support. Special heart-felt thanks go to my wife for her relentless and continuous support throughout my graduate studies. Her support started from the first day and has never ended. Thanks to all my friends for their moral encouragement and support.

Lastly, I would like to acknowledge King Fahd University of Petroleum and minerals for providing me with a scholarship to pursue my PhD at Georgia Tech.

TABLE OF CONTENTS

ACKNOWLEDGEMENTS	iv
LIST OF TABLES	x
LIST OF FIGURES	xi
LIST OF ABBREVIATIONS	xvii
SUMMARY	xix
CHAPTER 1: INTRODUCTION	1
1.1 Scarcity of Global Potable and Clean Water	1
1.2 Water Desalination Technologies	1
1.3 History of Water Desalination	4
1.4 Reverse Osmosis Membranes	6
1.4.1 Reverse Osmosis Process Fundamentals	8
1.4.2 Polymeric RO Membranes	9
1.4.3 Inorganic Membranes	11
1.5 Organization of The Dissertation	12
CHAPTER 2: LITERATURE REVIEW	14
2.1 Historical Development of RO Water Desalination Membranes	14
2.1.1 Thin Film Composite membranes	15
2.2 Transport Through RO membranes	15
2.3 RO Membranes Challenges	17
2.3.1 Membrane Fouling	18
2.3.1.1 Biofouling	18
2.3.2 Biofouling Negative Effects on RO Membranes	21
2.3.2.1 Loss of salt rejection	21
2.3.2.2 Water flux decline	22
2.3.2.3 Increase in operating pressure	24
2.3.2.4 Membrane bio-degradation	24
2.3.3 Chlorine Attack	24
2.4 Membranes Surface Modification	26
2.5 Utilizing Poly (vinyl alcohol) in RO Applications	29
CHAPTER 3: OBJECTIVES AND METHODOLOGY	32
3.1 Research Objectives	32
3.2 Methodology	33
3.2.1 Materials	33
3.2.2 Permeation Studies	34
3.2.3 Chlorine Resistance Testing	36
3.2.4 Biofouling Resistance Testing	36
3.2.5 Characterization Techniques	37
3.2.3.1 Fourier transform infrared spectroscopy (FTIR)	37

3.2.3.2	Scanning electron microscopy (SEM)	37
3.2.3.3	Atomic force microscopy (AFM)	38
3.2.3.4	Contact angle measurements	39
3.2.3.5	Mechanical Properties	39
3.2.3.6	X-ray diffraction Measurements (XRD)	39

CHAPTER 4: Highly Improved Reverse Osmosis Performance of Novel PVA/DGEBA Cross-linked Membranes by Incorporation of Pluronic F-127 and MWCNTs For Water Desalination **41**

4.1	Introduction	41
4.2	Experimental Procedure	44
4.2.1	Materials	44
4.2.2	Membrane Casting	44
4.2.2.1	Crosslinking of PVA with DGEBA	44
4.2.2.2	Incorporation of Pluronic F127 into the crosslinked PVA membranes	45
4.2.2.3	Inclusion of MWCNTs within the Pluronic F127 modified PVA membranes	46
4.2.3	Membranes Characterization	48
4.2.3.1	Fourier Transform Infrared Spectroscopy (FTIR)	48
4.2.3.2	Contact Angle Measurements	48
4.2.3.3	X-Ray Diffraction Measurements	49
4.2.3.4	Scanning Electron Microscopy (SEM)	49
4.2.3.5	Atomic Force microscopy (AFM)	49
4.2.3.6	Mechanical Testing	50
4.2.3.7	Permeation and Salt Rejection Testing	51
4.2.3.8	Chlorine Resistance Testing	53
4.2.3.9	Biofouling Resistance Testing	53
4.3	Results and Discussion	54
4.3.1	FTIR analysis	54
4.3.2	Contact Angle Analysis	55
4.3.2.1	Effect of Mixing Pluronic F127 on Hydrophilicity	56
4.3.2.2	Effect of Incorporating MWCNTs on Hydrophilicity	57
4.3.3	X-Ray Diffraction	59
4.3.4	Atomic Force Microscopy (AFM)	61
4.3.5	Scanning Electron Microscopy (SEM)	63
4.3.6	Mechanical Properties	66
4.3.7	Permeate Flux and Salt Rejection	68
4.3.7.1	Separation performance of DGEBA crosslinked PVA membranes	68
4.3.7.2	Separation performance of PVA membranes incorporated with Pluronic F127	70
4.3.7.3	Effect of MWCNTs infusion on PVA membranes separation performance	71
4.3.8	Effect of MWCNTs Infusion on Membrane's Chlorine Resistance	74
4.3.9	Effect of MWCNTs Infusion on Membrane's Biofouling Resistance	75
4.4	Conclusion	77

CHAPTER 5: Conjugation of Vanillin and Pluronic F-127 With Novel PVA/DGEBA Cross-linked Thin Film Membranes For Reverse Osmosis Performance Enhancement **79**

5.1	Introduction	79
-----	--------------	----

5.2	Experimental Procedure	82
5.2.1	Materials	82
5.2.2	Membrane Casting	82
5.2.2.1	Crosslinking of PVA with DGEBA	82
5.2.2.2	Incorporation of Pluronic F-127 into the crosslinked PVA membranes	83
5.2.2.3	Conjugation of Vanillin with the Pluronic F-127 modified PVA membranes	83
5.2.3	Membranes Characterization	85
5.2.3.1	Fourier Transform Infrared Spectroscopy (FTIR)	85
5.2.3.2	Contact Angle Measurements	86
5.2.3.3	X-Ray Diffraction Measurements	86
5.2.3.4	Scanning Electron Microscopy (SEM)	86
5.2.3.5	Atomic Force microscopy (AFM)	86
5.2.3.6	Mechanical Testing	87
5.2.3.7	Permeation and Salt Rejection Testing	88
5.2.3.8	Biofouling Resistance Testing	91
5.2.3.9	Chlorine Resistance Testing	91
5.3	Results and Discussion	92
5.3.1	FTIR Analysis	92
5.3.2	Contact Angle Analysis	93
5.3.2.1	Effect of Mixing Pluronic F-127 on Hydrophilicity	94
5.3.2.2	Effect of Vanillin Conjugation on Hydrophilicity	95
5.3.3	X-Ray Diffraction	96
5.3.4	Atomic Force Microscopy (AFM)	98
5.3.5	Scanning Electron Microscopy (SEM)	100
5.3.6	Mechanical Properties	103
5.3.7	Permeate Flux and Salt Rejection	105
5.3.7.1	Separation performance of DGEBA crosslinked PVA membranes	105
5.3.7.2	Separation performance of PVA membranes incorporated with Pluronic F-127	107
5.3.7.3	Effect of Vanillin conjugation on PVA membranes separation performance	108
5.3.8	Effect of Vanillin Conjugation on Membrane's Biofouling Resistance	110
5.3.9	Effect of Vanillin conjugation on Membrane's Chlorine Resistance	112
5.4	Conclusion	113

CHAPTER 6: Research on Novel Reverse Osmosis Membranes Composed of PVA Conjugated with Gum Arabic: Biofouling Mitigation and Chlorine Resistance

Enhancement	116	
6.1	Introduction	116
6.2	Experimental Procedure	119
6.2.1	Materials	119
6.2.2	Membrane Casting	119
6.2.2.1	Crosslinking of PVA with DGEBA	119
6.2.2.2	Incorporation of Pluronic F127 into the crosslinked PVA membranes	120
6.2.2.3	Conjugation of Gum Arabic with the modified PVA membranes	120
6.2.3	Membranes Characterization	122
6.2.3.1	Fourier Transform Infrared Spectroscopy (FTIR)	122
6.2.3.2	X-Ray Diffraction Measurements	122
6.2.3.3	Scanning Electron Microscopy (SEM)	123

6.2.3.4	Atomic force microscopy (AFM)	123
6.2.3.5	Contact Angle Measurements	124
6.2.3.6	Mechanical Testing	124
6.2.3.7	Permeation and Salt Rejection Testing	125
6.2.3.8	Chlorine Resistance Testing	127
6.2.3.9	Biofouling Resistance Testing	127
6.3	Results and Discussion	128
6.3.1	FTIR analysis	128
6.3.2	X-Ray Diffraction	129
6.3.3	Scanning Electron Microscopy (SEM)	131
6.3.4	Atomic Force Microscopy (AFM)	133
6.3.5	Contact Angle Analysis	135
6.3.5.1	Effect of mixing Pluronic F127 on hydrophilicity	135
6.3.5.2	Effect of conjugating Gum Arabic on Hydrophilicity	137
6.3.6	Mechanical Properties	139
6.3.7	Permeate Flux and Salt Rejection	141
6.3.7.1	Separation performance of DGEBA crosslinked PVA membranes	141
6.3.7.2	Separation performance of PVA membranes incorporated with Pluronic F127	142
6.3.7.3	Effect of Gum Arabic conjugation on PVA membranes separation performance	144
6.3.8	Effect of Gum Arabic Conjugation on Membrane's Chlorine Resistance	145
6.3.9	Effect of Gum Arabic Conjugation on Membrane's Biofouling Resistance	147
6.4	Conclusion	149

CHAPTER 7: High Performance and Chlorine Resistant PVA/DGEBA Crosslinked TFN-RO Polymer Membranes Infused with Pluronic F127/ZnO-NPs Using Natural Sea Salt for Desalination **152**

7.1	Introduction	152
7.2	Experimental procedure	154
7.2.1	Materials	154
7.2.2	Membrane Preparation	155
7.2.2.1	Preparation of single layer PVA/DGEBA crosslinked membrane	155
7.2.2.2	Membrane Casting	155
7.2.2.3	Synthesis of thin film composite (PVA/DGEBA/PluronicF127) membrane	156
7.2.2.4	Infusion of ZnO-NPs in TFC membrane	157
7.3	Membrane Characterization	159
7.3.1	Fourier Transform Infrared Spectroscopy	159
7.3.2	Contact Angle Measurements	159
7.3.3	Structural Investigation	159
7.3.4	Scanning Electron Microscopy	159
7.3.5	Atomic Force Microscopy (AFM)	160
7.3.6	Mechanical Testing	160
7.3.7	Reverse Osmosis Separation Performance Testing	161
7.3.8	Chlorine Resistance of The Prepared Membranes	163
7.4	Results and Discussion	163
7.4.1	FTIR Analysis	163
7.4.2	Contact Angle Measurements	165

7.4.3	Structural Investigation	167
7.4.4	Scanning Electron Microscopy	168
7.4.5	Atomic Force Microscopy	171
7.4.6	Mechanical Testing	173
7.4.7	Reverse Osmosis Separation Performance Testing	175
7.4.7.1	Effect of crosslinker on PVA membrane separation performance	175
7.4.7.2	Effect of Pluronic F127 loading on membrane separation performance	176
7.4.7.3	Effect of ZnO-NPs Loading on TFC membrane separation performance (TFN)	178
7.4.8	Chlorine Resistance of TFN-RO Membrane	179
7.5	Conclusion	181
CHAPTER 8: Hyperbranched Polyethyleneimine, A Polycation Induced Zwitterionic Membrane for Improved Fouling Resistance and High RO Performance		182
8.1	Introduction	182
8.2	Experimental	184
8.2.1	Materials	184
8.2.2	Membranes Synthesis	184
8.2.2.1	Synthesis of PVA/MA crosslinked membranes	184
8.2.2.2	Membrane modification as zwitterion membrane	185
8.3	Membrane characterization	187
8.3.1	Fourier Transform Infrared Spectroscopy	187
8.3.2	Contact Angle Measurements	187
8.3.3	Scanning Electron Microscopy	187
8.3.4	Atomic Force Microscopy (AFM)	188
8.3.5	Mechanical Testing	188
8.3.6	Biofouling Testing	188
8.3.7	Bacterial Adhesion Testing	189
8.4	Results and Discussion	189
8.4.1	Fourier Transform infrared spectroscopy	189
8.4.2	Contact Angle Measurements	191
8.4.3	Atomic force microscopy	192
8.4.4	Scanning Electron Microscopy	194
8.4.5	Membrane Fouling Resistance for HPEI-RO Membranes	196
8.4.6	Bacterial Adhesion test	197
8.5	Conclusion	200
CHAPTER 9: CONCLUSIONS AND FUTURE WORK		201
9.1	Conclusions	201
9.2	Future Work	204
REFERENCES		205

LIST OF TABLES

Table 1.1 Market historical and forecast data of desalination systems [12].	4
Table 4.1 Weight percentages of DGEBA, Pluronic F127 and MWCNTs in PVA solution.....	48
Table 5.1 Weight percentages of DGEBA, Pluronic F-127 and Vanillin in PVA solution.	84
Table 6.1 Weight percentages of DGEBA, Pluronic F127 and Gum Arabic in PVA solution.....	122
Table 7.1 Composition and effect of PVA/DGEBA, Pluronic F127 and ZnO-NPs on average and root mean square roughness values (Rms and Ra) of the membranes.	158
Table 8.1 Weight percentages of PVA/MA, Pluronic F127 and HPEI.	186

LIST OF FIGURES

Figure 1.1 Global water withdrawal and consumption [13].	2
Figure 1.2 Worldwide installed desalination capacity by technology [12].	3
Figure 1.3 RO seawater desalination unit at Jeddah, Saudi Arabia in the 1970s [16].	5
Figure 1.4 Modern RO plant in Spain [17].	6
Figure 1.5 Reverse osmosis principle (source: Aqualyng) [19].	7
Figure 1.6 Schematic of (a) reverse osmosis (RO) desalination process and (b) membrane configurations including integrally asymmetric membrane (left) and thin film composite membrane (right) [20].	9
Figure 1.7 The polyamide derived from m-phenylenediamine (MPD) and trimesoyl chloride (TMC) via interfacial polymerization [20].	11
Figure 1.8 (a) SEM image of a cross section of zeolite NaA membrane supported on porous α -Al ₂ O ₃ ceramic. (b) Illustrations of an inter-crystal pore and zeolite pore in zeolite membranes [20].	12
Figure 2.1 Biofilm Maturation Stages. Each stage of development in the diagram is paired with a photomicrograph of a developing <i>P. aeruginosa</i> biofilm. All photomicrographs are shown to same scale. (Image Credit: D. Davis) [63].	20
Figure 2.2 Schematic drawing illustrating internal and external concentration polarization when an asymmetric membrane is used for pressure retarded osmosis [66].	22
Figure 2.3 Normalized flux decline and loss of salt rejection upon induced biofouling with <i>P. aeruginosa</i> [61].	23
Figure 2.4 Orton rearrangement of an aromatic amide with active Chlorine [43, 70].	25
Figure 2.5 Schematic diagrams of antifouling mechanisms: (a) pure water layer; (b) electrostatic repulsion [80].	28
Figure 3.1 Manufacturer supplied schematic diagram of the permeation unit.	35
Figure 4.1 Schematic diagram of the crosslinking of PVA with DGEBA and the intermolecular hydrogen bonding with Pluronic F127.	47

Figure 4.2 Dead-end filtration system for RO membranes.....	52
Figure 4.3 ATR-FTIR spectra of pure PVA and MWCNTs modified PVA membranes.	55
Figure 4.4 Effect of Mixing Pluronic F127 on the hydrophilicity of the PVA membrane.	57
Figure 4.5 Effect of Mixing MWCNTs on the hydrophilicity of the PVA membrane.....	59
Figure 4.6 XRD patterns of pure PVA and MWCNTs modified membranes.....	60
Figure 4.7 3-D AFM images of (a) PVA membranes and PVA modified with (b) 0.02, (c) 0.04, (d) 0.06, (e) 0.08 and (f) 0.1 wt% MWCNTs.	62
Figure 4.8 Effect of MWCNTs loading on surface roughness of PVA membranes.....	63
Figure 4.9 SEM images of (a) pristine PVA, (b) PVA with Pluronic F127 and (c) PVA modified with 0.02, (d) 0.04, (e) 0.06, (f) 0.08 and (g) 0.1 wt% MWCNTs.	66
Figure 4.10 Stress-strain Curves for different MWCNTs wt%.	67
Figure 4.11 Effect of MWCNTs wt% on Young's modulus of the membranes.....	68
Figure 4.12 Effect of crosslinker wt% on the permeation and selectivity of the membrane.	69
Figure 4.13 Effect of Pluronic F127 wt% on the permeation and selectivity of the membrane.....	71
Figure 4.14 Effect of MWCNTs wt% on the permeation and selectivity of the membrane.	73
Figure 4.15 Effect of MWCNTs wt% on salt rejection before and after Chlorination.....	75
Figure 4.16 Relative amount and viability of E.coli cells adhering onto pristine and modified PVA membranes.....	76
Figure 4.17 Target plot comparing RO performance properties for unmodified and MWCNTs modified PVA membranes.....	78
Figure 5.1 Schematic diagram of the crosslinking of PVA with DGEBA and the intermolecular hydrogen bonding with Pluronic F-127.....	85
Figure 5.2 Dead-end filtration system for RO membranes.....	90

Figure 5.3 ATR-FTIR spectra of pure PVA and the PVA modified membranes with different wt% of Vanillin.....	93
Figure 5.4 Effect of mixing Pluronic F-127 on the hydrophilicity of the PVA membrane.	95
Figure 5.5 Effect of mixing Vanillin on the hydrophilicity of the PVA membrane.....	96
Figure 5.6 XRD patterns of pure PVA and Vanillin modified membranes.....	97
Figure 5.7 3-D AFM images of (a) pristine PVA membrane, (b) PVA-V1, (c) PVA-V2, (d) PVA-V3, (e) PVA-V4 and (f) PVA-V5.....	99
Figure 5.8 Effect of Vanillin loading on surface roughness of PVA membranes.	100
Figure 5.9 SEM images of (a) pristine PVA membrane, (b) PVA with Pluronic F-127 (c) PVA-V1, (d) PVA-V2, (e) PVA-V3, (f) PVA-V4 and (g) PVA-V5.....	102
Figure 5.10 Stress-strain Curves for different Vanillin wt%.	104
Figure 5.11 Effect of Vanillin wt% on Young's modulus of the membranes.	105
Figure 5.12 Effect of DGEBA (crosslinker) wt% on the permeation and selectivity of the membrane.....	106
Figure 5.13 Effect of Pluronic F-127 wt% on the permeation and selectivity of the membrane.....	108
Figure 5.14 Effect of Vanillin wt% on the permeation and selectivity of the membrane.	109
Figure 5.15 Bacteria Bacillus Subtilis DIZ photos of (a) unmodified PVA and (b) PVA conjugated with Vanillin.....	111
Figure 5.16 Effect of Vanillin wt% on the Chlorine resistance of the membrane.....	113
Figure 5.17 Target plot comparing RO performance properties for unmodified membranes and PVA membranes conjugated with Vanillin.	115
Figure 6.1 Schematic diagram of the crosslinking of PVA with DGEBA and the intermolecular hydrogen bonding with Pluronic F127.	121
Figure 6.2. Dead-end filtration system for RO membranes.....	126

Figure 6.3 ATR-FTIR spectra of pure PVA and PVA conjugated with Gum Arabic membranes.....	129
Figure 6.4 Diffractograms of pure PVA and Gum Arabic modified membranes.....	130
Figure 6.5 SEM images of (a) pristine PVA, (b) PVA with Pluronic F127, (c) PVA-GA-1, (d) PVA-GA-2, (e) PVA-GA-3, (f) PVA-GA-4 and (g) PVA-GA-5.	133
Figure 6.6 3-D AFM images of (a) PVA membranes with Pluronic F127, (b) PVA-GA-1, (c) PVA-GA-2, (d) PVA-GA-3, (e) PVA-GA-4 and (f) PVA-GA-5.	134
Figure 6.7 Effect of Gum Arabic conjugation on surface roughness of PVA membranes.	135
Figure 6.8 Effect of Mixing Pluronic F127 on the hydrophilicity of the PVA membrane.	137
Figure 6.9 Effect of Mixing Gum Arabic on the hydrophilicity of the PVA membrane.	138
Figure 6.10 Stress-strain Curves for different Gum Arabic wt%.	140
Figure 6.11 Effect of Gum Arabic wt% on Young's modulus of the membranes.....	140
Figure 6.12 Effect of crosslinker wt% on the permeation and selectivity of the membrane.	142
Figure 6.13 Effect of Pluronic F127 wt% on the permeation and selectivity of the membrane.....	143
Figure 6.14 Effect of Gum Arabic wt% on the permeation and selectivity of the membrane.....	145
Figure 6.15 Effect of Gum Arabic conjugation on salt rejection before and after Chlorination.	147
Figure 6.16 Relative amount and viability of E. coli cells adhering onto pristine and modified PVA membranes.....	149
Figure 6.17 Target plot comparing RO performance properties for the unmodified PVA membranes and the membranes conjugated with Gum Arabic.	151
Figure 7.1 Schematic diagram of the crosslinking of PVA with DGEBA and the intermolecular hydrogen bonding with Pluronic F127.	156

Figure 7.2. Dead-end filtration system for RO membranes.....	162
Figure 7.3 ATR-FTIR spectra of pure PVA, PVA-0.16 and TFN (1-5) membranes	165
Figure 7.4 Contact angle of the prepared PVA-0.16, TFC3 and TFN (1-5) RO membranes	167
Figure 7.5 XRD patterns of pure PVA, PVA-0.16, TFC3 and TFN4 membranes	168
Figure 7.6 SEM micrographs of PVA-0.16, TFC3 and TFN 1-5 (a) top surface and (b) cross-section.....	170
Figure 7.7 AFM images of single layer crosslinked PVA-0.16 and TFN (1-5) membrane	172
Figure 7.8 Stress-strain curves of PVA-0.16 and TFN (1-5) membranes	174
Figure 7.9 Young's modulus, Ultimate tensile strength and Elongation at break of PVA- 0.16 and TFN (1-5) membranes.....	174
Figure 7.10 Effect of different concentration (0-0.2wt%) of crosslinker (DGEBA) on pure PVA membrane for separation performance.	176
Figure 7.11 Effect of Pluronic F127 loading (0-10 wt%) on PVA-0.16 membrane for separation performance.....	177
Figure 7.12 Effect of ZnO-NPs loading (0-0.1wt%) on TFC3 membrane for separation performance.	179
Figure 7.13 Chlorine resistance analysis before and after Chlorination for PVA-0.16, TFC3 and TFN (1-5).....	180
Figure 8.1 Schematic representation of Zwitterion membrane formation.....	186
Figure 8.3 FTIR of control and HPEI-RO (1-4) membranes.....	190
Figure 8.4 Contact angles of control and HPEI-RO (1-4) membranes.....	191
Figure 8.5 AFM images of control and HPEI-RO (1-4) membrane.	193
Figure 8.6 SEM micrographs of control and HPEI-RO(1-4) (a) top surface and (b) cross- section.	195

Figure 8.7 Permeation fluxes of control and HPEI-RO3 membranes during RO tests with NaCl solutions (3.28wt.%) containing different level of CTAB. The modified membranes were surface modified with 3000ppm HPEI..... 197

Figure 8.8 Relative amount and viability of S.epidermidis and E.coli adhering onto the control and HPEI-RO (1-4) membranes. S.epidermidis and E.coli had been cultured until initial stationary phase and membranes were kept in broths for 3h..... 198

Figure 8.9 Schematic representation of the zwitterionic membranes for anti-bacterial adhesion. 199

LIST OF ABBREVIATIONS

MED	Multi-effect distillation
MSF	Multistage flashing
VC	Vapor compression
RO	Reverse osmosis
FO	Forward osmosis
SWRO	Seawater reverse osmosis
CA	Cellulose Acetate
PA	Polyamide
TFC	Thin film composite
MPD	M-phenylenediamine
TMC	Trimesoyl chloride
PVA	Poly (vinyl alcohol)
MWCNT	Multi-wall carbon nano-tubes
CTA	Cellulose triacetate
CDA	Cellulose diacetate
NOM	Natural organic matter
NF	Nano filtration
UV	Ultraviolet
PVDF	Poly (vinylidene fluoride)
BSA	Bovine serum albumin
SDS	Sodium dodecyl sulfate

DTAB	Dodecyltrimethyl ammonium bromide
PHMG	Polyhexamethylene guanidine
DGEBA	Bisphenol A diglycidyl ether
DMSO	Dimethyl sulphoxide
HPEI	Hyperbranched polyethyleneimine
LMH	(L/(m ² .h))
OD	Optical density
DIZ	Diffusion inhibition zone
CLSI	Clinical Laboratory Standards Institute
FTIR	Fourier transform infrared spectroscopy
ATR	Attenuated total reflectance
SEM	Scanning electron microscopy
AFM	Atomic force microscopy
XRD	X-ray diffraction
PEO	Poly (ethylene oxide)
PPO	Poly (propylene oxide)
GA	Gum Arabic
TFN	Thin film nanocomposite
MA	Maleic acid
ZP	Zwitterionic polymers
PBS	Phosphate-buffered saline

SUMMARY

Water is becoming increasingly scarce as the demand for fresh water continues to increase in a drastic manner. One potential new water resource is desalination of sea and brackish water. Reverse osmosis (RO) membranes desalination is one of the many processes used to obtain potable water fit for human consumption from seawater. Nevertheless, the membranes used in this process are prone to fouling by microorganisms and Chlorine attack.

It has been shown from literature that developing an anti-fouling, Chlorine resistant, highly selective and highly permeable reverse osmosis membrane is a necessity. To develop such a membrane, one should improve the hydrophilicity of the membrane surface, reduce its roughness and make the surface negatively charged. The overall goal of this research was the development of high performance reverse osmosis membranes materials with improved permeability, high salt rejection and superior biofouling and Chlorine resistance.

The present research was designed to investigate novel poly (vinyl alcohol) (PVA) RO membranes with various fillers and combinations and their effectiveness as active RO separation layers with improved biofouling and Chlorine resistance. The uniqueness of this work was that the PVA polymer matrix was utilized as an active RO layer without the use of any polymeric or ceramic substrate.

The crosslinked PVA RO membranes incorporated with various fillers were fabricated using dissolution casting method. The fabricated membranes were then characterized and analyzed using various techniques like attenuated total reflection Fourier transform infrared spectroscopy (ATR-FTIR), contact angle measurements, X-ray diffraction

(XRD), scanning electron microscope (SEM), atomic force microscope (AFM) and mechanical testing. The actual reverse osmosis performance of the membranes, including permeation testing, salt rejection and Chlorine resistance was examined using a reverse osmosis permeation unit.

This study showed that the incorporation of Pluronic F127 and MWCNTs into the PVA polymer matrix improved the overall RO performance of the membrane in terms of hydrophilicity, surface roughness, water permeability, salt rejection, Chlorine resistance and biofouling resistance. The membranes that contain 0.08 and 0.1 wt% MWCNTs provided optimal salt rejection, Chlorine and biofouling resistance and mechanical strength. Although the permeation of these two membranes is not the best, they relatively have an excellent water flux.

Furthermore, It has been shown that the conjugation of Vanillin and Pluronic F-127 improved the overall RO performance of the membrane in terms of hydrophilicity, surface roughness, salt rejection, Chlorine resistance, biofouling resistance and mechanical strength. Membranes PVA-V4 and PVA-V5 provided optimal salt rejection, Chlorine resistance, mechanical strength and surface hydrophilicity. Although the permeation of these two membranes is not the best, they relatively have an excellent water flux.

It has been shown that conjugating PVA with Gum Arabic and Pluronic F127 improved the overall RO performance of the membrane in terms of hydrophilicity, surface roughness, water permeability, salt rejection, Chlorine resistance, biofouling resistance and mechanical strength. The membrane PVA-GA-5 that contains 0.9 wt% Gum Arabic

provided optimal salt rejection, Chlorine and biofouling resistance, mechanical strength, permeability, surface roughness and surface hydrophilicity.

The incorporation of ZnO-NPs and Pluronic F-127 improved the performance of RO membrane, as well. The improvement was in terms of water permeability, salt rejection and Chlorine resistance by increasing hydrophilicity and affecting the roughness of the membrane. The membrane TFN4, containing 0.08 wt% ZnO-NPs, exhibited superior permeation flux, salt rejection and Chlorine resistance.

HPEI-RO membranes having zwitterions were effectively synthesized, as well. FTIR analysis confirmed the HPEI and MA functional group of the membranes. The AFM roughness value of all HPEI-RO membranes decreased with increasing HPEI content in zwitterionic membranes. Both water contact angle and RO performance test measurements demonstrated that HPEI-RO membranes had high permeation flux and could bind high amount of water molecules with zwitterions in membranes. In addition, the HPEI-RO3 exhibited the stability during desalination process and good fouling resistance property.

Lastly, the outcomes of this study have shown a great promise for the proposed crosslinked PVA membrane as an active RO separation layer without a substrate. The results of this investigation showed that the fabricated RO membrane overcame PVA drawbacks through appropriate crosslinking and through appropriate selection of fillers. The synthesized membranes had an improved RO performance and an enhanced Chlorine and biofouling resistance.

CHAPTER 1

INTRODUCTION

1.1 Scarcity of Global Potable and Clean Water

Around one billion people worldwide are suffering from the lack of clean water, according to the World Health Organization. Approximately 2.3 billion live in areas that are water-stressed. Another factor that enormously affects the water demand equation is the global population increase. The global population increase is around 80 million a year [1-4]. Figure 1.1 shows the increasing demand of water worldwide.

Although most of earth's surface is water, only 2.5% is fresh water and a small amount of the fresh water is easily reachable. This is because most of the fresh water is stored as glaciers or is very deep underground [3, 5]. Therefore, tremendous effort to provide clean, fresh water for the world populations is necessary.

1.2 Water Desalination Technologies

Water desalination techniques can be classified under the following two general processes: (a) Phase change processes (thermal methods) or (b) single phase processes (membrane processes). Multi-effect distillation (MED), multistage flashing (MSF) and vapor compression (VC) are the most commonly used phase change processes. Reverse osmosis (RO) (a membrane technique) is widely used nowadays [6]. Forward osmosis (FO) is an emerging, low-cost membrane technology that has a bright future [7-11]. For very salty seawaters, Thermal techniques showed better effectiveness compared to membrane techniques [6]. As shown in Figure 1.2, around 60% of the worldwide installed desalination capacity of water is produced using RO technology [12].

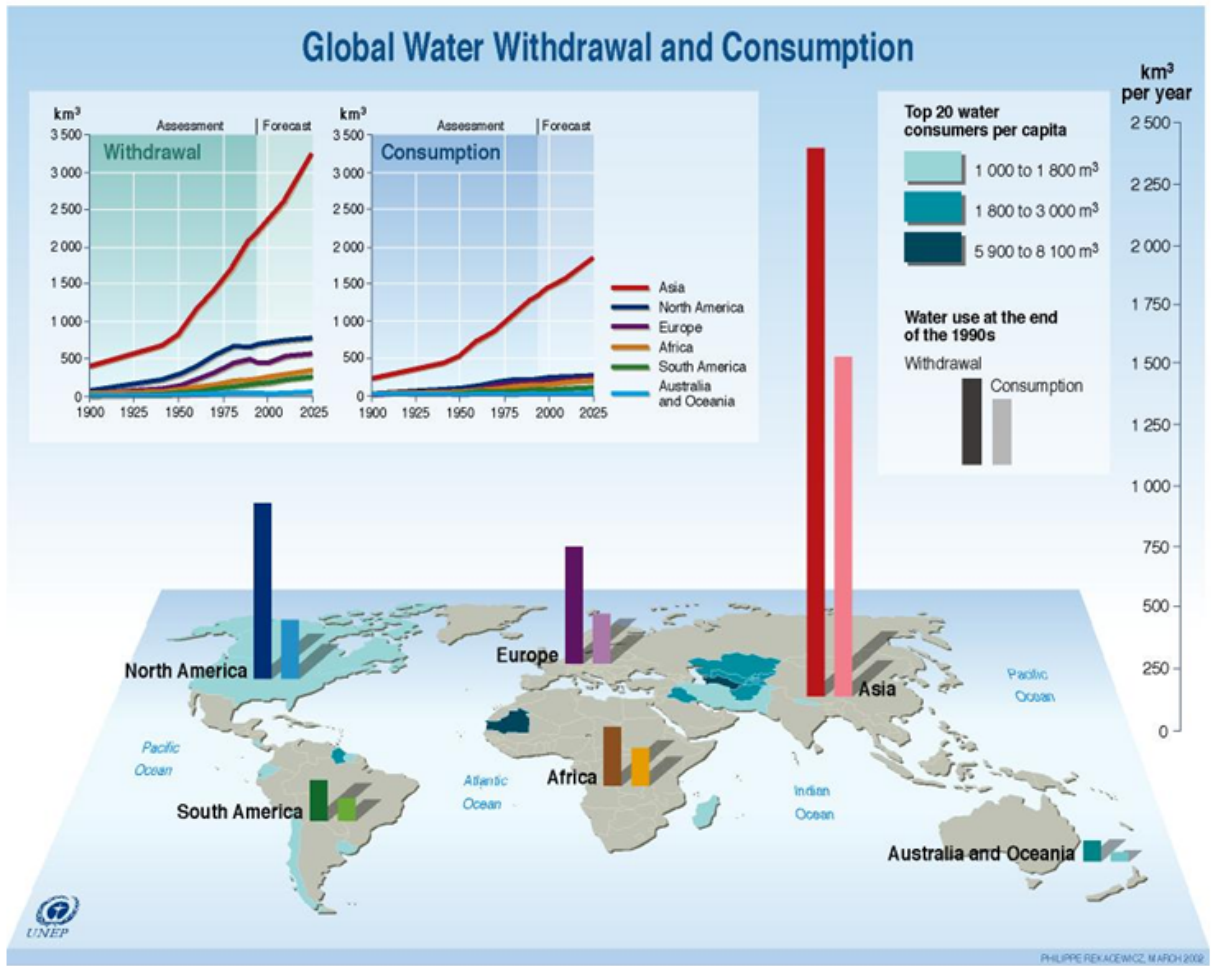


Figure 1.1 Global water withdrawal and consumption [13].

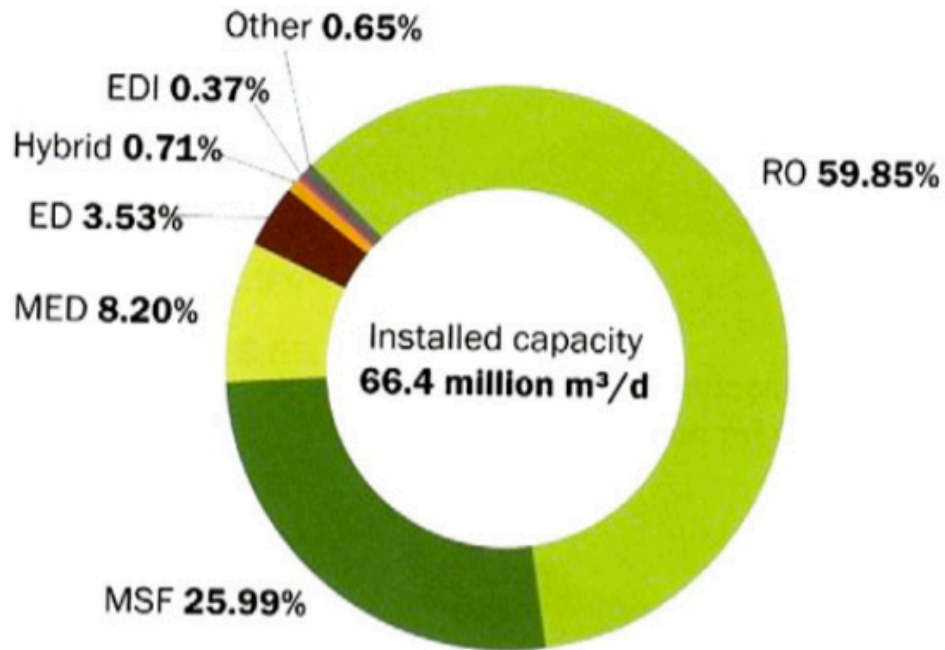


Figure 1.2 Worldwide installed desalination capacity by technology [12].

Advances in water desalination technologies have been rapid. The cost to desalinate seawater lowers from about $\$9.0/\text{m}^3$ around 1960, to around $\$1.0/\text{m}^3$ in 2005 for the MSF process. The costs have fallen to $\$0.6/\text{m}^3$ for saline water desalination using RO [14]. The total desalination market reached over US\$31 billion in 2015, as shown in Table 1.1. Around 50% of the total desalination investments are for seawater RO (SWRO) projects. This is mainly due to its lower total cost. The utilization of thermal techniques will continue in areas where energy is available at low-cost [12].

Table 1.1 Market historical and forecast data of desalination systems [12].

Project type	2006–2010 (\$billion USD)	2011–2015 (\$billion USD)
Seawater RO	9.92	15.48
Seawater MED	3.03	4.04
Seawater MSF	8.39	7.07
Small thermal	2.06	2.33
Brackish RO	1.43	2.18
Ultrapure RO	0.21	0.30
Total (\$Billion USD)	25.04	31.40

1.3 History of Water Desalination

Desalination first began to get commercialized at the early days when they first tried to desalt water at ships or boats long journeys. To avoid depletion of fresh water on board, they used some sort of heat to distill seawater. Japanese sailors used a very basic distillation technique; they heated pots of salty water and used bamboo tubes to collect the evaporated fresh water. This was in the beginning of the 17th century [15]. Many countries began to develop advanced distillation technologies in the late 18th century. Some of the first desalination plants worldwide include the plants in Tigne, Malta in 1881 and in Jeddah, Saudi Arabia in 1907 [15]. Middle Eastern countries are the first to use desalination on a large scale for municipal drinking water production. Seawater distillation plants were first developed in the 1950s and the 1960s. In the late 1960s,

membranes entered the desalination market, and the first successful RO plants that used brackish water as the feed were established. In the following decade, after further developments in the membranes materials, the permeability and salt rejection were improved, which allowed for the utilization of RO technology in seawater desalination. Over the past 40 years, RO became the primary choice for new desalination facilities [15].

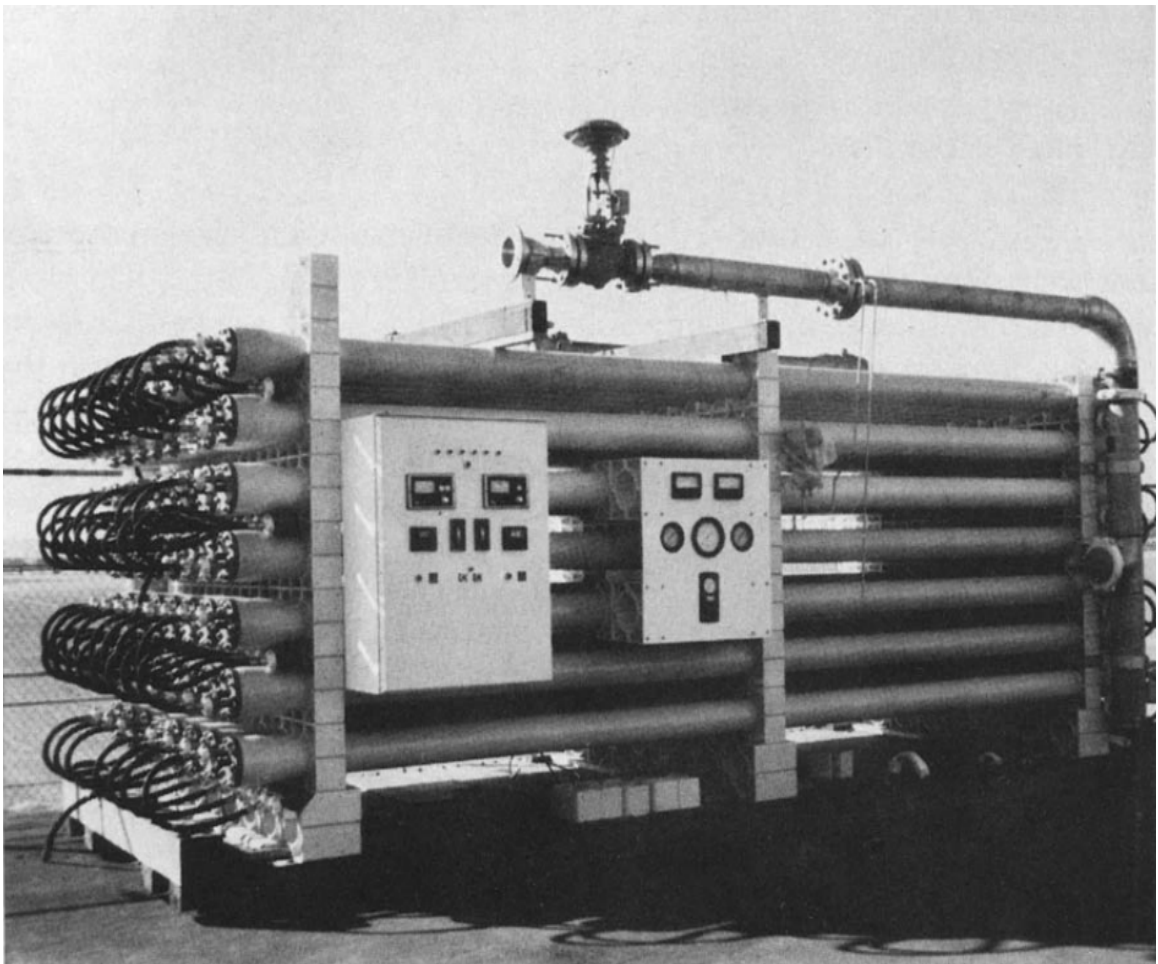


Figure 1.3 RO seawater desalination unit at Jeddah, Saudi Arabia in the 1970s [16].



Figure 1.4 Modern RO plant in Spain [17].

1.4 Reverse Osmosis Membranes

Nowadays, RO is the prominent desalination technology. It took the leadership over conventional thermal technologies and is expected to maintain its leadership in the near future. RO attracts interests commercially due to continuous process improvements and significant cost reductions. These improvements include developments in membrane materials and module design, process design, feed pre-treatment and energy recovery and reduction in energy consumption [18].

Some polymers have a property called semi-permeability, which means that they are very permeable for water but their permeability for dissolved substances is low. When applying a pressure difference across the membrane, the contaminated water in the feed is forced to permeate through the membrane surface [19]. Fairly high feed pressure is required to overcome the feed side osmotic pressure, a process called reverse osmosis. The Operating pressure ranges from 55 to 68 bar in seawater desalination. On the other hand, for brackish water, the operating pressure is lower due to the lower osmotic pressure, since the water is less saline [19]. Figure 1.5 shows the basic schematic for reverse osmosis principle.

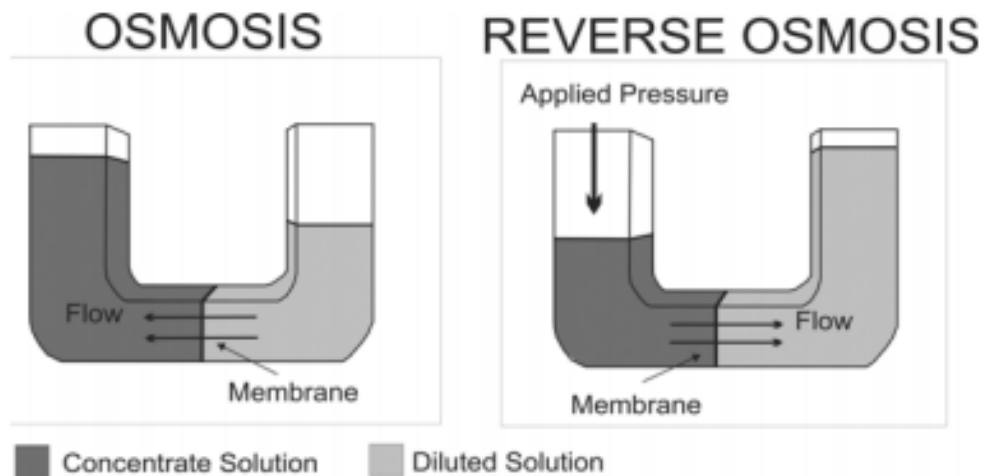


Figure 1.5 Reverse osmosis principle (source: Aqualyng) [19].

1.4.1 Reverse Osmosis Process Fundamentals

When the pressure and temperature on both sides of the membrane are equal, water will permeate from the high concentration side of the membrane to the low concentration side. This process will continue even if there is a pressure difference between the two sides until the pressure difference, Δp reaches the osmotic pressure, $\Delta\pi$. If Δp is larger than $\Delta\pi$, the direction of flow is reversed and water goes from the high concentration side to the low concentration side. This process is called reverse osmosis (RO) [19].

A crucial feature an RO membrane should have is high permeate flux and high salt rejection [19]. In addition to that, excellent Chlorine and fouling resistance, mechanical durability, and low cost are very important features [20]. Very thin membranes are required to achieve high permeability, since the flux is inversely proportional to the membrane thickness. RO membranes generally consist of a very thin active non-porous layer and a porous supporting layer for mechanical support. The thin active layer is responsible for almost all resistance to mass transport and salt rejection. The support layer, on the other hand, protects the membrane from breaking. Membranes featuring this combination of active layer and supporting structure are called asymmetric membrane, as shown in Figure 1.6 [19]. In symmetric membranes, the structure and transport properties are undistinguishable over the entire membrane cross-section; and the flux is directly proportional to the membrane thickness [21].

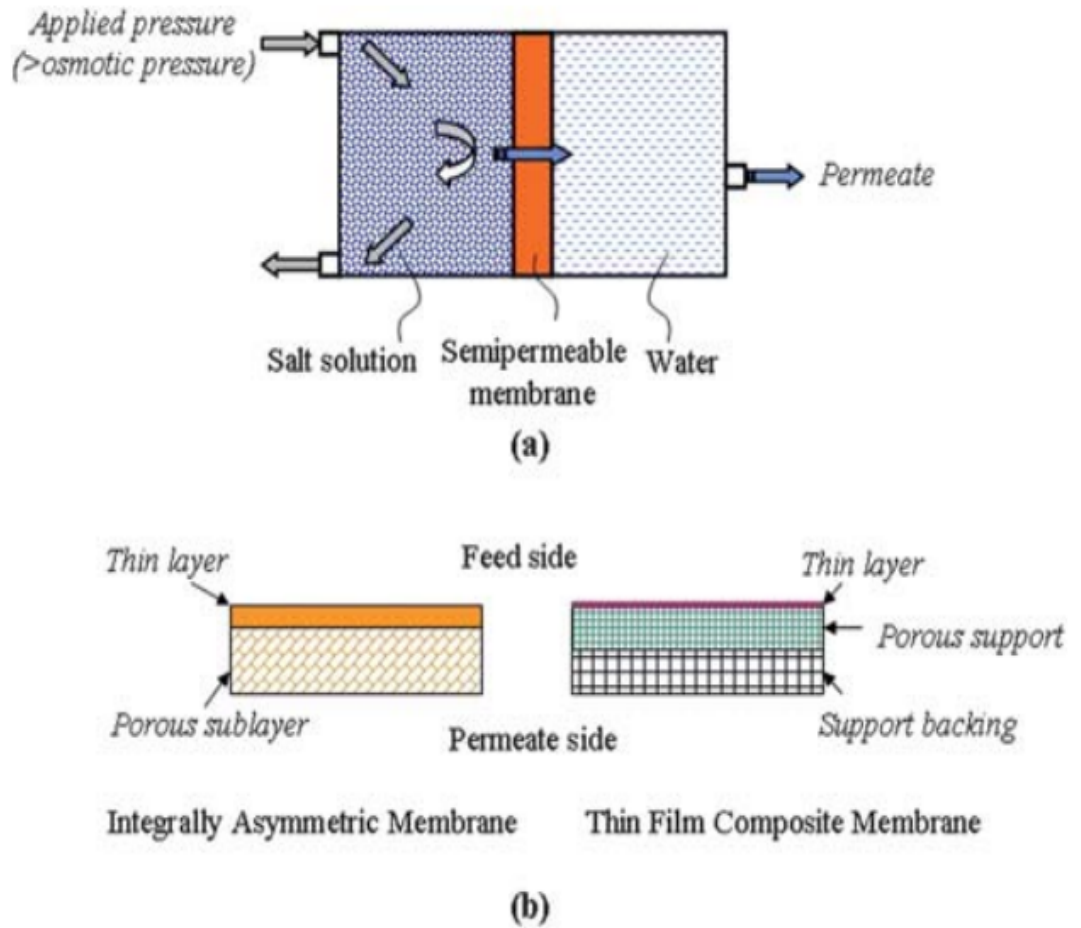


Figure 1.6 Schematic of (a) reverse osmosis (RO) desalination process and (b) membrane configurations including integrally asymmetric membrane (left) and thin film composite membrane (right) [20].

1.4.2 Polymeric RO Membranes

Commercially, Polymeric RO membranes have dominated applications since the very first RO desalination plant. They are low-cost membranes, very easy to handle and they have great permeability and salt rejection [18]. Commercially available RO membranes are basically synthesized from two types of polymers: cellulose acetate (CA) and

aromatic polyamides (PA). In 1960's, the first cellulose acetate membrane was commercially applied for seawater desalination. Nowadays, cellulose acetate membranes are derived from either cellulose acetate, triacetate, diacetate or their blends, in the form of asymmetric configuration (Figure 1.6, b) [20]. Since they are derived from naturally occurring cellulose, CA membranes are relatively low-cost membranes. However, there are some drawbacks, such as a narrow operating pH range (4.5–7.5), sensitivity to biological attack, structural compaction under high pressure and low upper temperature limit [20]. In the mid-1970s, Cadotte, at North Star Research, developed the interfacial polymerization method for producing polyamide (PA) thin film composite (TFC) membranes (Figure 1.7) [19, 20, 22-24]. The PA TFC membranes are composed of a thin highly selective aromatic polyamide layer bottomed by a reinforced micro-porous sub-layer, which has another polymer (Figure 1.6, b). PA membranes, when compared to CA membranes, show much better water flux, salt and organic rejections, and pressure compaction resistance. They also operate under wider operating temperatures and pH ranges [20, 24, 25].

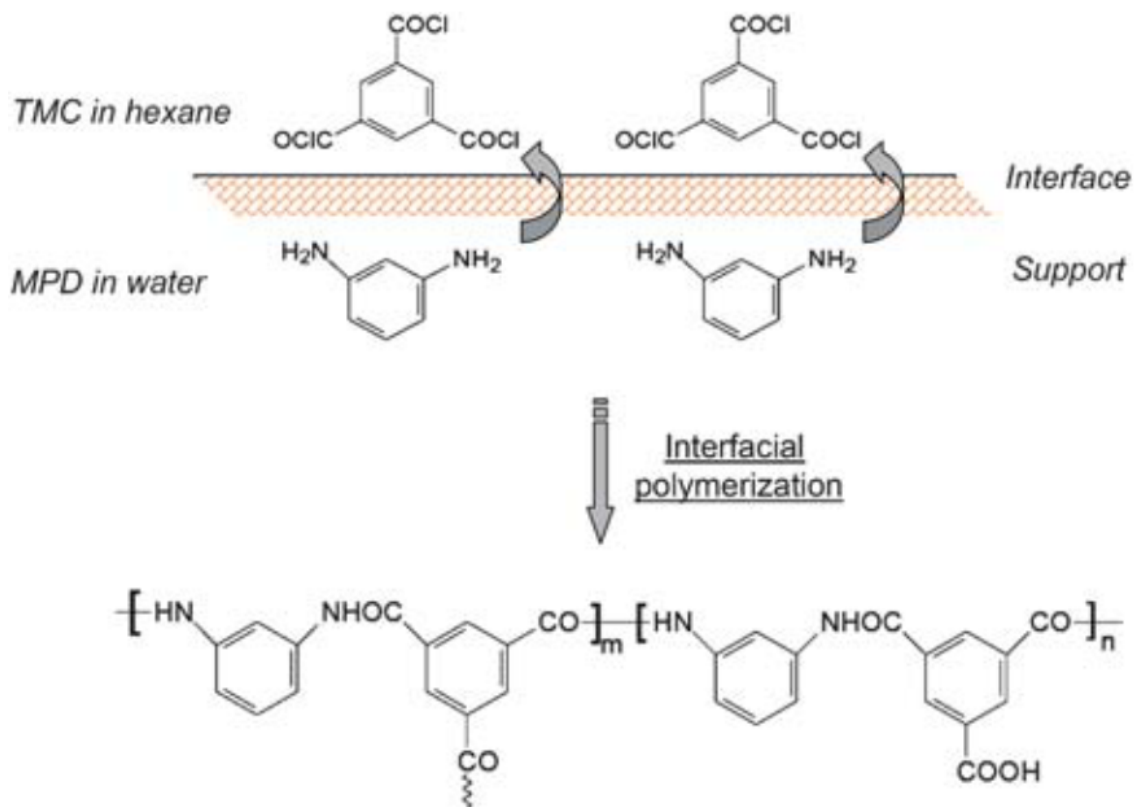


Figure 1.7 The polyamide derived from m-phenylenediamine (MPD) and trimesoyl chloride (TMC) via interfacial polymerization [20].

1.4.3 Inorganic Membranes

In recent decades, zeolite and other inorganic membranes have been studied extensively for gas separation and liquid pervaporation. Zeolite membranes, in particular, have shown potential advantages for desalination in terms of superior permeability and selectivity, compared to polymeric membranes, since they have very specific pore structure and narrow pore size distribution. Zeolite membranes are synthesized by the hydrothermal deposition on suitable porous ceramic or stainless steel supports, as shown in Figure 1.8 [20, 26-28].

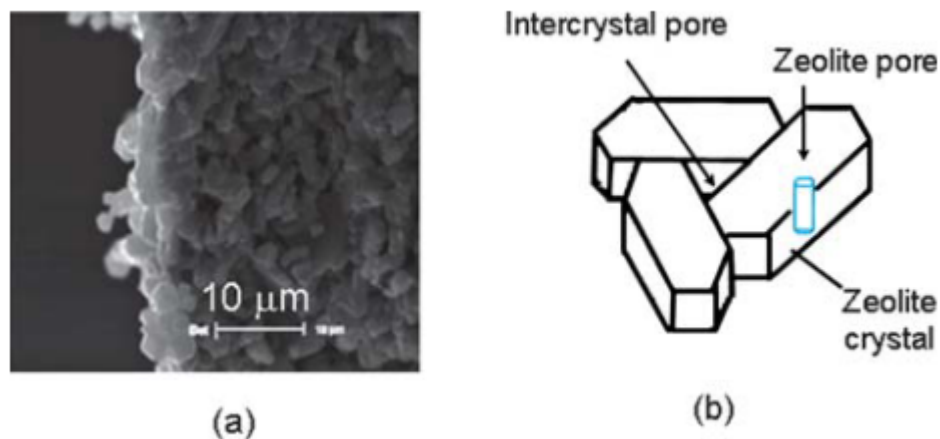


Figure 1.8 (a) SEM image of a cross section of zeolite NaA membrane supported on porous α - Al_2O_3 ceramic. (b) Illustrations of an inter-crystal pore and zeolite pore in zeolite membranes [20].

1.5 Organization of The Dissertation

This dissertation contains 9 chapters including this introductory chapter. Chapter 2 offers a detailed literature review about the process of reverse osmosis desalination including its history, its background and theory, the challenges facing its utilization and how to address them. Chapter 3 detailed the overall and specific objectives of this research followed by the procedures and methods. Chapter 4 discusses the influence of utilizing crosslinked poly (vinyl alcohol) (PVA) as an active RO membrane with the incorporation of Pluronic F-127 and MWCNTs on the RO performance including Chlorine and biofouling resistance. Chapter 5 offers a comprehensive study on the effect of incorporating Vanillin into the PVA membrane system on the membrane performance. Chapter 6 describes a research on conjugating Gum Arabic and Pluronic F-127 with the

membrane matrix and their influence on Chlorine resistance enhancement and biofouling mitigation. Chapter 7 displays an investigation on the influence of incorporating ZnO nano-particles (ZnO-NPs) into the membrane matrix and their effect on permeability, selectivity and Chlorine and biofouling resistance. Chapter 8 describes the feasibility of utilizing hyperbranched polyethyleneimine as biofouling resistant agent and its effect on the RO performance of the PVA-based membrane. Chapter 9 closes with conclusions and future work recommendations.

CHAPTER 2

LITERATURE REVIEW

2.1 Historical Development of RO Water Desalination Membranes

In 1949, researchers reported that the report entitled “The Sea as a Source of Fresh Water” has initiated the research in the area of salt-rejecting membranes [18]. In 1959, Reid and Breton showed that a thin symmetrical cellulose acetate (CA) membrane could be used to desalinate water with 98% salt rejection; unfortunately, the water flux was very low, of the order of less than $10 \text{ mL}/(\text{m}^2 \cdot \text{h})$ [29]. In 1963, Loeb-Sourirajan invented the first asymmetric CA membrane. The thin layer of CA was formed on top of a thick micro-porous layer. The flux of this membrane was an order of magnitude higher than that of the previous symmetric model [30, 31]. Due to its stability in a wider range of temperatures and pH, cellulose triacetate (CTA) membrane was developed. CTA has higher resistance to chemical and biological attack when compared to the initial cellulose diacetate (CDA) material. However, the drawback of CTA is that it has a very low mechanical strength which results in possible compaction that causes flux decline even at moderate pressures [18, 32]. It has been reported that blending CDA with CTA offered higher permeability and selectivity and better resistance to compaction compared to CA membranes [18, 33].

Richter and Hoehn developed the first non-cellulosic asymmetric membrane. It consisted of an aromatic polyamide (PA) asymmetric hollow-fiber membrane [18]. The trade name of this membrane was B-9 Permasep® and it was commercialized by Du Pont for brackish water desalination applications. This membrane had better durability, stability

and versatility compared to CA membranes. Unfortunately, the flux and salt rejection were low [18, 34, 35].

2.1.1 Thin Film Composite membranes

Due to the fact that it is difficult to form asymmetric membranes from most soluble polymers in one step casting, two-step casting methods were utilized. This method yields anisotropic membrane morphologies. Using this method, one can optimize the properties of each, the support layer and the active layer independently. The support layer is optimized for better mechanical stability and strength, while the active layer is optimized for salt rejection and permeability. Furthermore, a wide variety of polymers can be tested for the barrier layer and support layer separately. Membranes synthesized using this method are called thin film composite membranes (TFC) [18, 36].

The first thin film composite membrane was proposed by Morgan using interfacial polymerization method [24]. Cadotte and his co-workers made it commercially available by optimizing the polymerization conditions to get high flux and high rejection membranes. They achieved the optimum performance by interfacial crosslinking of piperazine with trimesoyl chloride/isophthaloyl chloride mixture [24, 37]. After the invention of the interfacial polymerization method to synthesize thin film composite (TFC) membranes by Cadotte and his coworkers, multiple corporations started to develop and produce TFC membranes commercially [24, 37].

2.2 Transport Through RO membranes

The transport through RO membranes is governed by the solution-diffusion theory [38-40]. The theory states that, initially, a molecule from the feed solution gets absorbed onto

the upstream face of the membrane. Afterwards, it diffuses through the membrane with the aid of the chemical potential gradient in the membrane. Lastly, it desorbs from the downstream face of the membrane towards the permeate solution. The applied pressure stimulates the activity gradient, which is the driving force for transport through RO membranes. The governing equation describing solution-diffusion transport is [38, 39]:

$$J_w = L_p (\Delta P - \Delta \pi)$$

where J_w is volumetric water flux (L/(m² hr)), L_p is membrane permeance (L/(m² hr bar)), Δp is the applied trans-membrane pressure difference (bar) and $\Delta \pi$ is the osmotic pressure difference between the feed and the permeate solutions (bar). The flux could be defined as the volume of water passing through the membrane across a unit cross-sectional area in a unit time [23, 41, 42]. For a nonporous, defect-free RO membrane, L_p is given by [38, 39]:

$$L_p = \frac{DSV}{RTl}$$

where D is the diffusion coefficient of water in the membrane (cm²/s), S is the water solubility in the membrane, equivalent to the water volume fraction in the membrane, V is the molar volume of water (18 cm³/mole), R is the ideal gas constant (83.1 (cm³ bar)/(mol K)), T is the ambient temperature (K) and l is the membrane thickness (cm). In membrane-based desalination, purified water is forced through the membrane by the application of high pressure. The external applied pressure is needed to overcome the osmotic pressure present in the system that is caused by the difference in the salt concentration of both sides of the membrane. The osmotic pressure is proportional to the solute concentration. For an ideal solution, with all salt ions being completely dissociated, the osmotic pressure is given by the following equation [38-40]:

$$\pi = iMRT$$

where i is the dimensionless Van't Hoff factor, M is the molarity, R is the gas constant and T is the thermodynamic (absolute) temperature. Salt transport through the membrane is also governed by the solution-diffusion theory [38-40]:

$$J_s = B (C_f - C_p)$$

where J_s is salt flux ($\text{mg}/(\text{m}^2 \text{ hr})$), B is the membrane salt permeance ($\text{L}/(\text{m}^2 \text{ hr})$), and C_f and C_p are the salt concentrations in the feed and permeate streams, respectively (mg/L). For a nonporous, defect-free membrane, the membrane salt permeance is calculated by the following equation [38-40]:

$$B = \frac{D_s K_s}{l}$$

where D_s is the salt diffusivity in the membrane (cm^2/s), K_s is the salt partition coefficient and l is the membrane thickness (cm). Therefore, salt flux is related to water flux by:

$$J_s = J_w C_p$$

The selectivity of RO membranes is usually quantified in terms of salt rejection rather than salt flux. Salt rejection is calculated by the following equation [38-40]:

$$SR = \left(1 - \frac{C_p}{C_f} \right) \times 100$$

2.3 RO Membranes Challenges

Despite the relative success of RO membranes technologies, there are some challenges. Membrane fouling and Chlorine attack are the major problems facing reverse osmosis applications.

2.3.1 Membrane Fouling

Fouling can be defined as the deposition of foulants on top of the membrane surface or within the pores of the membrane. Membrane fouling can be classified into inorganic fouling, colloidal fouling, organic fouling and biofouling. Fouling is the major factor that negatively affects the membrane performance and reduces its life, which increases the overall cost of the desalination process [43-48]. The scientific cause of fouling is agreed to be the reversible and irreversible adsorption of dissolved species onto the surface or inside the pores of the membrane [49-51].

2.3.1.1 Biofouling

Most of the foulants, other than bio-foulants, can be removed or their effect can be minimized to some extent by pretreatment. Biofouling, on the other hand, is different. Membrane biofouling is defined as the buildup of microbial layers on the surface or within the pores of the membrane. Those micro-organisms such as bacteria, algae and fungi are pseudo particles, which means that even if pre-treatment gets rid of 99.99% of them, the remaining 0.01% can grow, multiply or even relocate. Therefore, it has been found that biofouling occurs even after feed water pretreatment and after the addition of disinfectants [42, 48, 51-55]. Micro-organisms can withstand extreme conditions like temperatures ranging from -12°C to 110°C and pH values between 0.5 and 13. The attached microorganisms embed and form biofilms. This means that the originally dissolved species are now locally restrained and converted from solution into a semisolid state [52, 53, 56, 57].

Biofouling follows a series of events. These include the transport, deposition and adhesion of cells followed by biofilm production and cell progression and spread, as

shown in Figure 2.1 [22, 51, 57, 58]. The worst thing about biofouling is that the cells are able to survive with insignificant amount of nutrients. Biofouling could decrease the membrane flux, deteriorate the membrane structure, increase salt passage and negatively affect membrane module [59-62]

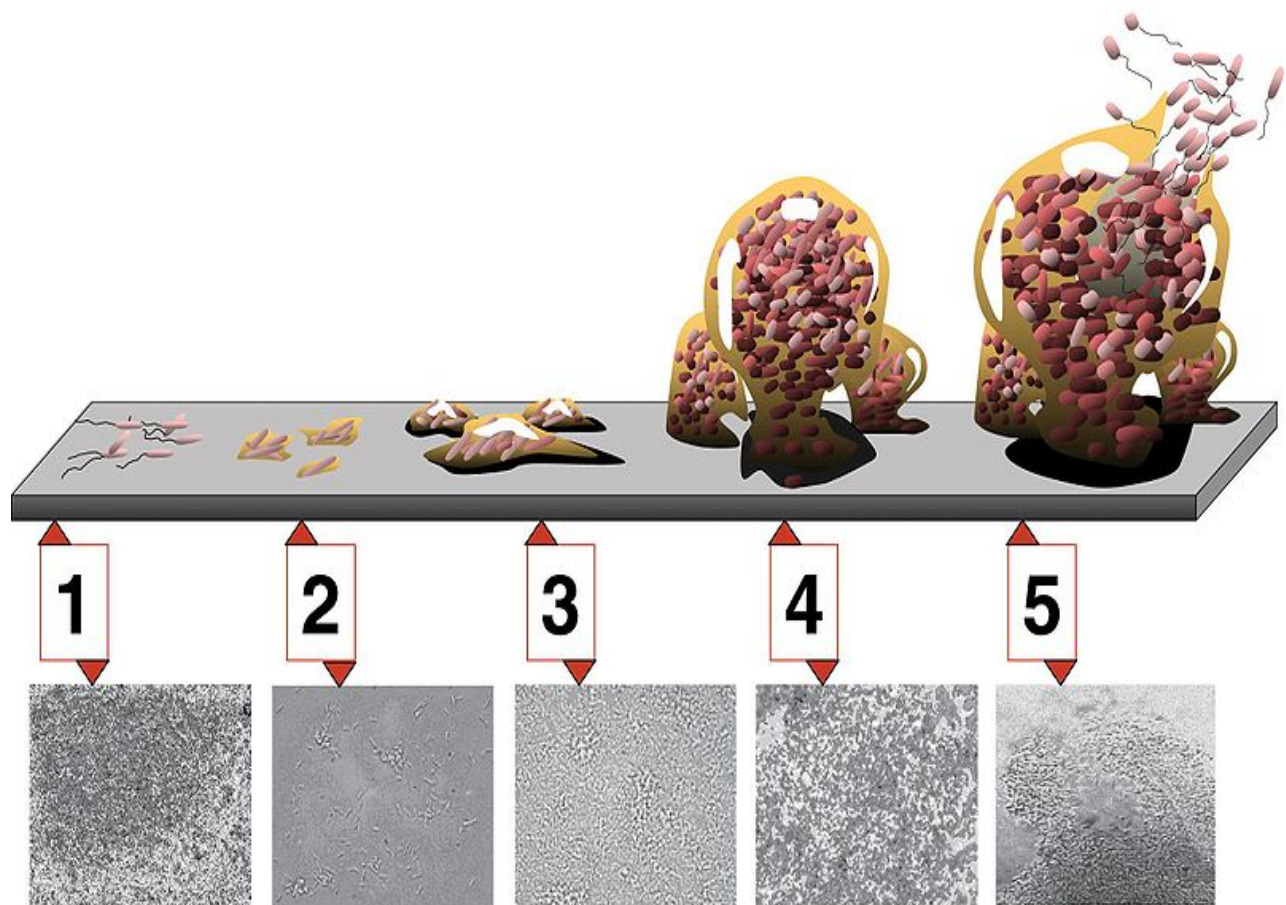


Figure 2.1 Biofilm Maturation Stages. Each stage of development in the diagram is paired with a photomicrograph of a developing *P. aeruginosa* biofilm. All photomicrographs are shown to same scale. (Image Credit: D. Davis) [63].

2.3.2 Biofouling Negative Effects on RO Membranes

The development of a biofilm on the surface of the membrane causes several undesirable consequences on the RO process. These include the following:

2.3.2.1 Loss of salt rejection

It has been reported that the formation of a biofilm causes an increase in solute content of the purified water through reverse osmosis membranes [64]. That loss of salt rejection is primarily due to the increase in concentration polarization at the membrane surface (Figure 2.2). The formation of a biofilm on the surface of the membrane may spread and stabilize the viscous sub-layer. Dissolved solutes tend to build up at that viscous sub-layer, which, in turn, promotes the concentration polarization across the membrane [65].

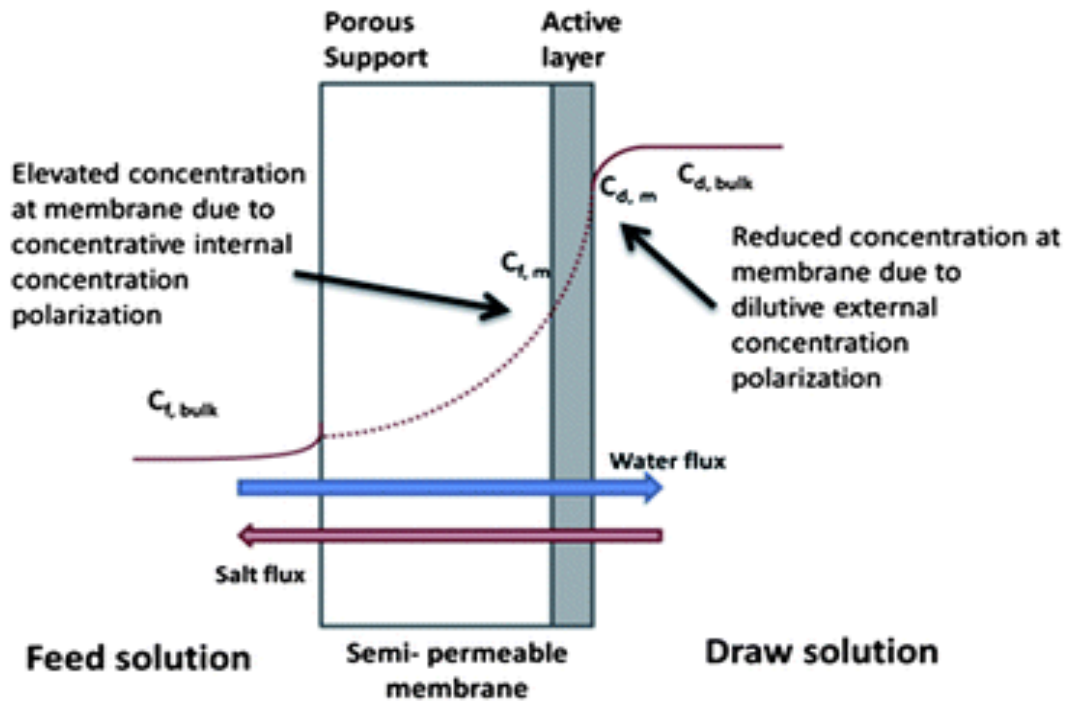


Figure 2.2 Schematic drawing illustrating internal and external concentration polarization when an asymmetric membrane is used for pressure retarded osmosis [66].

2.3.2.2 *Water flux decline*

The flux decline is caused by the formation of the low permeability biofilm on top of the membrane surface. One more reason is the irreversible change in the composition or structure of the RO polymer. The biofilm and the associated biopolymers are the major barrier for the passage of water molecules. If the biofilm is removed partially by chemical cleaning, water transport could be restored to near pre-fouling levels. Flux decline due to biofouling usually starts with an initial rapid decline followed by a gradual decay. The initial decline results from the initial adhesion of the microorganisms and the synthesis of the biopolymer. That stage is followed by the growth, which is more of a gradual behavior [51, 54, 65]. Figure 2.3 shows a typical normalized flux decline upon induced

biofouling with *P. aeruginosa* in four independent biofouling experiments terminated at different times. Also shown in the inset graph are the corresponding increases in salt passage at the end of the fouling experiments [61].

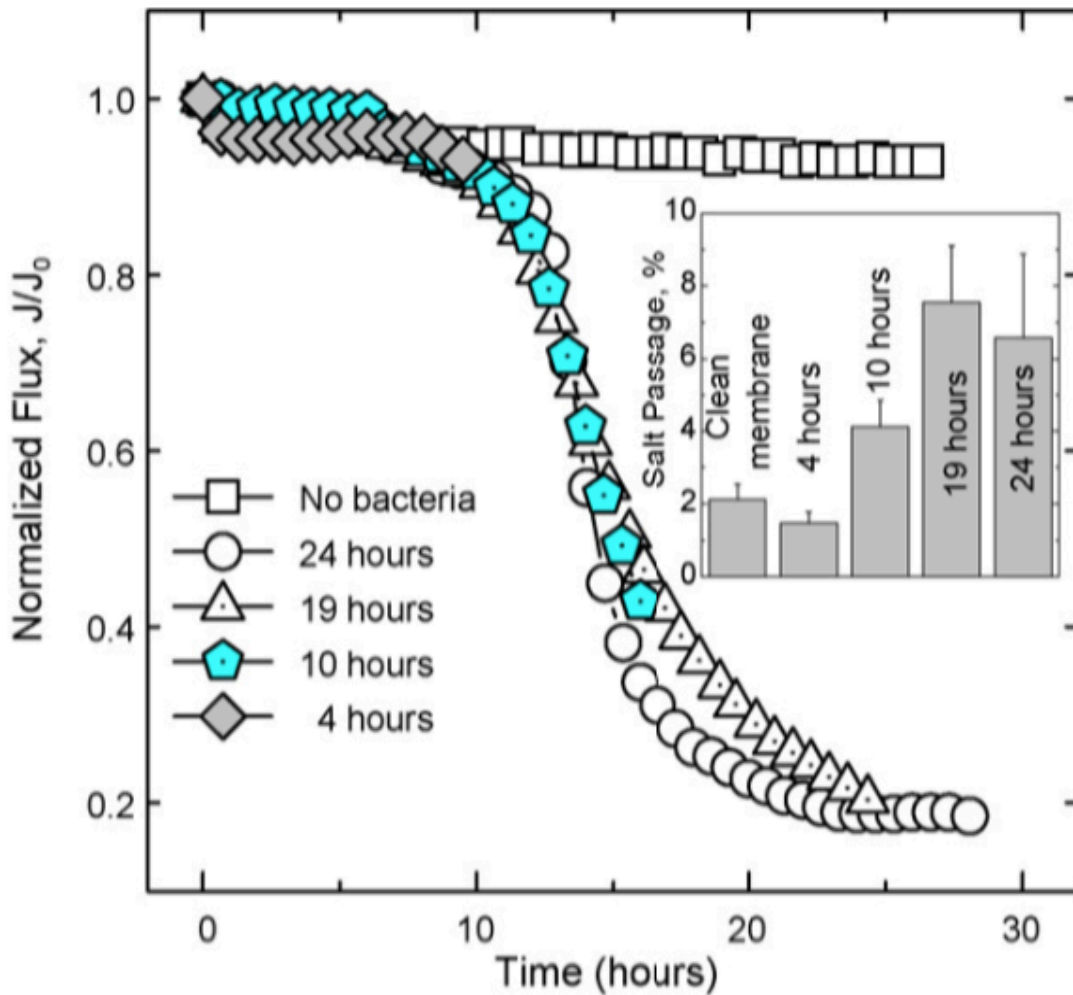


Figure 2.3 Normalized flux decline and loss of salt rejection upon induced biofouling with *P. aeruginosa* [61].

2.3.2.3 *Increase in operating pressure*

Biofouling usually causes some frictional drag forces within the membrane module. That friction increase causes energy loss, which causes pressure dissipation, in turn. Due to biofouling, that trans-membrane pressure (ΔP) may exceed the design specification for the reverse osmosis module. This may result in compression or collapse of the module [65].

2.3.2.4 *Membrane bio-degradation*

Micro-organisms attachment to the surface may destabilize the reverse osmosis membrane polymer, which makes it prone to oxidation or hydrolytic cleavage. Moreover, some bacteria and fungi may secrete some enzymes that degrade the membrane polymer directly [65].

2.3.3 Chlorine Attack

Another challenge that faces most commercially available RO membranes is membrane polymer degradation through direct contact with Chlorine, which is commonly used as disinfectant in water and wastewater treatment. It has been reported that Chlorine exposure changes the chemical structure of the RO polymer, which affects membrane performance and shortens its lifespan [24, 67, 68].

For PA RO membranes, vulnerability to Chlorine attack is due to the presence of Chlorine-sensitive sites of amide linkages ($-\text{CONH}-$) and end amine groups ($-\text{NH}_2$) in the polyamide chains [69]. Chlorine forms N-Chlorinated amides in the preliminary stage. Then, it is followed by a non-reversible reaction, which is ring-Chlorination through intramolecular rearrangement of Chlorine atom into the aromatic ring of the

diamine moiety via Orton rearrangement. Figure 2.4 shows the effect of the exposure to Chlorine on the chemical structure of PA. It has been reported that membrane polymer degradation due to Chlorine presence is independent of feed pH; rather, it strongly relies on Chlorine concentration in the feed solution and the exposure time [43].

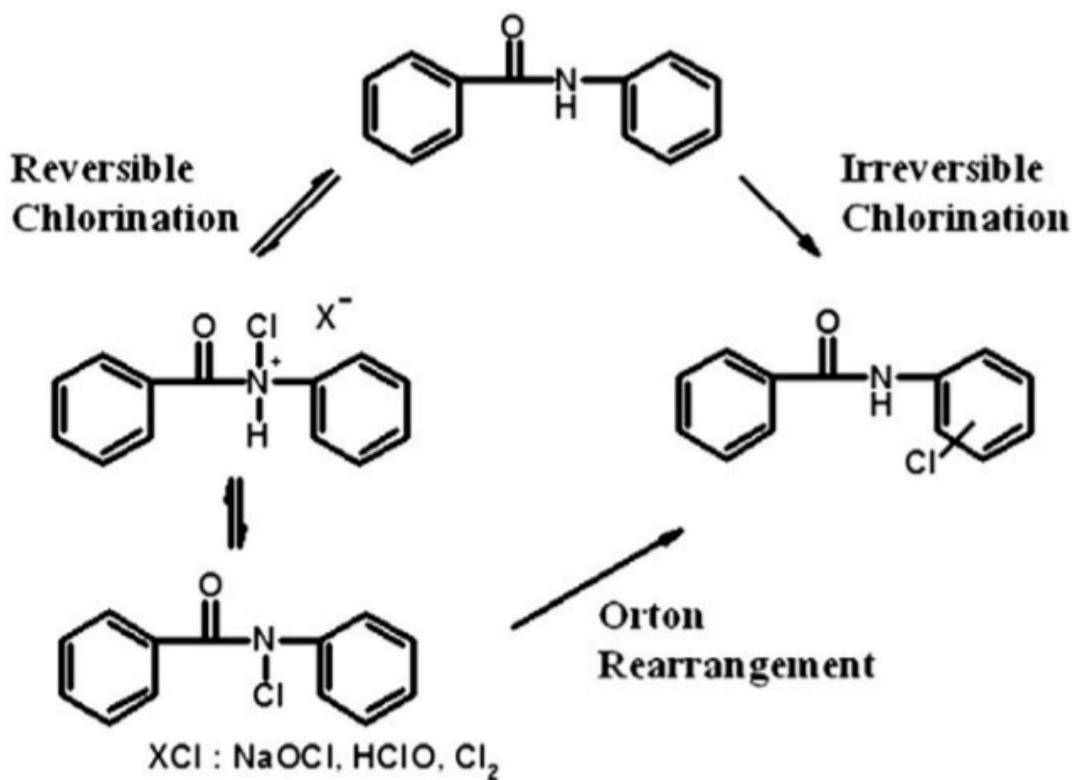


Figure 2.4 Orton rearrangement of an aromatic amide with active Chlorine [43, 70].

2.4 Membranes Surface Modification

As reported earlier, the important stages in biofilm formation are bacterial adhesion, micro-colony formation, and biofilm maturation. Membrane surface modification is done primarily to prevent one or more of these stages [51]. Furthermore, surface modification is performed to mitigate Chlorine attack.

Membrane surface hydrophilicity, charge, and roughness are known to be strongly related to biofouling. This is because they determine the interaction between the membrane and the foulants [71, 72].

- Surface Hydrophilicity

Most of the commercial membranes are made from hydrophobic polymers with high thermal, chemical and mechanical stability. Since they are hydrophobic, they are susceptible to adsorption by biofoulants, which are essentially hydrophobic, as well. Fane and Fell and Hilal and coworkers reported that membranes with hydrophilic surfaces are less susceptible to fouling. This means that making the surface of the membrane more hydrophilic is a goal to make the surface more biofouling resistant [41, 73]. A hydrophilic surface forms a thin layer of water on top of the surface due to hydrogen bonding. This layer plays an important role in preventing or reducing the adsorption of biofoulants [72].

- Surface Charge

The charge of the membranes is an important factor in biofouling resistance, since most of the foulants are charged. It is preferred to use a membrane with the same electrical charge as the foulants. Electrostatic repulsion forces between the solute and the

membrane, when they carry the same charge, prevent the solute deposition on the membrane, which, in turn, reduce fouling [74, 75]. Ulbricht found out that if the surface is negatively charged, it would generate better results with the separation of proteins around neutral pH [76]. This is because the proteins are negatively charged, as well. Furthermore, most of the colloidal particles, such as natural organic matter (NOMs), that are attached to the surface are negatively charged [49]. Similar to the negatively charged surface, the positively charged membrane surfaces exhibited electrochemical repulsion against positively charged foulants [72, 77].

- Surface Roughness

It has been found that there is a strong correlation between fouling and the surface roughness of the RO and the nano filtration (NF) membranes [78]. A higher roughness increases the total surface area that foulants could be attached to, and the ridge-valley structure favors the accumulation of foulants on the surface. As a consequence, the rougher the membrane surface, the more it will be favorable for foulants to attach to the membrane surface [79]. In general, membrane development is currently focused on the reduction of membrane surface roughness.

The goal of membrane surface modification is, therefore, to enhance surface hydrophilicity, reduce surface roughness and to introduce charged/bactericide groups on the membrane surface to prevent biofouling [71-74]. Some of the commonly used surface modification techniques are ultraviolet (UV) and redox-initiated surface grafting of the hydrophilic compounds, low-temperature plasma treatment, physical coating/adsorption of a thin layer of hydrophilic polymer on the membrane surface, chemical reactions on

the membrane surface, and surface modification of the polymer membranes with nanoparticles [72]. Figure 2.5 shows some antifouling mechanisms.

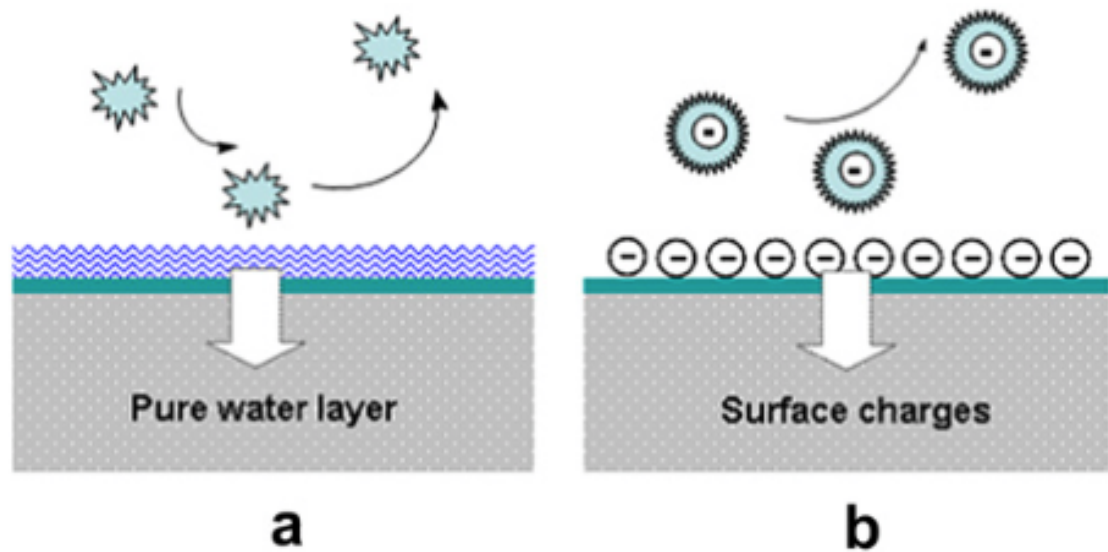


Figure 2.5 Schematic diagrams of antifouling mechanisms: (a) pure water layer; (b) electrostatic repulsion [80].

2.5 Utilizing Poly (vinyl alcohol) in RO Applications

Poly (vinyl alcohol) (PVA) is a water-soluble biodegradable polymer with intrinsic hydrophilicity, good film-forming properties and outstanding thermal, mechanical and chemical stability. PVA has been one of the best polymers to fabricate membranes with high chemical stability, good Chlorine tolerance and excellent fouling resistance. Consequently, PVA has been used broadly to synthesize membranes for separation and pressure driven processes such as microfiltration, ultrafiltration, reverse osmosis and pervaporation [81-87]. Swelling of PVA membranes in aqueous medium is observed due to its very high hydrophilicity, which makes it an open structure that affects the membrane performance, predominantly the membrane solute rejection. Therefore, crosslinking of PVA is needed to balance the hydrophilic-hydrophobic properties of such membranes [88-90]. PVA may be crosslinked by using multifunctional compounds, such as dicarboxylic acids, dialdehydes and dianhydrides, which could react with the –OH groups of PVA [91-96]. The highly polar nature of PVA mitigates fouling greatly, since non-polar surfaces enhance adsorption of water contaminants due to hydrophobic interactions [82].

PVA has been used as a surface coating agent by many researchers. Hachisuka and Ikeda coated PVA onto polyamide RO membrane to improve the antifouling properties [97]. The hydrophilicity and biofouling resistance of the membrane surface improved greatly [80]. Kim and Lee coated RO membranes with PVA to decrease surface charge and surface roughness. The resultant membrane showed great fouling resistance [80, 98]. Rana and coworkers investigated a redox system mediated rapid surface modification of polyamide thin film composite (TFC) reverse osmosis (RO) membrane using Cerium

(IV)/polyvinyl alcohol (PVA) for the improvement of both antifouling and Chlorine resistant properties. The modified membranes exhibited much enhanced antifouling property and Chlorine resistance during desalination of water in the presence of scale forming salt and protein [99]. Rajaeian et al. examined a series of thin film nanocomposite membranes developed by coating a surface-modified porous poly (vinylidene fluoride) (PVDF) support with PVA doped solution containing carboxylated TiO₂ nanoparticles. The produced membrane had improved performance including solute rejection, antifouling properties and flux recovery ratio [100]. Liu et al. reported the chemical linkage of PVA on the surface of a commercial PA TFC membrane through a single step of grafting with potassium persulfate as thermal dissociation initiator. They found that the membrane surface became smoother, more hydrophilic and less charged with increased salt rejection. Furthermore, the surface had a slightly declined water flux, an improved Chlorine and fouling resistances to the model foulants of bovine serum albumin (BSA), sodium dodecyl sulfate (SDS) and dodecyltrimethyl ammonium bromide (DTAB) [69]. Bano et al. prepared a composite membrane by coating a thin layer of sodium alginate (NaAlg)/PVA blend on polysulfone support, then cross linked it in two steps with calcium chloride and glutaraldehyde, respectively. The produced membrane had enhanced flux and Chlorine resistance [101]. Nikkola et al. prepared PVA coatings on commercial TFC PA membranes to enhance anti-biofouling performance. The PVA coating was modified with cationic polyhexamethylene guanidine hydrochloride (PHMG) polymer to obtain antimicrobial performance. All coated membranes exhibited more hydrophilic and lower surface roughness. The coated membranes showed anti-microbial property against *Escherichia coli* (*E. coli*) and *Bacillus subtilis* (*B. subtilis*) [102].

Mohammed and others prepared thin film multi-layers membranes composed of PVA, cellulose acetate and PEG. They were prepared using interfacial polymerization and the PVA layer was crosslinked by a varying maleic acid concentrations. Their membrane had smoother surface but low permeability [103].

CHAPTER 3

OBJECTIVES AND METHODOLOGY

3.1 Research Objectives

It has been shown from the literature review that developing an anti-fouling, highly selective and highly permeable reverse osmosis membrane is a necessity. To develop such a membrane, one should improve the hydrophilicity of the membrane surface, reduce its roughness and make the surface biofouling resistant. The overall goal of this research is the development of high performance, economical reverse osmosis membranes materials with improved permeability, high salt rejection and superior biofouling and Chlorine resistance. The specific objectives are as follows:

- To synthesize novel PVA RO membranes with chemical and mechanical stability.

As has been discussed in the literature review, PVA has a great potential in RO applications. Nevertheless, the utilization of PVA as an active RO separation layer without a substrate has been limited due to PVA well known drawbacks, such as swelling and rupture under very high pressure. One objective of this research is to try to mitigate these downsides through proper crosslinking and mechanical strength enhancement.

- To incorporate various fillers within the PVA membrane matrix.

Various nano or micro fillers could be incorporated within the membrane matrix to further enhance the overall RO performance of the PVA membrane. These fillers include Pluronic F-127, MWCNTs, ZnO-NPs, Vanillin, Gum Arabic, hyperbranched polyethyleneimine and various crosslinkers.

- To characterize and analyze the newly synthesized membranes.

Excessive characterization is needed after synthesizing the membranes to make sure that the synthesis parameters and conditions are in accord with the synthesized membrane properties. For example, chemical identification after synthesis is very important to make sure that the reactants have been fully reacted.

- To evaluate the overall reverse osmosis performance of the newly synthesized membranes.

Lastly, those newly synthesized membranes will be evaluated and their performance will be assessed. Permeation tests will be carried out to determine the permeability and the selectivity of the membranes. In addition, the membrane Chlorine and biofouling resistance will be evaluated. Those membranes will be tested in realistic conditions with the feed water resembling seawater and the operating pressure will be similar to that used in actual reverse osmosis desalination plants.

3.2 Methodology

3.2.1 Materials

Analytical grade PVA ($M_w=89000$), bisphenol A diglycidyl ether (DGEBA) (crosslinker), Pluronic F-127 (average molecular weight: 12.6 kDa), dimethyl sulphoxide (DMSO), Sodium hypochlorite (NaClO), Vanillin ($\text{C}_8\text{H}_8\text{O}_3$), Gum Arabic ($M_w=250,000$), hyperbranched polyethyleneimine (HPEI) and maleic acid ($\text{C}_4\text{H}_4\text{O}_4$; MA > 99%) were acquired from Sigma Aldrich (St Louis, MO, USA). MWCNTs (>99%) produced by chemical vapor deposition followed by HCl mineralization, with 12 nm

diameter and 10 μm length, were purchased from Aldrich. Zinc Oxide nanoparticles (ZnO-NPs) with 99.7% purity were obtained from Inframat Advance Materials (USA). All chemicals were used without further purification.

3.2.2 Permeation Studies

A dead-end filtration system (Model HP4750 Stirred Cell, Sterlitech Corp., Kent, WA), shown in Figure 3.1, made of stainless steel 316 to ensure the chemical stability, with 300 ml of feed, was used for all the permeation tests. It has an active filtration area of 14.6 cm^2 . The permeation cell can withstand a maximum pressure rating of 1000 psig (69 bar) and has been widely used and described for various membrane filtration studies [31]. Nitrogen gas was compressed in the solution into the cell.

Water flux through the membrane could be calculated using the following equation [99]:

$$J = \frac{V}{A t},$$

where J is the water flux ($\text{L}/(\text{m}^2 \cdot \text{h})$) or simply LMH, V is the volume of water permeated (L), A is the membrane active area (m^2), and t is permeate sampling time (h). Salt concentration before and after permeation is measured using a salinity meter.

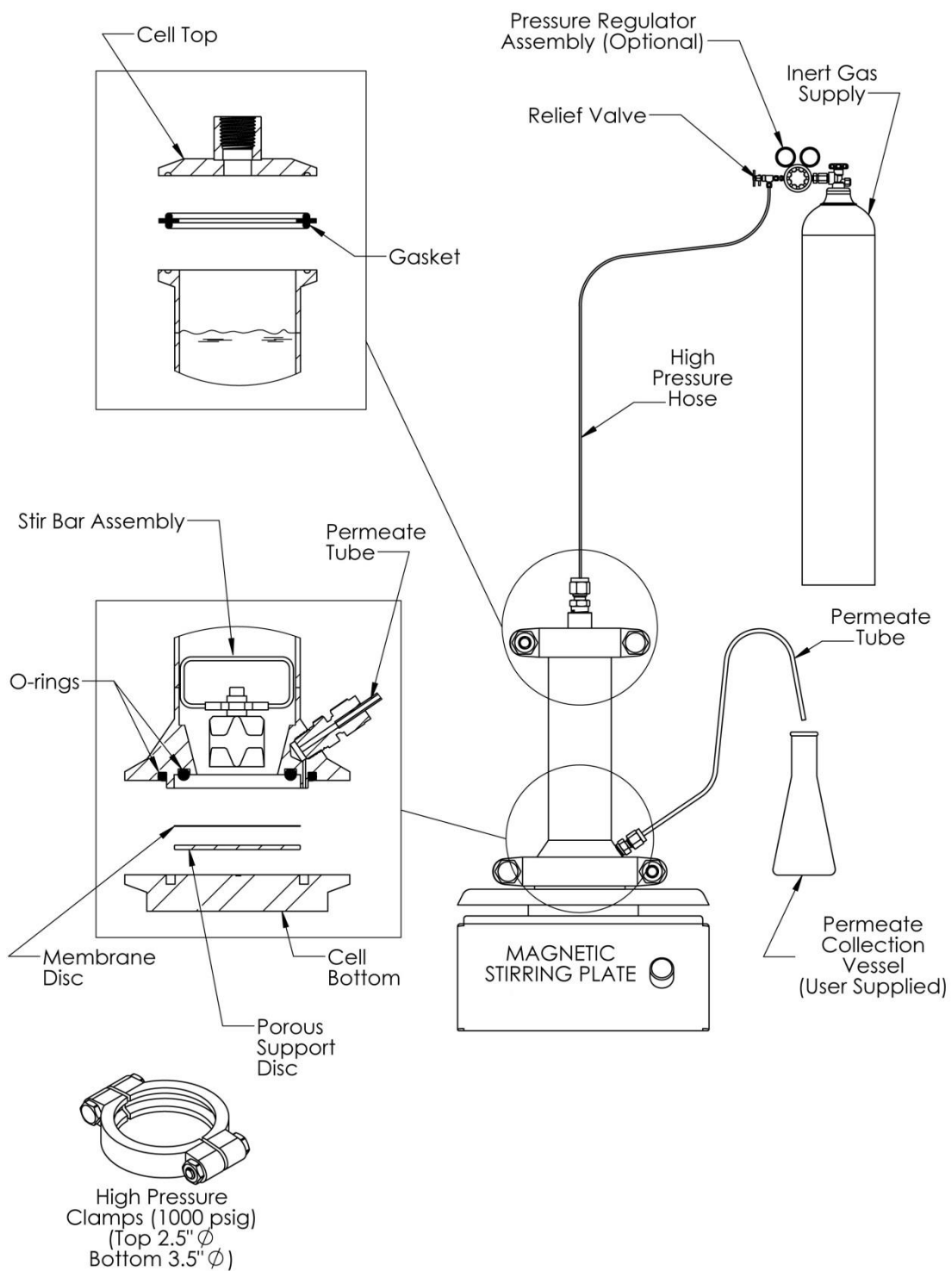


Figure 3.1 Manufacturer supplied schematic diagram of the permeation unit.

3.2.3 Chlorine Resistance Testing

It has been reported that there is an equivalent resultant effect when comparing high concentration Chlorine exposure for a short period of time to low concentration Chlorine exposure for a longer period of time [104, 105]. Thus, it is more convenient to expose the membrane surface to a high concentration of Chlorine for a short period of time for Chlorine resistance testing in the lab. Chlorinated solution (2000 mg/L) was prepared by diluting a commercial NaClO solution (free Chlorine content of 10 wt%) with distilled water. The pH of the prepared hypochlorite solution was adjusted to 4.0 by HCl (0.1 M) to make it more oxidative and harsh environment [106]. To perform the Chlorination experiments, water flux and salt rejection performance of the membranes were evaluated using 2000 mg/L NaCl solution and after that, the membranes were taken out of the test cells, washed with distilled water and exposed to 2000 mg/L hypochlorite solution for 2 h at pH=4.0 and 25° C. After exposure, the Chlorinated membranes were washed thoroughly with distilled water and re-loaded in the test cells. The performance of the membranes was evaluated again with 2000 mg/L NaCl aqueous solution.

3.2.4 Biofouling Resistance Testing

Antibacterial test was carried out using *Escherichia coli* by JIS L 1902–2002 methodology. Broth (30 mL) was arranged in conical flasks. All flasks were autoclaved at 125 °C having a pressure of 15 psi for 30 min. After autoclaving, alpha E. coli strain (100µl) was protected in the flasks. The unmodified and modified membranes were added in each conical flask. All flasks were nurtured at 35 °C in an incubator for 24 h. After nurturing, 600 nm optical density (OD) was observed by a spectrophotometer.

Diffusion Inhibition Zone (DIZ) method was also conducted to examine the antimicrobial performance of the modified membranes. DIZ test was performed following the procedure of Clinical Laboratory Standards Institute (CLSI) document M2-A9 26:1 [107]. 100 μL bacterial inoculums were spread on the agar plates. Modified membranes were then placed in the plates and incubated for 24 hours maintaining the temperature at 30°C for the cultivation of model bacteria *Bacillus Subtilis*. The diffusion inhibition zones developed around the modified membranes were defined visually [102].

3.2.5 Characterization Techniques

3.2.3.1 Fourier transform infrared spectroscopy (FTIR)

An IR Prestige-21 (Shimadzu) using attenuated total reflectance (ATR) accessory equipped with Zinc Selenide (ZnSe) crystal was used to obtain FTIR spectra of the composite membrane samples. Before each sample scan, an air background of the instrument was run. The frequency range was from 4000-600 cm^{-1} at a resolution of 4.0 cm^{-1} and an average of 120 scans per spectrum were reported.

3.2.3.2 Scanning electron microscopy (SEM)

A Scanning Electron Microscope (S-3400N Hitachi, USA) was used to obtain SEM images of the synthesized membranes. The SEM was operated under low vacuum mode to characterize the samples. Sample gold sputtering was performed for 120 s before it is placed into the SEM to make sure no surface charging occurs. Gold sputtering was performed using Denton Vacuum Sputtering Automatico Desk IV.

3.2.3.3 Atomic force microscopy (AFM)

AFM imaging and analysis (Digital Instruments, Santa Barbara, CA, US) were utilized to characterize membrane surface morphological structure and to determine membrane's quantitative surface roughness, respectively. Topographical images were attained using standard tapping mode. A cantilever oscillated sinusoidally at 350 kHz resonant frequency, and briefly contacted the sample surface at the down stroke of each sinusoidal cycle. A user-established set point force was fixed so that the sample surface was minimally deformed and used as a feedback control. Scanned images were taken at 512 x 512 pixel resolution. Root mean square (RMS) roughness values (R_q) were obtained from AFM images that were taken from the average of the values measured from random areas. Membrane surface morphology was expressed in terms of several roughness parameters, such as mean roughness (R_a). It is calculated by the following equation [108, 109]:

$$R_a = \frac{1}{n} \sum_{i=1}^n |z_i|$$

where z_i is the height or depth of the i^{th} highest or lowest deviation and n is the number of discrete profile deviations. Root-mean-square surface roughness (R_q) is another roughness parameter and is defined as the root-mean-square (RMS) of the deviations in height from the profile mean and it is calculated by [109]:

$$R_q = \sqrt{\frac{1}{n} \sum_{i=1}^n z_i^2}$$

3.2.3.4 Contact angle measurements

A Goniometer (Digidrop, KSV Instruments) was used to calculate sessile drop contact angles of the reverse osmosis membranes. The equilibrium value was average of right and left angles of the drop that are calculated from the software fitting. The reported data is the average of three measurements for each membrane sample. All angles were measured upon immediate release of the drops to avoid errors due to evaporation.

3.2.3.5 Mechanical Properties

An Instron 5567 Tensile Testing Machine fitted with a 10 kN load cell was used to calculate the mechanical properties of the fabricated membranes. Those mechanical properties include the stress strain curves, ultimate tensile strength, elongation at break and the Young's modulus. The shape of the membrane sample was used as per ASTM D-638 standard with gauge length and width of 50 and 10 mm, respectively. Three specimens were tested for each membrane and the average value was recorded at a crosshead speed of 10 mm/min. The thickness of the membrane samples was measured using a micro-caliper and maintained at 0.1 mm for all of the tested samples. All specimens were drawn at ambient temperature and the Young's modulus was calculated in triplicate using stress-strain curves, which were instantaneously recorded by a computer.

3.2.3.6 X-ray diffraction Measurements (XRD)

An X'pert PRO Diffractometer (PANalytical) was used to analyze the structure of the synthesized composite membranes. The instrument uses monochromatized CuK α 1 radiation with wavelength of 1.540 Å from a fixed source operated at voltage 40 kV and

current 40 mA. The scanning range was from 4° to 80°.

CHAPTER 4

Highly Improved Reverse Osmosis Performance of Novel PVA/DGEBA Cross-linked Membranes by Incorporation of Pluronic F-127 and MWCNTs For Water Desalination

4.1 Introduction

Availability of clean water is becoming increasingly scarce in many parts of the world. Approximately, 2.3 billion people live in areas that are water-stressed and around one billion people worldwide are suffering from the lack of clean water, according to the World Health Organization [15]. Another factor that is significantly increasing the demand for clean water is the global population increase, now roughly around 80 million per year [1-4, 12, 23, 42, 80, 110, 111].

Although most of earth's surface is water, only 2.5% of the water mass is fresh water and a small fraction of the available fresh water is easily reachable. This is because most of the fresh water is stored as glaciers in the frozen form or collected in water reservoirs deep underground [3, 5, 110]. Therefore, tremendous effort is required to extract and provide clean, fresh water for the world population. One route to address this problem is to use salt water from oceans after subjecting it to a desalination process. Although desalination processes are energy intensive and costly, recent developments have opened up new opportunities for reducing the energy demands for desalination.

Recently, Reverse Osmosis (RO) has emerged as one of the predominant desalination technologies surpassing conventional thermal technologies, like Multi-Stage Flashing (MSF) and Multi-Effect Distillation (MED) [6].

The RO approach is expected to continue to maintain its leadership in the near future. RO attracts interests commercially due to its continuous process improvements and significant cost reductions. These improvements include developments in new membrane materials, modular design, overall process design, water pre-treatment, energy recovery, and energy consumption reduction [18, 22, 51, 112].

In this research, a novel crosslinked PVA reverse osmosis membranes incorporated with Pluronic F-127 and MWCNTs were synthesized using dissolution casting.

Poly (vinyl alcohol) (PVA) is a water-soluble biodegradable polymer with intrinsic hydrophilicity, good film-forming properties and outstanding thermal, mechanical and chemical stability. PVA has been one of the best polymers to fabricate membranes with high chemical stability, good Chlorine tolerance and excellent fouling resistance. Consequently, PVA has been used broadly to synthesize membranes for separation and pressure driven processes such as microfiltration, ultrafiltration, reverse osmosis and pervaporation [81-87]. Swelling of PVA membranes in aqueous medium is observed due to its very high hydrophilicity, which makes it an open structure that affects the membrane performance, predominantly the membrane solute rejection. Therefore, crosslinking of PVA is needed to balance the hydrophilic-hydrophobic properties of such membranes [88-90]. PVA may be crosslinked by using multifunctional compounds, such as dicarboxylic acids, dialdehydes and dianhydrides, which could react with the -OH groups of PVA [91-96].

Polyethylene oxide–polypropylene oxide–polyethylene oxide (PEO–PPO–PEO) triblock copolymers are amphiphilic copolymers comprising hydrophilic PEO sections and

hydrophobic PPO sections. These copolymers are known as Poloxamers or Pluronics. Pluronic F-127 has high molecular weight (M_w 12,600), proper hydrophilic/lipophilic balance value (HLB = 22), and high extractability into aqueous phase compared to other Poloxamers or Pluronics [113, 114]. It has been reported in literature that the incorporation of Pluronic F-127 into PVA thin films enhances the separation performance of membranes [114, 115]. Furthermore, it is documented that amphiphilic copolymers can alter the diffusion rate of the coagulation solution (mainly water), which increases the permeation flux of water through the membrane [114, 116-118].

Carbon nanotubes (CNTs) have caught the attention of researchers in chemistry and material science due to their unique properties such as low density, high aspect ratio, high chemical, thermal, and mechanical strengths and remarkable electrical and optical properties [119-122]. It has been shown in literature that the incorporation of CNTs into polymer membrane matrix made it possible to manipulate membrane properties especially through modifying nanotubes resulting in improved permeability and solute rejection, decreased fouling tendency, improved hydrophilicity, increased tensile strength and electrical conductivity along with controlled pore size, surface chemistry and polymer crystallinity [123-128].

Many researchers have used PVA as a hydrophilic modifier or as a coating on polymeric or ceramic surfaces for many separation applications [69, 81, 100, 101, 111, 129-150]. Nevertheless, to the best of our knowledge, no study has been presented on the use of crosslinked PVA as an active RO separation layer under typical RO pressure without polymeric or ceramic substrates. The crosslinked PVA has been incorporated with Pluronic F-127 and Multiwall Carbon Nanotubes (MWCNTs) to counteract common

PVA downsides, mainly swelling and rupture under high pressure. As mentioned before, here we used crosslinked PVA membranes incorporated with Pluronic F-127 and MWCNTs for RO. The newly synthesized membranes with crosslinked PVA were then characterized and analyzed using various techniques like attenuated total reflection Fourier transform infrared spectroscopy (ATR-FTIR), contact angle measurements, X-ray diffraction (XRD), scanning electron microscopy (SEM), atomic force microscopy (AFM) and mechanical testing. The actual reverse osmosis performance of the membranes, including permeation testing, salt rejection and Chlorine resistance, was analyzed using a dead-end RO permeation unit.

4.2 Experimental Procedure

4.2.1 Materials

Analytical grade PVA ($M_w=89000$), bisphenol A diglycidyl ether (DGEBA) (crosslinker), Pluronic F-127 (average molecular weight: 12.6 kDa), dimethyl sulphoxide (DMSO) and sodium hypochlorite (NaClO) were acquired from Sigma Aldrich (St Louis, MO, USA). MWCNTs (>99%) produced by chemical vapor deposition followed by HCl mineralization, with 12 nm diameter and 10 μm length, were purchased from Aldrich. All chemicals were used without further purification.

4.2.2 Membrane Casting

4.2.2.1 Crosslinking of PVA with DGEBA

Various weight percentages of DGEBA crosslinker, as shown in Table 4.1, were mixed into PVA solutions, where DMSO was used as a solvent with a 17:83 solute/solvent

weight percent ratio. The mixing was performed at 70° C for 2 hours with continuous stirring until a homogenous, transparent solution was produced. Utilizing the dissolution casting method, the solution was then transferred slowly into identical Petri dishes with identical amounts of the solution to insure uniformity. Petri dishes were then heated to 65°C in a controlled evaporation environment to assure uniform film thicknesses of 0.1 mm, measured by a screw gauge. After complete evaporation, the thin film membranes were removed from the Petri dishes with the aid of sharp blades. Five membranes were synthesized from each concentration for testing. The resultant dense membranes were examined for swelling, permeation and salt rejection to come up with the optimal crosslinker weight percent. As will be demonstrated in the results section, the 0.16 wt% of DGEBA provided the optimum membrane properties, thus, the weight percent of 0.16 was used for further modifications.

4.2.2.2 Incorporation of Pluronic F127 into the crosslinked PVA membranes

Various weight percentages of Pluronic F127, as shown in Table 4.1, were blended into the solutions of PVA and 0.16 wt% of DGEBA. The solution preparation and the film casting method followed the procedure mentioned in the previous section. The resultant composite membranes with different weight percentages of Pluronic F127 were characterized and evaluated. The overall evaluation of the Pluronic F127 membranes as will be detailed later on, showed that 6 wt% of Pluronic F127 was the optimal percentage and was used for further modifications. Figure 4.1 shows a scheme of the chemical reaction.

4.2.2.3 *Inclusion of MWCNTs within the Pluronic F127 modified PVA membranes*

Five weight percentages of MWCNTs, shown in Table 4.1, were incorporated within the solution of crosslinked PVA and 6 wt% of Pluronic F127 to synthesize the thin film nano composite membranes. To assure appropriate dispersion of MWCNTs within the solution and to avoid agglomeration of the nano tubes, the solution containing PVA, DGEBA, Pluronic F127 and the MWCNTs was sonicated at 70° C for 2 hours. After sonication, the membrane casting followed the abovementioned dissolution casting method.

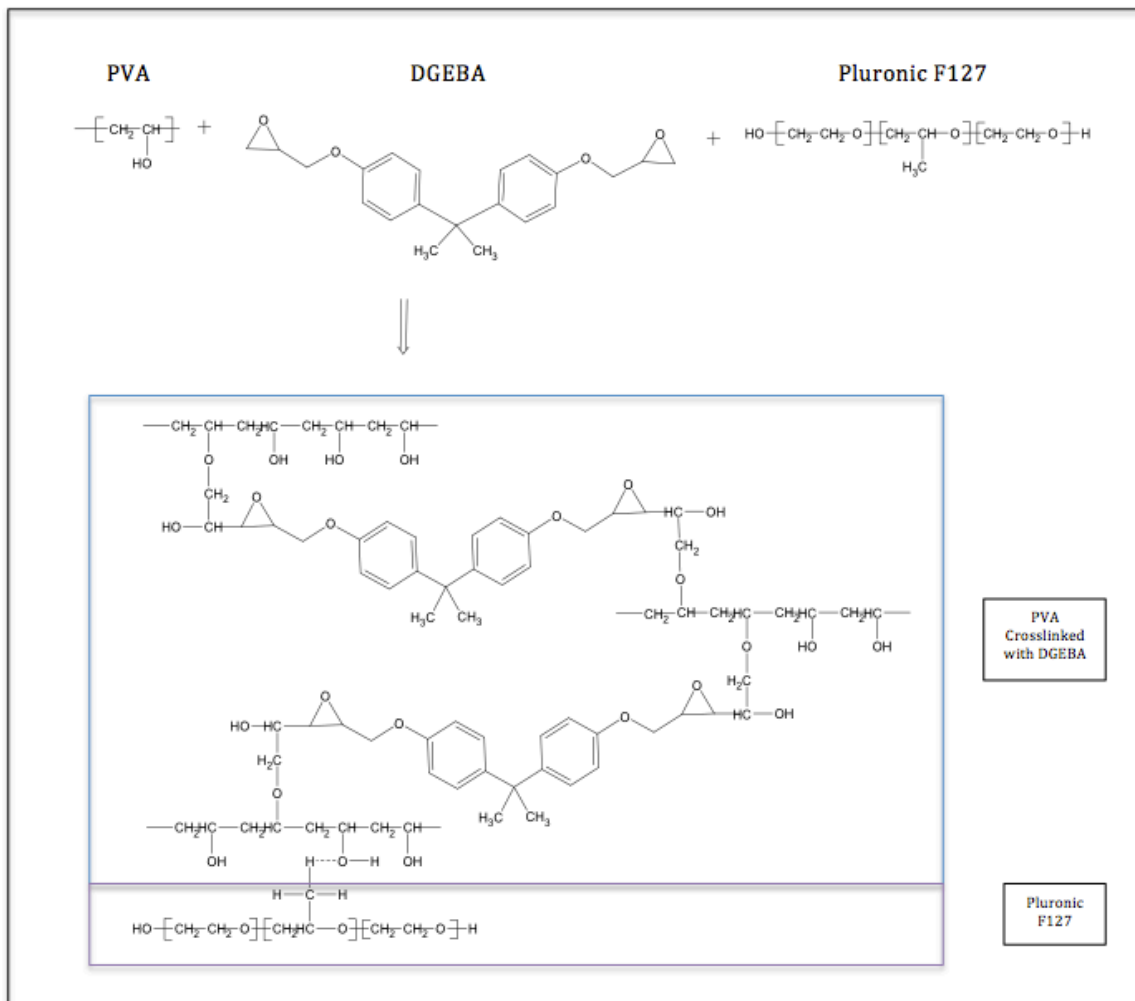


Figure 4.1 Schematic diagram of the crosslinking of PVA with DGEBA and the intermolecular hydrogen bonding with Pluronic F127.

Table 4.1 Weight percentages of DGEBA, Pluronic F127 and MWCNTs in PVA solution.

	Weight Percentages (wt%)									
DGEBA	0.02	0.04	0.06	0.08	0.1	0.12	0.14	0.16	0.18	0.2
Pluronic F127*	2	4	6	8	10					
MWCNTs**	0.02	0.04	0.06	0.08	0.1					
*with 0.16 wt% DGEBA.										
**with 0.16 wt% DGEBA and 6 wt% Pluronic F127										

4.2.3 Membranes Characterization

4.2.3.1 Fourier Transform Infrared Spectroscopy (FTIR)

An IR Prestige-21 (Shimadzu) using attenuated total reflectance (ATR) accessory equipped with zinc selenide (ZnSe) crystal was used to obtain FTIR spectra of the composite membrane samples. Before each sample scan, an air background of the instrument was run. The frequency range was from 4000-600 cm^{-1} at a resolution of 4.0 cm^{-1} and average of 120 scans per spectrum were reported.

4.2.3.2 Contact Angle Measurements

A Goniometer (Digidrop, KSV Instruments) was used to calculate sessile drop contact angle of the reverse osmosis membranes. The equilibrium value was average of right and

left angles of the drop that are calculated from the software fitting. The reported data was the average of three measurements from different locations for each membrane sample. All angles were measured upon immediate release of the drops to avoid errors due to evaporation.

4.2.3.3 X-Ray Diffraction Measurements

An X'pert PRO Diffractometer (PANalytical) was used to characterize the structure of the synthesized composite membranes. The instrument uses monochromatized CuK α 1 radiation with wavelength of 1.540 Å from a fixed source operated at voltage 40 kV and current 40 mA. The scanning range was from 4° to 80°.

4.2.3.4 Scanning Electron Microscopy (SEM)

A Scanning Electron Microscope (S-3400N Hitachi, USA) was used to attain SEM micrographs of the fabricated membranes. The SEM was operated under low vacuum mode to analyze the samples. Samples were gold sputtered for 120 s before they were placed into the SEM to make sure no surface charging occurs. Gold sputtering was performed using Denton Vacuum Sputtering Automatico Desk IV.

4.2.3.5 Atomic Force microscopy (AFM)

AFM imaging and analysis (Digital Instruments, Santa Barbara, CA, US) were utilized to characterize membrane surface morphological structures and to determine membrane's quantitative surface roughness, respectively. Topographical images were taken using standard tapping mode. A cantilever oscillated sinusoidally at 350 kHz resonant frequency, and briefly contacted the sample surface at the down stroke of each sinusoidal

cycle. A user-established set point force was fixed so that the sample surface was minimally deformed and used as a feedback control. Scanned images were taken at 512 x 512 pixel resolution. The values of root mean square (RMS) roughness were extracted from AFM images through the calculation of the average of the values measured in random areas. The membrane surface morphology was expressed in terms of various roughness parameters, like mean roughness (R_a). It is calculated by the following equation [108, 109]:

$$R_a = \frac{1}{n} \sum_{i=1}^n |z_i|$$

where z_i is the height or depth of the i th highest or lowest deviation and n is the number of discrete profile deviations. Root-mean-square surface roughness (R_q) is defined as the root-mean-square (RMS) of the deviations in height from the profile mean and it is calculated by [109]:

$$R_q = \sqrt{\frac{1}{n} \sum_{i=1}^n z_i^2}$$

4.2.3.6 *Mechanical Testing*

Universal Tensile Testing Machine Instron 5567 fitted with a 10 kN load cell was used to calculate the mechanical properties of the fabricated membranes. Those mechanical properties include the stress strain curves, ultimate tensile strength, elongation at break and the Young's modulus. The shape of the membrane sample was used as per ASTM D-638 standard with gauge length and width of 50 and 10 mm, respectively. Three

specimens were tested for each membrane and the average value was recorded at a crosshead speed of 10 mm/min. The thickness of the membrane samples was measured using a micro-caliper and maintained at 0.1 mm for all of the tested samples. All specimens were drawn at ambient temperature and the Young's modulus was calculated in triplicate using stress-strain curves, which were instantaneously recorded by a computer.

4.2.3.7 Permeation and Salt Rejection Testing

A dead-end filtration system made of stainless steel 316 (HP4750 Stirred Cell, Sterlitech Corp., Kent, WA, US), as shown in Figure 4.2, was used to evaluate the permeation performance and the salt rejection percentages of the newly synthesized membranes. The active surface area of the membrane inside the permeation cell is 14.6 cm². The feed solution was prepared using 3.28 wt% of commercially available natural sea salt and the pressure was kept at 800 psi (55.2 bar). The membranes were tested in the RO cell while the permeation flux of the membrane was calculated by determining the volume of the permeated water through the membrane over a certain period of time. It was calculated by the following Equation:

$$F \left(\frac{L}{m^2h} \right) = \frac{V(L)}{A(m^2) \times t(h)}$$

where (F) is the permeate flux through the membranes, which is the permeate volume (V) per effective area of the membrane (A) per unit time (t). Frequently, water flux unit is abbreviated as (LMH). Salt Rejection of the membranes was determined by a salinity meter (Traceble VWR, ISO 17025 Accredited). The reported RO experimental results were the average values obtained from at least three membrane samples prepared at

different times, and the error bars showed the standard deviation.

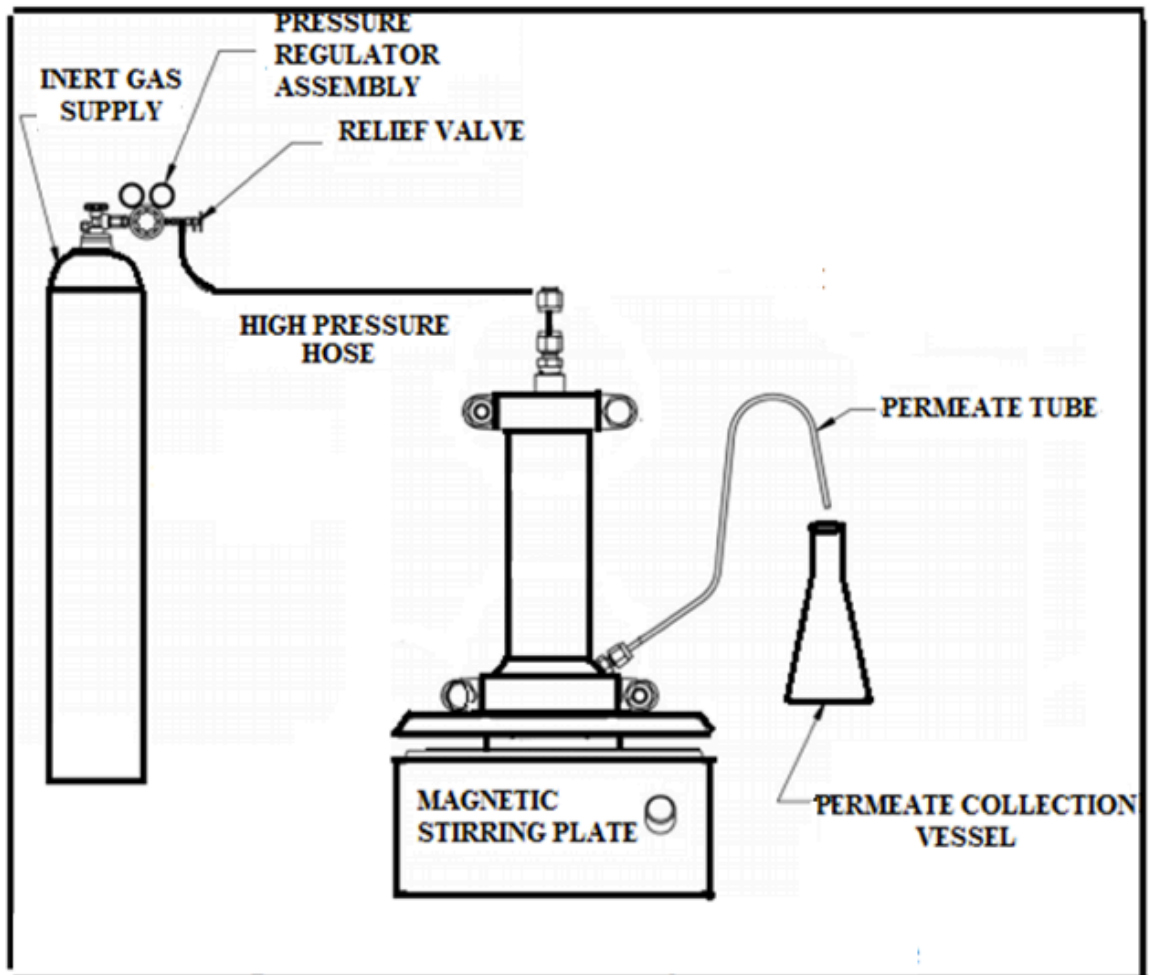


Figure 4.2 Dead-end filtration system for RO membranes.

4.2.3.8 *Chlorine Resistance Testing*

It has been reported that there is an equivalent resultant effect when comparing high concentration Chlorine exposure for a short period of time to low concentration Chlorine exposure for a longer period of time [104, 105]. Thus, it is more convenient to expose the membrane surface to a high concentration of Chlorine for a short period of time for Chlorine resistance testing. Chlorinated solution (2000 mg/L) was prepared by diluting a commercial NaClO solution (free Chlorine content of 10 wt%) with distilled water. The pH of the prepared hypochlorite solution was adjusted to 4.0 by HCl (0.1 M) to make it more oxidative and harsh environment [106]. To perform the Chlorination experiments, water flux and salt rejection performance of the membranes were evaluated using 2000 mg/L NaCl solution and after that, the membranes were taken out of the test cells, washed with distilled water and exposed to 2000 mg/L hypochlorite solution for 2 h at pH=4.0 and 25° C. After exposure, the Chlorinated membranes were washed thoroughly with distilled water and re-loaded in the test cells. The performance of the membranes was evaluated again with 2000 mg/L NaCl aqueous solution.

4.2.3.9 *Biofouling Resistance Testing*

Antibacterial test was carried out using *Escherichia coli* by JIS L 1902–2002 methodology. Broth (30 mL) was arranged in conical flasks. All flasks were autoclaved at 125 °C having a pressure of 15 psi for 30 min. After autoclaving DH5 alpha *E. coli* strain (100µl) was protected in the flasks. The unmodified and modified membranes were added in each conical flask. All flasks were nurtured at 35 °C in an incubator for 24 h. After nurturing, 600 nm optical density (OD) was observed by a spectrophotometer.

4.3 Results and Discussion

4.3.1 FTIR analysis

The FTIR analysis is carried out to confirm the proposed interactions between PVA and MWCNTs in the presence of constant amount of crosslinker (DGEBA), as shown in Figure 4.3. The strong bands at 3303 cm^{-1} are ascribed to hydrogen bonded -OH groups present in PVA [151]. The band at 1236 and 1082 cm^{-1} are characteristic for C-O-C cyclic and acyclic groups of epoxy present in DGEBA, respectively [152]. In addition, the band at 838 cm^{-1} confirmed the characteristic asymmetric vibration of epoxide ring [153]. The band at 1141 cm^{-1} in all spectra ascertained the existence of C-O bond in PVA. The band of C=C stretching at 1634 cm^{-1} confirmed the presence of pristine MWCNTs [154].

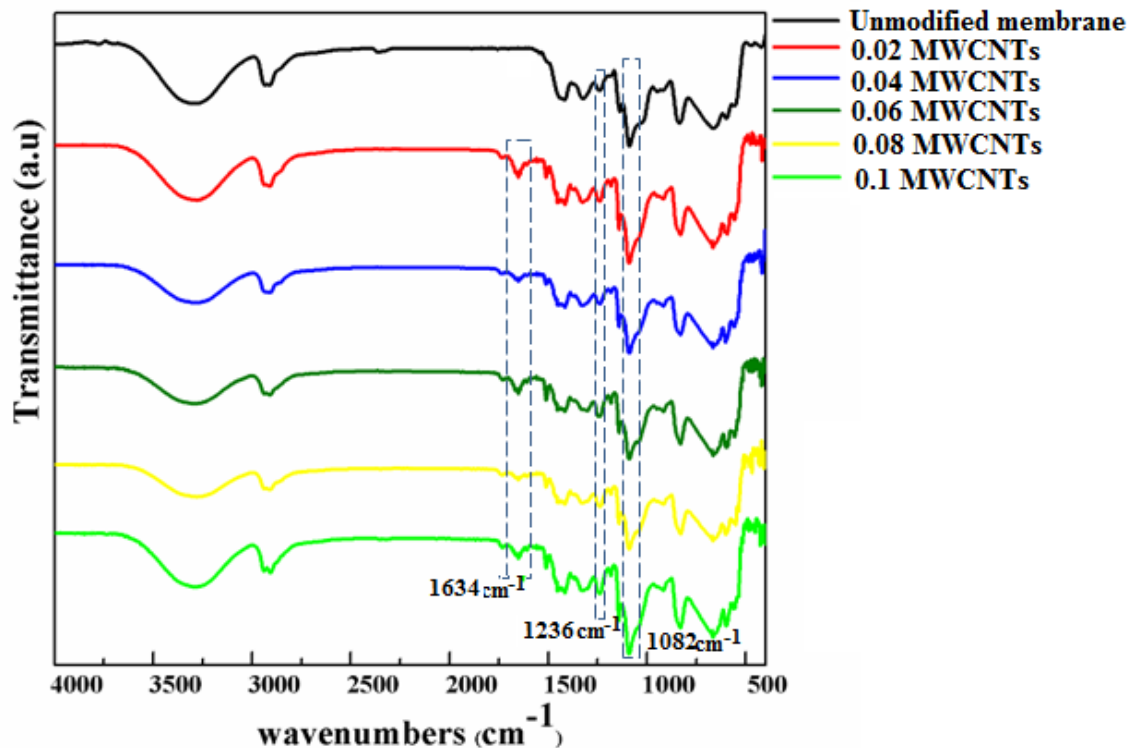


Figure 4.3 ATR-FTIR spectra of pure PVA and MWCNTs modified PVA membranes.

4.3.2 Contact Angle Analysis

The wettability of a solid surface is quantified by contact angle measurements. Typically, the surface is considered hydrophilic if the water contact angle is less than 90° . If it is more, the surface is hydrophobic [155]. Most of the commercial membranes are made from hydrophobic polymers with high thermal, chemical and mechanical stability. Since they are hydrophobic, they are susceptible to adsorption by biofoulants. It has been reported that membranes with hydrophilic surfaces are less vulnerable to fouling. This means that making the surface of the membrane more hydrophilic is a goal to make the surface more biofouling resistant and to enhance permeability [41, 73]. A hydrophilic

surface forms a thin layer of water on top of the surface due to hydrogen bonding. This layer plays an important role in preventing or reducing the adsorption of biofoulants and it also enhances the permeability of the membrane [72].

4.3.2.1 Effect of Mixing Pluronic F127 on Hydrophilicity

Figure 4.4 demonstrates the effect of modifying PVA with Pluronic F-127 on the hydrophilicity of the membrane surface. It is clear that Pluronic F-127 has a strong positive effect on the hydrophilicity of the membrane. Some researchers reported that the improvement in hydrophilicity is due to the pores formation, which is a characteristic feature of Pluronic F-127 [114, 156-158]. The hydrophilicity enhancement of the synthesized crosslinked PVA membranes was optimal with mixing 6 wt% of Pluronic F127. When more than 6 wt% was incorporated, the hydrophilicity started to decrease. It has been reported that the hydrophilicity reversal when additional amounts of Pluronic F-127 have been incorporated is due to the fact that the hydrophilic PEO segments of the excess amounts start to self-assemble themselves and adhere to the hydrophilic membrane surface. As a result, the hydrophobic PPO segments will form loops away from the surface facing the water [159]. Therefore, the overall hydrophilicity starts to decrease again at some point. Nevertheless, the hydrophilicity of the modified membranes was enhanced compared to the pristine PVA membrane, even after the reversal of hydrophilicity when more than 6 wt% Pluronic F-127 was incorporated.

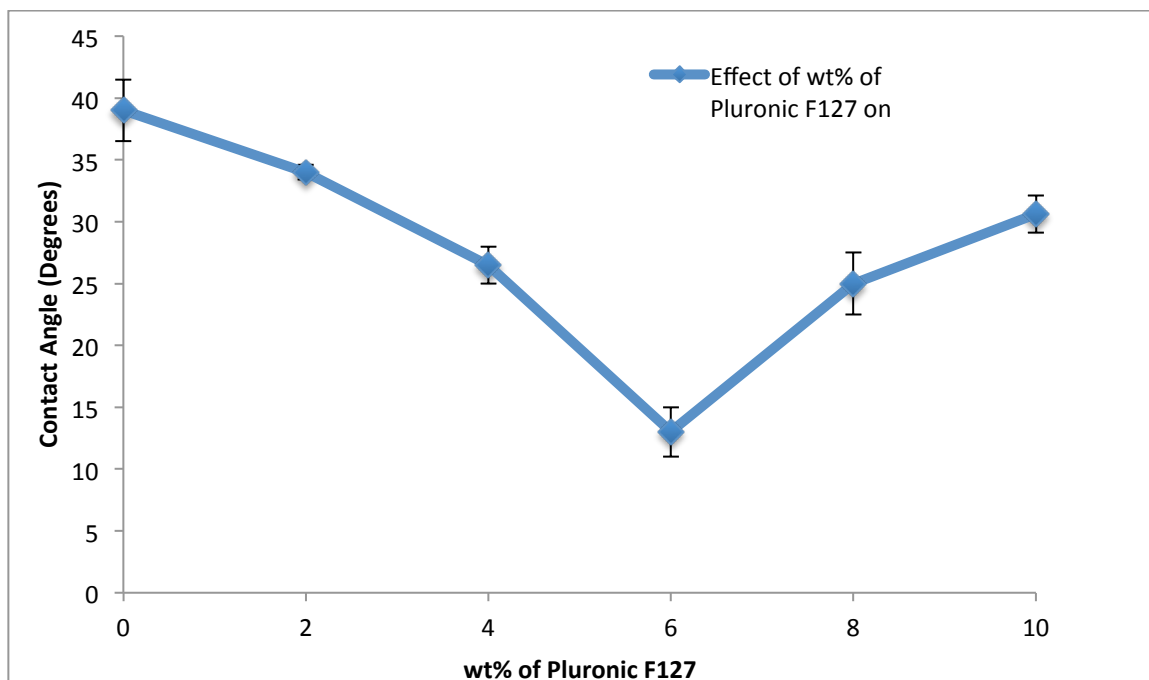


Figure 4.4 Effect of Mixing Pluronic F127 on the hydrophilicity of the PVA membrane.

4.3.2.2 *Effect of Incorporating MWCNTs on Hydrophilicity*

Multi-wall carbon nanotubes (MWCNTs) were introduced into the solution mixture to generate some effective nano-channels for improved water flux through the membrane and for enhanced mechanical strength and stability of the membrane [160]. Figure 4.5 shows the effect of the infusion of MWCNTs on the hydrophilicity of the membrane's surface. The curve shows that the hydrophilicity of the membranes surfaces has improved with the addition of MWCNTs, as indicated by the decrease in contact angle compared to the pure PVA membrane. MWCNTs are highly hydrophobic in nature. Nevertheless, some researchers found that the mixing or coating of MWCNTs with PVA improves their hydrophilicity significantly due to the fact that PVA surrounds MWCNTs with $-OH$

groups [161-163]. The contact angle of MWCNTs could go from 150° to 25° after the incorporation of PVA on the surface, which is a large modification of the surface properties [161-163]. Another explanation of the hydrophilicity improvement is related to the interactions between Pluronic F-127 and MWCNTs; The hydrophobic PPO segments in Pluronic F-127 get adsorbed into the hydrophobic MWCNTs sidewalls and form a coating layer, in which the hydrophilic PEO segments project away from the MWCNTs sidewalls in a brush-like structure [164, 165]. As a result, the MWCNTs become essentially hydrophilic, which improves the hydrophilicity of the membrane and enhance the blending of the MWCNTs within the polymer matrix. The optimal MWCNTs loading was 0.04 wt%, after which the hydrophilicity decreases. When more than 0.04 wt% was incorporated, the effective wrapping of MWCNTs with the hydrophilic groups may have decelerated due to the excess amounts of MWCNTs. Nonetheless, even after the hydrophilicity decrease, the incorporation of MWCNTs improved the hydrophilicity of the membrane compared to the pristine PVA membrane. This is an excellent improvement of the surface properties as enhancing surface hydrophilicity of the membrane has a strong effect on biofouling mitigation.

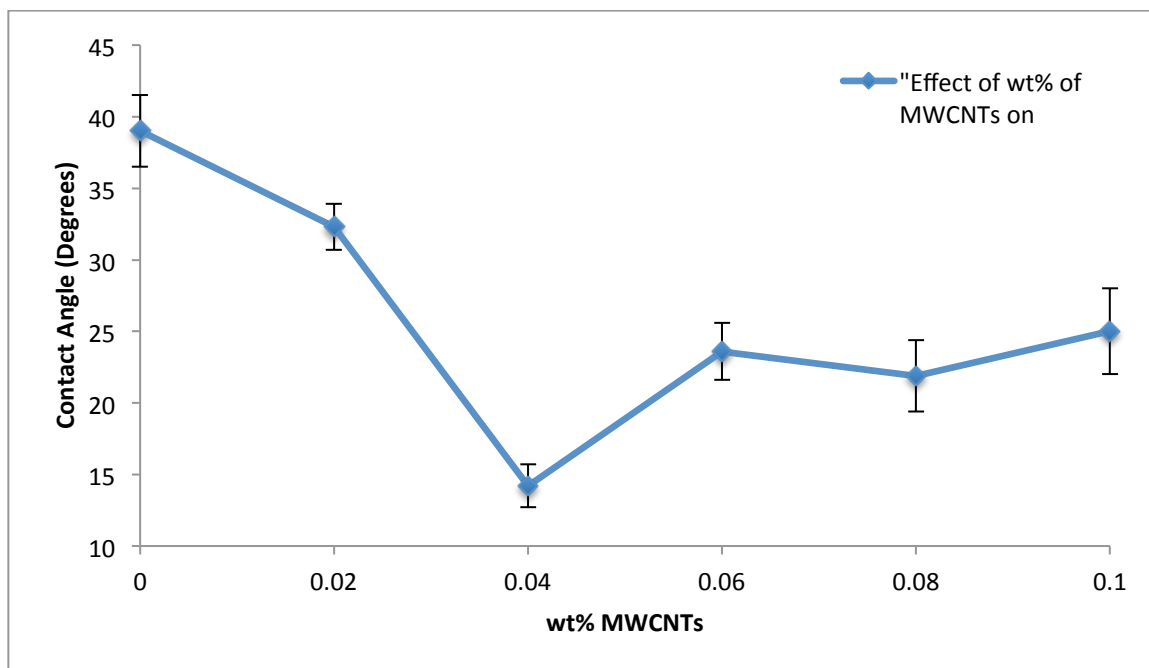


Figure 4.5 Effect of Mixing MWCNTs on the hydrophilicity of the PVA membrane.

4.3.3 X-Ray Diffraction

The microstructure of the synthesized membranes is characterized by X-ray diffraction. Diffraction patterns of the pure PVA and the MWCNTs infused PVA membranes are shown in Figure 4.6. The pure PVA XRD curve shows peaks at 11.4° , 20.02° , 23.23° , and 40.89° . The peak at 20.02° is the strongest and the most obvious. Those are characteristic peaks of Pure PVA demonstrating its semi-crystalline structure [141]. After mixing DGEBA, Pluronic F127 and MWCNTs with PVA, the strongest Peak for PVA at 20.02° became wider, which is an effect of DGEBA. Since the hydrogen bonding influence within PVA molecules reduces as a result of crosslinking with DGEBA, the crystallinity

of PVA is reduced, as well. As a result of this crystallinity decrease, the peaks become wider to represent the amorphous structure [141]. The XRD pattern of the MWCNTs modified PVA membranes shows additional peaks at 22.68° and 41.55° . Those peaks are believed to be representative of the (002) and (100) planes of the graphite structure of MWCNTs [166].

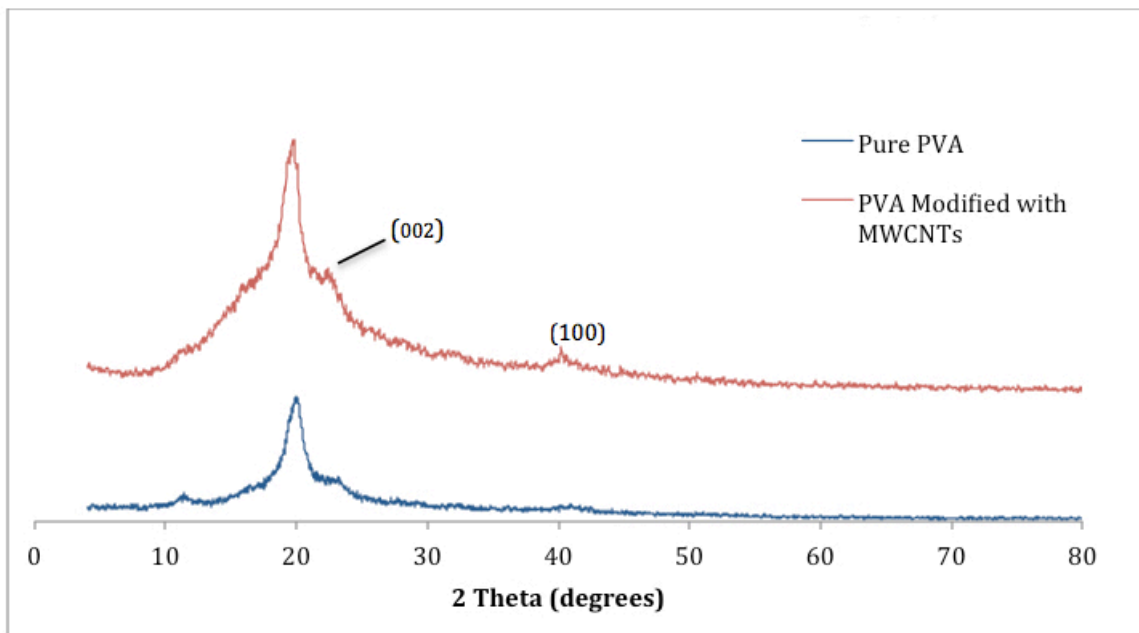


Figure 4.6 XRD patterns of pure PVA and MWCNTs modified membranes.

4.3.4 Atomic Force Microscopy (AFM)

There is a strong correlation between the surface roughness of the RO thin film membranes and biofouling [78]. A higher roughness increases the total surface area that microorganisms could be attached to, and the ridge-valley configuration enhances the accumulation of foulants on the surface. As a consequence, the rougher the membrane surface, the more it will be favorable for foulants to attach to the membrane surface [79]. An important goal in membrane development is to reduce surface roughness. Figures 4.7 & 4.8 show the effect of MWCNTs weight percent on the surface roughness of the PVA reverse osmosis membranes. The surface roughness decreased dramatically after the incorporation of very small amounts of MWCNTs. This could be explained by the fact that MWCNTs loading leads to an increase in viscosity of the casting solution which obstructs the exchange rate of solvent and non-solvent diffusion during the dissolution casting process, and hence, smoother membrane surfaces are formed [123]. Smoother RO membrane surfaces are of great interest; this is why this finding is crucial and expected to have a great impact on the permeation and biofouling resistance performance.

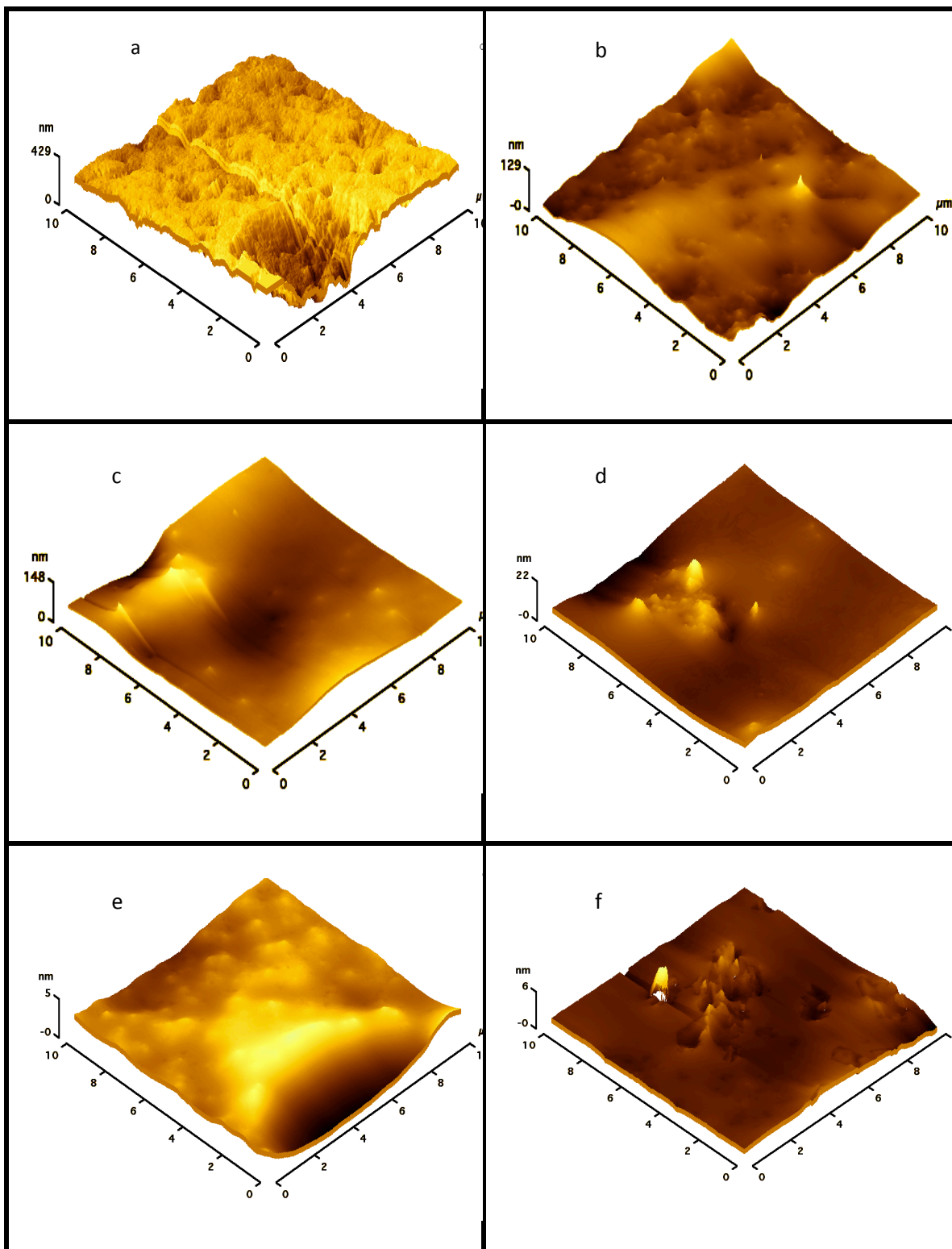


Figure 4.7 3-D AFM images of (a) PVA membranes and PVA modified with (b) 0.02, (c) 0.04, (d) 0.06, (e) 0.08 and (f) 0.1 wt% MWCNTs.

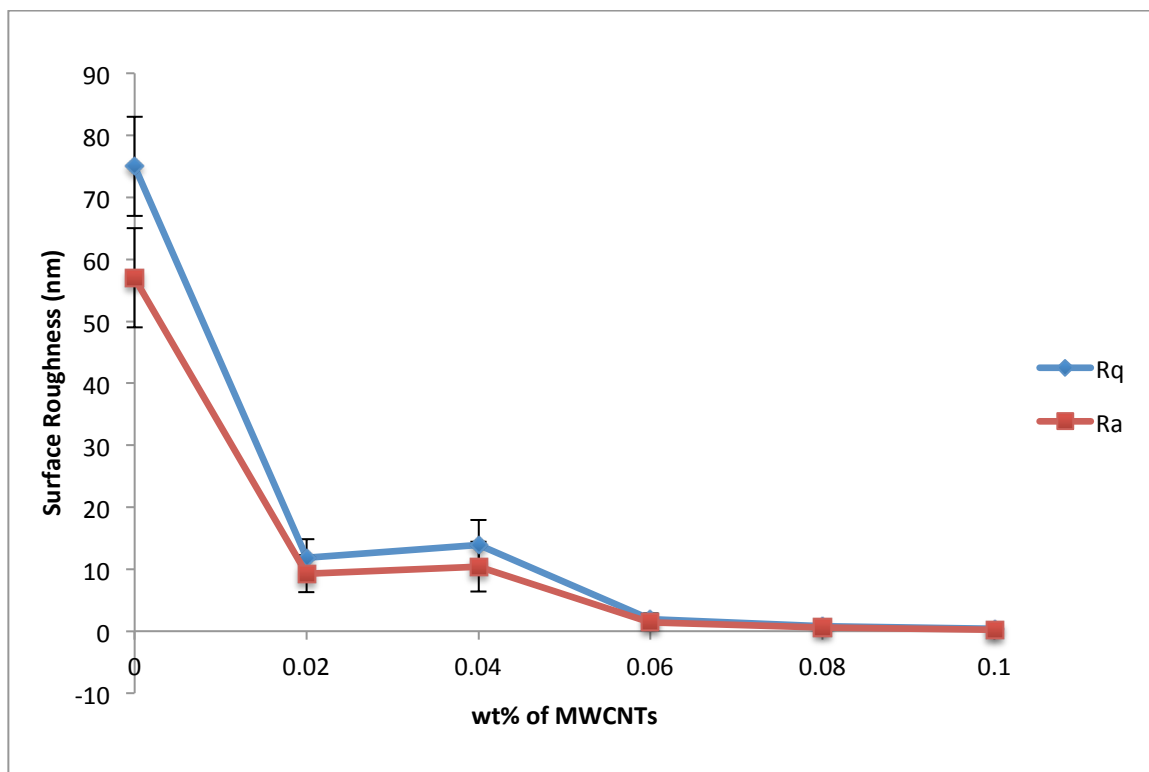


Figure 4.8 Effect of MWCNTs loading on surface roughness of PVA membranes.

4.3.5 Scanning Electron Microscopy (SEM)

Although RO membranes are often considered as having pore sizes ranging from 1 to 10 Å, they are assumed to be principally nonporous. These pores are more precisely referred to as transient free-volume elements. These elements actually vary in size and location as a function of time. Therefore, the solution-diffusion model is used to describe the flow. On the other hand, porous membranes, such as ultrafiltration membranes, have permanent pores and are governed by a different transport model, which is the pore-flow model [38, 51]. Pluronic F-127 can serve as a pore forming agent to enhance the porosity of the resultant reverse osmosis membranes. The pore forming mechanism is reported in details elsewhere [167]. Pluronic F-127 does not only increase the pore size and the water flux of

the resultant membranes, furthermore, it remarkably reduces irreversible fouling due to protein adsorption [167, 168]. Figure 4.9, (a) and (b) show SEM images of the pristine PVA reverse osmosis membrane and the modified membranes with 6 wt% of Pluronic F-127. It is very clear from surface morphology images that the incorporation of Pluronic F-127 resulted in pores formation. The pristine PVA membrane surfaces are dense, flat and smooth. The surface morphology has changed dramatically with the incorporation of Pluronic F-127. Manifold pores ranging in size from 1 μm to 10 μm are clearly noticeable on the surface. As mentioned earlier, the MWCNTs modified membranes already have Pluronic F-127 incorporated in them. Thus, it is expected that the morphological surface images will contain some pores because of that. Figure 4.9, (c-g), shows the SEM images of MWCNTs modified PVA membranes. The pores again are clearly visible, but there are no MWCNTs agglomerations visible on the surface.

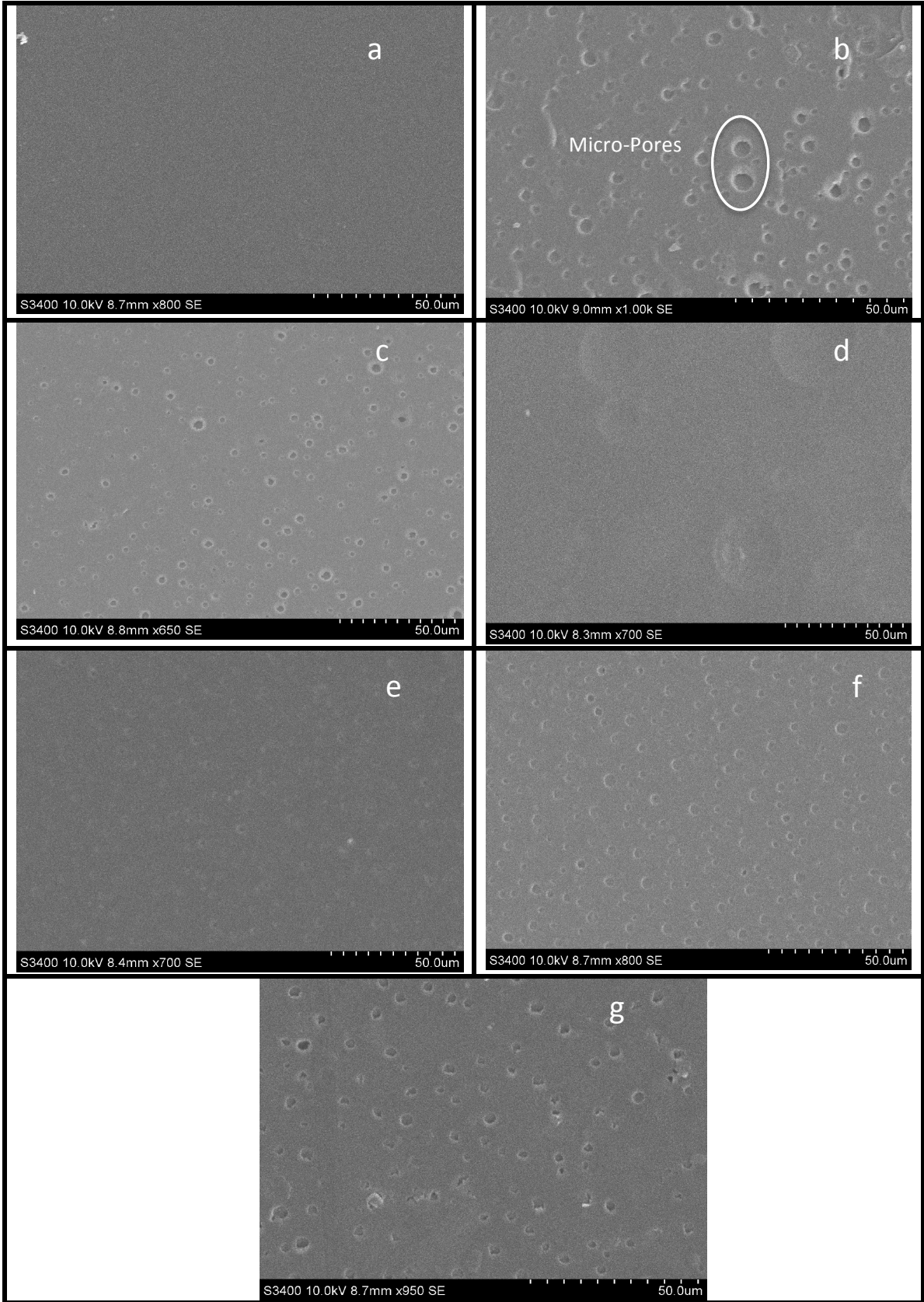


Figure 4.9 SEM images of (a) pristine PVA, (b) PVA with Pluronic F127 and (c) PVA modified with 0.02, (d) 0.04, (e) 0.06, (f) 0.08 and (g) 0.1 wt% MWCNTs.

4.3.6 Mechanical Properties

MWCNTs are allotropes of carbon, which are one-dimensional nano-materials. The unique carbon nanotube structure offers the MWCNTs with unique physical and chemical properties. The Carbon covalent bond that is the backbone of the carbon nanotubes is exceptionally strong; that is why carbon nanotubes have unique mechanical properties. MWCNTs are excellent fillers for reinforcement purposes [169-171]. Figures 4.10 & 4.11 show the stress-strain curves and the Young's modulus values for PVA RO membranes modified with different weight percentages of MWCNTs, respectively. The figures show that as the amount of MWCNTs increased the overall strength and ductility of the membrane improved. The yield strength of all of the tested membranes was around 20 MPa. The ductility of the resultant membranes was too high, almost 150%. Young's modulus increased slightly as the amount of MWCNTs increased. A very slight decrease in stiffness was observed when more the 0.06 wt% MWCNTs was incorporated. This effect could be attributed to the agglomeration of MWCNTs at high loadings [87]. These results illustrate that the synthesized PVA modified membranes are certainly mechanically stable. Practically, the membranes withstood the very high reverse osmosis pressure of 800 Psi without the need of a supportive layer or a substrate. This is an exceptional outcome, as the utilization of the membrane without a substrate eliminates unfavorable consequences, such as internal concentration polarization that may cause an increase in the applied pressure.

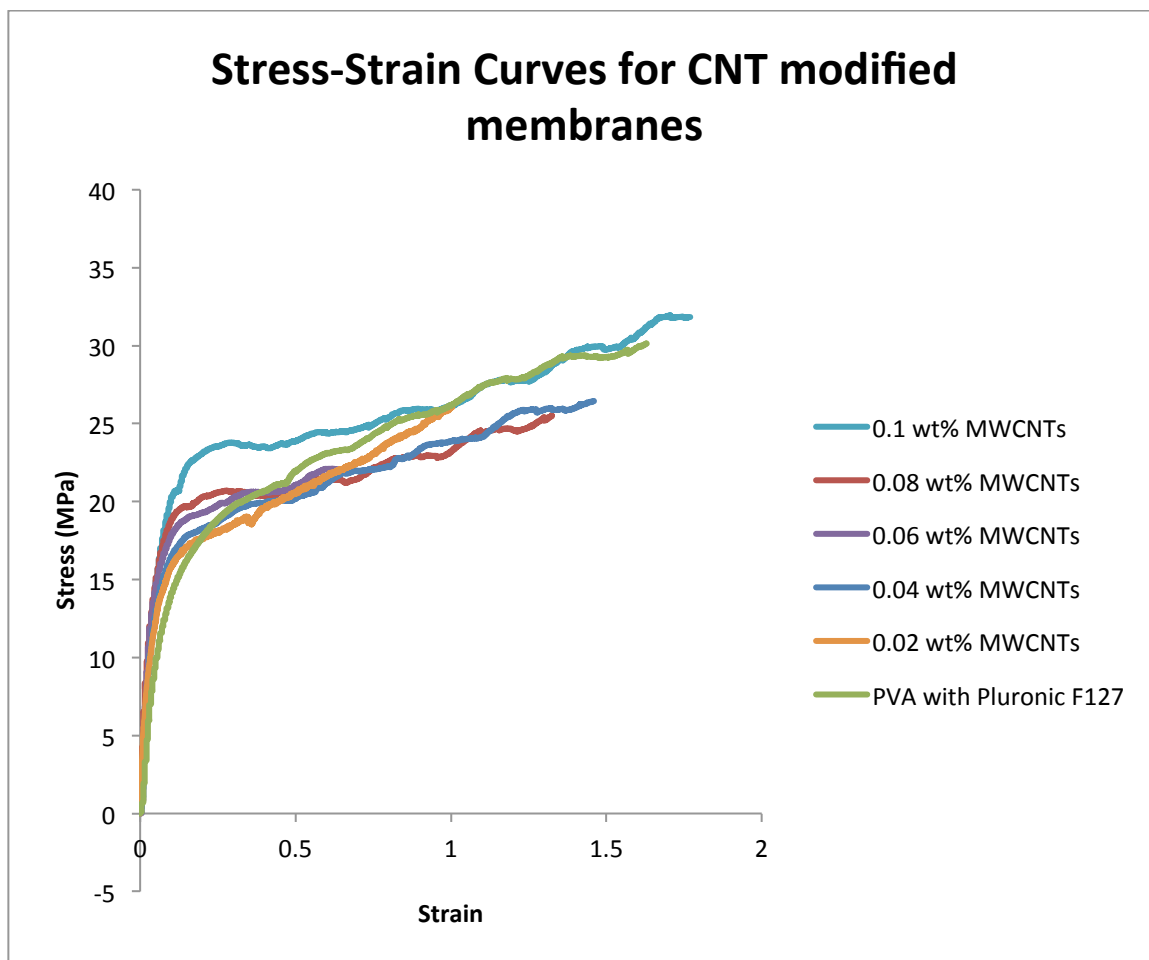


Figure 4.10 Stress-strain Curves for different MWCNTs wt%.

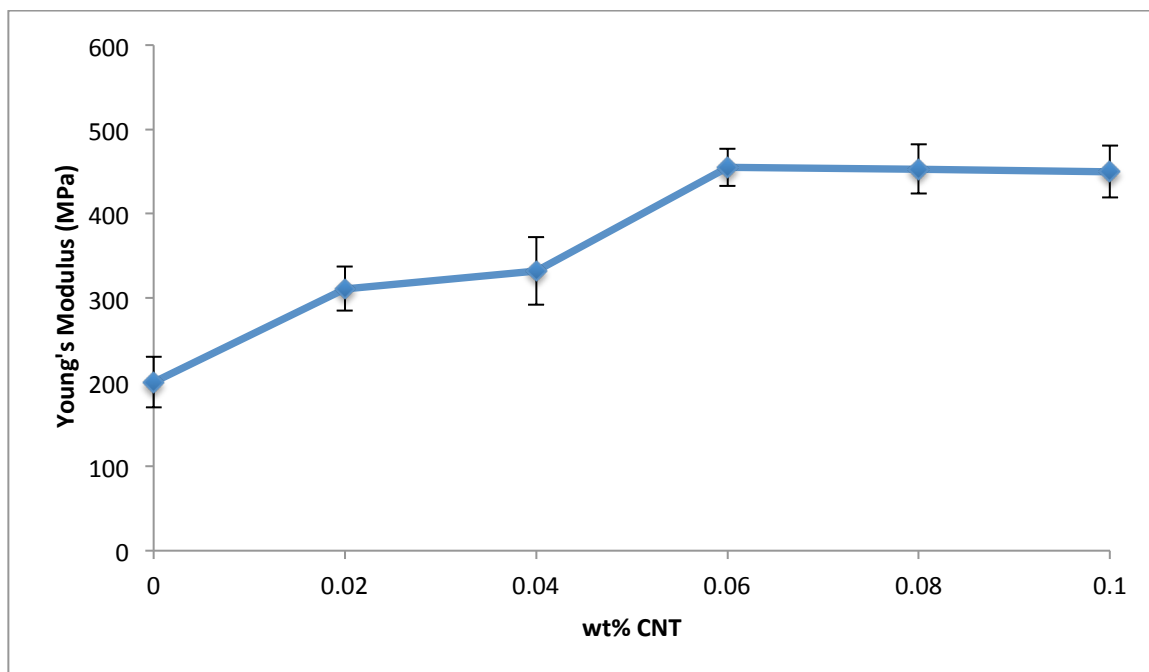


Figure 4.11 Effect of MWCNTs wt% on Young's modulus of the membranes.

4.3.7 Permeate Flux and Salt Rejection

4.3.7.1 Separation performance of DGEBA crosslinked PVA membranes

Figure 4.12 shows the permeation flux and the salt rejection percentages of the PVA crosslinked membranes with DGEBA. As the amount of the crosslinker increases, the salt rejection improves. This is a direct effect of polymer chains crosslinking of PVA with DGEBA. Characteristically, crosslinking of polymer chains generates tighter and denser structures as those polymer chains would interweave and form larger networks [88]. Those more complex structures will impede the free passage of salt molecules across the membrane. On the other hand, the permeate flux is reduced as the amount of DGEBA

increases. The reason is understandably the same. Those larger, tighter and denser networks will affect the flow of water molecules as well. At this stage, the synthesis of highly selective membranes is more significant since the purpose of the subsequent incorporation of Pluronic F127 is to enhance the permeation and the water flux through the membrane. Hence, the optimal wt% of the crosslinker is the one that produces optimal salt rejection. Figure 4.12 shows that the DGEBA wt% of 0.16 created the membrane with the optimal salt rejection. This specific weight percentage will be added to all of the PVA membranes for further modifications to enhance the permeability.

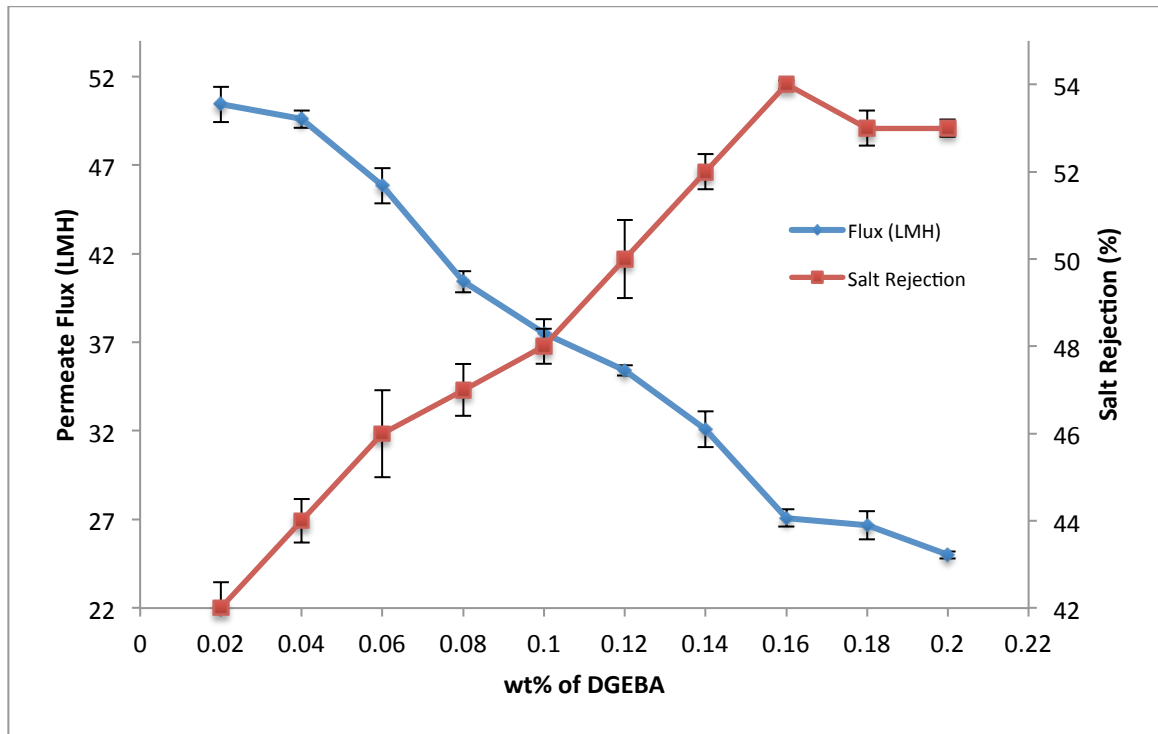


Figure 4.12 Effect of crosslinker wt% on the permeation and selectivity of the membrane.

4.3.7.2 *Separation performance of PVA membranes incorporated with Pluronic F127*

Pluronic F-127 was added to the solution with different weight percentages to investigate the effect on hydrophilicity and overall performance. Figure 4.13 illustrates the effect of the incorporation of Pluronic F-127 on the water flux through the reverse osmosis membrane after five hours of operation. It is clear from the curve that the addition of Pluronic F-127 enhanced the permeation greatly. Part of this is due to the hydrophilic nature of the membrane surface after the incorporation of the hydrophilic groups; the other part is evidently due to the pore formation, which is a characteristic of Pluronic F-127 as has been reported elsewhere [114, 156-158, 172]. The curves show that as the amount of the added Pluronic F-127 increases, the water flux increases. Interestingly, the salt rejection declines after the addition of 6 wt%. This could be attributed to the pores, as forming more and more pores with bigger sizes will allow more salt molecules to pass through. Consequently, the Pluronic F-127 wt% of 6 was selected as optimal weight percentage and was incorporated into subsequent membranes for further modifications.

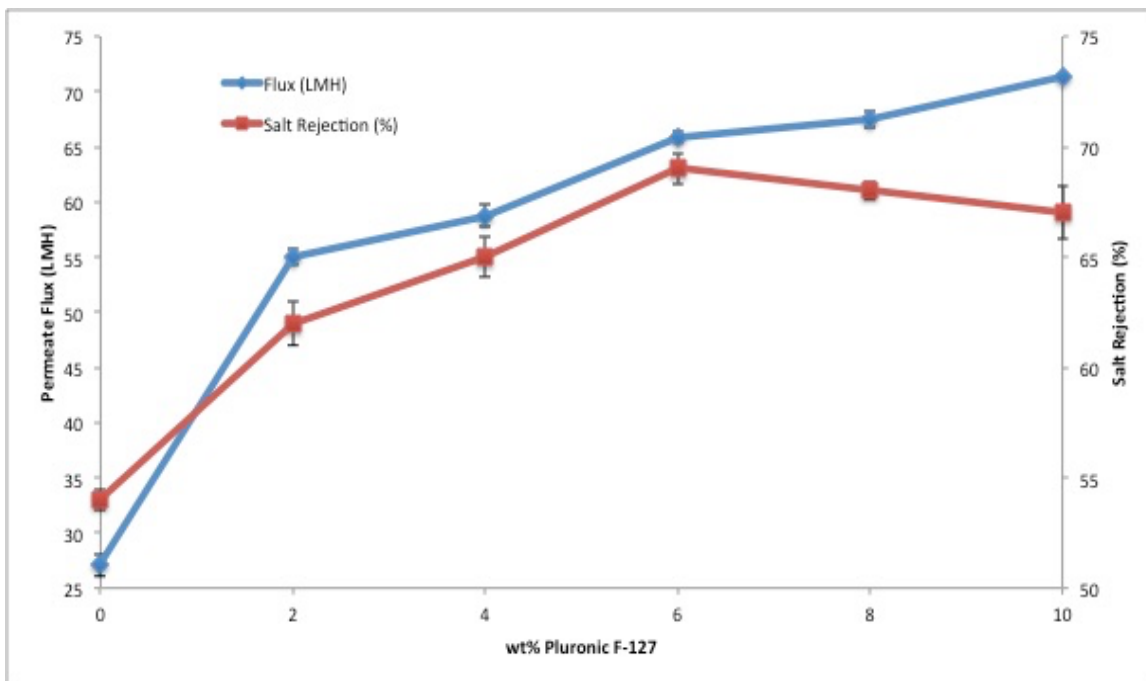


Figure 4.13 Effect of Pluronic F127 wt% on the permeation and selectivity of the membrane.

4.3.7.3 Effect of MWCNTs infusion on PVA membranes separation performance

Multi-wall carbon nanotubes (MWCNTs) were introduced into the solution mixture to generate some effective nano-channels for higher water flux and improved mechanical strength [160]. Figure 4.14 shows the effect of the addition of different weight percentages of MWCNTs on the water flux through the membrane. The water flux almost doubled after the addition of just a small amount of MWCNTs. These results match what was reported earlier that the incorporation of MWCNTs with PVA makes it remarkably more hydrophilic. That increase in hydrophilicity is the reason why the permeation gets improved vastly. Another explanation for this improvement of permeability is related to the stiffness and the mechanical strength of the synthesized membrane. Permeation

studies are performed under very high pressure, in the order of 800 Psi. Due to the exposure of this very high pressure, the membrane is deformed and the internal pores are deformed as well. As a result of this deformation, some pores get blocked or severely damaged, which negatively affect the permeation of the membrane. Thus, the higher the mechanical strength and stiffness of the membrane material the better the permeation performance will be. Figure 4.11 showed that the stiffness of the membrane increased with the addition of MWCNTs. There was a slight decline when more than 0.06 wt% is infused. This behavior clearly matches the permeation behavior as it is obvious that there was a slight decrease in water flux when more than 0.06 wt% was incorporated. The maximum permeate flux in this study was around 140 LMH. This flux is much higher than typical permeate flux of commercially available Polyamide RO membranes. For instance, SW30HR, a polyamide RO membrane from DOW FILMTEC, has a permeate flux of 27 LMH under the same operating conditions used in this study [173].

As reported earlier, the incorporation of MWCNTs into polymeric membranes enhances the separation performance and selectivity of the membrane. Figure 4.14, also, shows the effect of incorporating MWCNTs on the selectivity of the synthesized membranes. It is clear that infusing small amounts of MWCNTs into the polymer membrane matrix enhanced the selectivity enormously compared to unmodified membranes. The salt rejection improved from around 50% to 92% with the addition of .08 wt% MWCNTs. Incorporating MWCNTs into PVA membranes led to structural compactness of the membranes due to the strong interactions between MWCNTs and PVA matrix, resulting in a network structure [128, 174, 175]. This network structure hindered the free passage of salt molecules across the membrane, which improved the selectivity [128, 176]. This is

an excellent result as it is usually a tradeoff between permeability and selectivity; nonetheless, the incorporation of MWCNTs enhanced both.

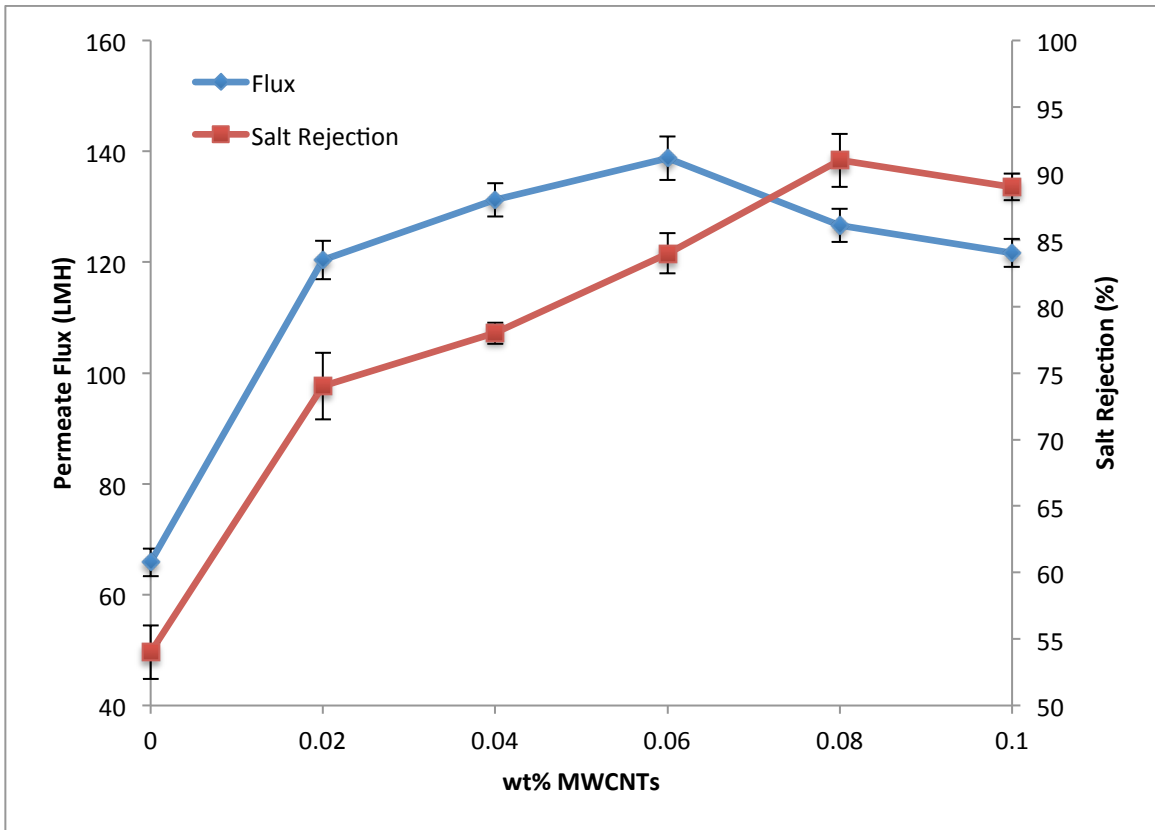


Figure 4.14 Effect of MWCNTs wt% on the permeation and selectivity of the membrane.

4.3.8 Effect of MWCNTs Infusion on Membrane's Chlorine Resistance

Figure 4.15 shows the comparison between the modified MWCNTs composite RO membranes with unmodified (PVA/DGEBA/PluronicF-127) ones. Without MWCNTs, the membrane shows poor Chlorine resistance as the salt rejection decreased from 54 to 40%, a 26% decrease in salt rejection efficiency. This indicates that the membrane surface has been affected greatly by the harsh environment caused by the presence of high concentration of Chlorine. On the other hand, once MWCNTs have been infused, the decline in salt rejection became negligible. The figure shows that the addition of 0.08 and 0.1 wt% MWCNTs provided a more chemically stable membrane as it became more Chlorine resistant. The improvement of Chlorine resistance upon incorporation of MWCNTs is due to the physical crosslinking effect of MWCNT that enhances the mechanical strength of the membrane, as well as reduces the degradation of the polymer by reducing the sites where Chlorine atoms could be attached to [177, 178].

Existing commercially available Polyamide (PA) RO membranes are severely affected by exposure to even lower levels of Chlorine than those used in the present study [179, 180]. The decrease of salt rejection of a typical commercially available PA membrane (SW30HR, Dow FilmTec) is more than 25% in less harsh conditions [179, 180]. In this research, the synthesized modified PVA membranes had a much better Chlorine resistance compared to commercial RO membranes. Chlorine resistance is a very important membrane property since it diminishes the need for the de-Chlorination process that is needed to protect the membrane material from the attack of Chlorine used for anti-fouling purposes [181].

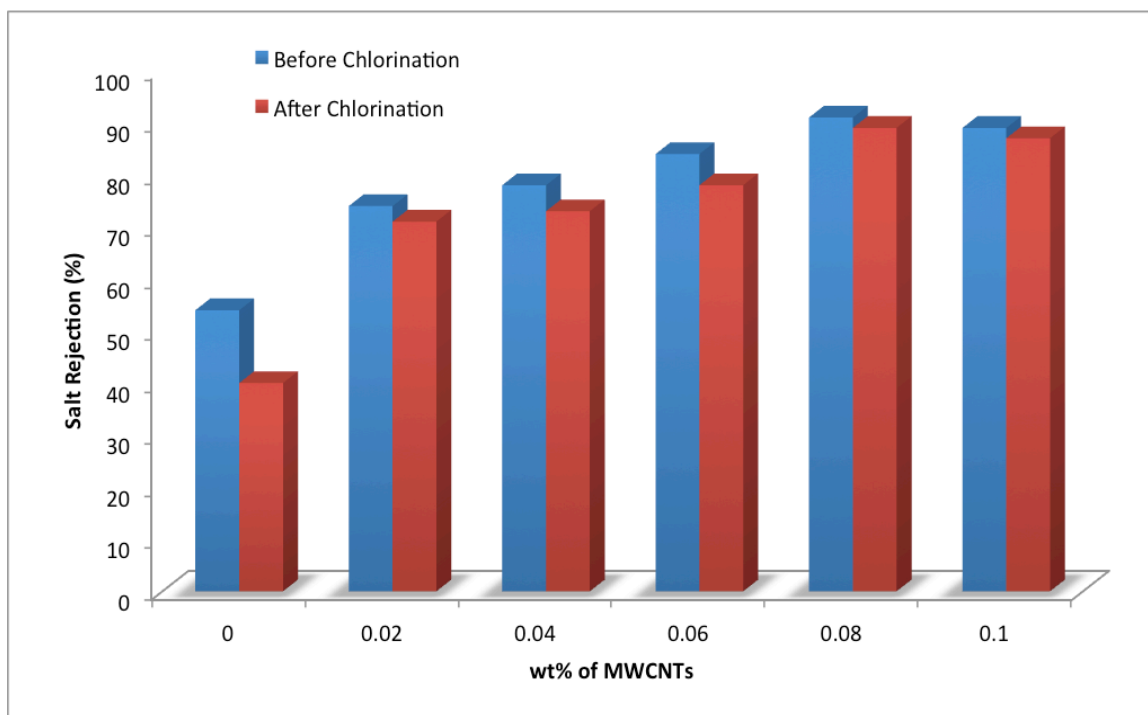


Figure 4.15 Effect of MWCNTs wt% on salt rejection before and after Chlorination.

4.3.9 Effect of MWCNTs Infusion on Membrane's Biofouling Resistance

The antibacterial activity of *E. coli* by JIS L 1902–2002 methodology was analyzed. It was noticed that conical flasks that contains unmodified membrane appeared muddled which show the bacterial growth while MWCNTs modified membranes displayed a clear transparent solution. The optical density (OD) noted for the unmodified and modified membranes are shown in Figure 4.16. The OD of MWCNTs modified membranes indicated that there was slight bacterial growth. The unmodified membrane, with 1.442 of OD, indicated the induction of *E. coli* on the membrane surface. It was concluded that modified membranes effectively restricted the bacterial growth. After the incorporation of MWCNTs into the membranes, most of the *E. coli* cells no longer have their cellular

integrity and became more rigid indicating irreversible cell death and/or cell damage. According to OD result, the bacterial attachment has been reduced by up to 80% with the incorporation of MWCNTs. This is a great improvement of the membrane surface, as enhancing biofouling and Chlorine resistance will extend the membrane life and maintain optimal salt rejection and permeability without the need of frequent cleaning.

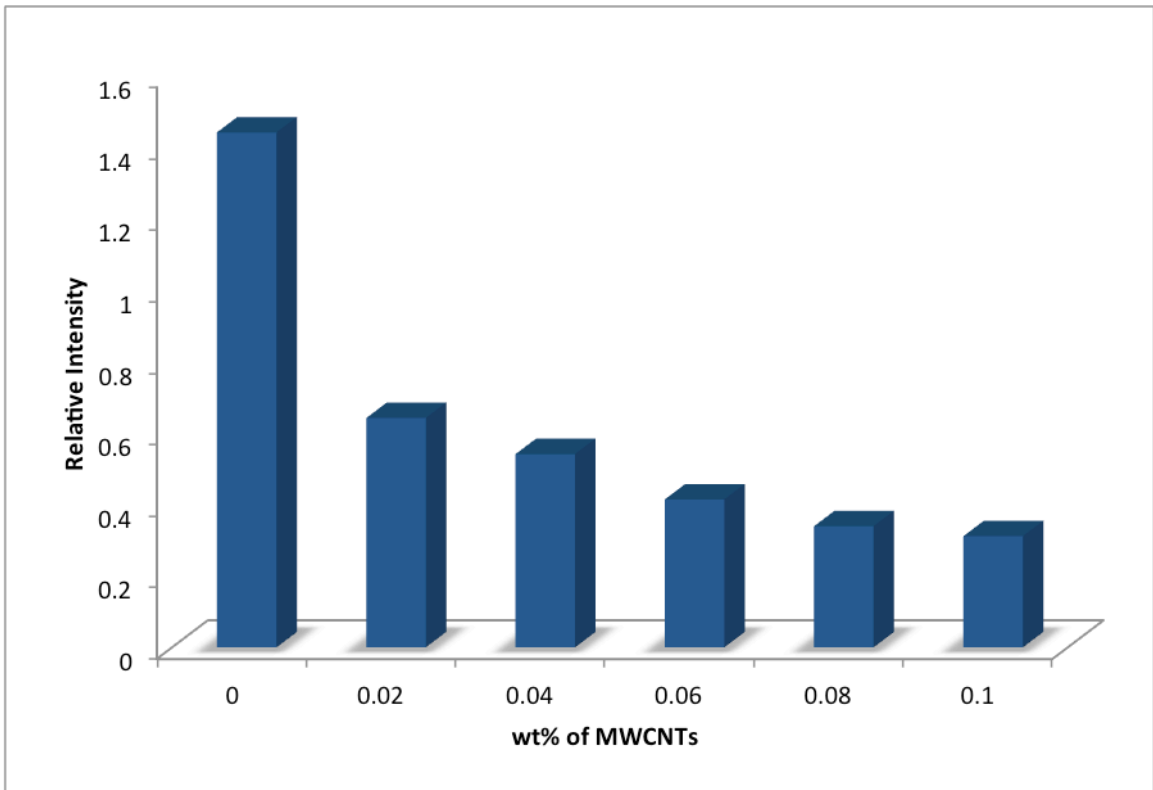


Figure 4.16 Relative amount and viability of E.coli cells adhering onto pristine and modified PVA membranes.

4.4 Conclusion

The purpose of the current research was to investigate the effect of incorporating Pluronic F127 and MWCNTs into DGEBA crosslinked PVA membranes on the overall reverse osmosis performance. The uniqueness of this work is that the PVA polymer matrix is utilized as an active RO layer without the use of any polymeric or ceramic substrate. Although PVA possesses excellent separation and film forming properties, researchers tend to avoid using PVA as an active layer in RO applications because of PVA swelling effect and the membrane collapse under a very high pressure for RO applications. Instead, they utilize PVA as a modifier. We succeeded to fabricate an RO membrane utilizing PVA as an active layer that overcame those issues through appropriate crosslinking and through incorporating Pluronic F127 and MWCNTs.

Crosslinked PVA membranes were prepared using dissolution casting method and MWCNTs were incorporated in the PVA polymer matrix by dispersion. The incorporation of Pluronic F127 and MWCNTs improved the overall RO performance of the membrane in terms of hydrophilicity, surface roughness, water permeability, salt rejection, Chlorine resistance and biofouling resistance. Figure 4.17 shows a target plot that determines which RO membrane has the optimal performance. The membrane properties and performance were ranked from level 1, the innermost loop on the target, to level 10, the outermost loop; level 10 indicates ideal properties. The target plot clearly illustrates that the incorporation of MWCNTs improved the overall performance vastly. From the plot, the membranes that contain 0.08 and 0.1 wt% MWCNTs provided optimal salt rejection, Chlorine and biofouling resistance and mechanical strength. Although the permeation of these two membranes is not the best, they relatively have an excellent

water flux.

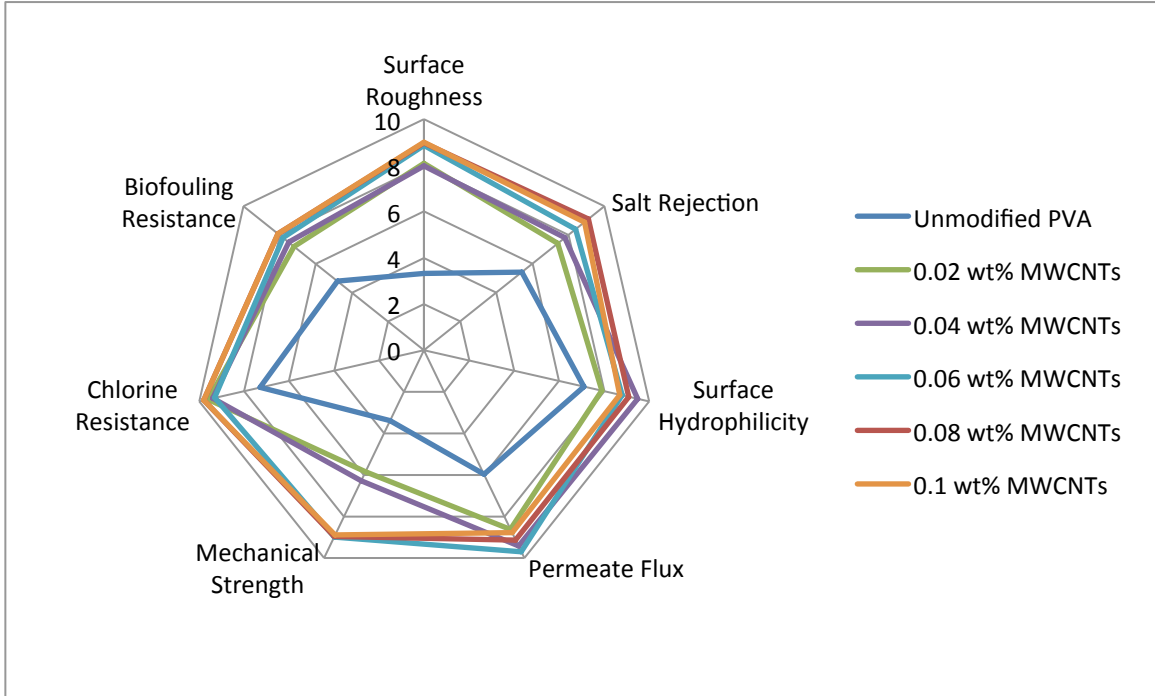


Figure 4.17 Target plot comparing RO performance properties for unmodified and MWCNTs modified PVA membranes.

CHAPTER 5

Conjugation of Vanillin and Pluronic F-127 With Novel PVA/DGEBA Cross-linked Thin Film Membranes For Reverse Osmosis Performance Enhancement

5.1 Introduction

Global water scarcity is increasingly becoming the most critical problem affecting people around the world. Coupling this with the exponential growth in population and economy yields a recipe for calamitous fresh water dearth. Global demand of fresh water is anticipated to jump from 4500 billion m³ to 6900 billion m³ by 2030 [5, 43].

Only 2.5% of earth's surface, which is predominantly covered with water, is fresh water and a small amount of the fresh water is easily accessible. The reason is the fact that most of the fresh water is accumulated as glaciers or is very deep underground [3, 5, 110]. With this substantial increase in fresh water demand, an effort to develop desalination technologies is necessary.

Reverse Osmosis (RO) is the predominant desalination technology nowadays. It is becoming the major desalination technology over conventional thermal technologies, like Multi-Stage Flashing (MSF) and Multi-Effect Distillation (MED). Due to desalination process developments and major cost and energy reductions, RO processes attract interests commercially [18, 22, 51, 112]. Membrane fouling causes a cutback in performance of reverse osmosis (RO) membranes, which is a major concern. Due to fouling, the membranes need to be chemically cleaned and treated frequently. This eventually abridges the membranes life, which will increase the cost of the overall reverse osmosis process [52, 61]. Most of the foulants, other than bio-foulants, can be

removed or their effect can be minimized to some extent by pretreatment. Biofouling, on the other hand, is different. Membrane biofouling is defined as the buildup of microbial layers on the surface or within the pores of the membrane. These micro-organisms such as bacteria, algae and fungi are pseudo particles, which means that even if pre-treatment gets rid of 99.99% of them, the remaining 0.01% can grow, multiply or even relocate. Therefore, it has been found that biofouling occurs even after feed water pretreatment and after the addition of disinfectants [42, 48, 51-55]. Micro-organisms can withstand extreme conditions like temperatures ranging from -12°C to 110°C and pH values between 0.5 and 13. The attached microorganisms embed, and form biofilms. This means that the originally dissolved species are now locally restrained and transformed from solution into a semisolid form [52, 53, 56, 57]. The development of a biofilm on the surface of the membrane causes several undesirable consequences on the RO process, such as flux decline, operating pressure increase, membrane bio-degradation and loss of salt rejection [64, 65].

In this study, novel crosslinked PVA reverse osmosis membranes infused with Pluronic F-127 and Vanillin were synthesized using dissolution casting methodology.

Poly (vinyl alcohol) (PVA) has been utilized extensively in applications related to water purification, since it possesses superb properties, such as water-solubility, biodegradability, intrinsic hydrophilicity, good film-forming properties, good Chlorine tolerance, excellent fouling resistance and exceptional thermal, mechanical and chemical stability [81-87]. Due to its very high hydrophilicity, swelling of PVA membranes is expected and it leads to an open structure that is not favorable, as the membrane will lose its selectivity. To solve such a problem, crosslinking of PVA is performed to generate a

membrane that has balanced permeability and selectivity [91-96].

Poloxamers or Pluronics are triblock amphiphilic copolymers comprising polyethylene oxide–polypropylene oxide–polyethylene oxide (PEO–PPO–PEO) as a monomer. Thus, the copolymer contains hydrophilic PEO segments and hydrophobic PPO segments. Compared to other Poloxamers and Pluronics, Pluronic F-127 (M_w 12,600) has a great hydrophilic/lipophilic balance value (HLB = 22), and better extractability into aqueous phase [113, 114]. Many researchers reported that the inclusion of Pluronic F-127 into PVA thin films improves the permeability and selectivity performance of the membrane. It is also used as a pore-forming agent [114-118].

Vanillin (4-hydroxy-3-methoxy-benzaldehyde) is the major constituent of *Vanilla planifolia* (Vanilla). It is used extensively in food industry as a natural flavoring agent. It has been reported that Vanillin has excellent antimicrobial properties [182, 183]. Many researchers proved that the incorporation of Vanillin into membrane systems enhanced biofouling resistance vastly [182, 184, 185].

PVA has been used by many investigators as a surface modifier to improve surface hydrophilicity or as a coating on polymeric or ceramic surfaces for many separation applications [69, 100, 101, 129-131, 133-136, 139, 141, 142, 144-150, 186]. To the best of our knowledge, no research has been presented on the utilization of crosslinked PVA incorporated with Pluronic F-127 and Vanillin as an active layer in reverse osmosis for seawater desalination without the use of polymeric or ceramic substrates. The crosslinked PVA has been conjugated with Pluronic F-127 and Vanillin to mitigate common PVA limitations, mainly swelling and rupture under high pressure.

In this research, a novel crosslinked PVA reverse osmosis membranes incorporated with Pluronic F-127 and Vanillin were fabricated using dissolution casting method. The fabricated membranes were then characterized and analyzed using various techniques like attenuated total reflection Fourier transform infrared spectroscopy (ATR-FTIR), contact angle measurements, X-ray diffraction (XRD), scanning electron microscope (SEM), atomic force microscope (AFM) and mechanical testing. The actual reverse osmosis performance of the membranes, including permeation testing, salt rejection and Chlorine resistance was examined using a reverse osmosis permeation unit.

5.2 Experimental Procedure

5.2.1 Materials

Analytical grade PVA ($M_w=89000$), bisphenol A diglycidyl ether (DGEBA) (crosslinker), Pluronic F-127 (average molecular weight: 12.6 kDa), dimethyl sulphoxide (DMSO), sodium hypochlorite (NaClO) and Vanillin ($\text{C}_8\text{H}_8\text{O}_3$) were acquired from Sigma Aldrich (St Louis, MO, USA). All the chemicals were used without further purification.

5.2.2 Membrane Casting

5.2.2.1 Crosslinking of PVA with DGEBA

Several weight percentages of DGEBA (crosslinker), as shown in Table 5.1, were incorporated into PVA solution, where DMSO was used as a solvent with a 17:83 solute/solvent weight percent ratio. The mixing was performed at 70°C for 2 hours with continuous stirring until a homogenous, transparent solution was produced. The solution was then transferred slowly into identical Petri dishes with identical amounts of the

solution to insure uniformity, following the dissolution casting method. The Petri dishes are then heated to 65°C in a controlled evaporation environment to assure uniform film thicknesses of 0.1 mm, measured by a screw gauge. After complete evaporation, the thin film membranes are removed from the Petri dishes with the aid of sharp blades. Five membranes are synthesized from each concentration for testing. The resultant dense membranes are examined for swelling, permeation and salt rejection to come up with the optimal crosslinker weight percent. As will be demonstrated in the results section, the 0.16 wt% of DGEBA provided the optimum membrane properties; thus, the weight percent of 0.16 will be used for further modifications.

5.2.2.2 Incorporation of Pluronic F-127 into the crosslinked PVA membranes

Various weight percentages of Pluronic F-127, as shown in Table 5.1, were incorporated into the solutions of PVA and 0.16 wt% of DGEBA. The solution preparation and the film casting method followed the procedure mentioned in the previous section. As previously done with the crosslinked PVA membranes, the resultant composite membranes with different weight percentages of Pluronic F-127 were characterized and evaluated. The overall evaluation of the Pluronic F-127 membranes, as will be detailed later on, yielded that 6 wt% of Pluronic F-127 is the optimal percentage and will be used for further modifications. Figure 5.1 shows a scheme of the chemical reaction.

5.2.2.3 Conjugation of Vanillin with the Pluronic F-127 modified PVA membranes

Five weight percentages of Vanillin, shown in Table 5.1, were conjugated to the solution of crosslinked PVA and 6 wt% of Pluronic F-127 to synthesize the thin film composite membranes. Vanillin was infused into the solution at 60°C for 2 hours with continuous

stirring until it dissolves completely and a homogeneous solution is formed. The membrane casting followed the abovementioned dissolution casting method.

Table 5.1 Weight percentages of DGEBA, Pluronic F-127 and Vanillin in PVA solution.

	Weight Percentages (wt%)							
DGEBA	0.02	0.04	0.06	0.08	0.1	0.12	0.14	0.16
	0.18	0.2						
Pluronic F-127*	2	4	6	8	10			
Vanillin**	0.01	0.03	0.05	0.07	0.09			
Labels	PVA-V1	PVA-V2	PVA-V3	PVA-V4	PVA-V5			
*with 0.16 wt% DGEBA.								
**with 0.16 wt% DGEBA and 6 wt% Pluronic F-127								

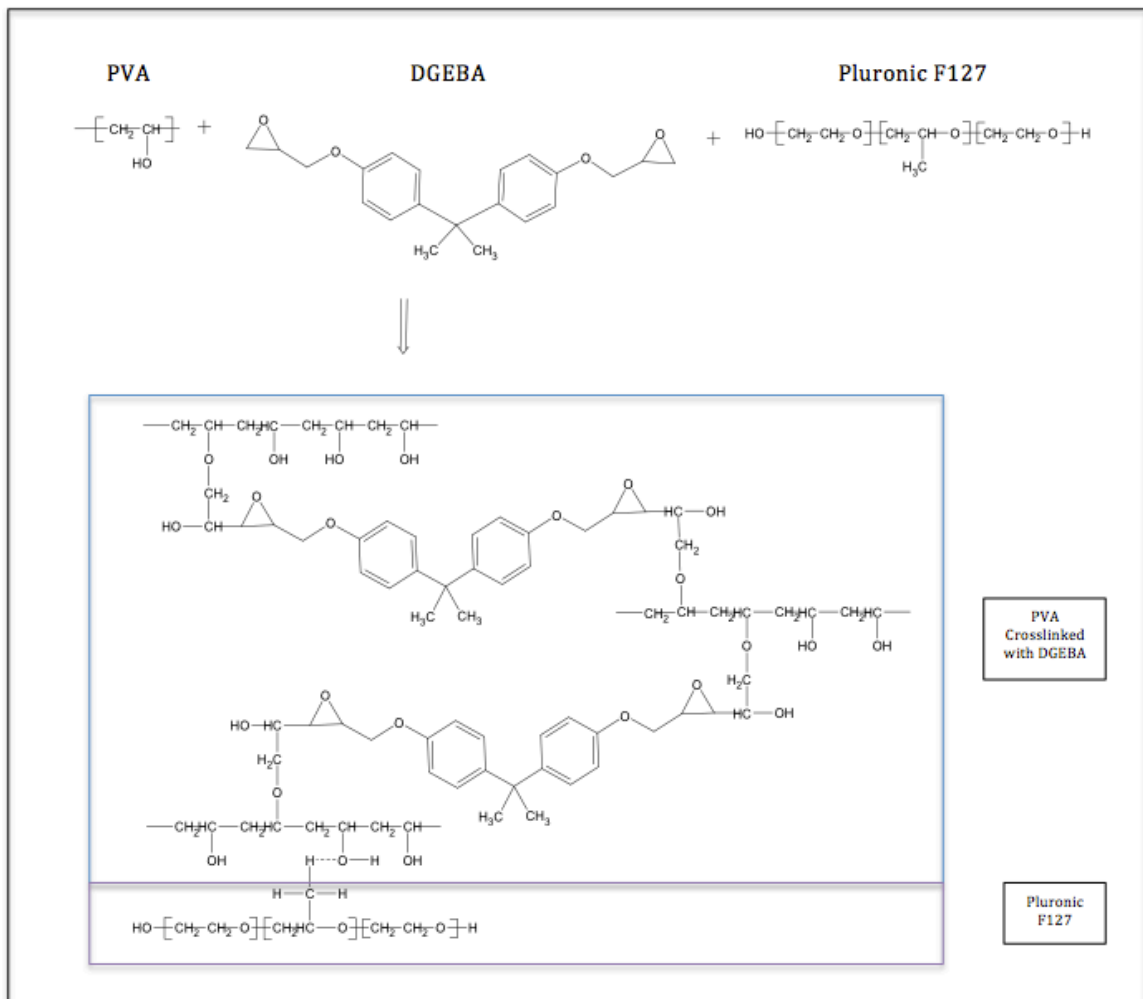


Figure 5.1 Schematic diagram of the crosslinking of PVA with DGEBA and the intermolecular hydrogen bonding with Pluronic F-127.

5.2.3 Membranes Characterization

5.2.3.1 Fourier Transform Infrared Spectroscopy (FTIR)

An IR Prestige-21 (Shimadzu) using attenuated total reflectance (ATR) accessory equipped with zinc selenide (ZnSe) crystal was used to obtain FTIR spectra of the composite membrane samples. Before each sample scan, an air background of the instrument was run. The frequency range was from $4000\text{-}600\text{ cm}^{-1}$ at a resolution of 4.0

cm⁻¹ and average of 120 scans per spectrum were reported.

5.2.3.2 Contact Angle Measurements

A Goniometer (Digidrop, KSV Instruments) was used to calculate sessile drop contact angles of the reverse osmosis membranes. The equilibrium value was average of right and left angles of the drop that are calculated from the software fitting. The reported data is the average of three measurements for each membrane sample.

5.2.3.3 X-Ray Diffraction Measurements

An X'pert PRO Diffractometer (PANalytical) was used to analyze the structure of the synthesized composite membranes. The instrument uses monochromatized CuK α 1 radiation with wavelength of 1.540 Å from a fixed source operated at voltage 40 kV and current 40 mA. The scanning range was from 4° to 80°.

5.2.3.4 Scanning Electron Microscopy (SEM)

A Scanning Electron Microscope (S-3400N Hitachi, USA) was used to obtain SEM images of the synthesized membranes. The SEM was operated under low vacuum mode to characterize the samples. Sample gold sputtering was performed for 120 s before it is placed into the SEM to make sure no surface charging occurs. Gold sputtering was performed using Denton Vacuum Sputtering Automatico Desk IV.

5.2.3.5 Atomic Force microscopy (AFM)

AFM imaging and analysis (Digital Instruments, Santa Barbara, CA, US) were utilized to characterize membrane surface morphological structure and to determine membrane's quantitative surface roughness, respectively. Topographical images were attained using

standard tapping mode. A cantilever oscillated sinusoidally at 350 kHz resonant frequency, and briefly contacted the sample surface at the down stroke of each sinusoidal cycle. A user-established set point force was fixed so that the sample surface was minimally deformed and used as a feedback control. Scanned images were taken at 512 x 512 pixel resolution. Root mean square (RMS) roughness values were obtained from AFM images that were taken from the average of the values measured in random areas. The membrane surface morphology was expressed in terms of various roughness parameters, like mean roughness (Ra). It is calculated by the following equation [108, 109]:

$$Ra = \frac{1}{n} \sum_{i=1}^n |z_i|$$

where z_i is the height or depth of the i^{th} highest or lowest deviation and n is the number of discrete profile deviations. Root-mean-square surface roughness (R_q) is defined as the root-mean-square (RMS) of the deviations in height from the profile mean and it is calculated by [109]:

$$R_q = \sqrt{\frac{1}{n} \sum_{i=1}^n z_i^2}$$

5.2.3.6 Mechanical Testing

An Instron 5567 Tensile Testing Machine fitted with a 10 kN load cell was used to calculate the mechanical properties of the fabricated membranes. Those mechanical properties include the stress strain curves, ultimate tensile strength, elongation at break

and the Young's modulus. The shape of the membrane sample was used as per ASTM D-638 standard with gauge length and width of 50 and 10 mm, respectively. Three specimens were tested for each membrane and the average value was recorded at a crosshead speed of 10 mm/min. The thickness of the membrane samples was measured using a micro-caliper and maintained at ~0.1 mm for all of the tested samples. All specimens were drawn at ambient temperature and the Young's modulus was calculated in triplicate using stress-strain curves, which were instantaneously recorded by a computer.

5.2.3.7 Permeation and Salt Rejection Testing

A dead-end filtration system made of stainless steel 316 (HP4750 Stirred Cell, Sterlitech Corp., Kent, WA, US), as shown in Figure 5.2, was used to evaluate the permeation performance and the salt rejection percentages of the newly synthesized membranes. The active surface area of the membrane inside the permeation cell is 14.6 cm². The feed solution was prepared using 3.28 wt% of commercially available natural sea salt and the pressure was kept at 800 psi (55.2 bar). The salinity of the feed solution and the applied pressure were chosen to imitate the average seawater salinity and the typical applied pressure at RO plants, respectively. The membranes were tested in the reverse osmosis cell while the permeation flux of the membrane was determined by measuring the volume of the permeated water through the membrane over a certain period of time. It was calculated by the following Equation:

$$F \left(\frac{L}{m^2h} \right) = \frac{V(L)}{A(m^2)xt(h)}$$

where F is the permeate flux through the membranes per effective area of the membrane

(A) per unit time (t). Frequently, water flux unit is abbreviated as (LMH). Salt rejection of the membranes was determined by a salinity meter (TRACEABLE VWR, ISO 17025 Accredited). The reported RO experimental results were the average values obtained from at least three membrane samples prepared at different times after 8 hours of operation to reach the steady state, and the error bars represent the standard deviation.

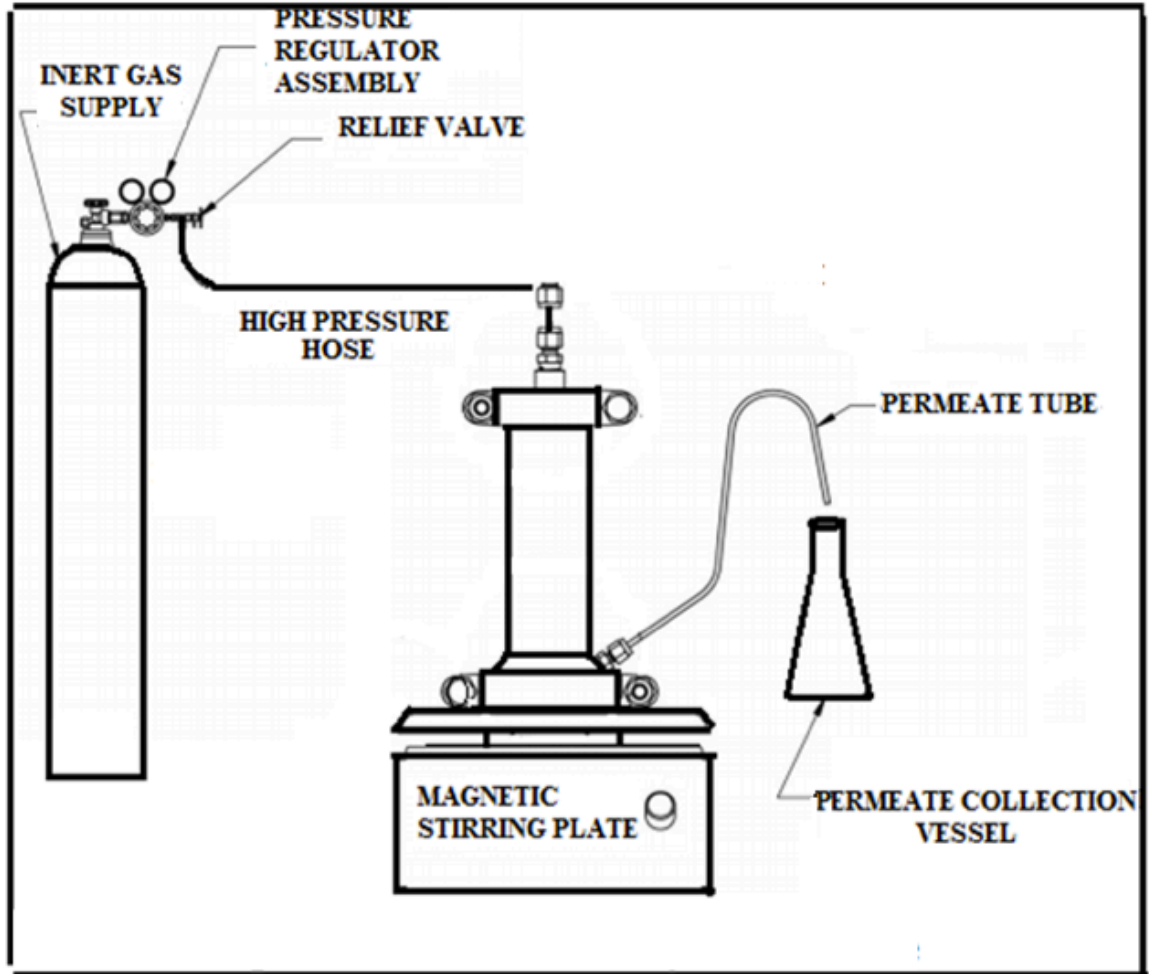


Figure 5.2 Dead-end filtration system for RO membranes.

5.2.3.8 Biofouling Resistance Testing

Diffusion Inhibition Zone (DIZ) method was conducted to examine the antimicrobial performance of the modified membranes. DIZ test was performed by following the Clinical Laboratory Standards Institute (CLSI) document M2-A9 26:1 [107]. 100 μ L bacterial inoculums were spread on the agar plates. Modified membranes were then placed in the plates and incubated for 24 hour maintaining the temperature at 30°C for the cultivation of model bacteria *Bacillus Subtilis*. The produced diffusion inhibition zones around the modified membranes were defined visually [102].

5.2.3.9 Chlorine Resistance Testing

It has been reported that the exposure to high concentration Chlorine for a short period of time is equivalent to the exposure to low concentration Chlorine for a longer period of time [104, 105]. Therefore, for lab testing purposes, it is more appropriate to expose membrane surfaces to high concentration of Chlorine for a short period of time for Chlorine resistance testing. Chlorinated solution (2000 mg/L) was prepared by diluting a commercial NaClO solution (free Chlorine content of 10 wt%) with distilled water. The pH of the prepared hypochlorite solution was adjusted to 4.0 by HCl (0.1 M) to make it more oxidative and harsh environment [106]. To perform the Chlorination experiments, water flux and salt rejection performance of the membranes were evaluated using 2000 mg/L NaCl solution and after that, the membranes were taken out of the test cells, washed with distilled water and exposed to 2000 mg/L hypochlorite solution for 2 h at pH=4.0 and 25° C. After exposure, the Chlorinated membranes were washed thoroughly with distilled water and reloaded in the test cells. The performance of the membranes was evaluated again with 2000 mg/L NaCl aqueous solution.

5.3 Results and Discussion

5.3.1 FTIR Analysis

FTIR analysis of the prepared films was conducted to confirm the existence of functional groups and all used ingredients, as shown in Figure 5.3. There is a strong and broad band at 3302 cm^{-1} , which is assigned to the hydroxyl group -OH presented in PVA and Vanillin. The band at $2977\text{-}2860\text{ cm}^{-1}$ is due to the symmetric and asymmetric vibration of the C-H of alkyl groups in PVA and DGEBA [151, 187]. The band at 1137 cm^{-1} is assigned to the C-O group in the PVA [188], while the bands at 1680 and 1584 cm^{-1} are attributed to the C=O of Vanillin and C=C of the aromatic ring present in Vanillin and DGEBA, respectively [189]. The band in the region of $1300\text{-}1200\text{ cm}^{-1}$ is assigned to C-O-C acyclic and epoxide group, while the band at 1089 cm^{-1} is associated with C-O-C cyclic group present in DGEBA [190, 191]. The -OH bending vibration is cleared at 656 cm^{-1} that is present in PVA and Vanillin.

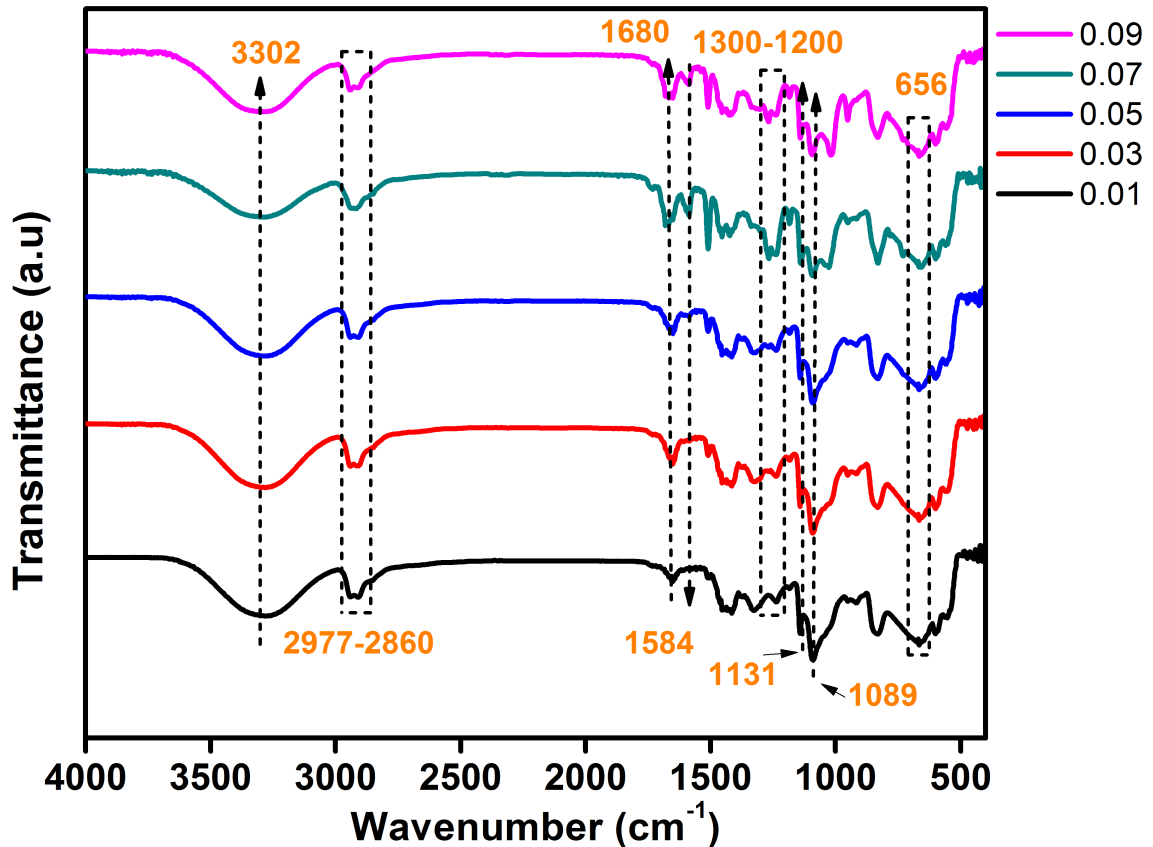


Figure 5.3 ATR-FTIR spectra of pure PVA and the PVA modified membranes with different wt% of Vanillin.

5.3.2 Contact Angle Analysis

Contact angle measurement is a tool that is used to quantify the wettability and the hydrophilicity/hydrophobicity of a solid surface [155]. Commercially available RO membranes are basically hydrophobic which makes them susceptible to adsorption by biofoulants. It has been reported that membranes with hydrophilic surfaces are less prone to fouling [41, 73]. Therefore, the synthesis of membranes with hydrophilic surfaces is favorable for fabricating biofouling resistant membranes. A thin layer of water is formed

on top of hydrophilic surfaces. This layer is important since it prevents or reduces the adsorption of biofoulants and it also enhances the permeability of the membrane [72].

5.3.2.1 Effect of Mixing Pluronic F-127 on Hydrophilicity

Figure 5.4 shows the effect of incorporating Pluronic F-127 on the surface contact angle. It is clear that Pluronic F-127 has a strong positive effect on the hydrophilicity of the membrane. It has been reported that the improvement in hydrophilicity is due to pores formation, which is a characteristic feature of Pluronic F-127 [114, 156-158]. Besides, it has been reported that Pluronic F-127 forms micelles when it is incorporated into the casting solution. The hydrophobic PPO segments amalgamate closer to the center of the micelle (core), whereas the hydrophilic PEO segments create the external layers of the micelle (corona) [156, 158, 159, 192]. Since the outer surface of the Pluronic F-127 micelle is hydrophilic, the overall hydrophilicity of the membrane improves. The hydrophilicity enhancement of the synthesized crosslinked PVA membranes was optimal with mixing 6 wt% of Pluronic F-127. A hydrophilicity decay was noticed when more than 6 wt% was incorporated. It has been reported elsewhere that the hydrophilicity reversal when additional amounts of Pluronic F-127 have been incorporated is due to the fact that the hydrophilic PEO segments of the excess amounts start to self-assemble themselves and adhere to the hydrophilic membrane surface due to the hydrophilic/hydrophilic interactions. As a consequence, the hydrophobic PPO segments will form loops away from the surface facing the feed solution [159]. Consequently, the overall hydrophilicity starts to decline after the initial enhancement. Nonetheless, even after the reversal of hydrophilicity, the modified membranes had better hydrophilicity compared to the pristine PVA membrane.

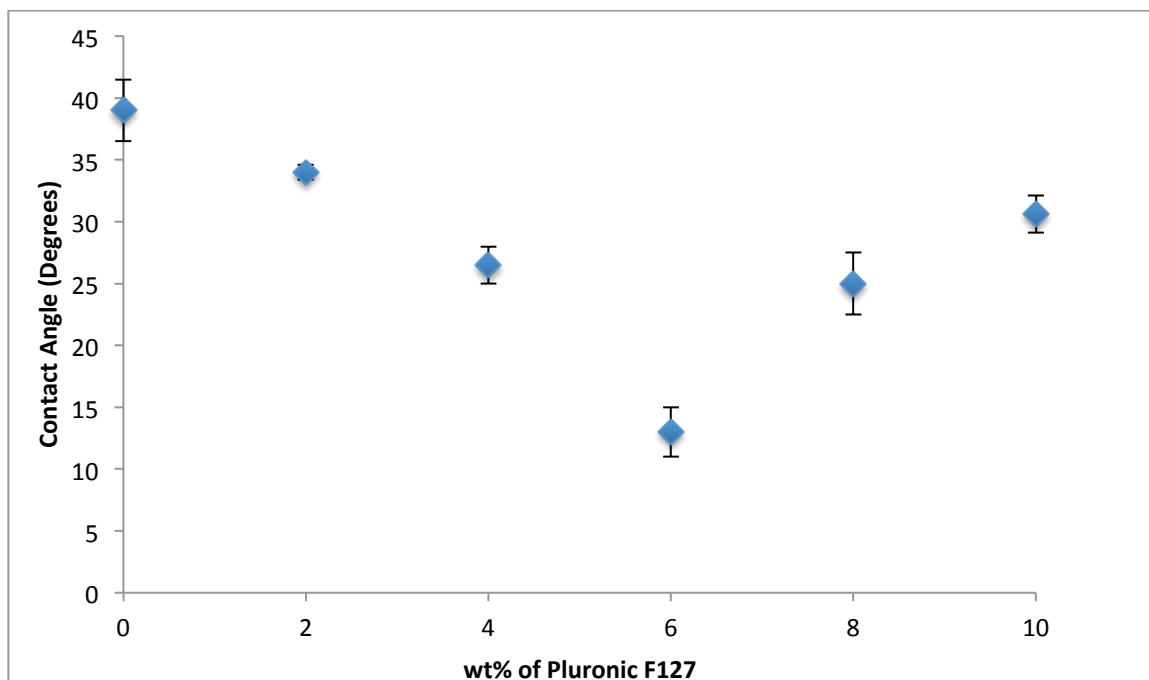


Figure 5.4 Effect of mixing Pluronic F-127 on the hydrophilicity of the PVA membrane.

5.3.2.2 Effect of Vanillin Conjugation on Hydrophilicity

Figure 5.5 demonstrates the effect of incorporating Vanillin into the membrane matrix on the hydrophilicity of the membrane surface. The curve shows reduction in the water contact angle, which indicates that the conjugation of Vanillin made the surface more hydrophilic. Vanillin is hydrophilic in nature and contains $-OH$ groups amply [193, 194]. Thus, the mixing of Vanillin with the highly hydrophilic PVA was expected to improve the overall hydrophilicity of the membrane surface.

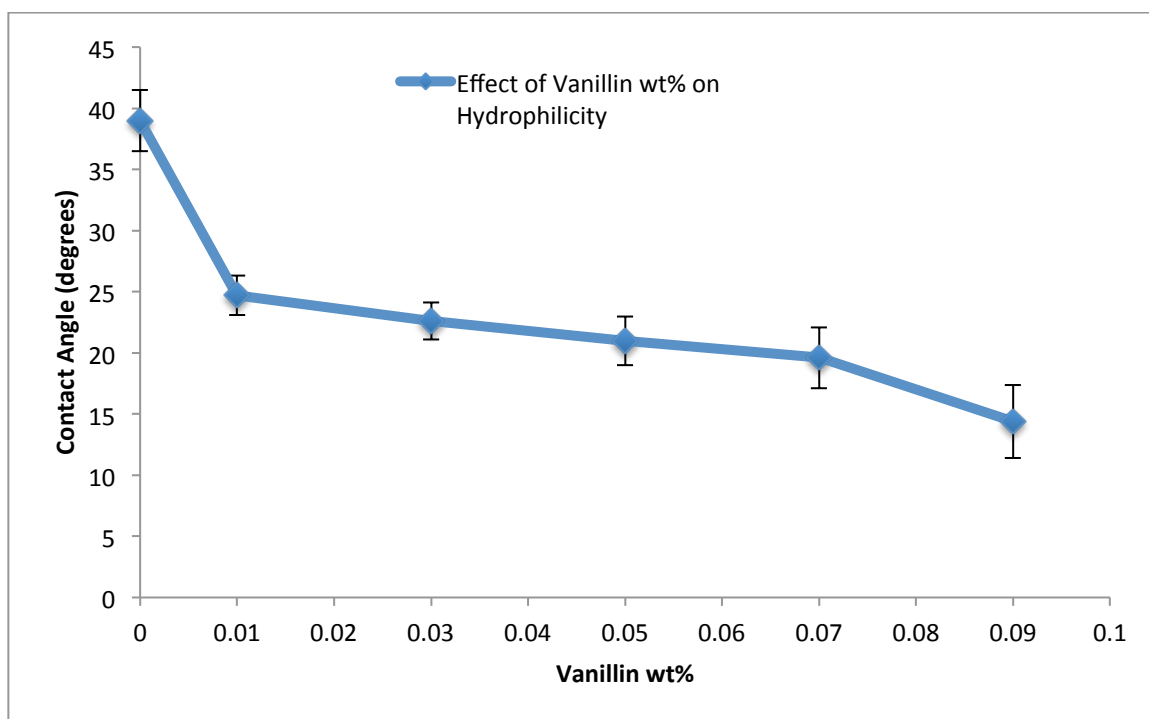


Figure 5.5 Effect of mixing Vanillin on the hydrophilicity of the PVA membrane.

5.3.3 X-Ray Diffraction

X-ray diffraction characterizes the microstructure of the synthesized membranes. Diffraction patterns of the pure PVA and the PVA membranes conjugated with Vanillin are shown in Figure 5.6. The pure PVA curve displays peaks at 11.4° , 20.02° , 23.23° , and 40.89° . The peak at 20.02° is the strongest and the sharpest. Those peaks are characteristic peaks of Pure PVA showing its semi-crystalline structure [141]. After mixing DGEBA, Pluronic F-127 and Vanillin with PVA, the strongest Peak for PVA at 20.02° becomes a little wider, which is an effect of DGEBA crosslinking. Since the hydrogen bonding influence within PVA molecules reduces as a result of crosslinking with DGEBA, the crystallinity of PVA is reduced, as well. The peaks become wider as a

result of this crystallinity decrease to represent the amorphous structure [141]. Crystalline Vanillin has a sharp characteristic peak at 13° . The absence of this peak in the XRD pattern indicates that there is a good miscibility between Vanillin and PVA. Furthermore, the new peak at 5.2° implies that there are intermolecular interactions between vanillin and PVA [195, 196].

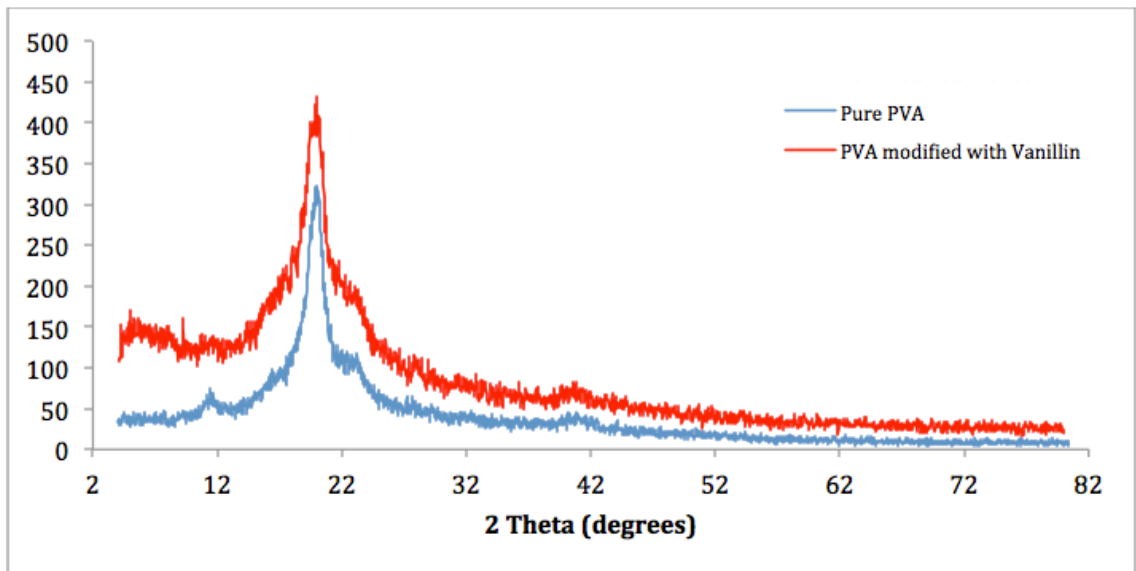


Figure 5.6 XRD patterns of pure PVA and Vanillin modified membranes.

5.3.4 Atomic Force Microscopy (AFM)

Surface roughness has a strong effect on biofouling inhibition [78]. If the membrane surface becomes increasingly rougher, the total surface area that microorganisms could be adhered to will increase. Furthermore, the ridge-valley pattern, which is a characteristic of rough surfaces, enhances the buildup of foulants on the surface [79]. Figures 5.7 & 5.8 show the effect of Vanillin weight percent on the surface roughness of the PVA reverse osmosis membranes. The surface roughness decreased considerably after the incorporation of very small amounts of Vanillin. That excellent effect on surface roughness is explained by the fact that conjugating Vanillin with PVA causes an increase in viscosity of the casting solution. This increase in viscosity impedes the exchange rate of solvent/solute diffusion during dissolution casting process and that will lead to the formation of smooth membrane surfaces [123, 197]. The small increase in surface roughness with the inclusion of larger amounts of Vanillin could be due to the fact that the excess amount of Vanillin will adhere to the surface and form the unwanted ridge-valley structure that increase the surface roughness. That effect could be seen from surface morphology images taken by SEM, which will be discussed in the following section. Nevertheless, even with the abovementioned effect, the surface roughness has improved overall with the conjugation of Vanillin. This result is excellent because, as mentioned earlier, reducing the surface roughness of the membrane leads to improved biofouling resistance and permeability.

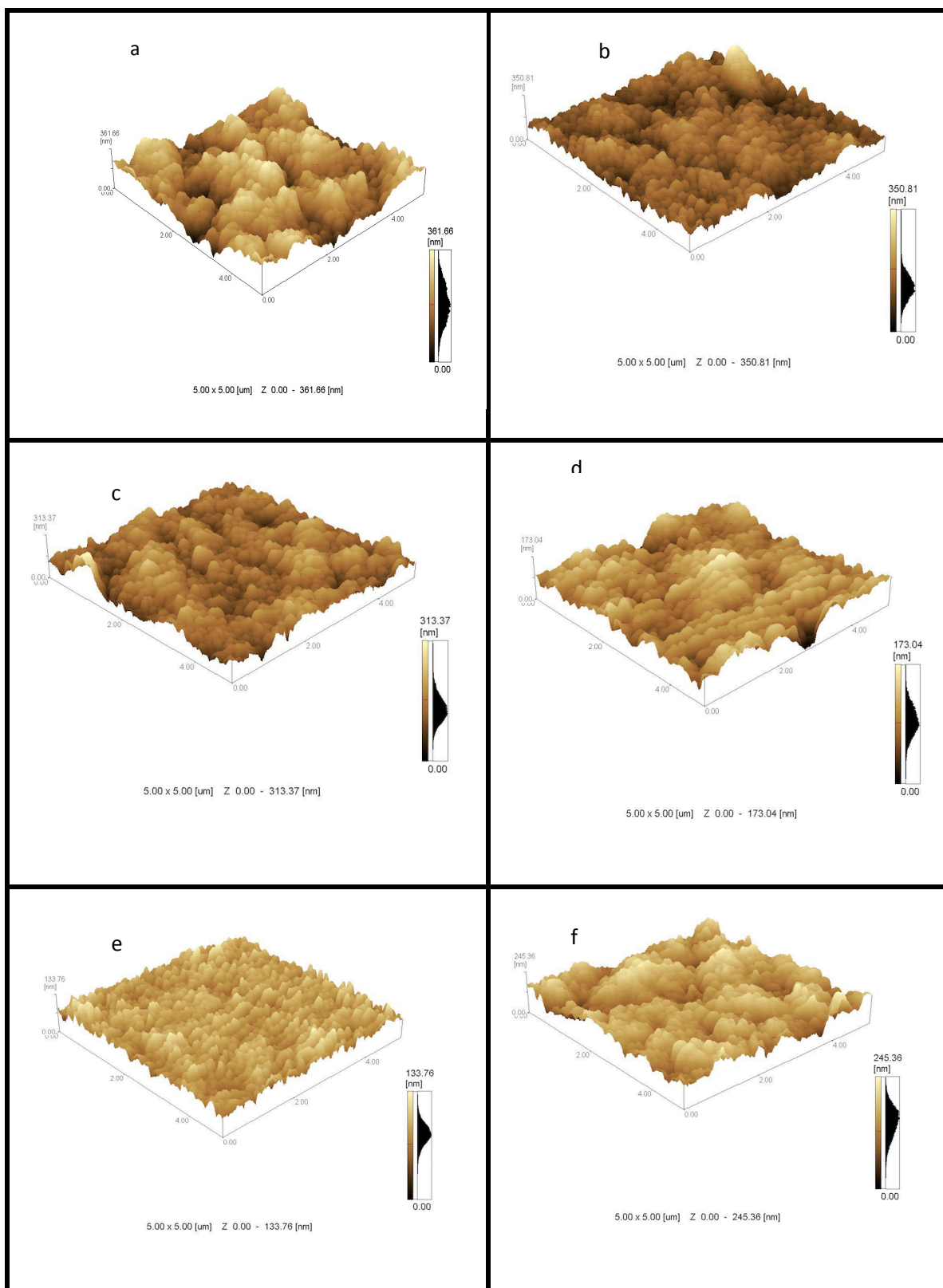


Figure 5.7 3-D AFM images of (a) pristine PVA membrane, (b) PVA-V1, (c) PVA-V2, (d) PVA-V3, (e) PVA-V4 and (f) PVA-V5.

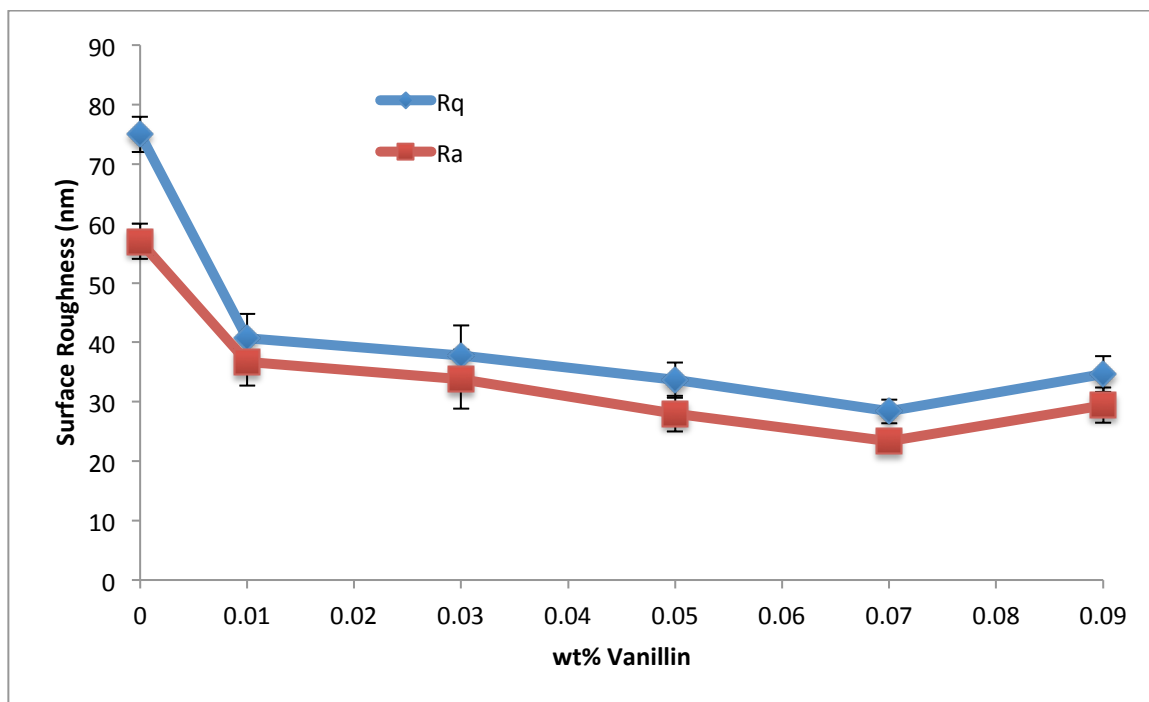
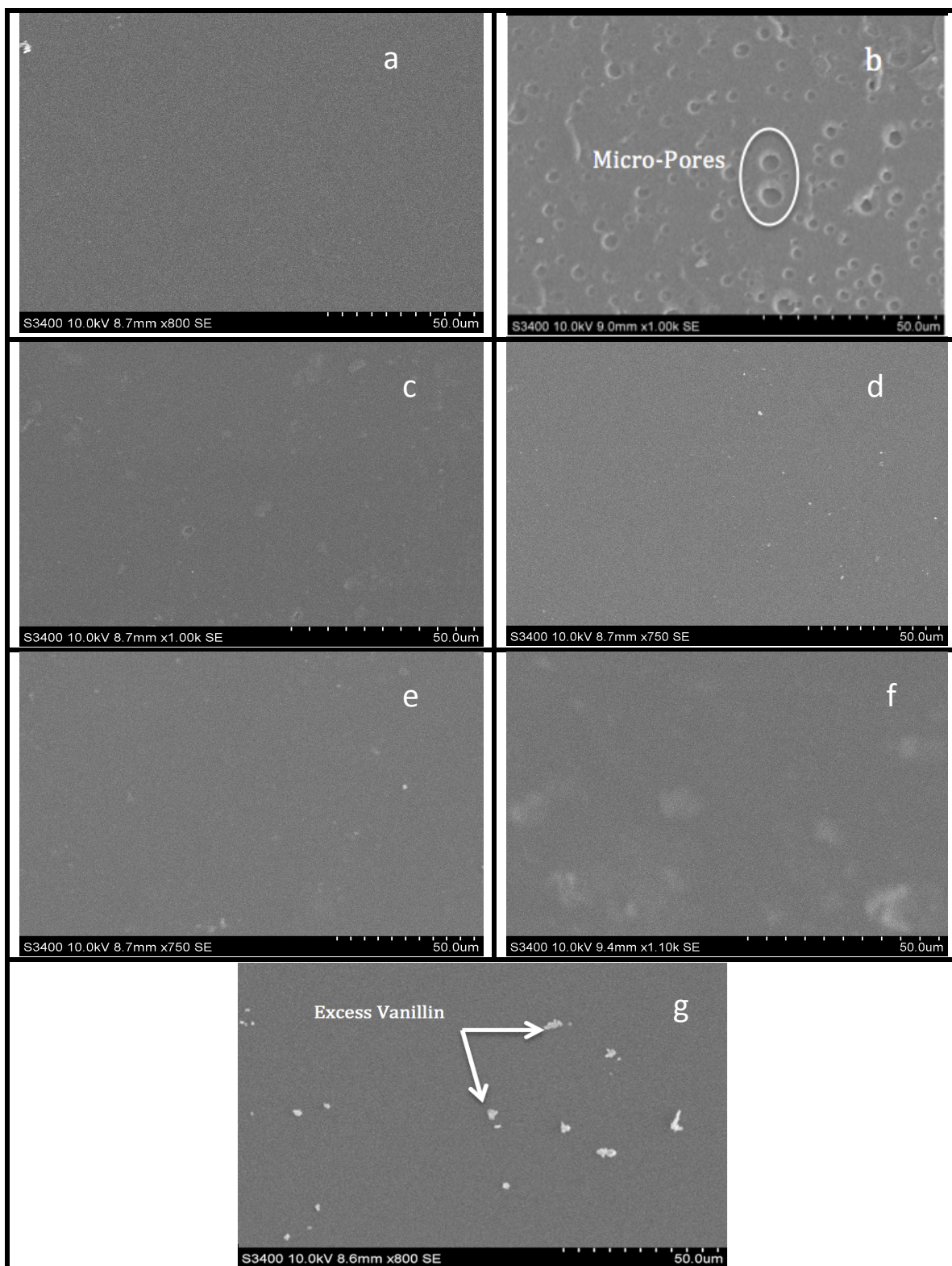


Figure 5.8 Effect of Vanillin loading on surface roughness of PVA membranes.

5.3.5 Scanning Electron Microscopy (SEM)

Reverse osmosis membranes are considered as dense membranes since the pore size is ranging from 1 to 10 Å, which is basically the size of a free volume rather than a pore [38, 51]. It has been reported that Pluronic F-127 is a pore-forming agent that increases the pore size and porosity of the resultant reverse osmosis membranes [167, 168]. Figure 5.9, (a) and (b) show SEM images of the Pristine PVA reverse osmosis membrane and the modified membranes with 6 wt% of Pluronic F-127, respectively. It is very clear from surface morphology images that the incorporation of Pluronic F-127 resulted in large pores formation. The surface morphology has changed noticeably with the inclusion of Pluronic F-172. Multiple pores ranging in size from 1 to 10 μm are clearly visible on the membrane surface.

Figure 5.9, (c-g), show the SEM images of Vanillin modified PVA membranes. It is clear from the images that as the amount of Vanillin increases, the pores sizes and the overall porosity decrease. Furthermore, excess amounts of Vanillin are visible when more than 0.5 wt% is incorporated. An explanation to this behavior is that Vanillin particles inhabit the pores that have been formed by the incorporation of Pluronic F-127. When those pores are packed, excess amounts of Vanillin will agglomerate and adhere to the membrane surface [198].



5.3.6 Mechanical Properties

Figures 5.10 & 5.11 show the stress-strain curves and the Young's modulus values for the modified PVA RO membranes with different weight percentages of Vanillin. The stress-strain curves show that as the amount of Vanillin increases the yield and tensile strengths of the modified membranes are almost doubled. The maximum yield strength of 27 MPa has been reached when maximum loading of Vanillin was conjugated, PVA-V5. The ductility of the resultant membranes was around 150%, which is too high. The membranes stiffness, represented by the Young's modulus, has improved with the conjugation of Vanillin. For PVA-V5, the stiffness of the membrane improved by 77%. The conjugation of Vanillin into the PVA matrix acts like a crosslinking agent that forms denser network structure. That dense structure will hinder internal structural relative movements during the tensile experiment, which enhances the stiffness of the membrane [195]. These results proved that the fabricated modified PVA membranes are certainly mechanically stable. During practical conditions with extremely high reverse osmosis pressure of 800 Psi, the membranes functioned properly and withstood that high pressure without damage or rupture and without the need of a supportive layer or a substrate. The utilization of the RO membranes without the use of a substrate reduces negative consequences, such as internal concentration polarization that causes an increase in the applied RO pressure.

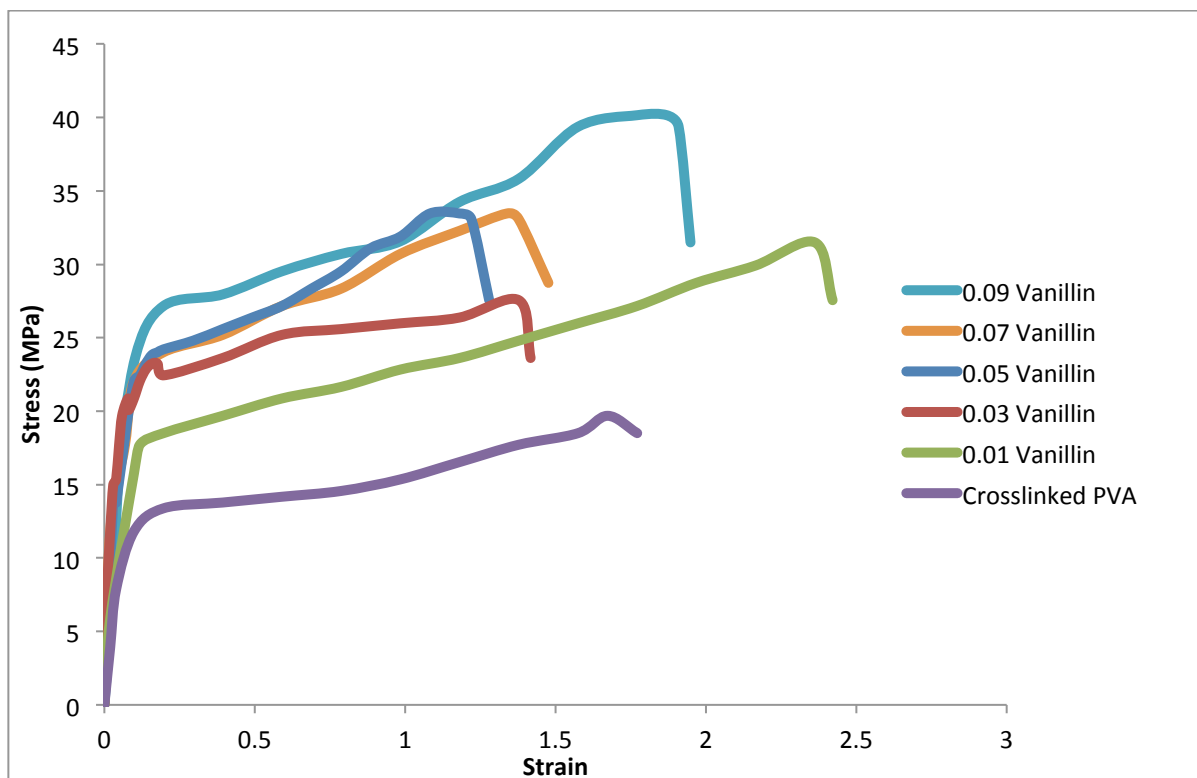


Figure 5.10 Stress-strain Curves for different Vanillin wt%.

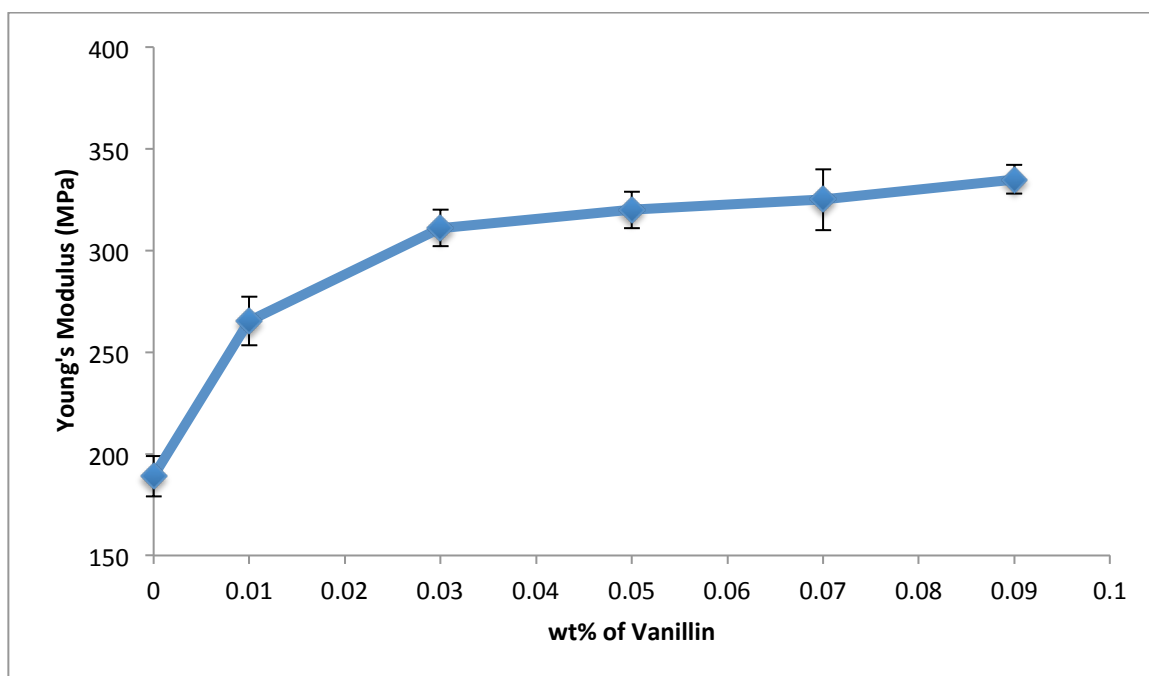


Figure 5.11 Effect of Vanillin wt% on Young's modulus of the membranes.

5.3.7 Permeate Flux and Salt Rejection

5.3.7.1 Separation performance of DGEBA crosslinked PVA membranes

Figure 5.12 shows the permeation and selectivity of the PVA crosslinked membranes with DGEBA. It shows that as the crosslinker amount increased, the selectivity improved. This is a direct effect of polymer crosslinking that creates tighter and denser morphologies due to polymer chains interlacing [88]. Conversely, permeability is reduced as the amount of DGEBA increases. This behavior could be explained the same way, as those tighter and denser polymer chains will hinder the free flow of water molecules, as well. The main reasons behind PVA membrane crosslinking are to eliminate polymer swelling and to enhance the selectivity of the membrane. Consequently, the ideal

crosslinker wt% is the one that gives the best selectivity. The optimum DGEBA weight percent of 0.16 was incorporated into all of the PVA membranes for further modifications.

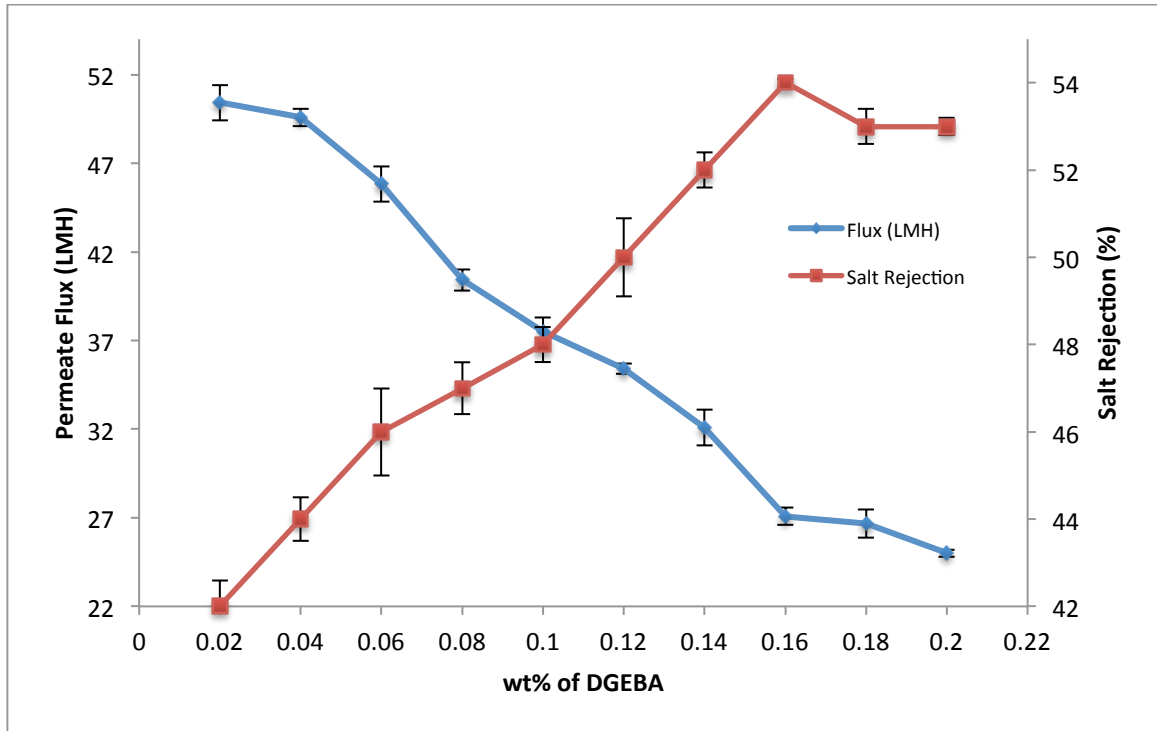


Figure 5.12 Effect of DGEBA (crosslinker) wt% on the permeation and selectivity of the membrane.

5.3.7.2 Separation performance of PVA membranes incorporated with Pluronic F-127

Figure 5.13 demonstrates the effect of the incorporation of Pluronic F-127 on the water flux and salt rejection. The water flux curve shows that as the amount of Pluronic F-127 increased, the permeation improved significantly. This could be explained by the fact that the presence of Pluronic F-127 made the membrane surface highly hydrophilic, which enhanced the diffusion of water across the membrane. Another explanation is that Pluronic F-127 is known as a pore-forming agent and it is reported that higher porosity leads to higher water fluxes [114, 156-158, 172]. The salt rejection curve shows that the selectivity improved as the amount of the added Pluronic F-127 increased up to 6 wt%. The salt rejection declines after the addition of more than 6 wt%. The reason is that adding larger amounts of Pluronic F-127 will lead to the formation of larger pores that could permit larger salt molecules to pass through the membrane. Therefore, 6 wt% of Pluronic F-127 was chosen as an optimum loading and will be infused into all of the subsequent modified membranes.

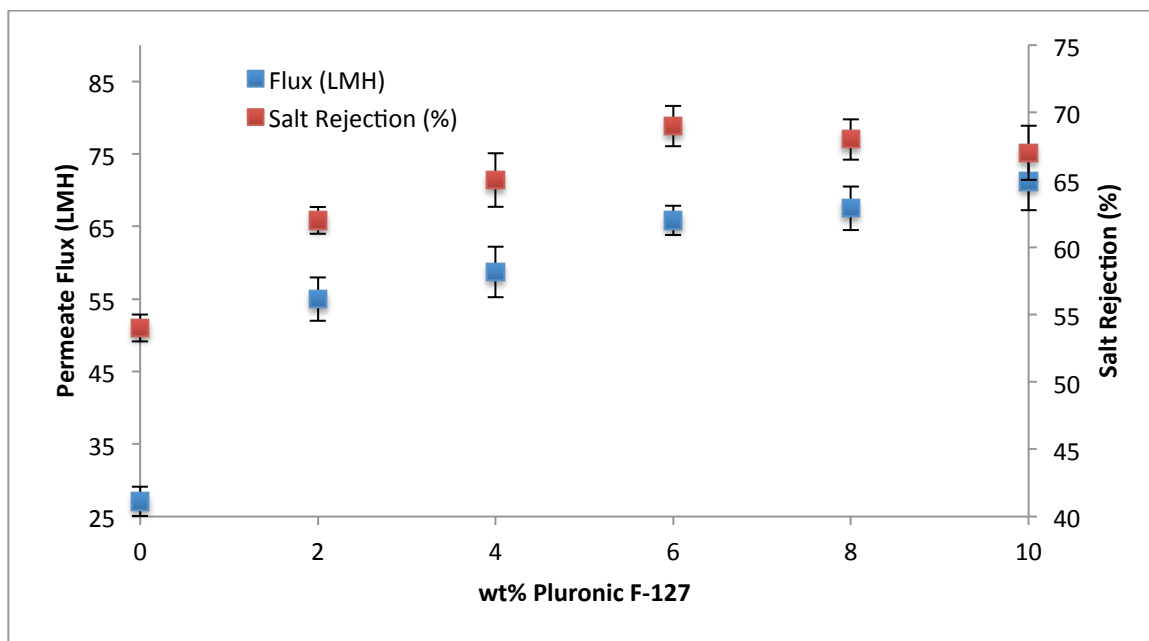


Figure 5.13 Effect of Pluronic F-127 wt% on the permeation and selectivity of the membrane.

5.3.7.3 Effect of Vanillin conjugation on PVA membranes separation performance

Figure 5.14 shows the effect of the conjugation of different weight percentages of Vanillin on the water flux through the membrane and salt rejection. The permeability was reduced slightly (less than 10%) with the conjugation of more and more Vanillin. As has been discussed earlier, the additional amounts of Vanillin tend to occupy the pores created by Pluronic F-127, which marginally affect the flow of water across the membrane. The SEM images showed that the pores get smaller and smaller as the Vanillin wt% increased.

Figure 5.14, also, shows the effect of conjugation Vanillin on the salt rejection of the synthesized membranes. Infusing small amounts of Vanillin into the polymer membrane

matrix improved the salt rejection immensely compared to the unmodified membranes. The salt rejection improved from around 50% to around 98% with the addition of 0.07 wt% Vanillin, PVA-V4. The conjugation of Vanillin into the PVA matrix acts like a crosslinking agent that forms denser network structure. That dense structure will obstruct the free passage of salt molecules [195].

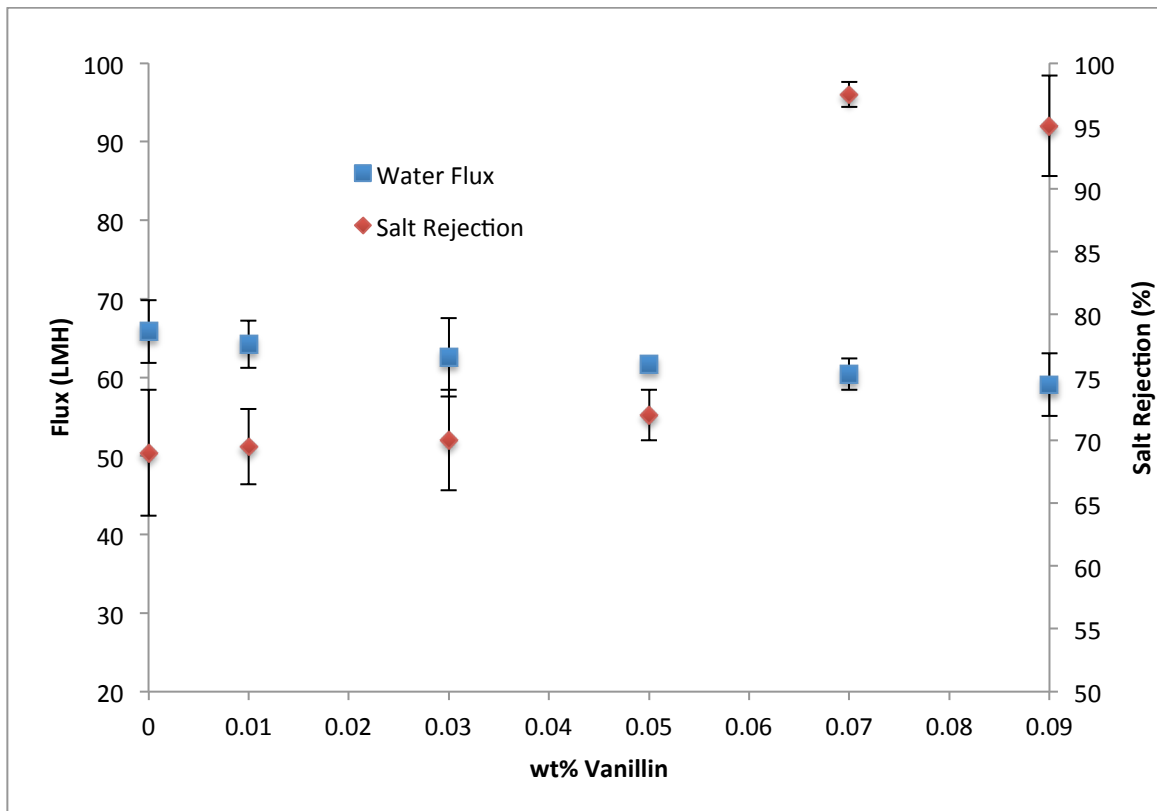


Figure 5.14 Effect of Vanillin wt% on the permeation and selectivity of the membrane.

5.3.8 Effect of Vanillin Conjugation on Membrane's Biofouling Resistance

The Diffusion Inhibition Zone (DIZ) test was conducted to analyze the biofouling resistance of the RO membranes. When an inhibition circle is generated around a membrane sample, it indicates that the membrane has an anti-microbial property [102]. Figure 5.15 shows DIZ results for *Bacillus Subtilis* bacteria. Unmodified PVA membrane sample, Figure 15 (a), showed no inhibition zones, which implies that the membrane does not possess an anti-microbial property. On the other hand, after the conjugation with Vanillin, the membrane sample displayed a clear inhibition zone, as shown in Figure 15 (b). The transversally calculated diameter of the inhibition zone was ~ 0.6 mm. This is an indication that the PVA membranes conjugated with Vanillin truly possess an anti-microbial property and are biofouling resistant.

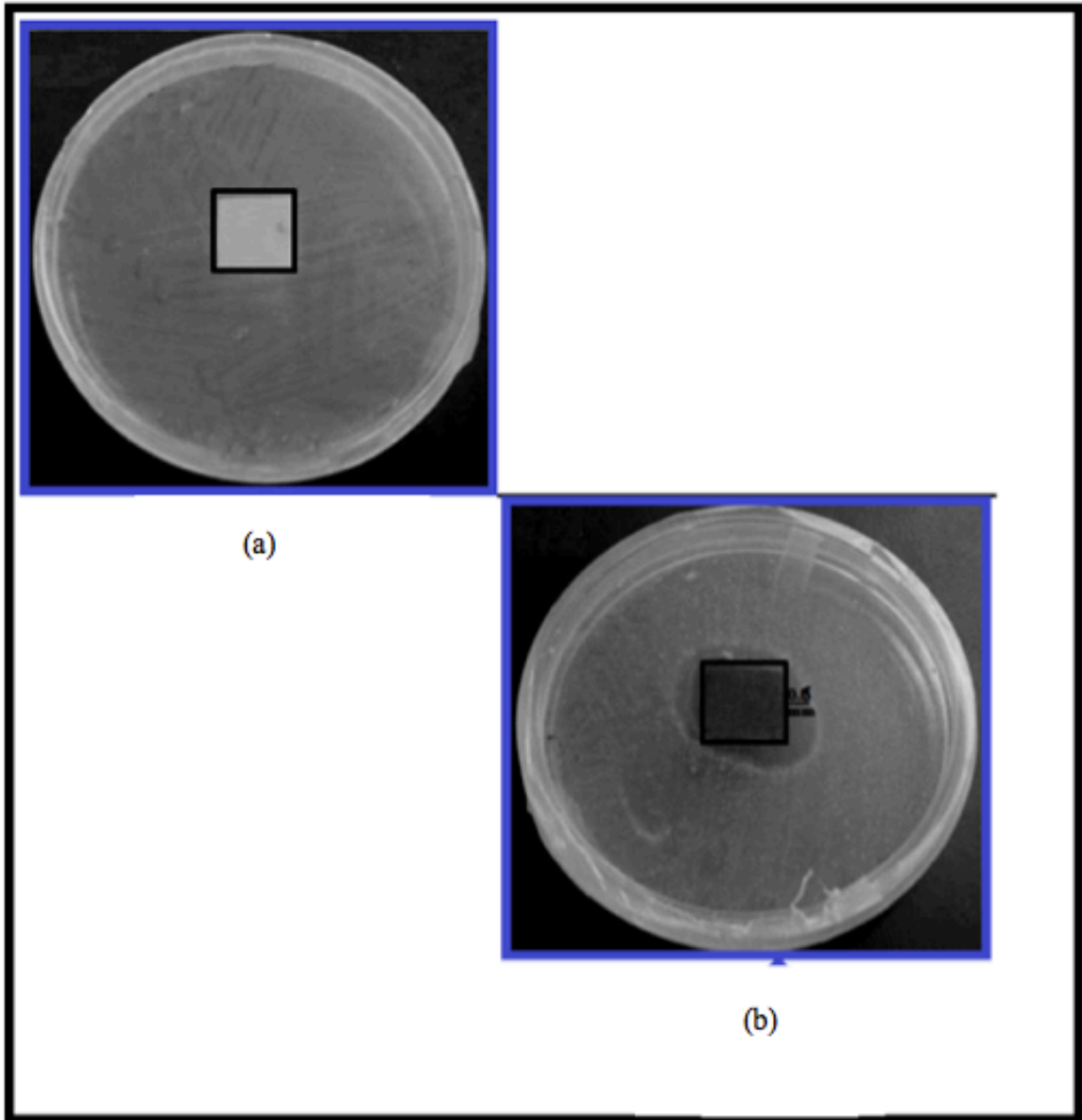


Figure 5.15 Bacteria *Bacillus Subtilis* DIZ photos of (a) unmodified PVA and (b) PVA conjugated with Vanillin.

5.3.9 Effect of Vanillin conjugation on Membrane's Chlorine Resistance

Figure 5.16 shows the comparison between the Pristine PVA membrane and the PVA membranes conjugated with Vanillin. The unmodified membrane showed poor Chlorine resistance as the salt rejection decreased from 69.1 to 41.1%, a 40% decrease in salt rejection efficiency. This indicates that the membrane surface is not Chlorine resistant and has been affected by the harsh environment caused by the presence of high concentration of Chlorine. On the other hand, once Vanillin was conjugated, the decline in salt rejection became negligible, which implies that the conjugation with Vanillin provided a more chemically stable membrane as it became more Chlorine resistant. For instance, for PVA-V3, the reduction in salt rejection was less than 4%, which is a 90% improvement of Chlorine resistance compared to pristine PVA.

Commercially available RO membranes fabricated using Polyamide (PA) are severely affected by exposure to even lower levels of Chlorine than those used in this study. The decrease of salt rejection of a typical commercially available PA membrane (SW30HR, Dow FilmTec) is more than 25% in less harsh conditions [179, 180]. The membranes fabricated in this research have a superior Chlorine resistance compared to commercial RO membranes. Chlorine resistance is crucial as it reduces the need for the de-Chlorination process that is necessary to protect the membrane material from the attack of Chlorine used for anti-fouling purposes [181].

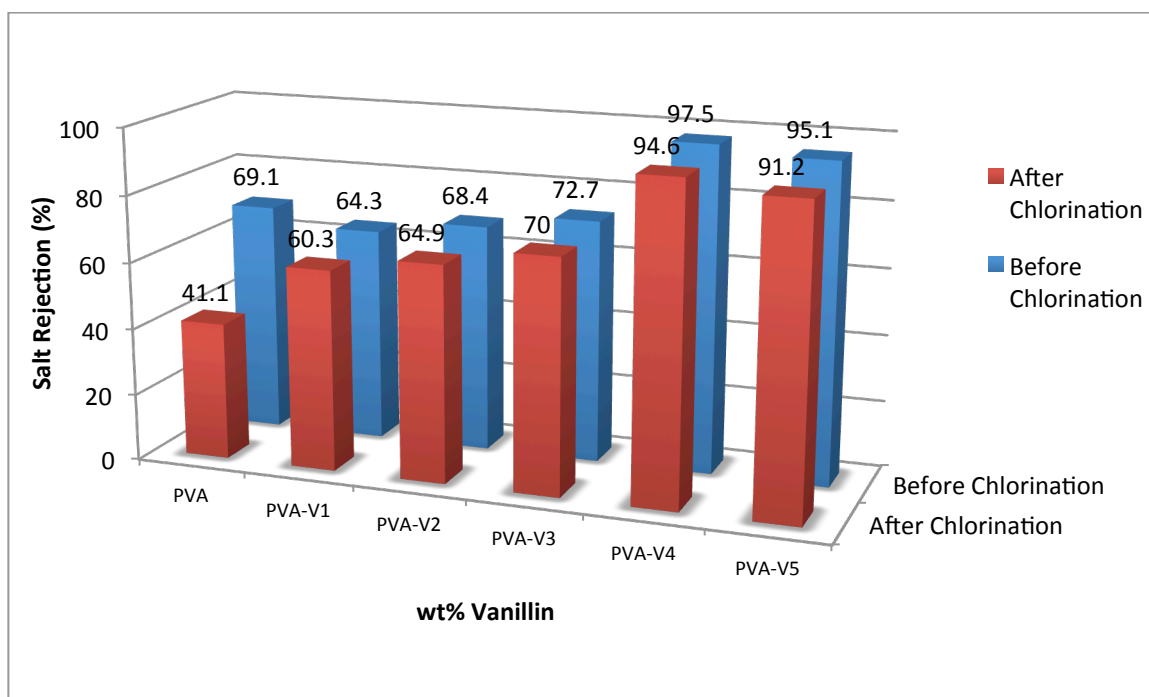


Figure 5.16 Effect of Vanillin wt% on the Chlorine resistance of the membrane.

5.4 Conclusion

The present study was designed to determine the effect of conjugating Vanillin with DGEBA crosslinked PVA membranes on the overall reverse osmosis performance. The novelty of this work is that the PVA polymer matrix membrane is utilized as an active RO layer without the use of any polymeric or ceramic substrate. Although PVA possesses excellent separation and film forming properties, researchers tend not to use PVA as an active layer in RO applications because of PVA swelling effect and the membrane rupture under high pressure. Instead, they utilize PVA as a modifier. The results of this investigation showed that the fabricated RO membrane overcame those issues through appropriate crosslinking and through incorporating Pluronic F-127 and Vanillin.

The conjugation of Vanillin improved the overall RO performance of the membrane in terms of hydrophilicity, surface roughness, salt rejection, Chlorine resistance, biofouling resistance and mechanical strength. Figure 5.17 shows a target plot that defines which RO membrane has the optimal performance. The membrane properties and performance were ranked from level 1, the innermost loop on the target, to level 10, the outermost loop; level 10 indicates ideal properties. The target plot clearly illustrates that the conjugation of Vanillin improved the overall performance vastly. From the plot, membranes PVA-V4 and PVA-V5 provided optimal salt rejection, Chlorine resistance, mechanical strength and surface hydrophilicity. Although the permeation of these two membranes is not the best, they relatively have an excellent water flux. This study paves the way for the utilization of PVA as an active layer in RO plants in the near future.

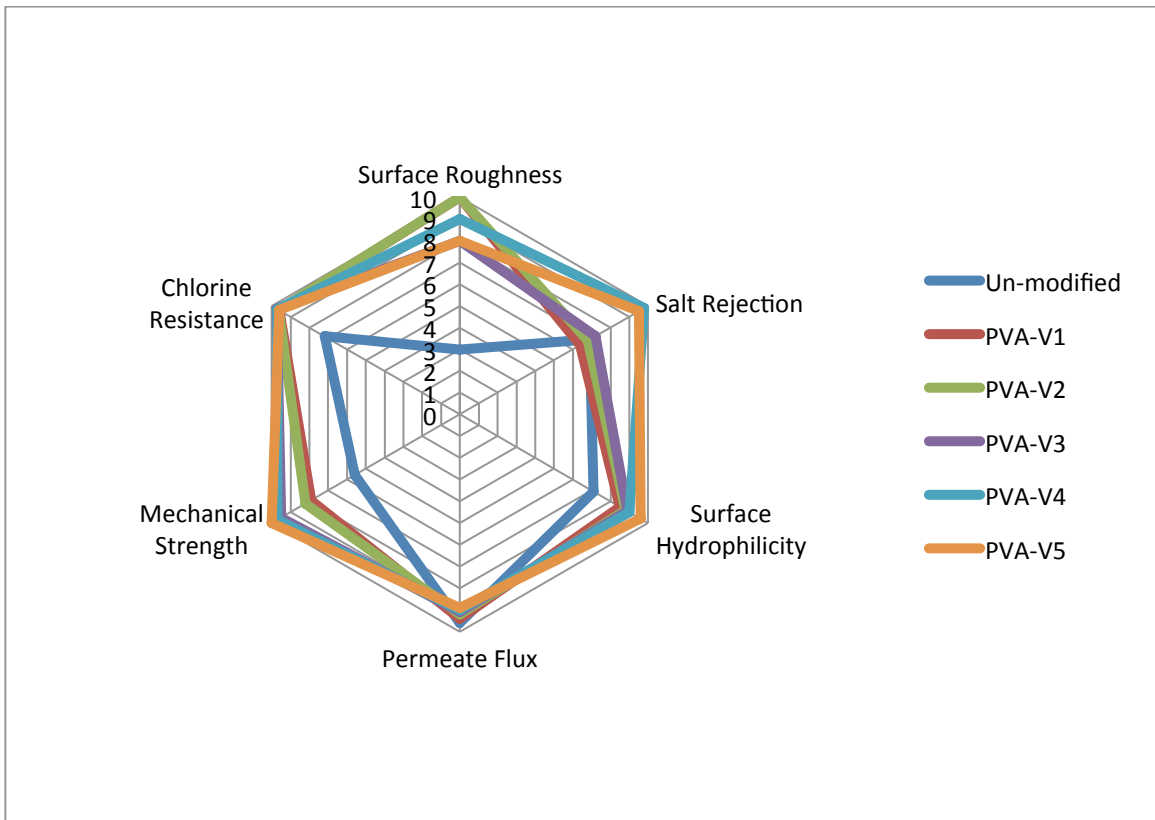


Figure 5.17 Target plot comparing RO performance properties for unmodified membranes and PVA membranes conjugated with Vanillin.

CHAPTER 6

Research on Novel Reverse Osmosis Membranes Composed of PVA Conjugated with Gum Arabic: Biofouling Mitigation and Chlorine Resistance Enhancement

6.1 Introduction

Desalination and purification of seawater and brackish water utilizing reverse osmosis (RO) technology has been progressively crucial in an effort to tackle the issue of the calamitous global fresh water resources scarcity [15, 18, 199, 200]. Due to the up-to-date advances in RO membrane technologies and their reduced cost compared to thermal desalination methods, RO became the predominant desalination technology nowadays [201].

One of the challenges that affect the RO process is membrane biofouling that causes a significant decline in performance. Due to membrane fouling, RO modules need to be cleaned and chemically treated frequently. Cleaning and pretreatment ultimately shorten the membrane life, and that increases the cost of the overall process [52, 61]. Membrane biofouling is the buildup of microbial layers on the surface or within the pores of the membrane. Micro-organisms such as bacteria, algae and fungi are pseudo particles, which means that they can grow, multiply or even relocate. Hence, biofouling occurs even after feed water pretreatment and after the application of disinfectants [42, 48, 51-55]. The buildup of a biofilm on the surface of the membrane causes several adverse effects including, operating pressure increase, loss of salt rejection, membrane bio-degradation and flux decline [64, 65].

In this research, novel crosslinked PVA/Pluronic F127 membranes conjugated with Gum

Arabic were synthesized using dissolution casting to investigate the biofouling and Chlorine resistance and to analyze the overall RO performance.

Poly (vinyl alcohol) (PVA) is a highly hydrophilic water-soluble biodegradable polymer with good film-forming properties and outstanding thermal, mechanical and chemical stability. It is considered as one of the best polymers to fabricate membranes with high chemical stability, good Chlorine tolerance and excellent fouling resistance. Subsequently, PVA has been utilized by many researchers to fabricate membranes for separation and pressure driven processes such as microfiltration, ultrafiltration, reverse osmosis and pervaporation [81-87]. One of the drawbacks that are associated with the use of PVA in aqueous media is swelling, which occurs due to its very high hydrophilicity that makes it an open structure. Swelling affects the membrane performance, primarily the membrane solute rejection. Therefore, crosslinking of PVA is needed to balance the hydrophilic-hydrophobic properties of such membranes [88-90]. PVA could be crosslinked using multifunctional compounds like dicarboxylic acids, dialdehydes and dianhydrides, which could react with the -OH groups of PVA [91-96].

Gum Arabic (GA) is a well-known hydrophilic, negatively charged, non-toxic natural composite polysaccharide derived from the excretions of Acacia Senegal and Vachellia Seyal trees [202, 203]. It is an arabinogalactan polysaccharide that consists of three distinctive segments and is composed of more than 97% carbohydrates and less than 3% proteins [204]. It is one of the widely accepted constituents in the pharmaceutical, cosmetic and food industries [204, 205]. Gum Arabic is proven to have excellent antibacterial properties, which play an important role in membranes biofouling mitigation [206-208]. Furthermore, Gum Arabic has shown superb surface activity and viscoelastic

film forming capabilities [209-211].

Polyethylene oxide–polypropylene oxide–polyethylene oxide (PEO–PPO–PEO) triblock copolymers, known as Poloxamers or Pluronics are amphiphilic copolymers comprising hydrophilic PEO segments and hydrophobic PPO segments. Compared to other Pluronics, Pluronic F127 has high extractability into aqueous phase, high molecular weight (M_w 12,600) and good hydrophilic/lipophilic balance value (HLB = 22) [113, 114]. The incorporation of Pluronic F127 into PVA thin films enhances the separation performance of membranes, as it has been reported in literature [114, 115]. Additionally, It has been reported that amphiphilic copolymers can alter the diffusion rate of water through membranes, which increases the permeate flux through the membrane [114, 116-118].

Many researchers have used PVA as a hydrophilic modifier or as a coating on polymeric or ceramic surfaces for many separation applications [69, 81, 100, 101, 111, 129-150, 186]. Nonetheless, to the best of our knowledge, no research has been presented on the use of crosslinked PVA incorporated with Pluronic F127 and conjugated with Gum Arabic as an active layer in reverse osmosis application without the use of polymeric or ceramic substrates. The use of the polymer as an active layer without a substrate reduces some negative consequences, such as internal concentration polarization that may cause an increase in the applied pressure. As mentioned earlier, in this research, crosslinked PVA membranes incorporated with Pluronic F127 and conjugated with Gum Arabic for RO were fabricated. The newly synthesized membranes were then characterized and analyzed using various techniques like attenuated total reflection Fourier transform infrared spectroscopy (ATR-FTIR), contact angle measurements, X-ray diffraction

(XRD), scanning electron microscopy (SEM), atomic force microscopy (AFM) and mechanical testing. The actual reverse osmosis performance of the membranes, including permeation testing, salt rejection and Chlorine resistance, was analyzed using a dead-end RO permeation unit.

6.2 Experimental Procedure

6.2.1 Materials

Analytical grade PVA (Mw=89000), Gum Arabic (Mw=250,000), bisphenol A diglycidyl ether (DGEBA) (crosslinker), Pluronic F127 (average molecular weight: 12.6 kDa), dimethyl sulphoxide (DMSO) and sodium hypochlorite (NaClO) were acquired from Sigma Aldrich (St Louis, MO, USA). All chemicals were used without further purification.

6.2.2 Membrane Casting

6.2.2.1 Crosslinking of PVA with DGEBA

Various weight percentages of DGEBA crosslinker, as shown in Table 6.1, were mixed into PVA solutions, where DMSO was used as a solvent with a 17:83 solute/solvent weight percent ratio. The mixing was performed at 70° C for 2 hours with continuous stirring until a homogenous, transparent solution was produced. Utilizing the dissolution casting method, the solution was then transferred slowly into identical Petri dishes with identical amounts of the solution to insure uniformity. Petri dishes were then heated to 65°C in a controlled evaporation environment to assure uniform film thicknesses of 0.1 mm, measured by a screw gauge. After complete evaporation, the thin film membranes

are removed from the Petri dishes with the aid of sharp blades. Five membranes are synthesized from each concentration for testing. The resultant dense membranes are examined for swelling, permeation and salt rejection to come up with the optimal crosslinker weight percent. As will be demonstrated in the results section, the 0.16 wt% of DGEBA provided the optimum membrane properties, thus, the weight percent of 0.16 was used for further modifications.

6.2.2.2 Incorporation of Pluronic F127 into the crosslinked PVA membranes

Various weight percentages of Pluronic F127, as shown in Table 6.1, were blended into the solutions of PVA and 0.16 wt% of DGEBA. The solution preparation and the film casting method followed the procedure mentioned in the previous section. The resultant composite membranes with different weight percentages of Pluronic F127 were characterized and evaluated. The overall evaluation of the Pluronic F127 membranes as will be detailed later on, showed that 6 wt% of Pluronic F127 is the optimal percentage and was used for further modifications. Figure 6.1 shows a scheme of the chemical reaction.

6.2.2.3 Conjugation of Gum Arabic with the modified PVA membranes

Five weight percentages of Gum Arabic, shown in Table 6.1, were conjugated with the solution of crosslinked PVA and 6 wt% of Pluronic F127 to synthesize the thin film membranes. The membrane casting followed the abovementioned dissolution casting method.

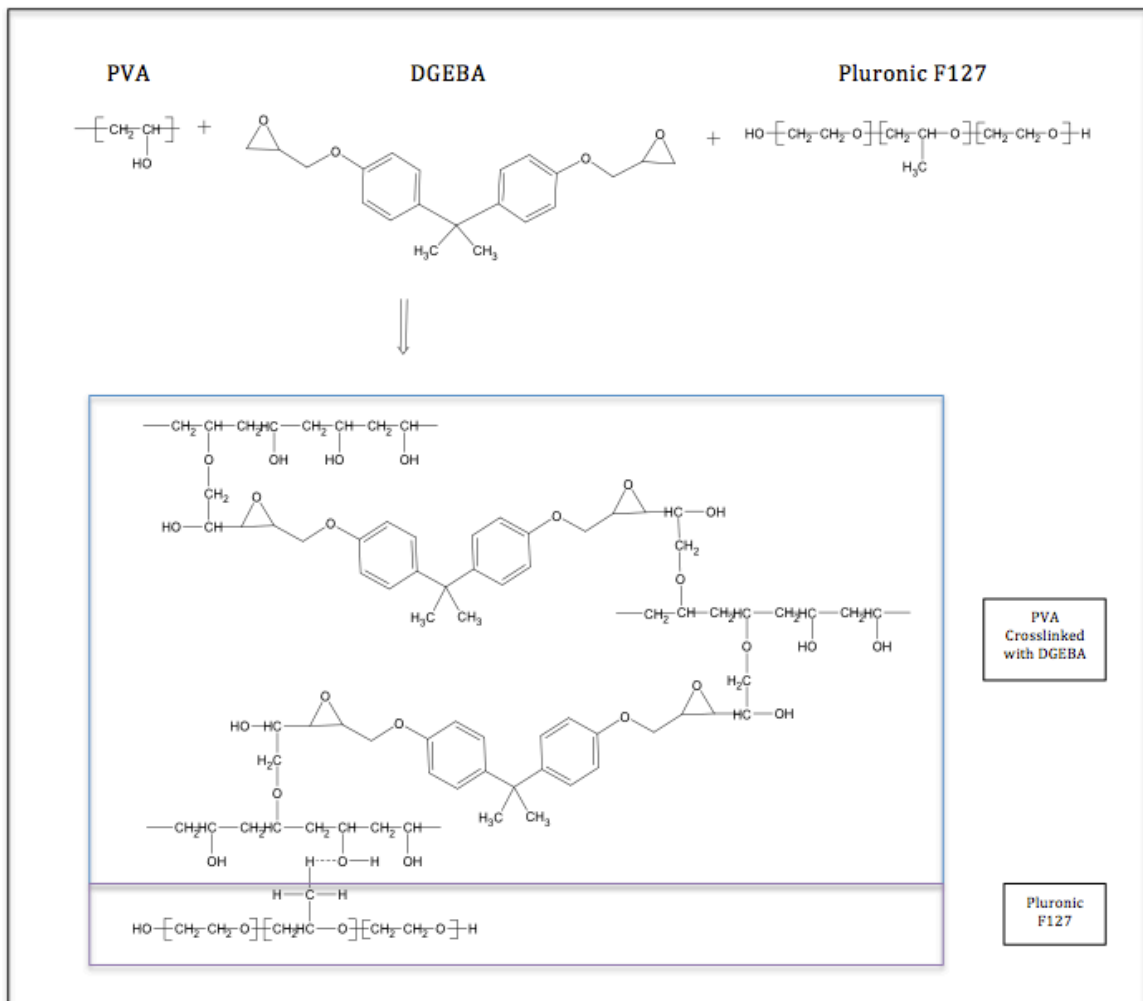


Figure 6.1 Schematic diagram of the crosslinking of PVA with DGEBA and the intermolecular hydrogen bonding with Pluronic F127.

Table 6.1 Weight percentages of DGEBA, Pluronic F127 and Gum Arabic in PVA solution.

	Weight Percentages (wt%)									
DGEBA	0.02	0.04	0.06	0.08	0.1	0.12	0.14	0.16	0.18	0.2
Pluronic F127*	2	4	6	8	10					
Gum Arabic**	0.1	0.3	0.5	0.7	0.9					
Labels	PVA-GA-1	PVA-GA-2	PVA-GA-3	PVA-GA-4	PVA-GA-5					
*with 0.16 wt% DGEBA.										
**with 0.16 wt% DGEBA and 6 wt% Pluronic F127										

6.2.3 Membranes Characterization

6.2.3.1 Fourier Transform Infrared Spectroscopy (FTIR)

An IR Prestige-21 (Shimadzu) using attenuated total reflectance (ATR) accessory equipped with zinc selenide (ZnSe) crystal was used to obtain FTIR spectra of the composite membrane samples. Before each sample scan, an air background of the instrument was run. The frequency range was from 4000-600 cm^{-1} at a resolution of 4.0 cm^{-1} and average of 120 scans per spectrum were reported.

6.2.3.2 X-Ray Diffraction Measurements

An X'pert PRO Diffractometer (PANalytical) was used to characterize the structure of the synthesized composite membranes. The instrument uses monochromatized $\text{CuK } \alpha_1$

radiation with wavelength of 1.540 Å from a fixed source operated at voltage 40 kV and current 40 mA. The scanning range was from 4° to 80°.

6.2.3.3 Scanning Electron Microscopy (SEM)

A Scanning Electron Microscope (S-3400N Hitachi, USA) was used to attain SEM micrographs of the fabricated membranes. The SEM was operated under low vacuum mode to analyze the samples. Samples were gold sputtered for 120 s before they are placed into the SEM to make sure no surface charging occurs. Gold sputtering was performed using Denton Vacuum Sputtering Automatico Desk IV.

6.2.3.4 Atomic force microscopy (AFM)

AFM imaging and analysis (Digital Instruments, Santa Barbara, CA, US) were utilized to characterize membrane surface morphological structures and to determine membrane's quantitative surface roughness, respectively. Topographical images were taken using standard tapping mode. A cantilever oscillated sinusoidally at 350 kHz resonant frequency, and briefly contacted the sample surface at the down stroke of each sinusoidal cycle. A user-established set point force was fixed so that the sample surface was minimally deformed and used as a feedback control. Scanned images were taken at 512 x 512 pixel resolution. The values of root mean square (RMS) roughness were extracted from AFM images through the calculation of the average of the values measured in random areas. The membrane surface morphology was expressed in terms of various roughness parameters, like mean roughness (Ra). It is calculated by the following equation [108, 109]:

$$Ra = \frac{1}{n} \sum_{i=1}^n |z_i|$$

where z_i is the height or depth of the i th highest or lowest deviation and n is the number of discrete profile deviations. Root-mean-square surface roughness (R_q) is defined as the root-mean-square (RMS) of the deviations in height from the profile mean and it is calculated by [109]:

$$R_q = \sqrt{\frac{1}{n} \sum_{i=1}^n z_i^2}$$

6.2.3.5 Contact Angle Measurements

A Goniometer (Digidrop, KSV Instruments) was used to calculate sessile drop contact angle of the reverse osmosis membranes. The equilibrium value was average of right and left angles of the drop that are calculated from the software fitting. The reported data is the average of three measurements from different locations for each membrane sample.

6.2.3.6 Mechanical Testing

Universal Tensile Testing Machine Instron 5567 fitted with a 10 kN load cell was used to calculate the mechanical properties of the fabricated membranes. Those mechanical properties include the stress strain curves, ultimate tensile strength, elongation at break and the Young's modulus. The shape of the membrane sample was used as per ASTM D-638 standard with gauge length and width of 50 and 10 mm, respectively. Three specimens were tested for each membrane and the average value was recorded at a crosshead speed of 10 mm/min. The thickness of the membrane samples was measured

using a micro-caliper and maintained at 0.1 mm for all of the tested samples. All specimens were drawn at ambient temperature and the Young's modulus was calculated in triplicate using stress-strain curves, which were instantaneously recorded by a computer.

6.2.3.7 Permeation and Salt Rejection Testing

A dead-end filtration system made of stainless steel 316 (HP4750 Stirred Cell, Sterlitech Corp., Kent, WA, US), as shown in Figure 6.2, was used to evaluate the permeation performance and the salt rejection percentages of the newly synthesized membranes. The active surface area of the membrane inside the permeation cell is 14.6 cm². The feed solution was prepared using 3.28 wt% of commercially available natural sea salt and the pressure was kept at 800 psi (55.2 bar). The membranes were tested in the RO cell while the permeation flux of the membrane was calculated by determining the volume of the permeated water through the membrane over a certain period of time. It was calculated by the following Equation:

$$F \left(\frac{L}{m^2h} \right) = \frac{V(L)}{A(m^2) \times t(h)}$$

where (F) is the permeate flux through the membranes, which is the permeate volume (V) per effective area of the membrane (A) per unit time (t). Frequently, water flux unit is abbreviated as (LMH). Salt rejection of the membranes was determined by a salinity meter (Traceble VWR, ISO 17025 Accredited). The reported permeate flux and salt rejection values were the average values obtained from at least three membrane samples prepared at different times after 8 hours of operation to reach the steady state, and the error bars represent the standard deviation.

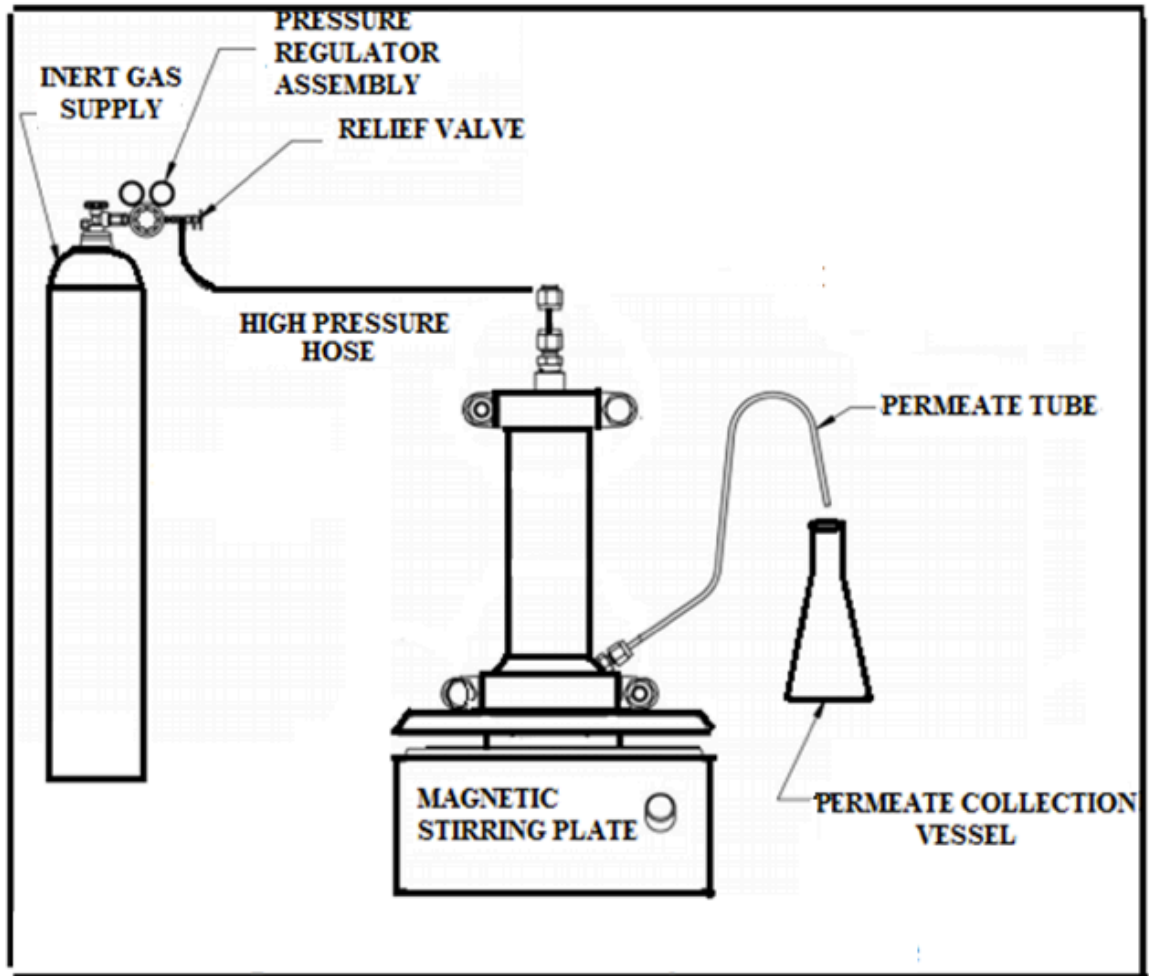


Figure 6.2. Dead-end filtration system for RO membranes.

6.2.3.8 Chlorine Resistance Testing

It has been reported that there is an equivalent resultant effect when comparing high concentration Chlorine exposure for a short period of time to low concentration Chlorine exposure for a longer period of time [104, 105]. Thus, it is more convenient to expose the membrane surface to a high concentration of Chlorine for a short period of time for Chlorine resistance testing. Chlorinated solution (2000 mg/L) was prepared by diluting a commercial NaClO solution (free Chlorine content of 10 wt%) with distilled water. The pH of the prepared hypochlorite solution was adjusted to 4.0 by HCl (0.1 M) to make it more oxidative and harsh environment [106]. To perform the Chlorination experiments, water flux and salt rejection performance of the membranes were evaluated using 2000 mg/L NaCl solution and after that, the membranes were taken out of the test cells, washed with distilled water and exposed to 2000 mg/L hypochlorite solution for 2 h at pH=4.0 and 25° C. After exposure, the Chlorinated membranes were washed thoroughly with distilled water and re-loaded in the test cells. The performance of the membranes was evaluated again with 2000 mg/L NaCl aqueous solution.

6.2.3.9 Biofouling Resistance Testing

Antibacterial test was carried out using *Escherichia coli* by JIS L 1902–2002 methodology. Broth (30 mL) was arranged in conical flasks. All flasks were autoclaved at 125 °C having a pressure of 15 psi for 30 min. After autoclaving DH5 alpha *E. coli* strain (100µl) was protected in the flasks. The unmodified and modified membranes were added in each conical flask. All flasks were nurtured at 35 °C in an incubator for 24 h. After nurturing, 600 nm optical density (OD) was observed by a spectrophotometer.

6.3 Results and Discussion

6.3.1 FTIR analysis

FTIR analysis was carried out to confirm the interactions between PVA and Gum Arabic in the presence of the crosslinker (DGEBA) and Pluronic F127, as shown in Figure 6.3. The strong bands at 3324 and 2932 cm^{-1} are ascribed to hydrogen bonded $-\text{OH}$ and $-\text{CH}$ stretching vibrations, respectively, existed in PVA and DGEBA [151, 187]. The bands at 1300 and 1089 cm^{-1} are characteristic bands for C-O-C cyclic in gum Arabic and DGEBA and C-O-C acyclic groups present in, Pluronic F127, Gum Arabic and DGEBA, respectively, while a weak band at around 1500 cm^{-1} is attributed to the aromaticity of the ring present in DGEBA [152, 190]. The band at 1408 cm^{-1} in all spectra ascertained the existence of C-O bond in PVA and Gum Arabic [188]. The sharp band at 1648 cm^{-1} denotes the presence of carbonyl group that Pluronic F127 possesses.

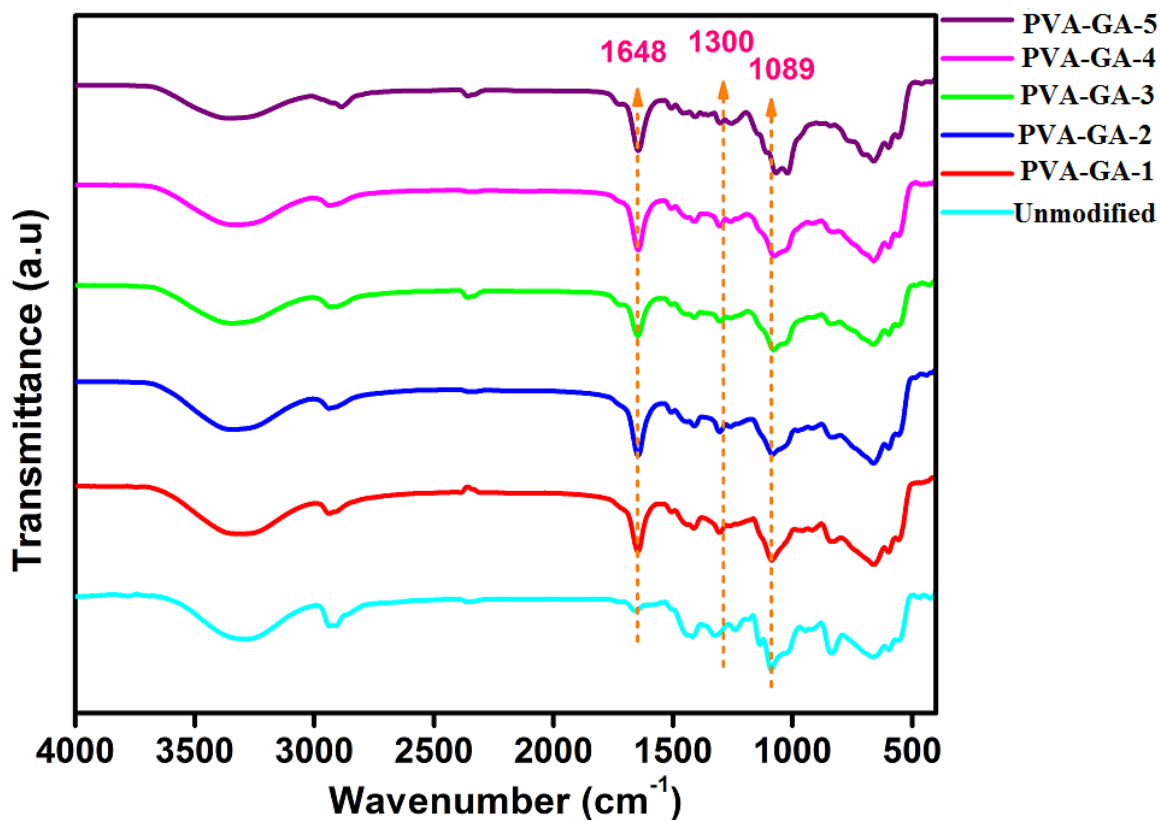


Figure 6.3 ATR-FTIR spectra of pure PVA and PVA conjugated with Gum Arabic membranes.

6.3.2 X-Ray Diffraction

Figure 6.4 shows the XRD curves for the Pure PVA membrane and the modified membranes with different weight percentages of Gum Arabic. The pure PVA XRD curve shows peaks at 11.4° , 20.02° , 23.23° , and 40.89° . The strongest and most obvious peak is at 20.02° . Those are distinctive peaks of Pure PVA that demonstrate its semi-crystalline structure [141]. Upon conjugation of DGEBA, Pluronic F127 and Gum Arabic with PVA, the sharp Peak for PVA at 20.02° became wider. This observation implies that the crystalline structure of PVA was disturbed after conjugation with naturally amorphous

Gum Arabic [209]. It has been reported that incorporation of polysaccharides would increase polymer chains mobility and this causes rapid growth of film structures. Those structures hinder the molecular chains arrangements, which leads to decreased crystallinity [210]. At the maximum loading of Gum Arabic, PVA-GA-5, the sharp PVA peak completely diminished which implies that the microstructure became essentially amorphous.

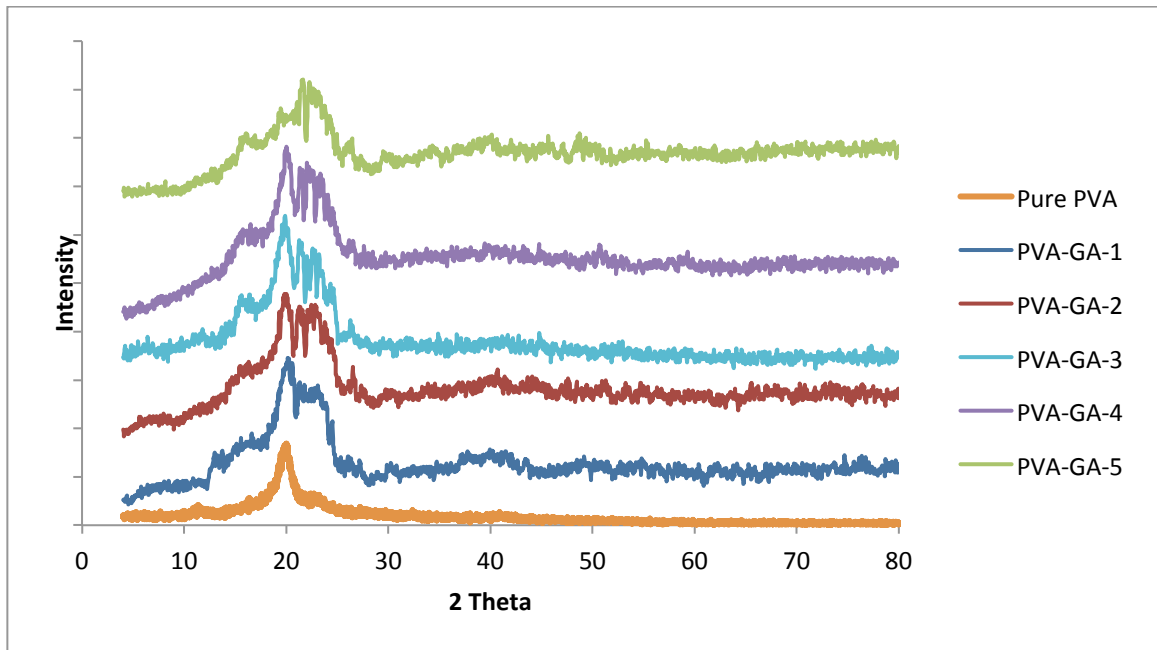


Figure 6.4 Diffractograms of pure PVA and Gum Arabic modified membranes.

6.3.3 Scanning Electron Microscopy (SEM)

Figure 6.5, (a) and (b) display SEM images of the Pristine PVA reverse osmosis membrane and the modified membranes with Pluronic F127, respectively. The surface morphology images proved that the incorporation of Pluronic F127 resulted in large pores formation in the order of 1-10 μm . It has been reported that Pluronic F127 is a pore-forming agent that increases the pore size and porosity of the resultant reverse osmosis membranes [167, 168]. Figure 6.5 (c-g) show the SEM images of PVA membranes conjugated with several weight percentages of Gum Arabic. The images show that as the amount of Gum Arabic increases, the pores sizes and the overall porosity decrease. Besides, PVA-GA-4 and PVA-GA-5 showed some agglomerations of the excess amounts of Gum Arabic. The crosslinking effect that the polysaccharide imposed on PVA polymer chains made the membrane surface more compact and smooth with fewer pores and less overall porosity [210].

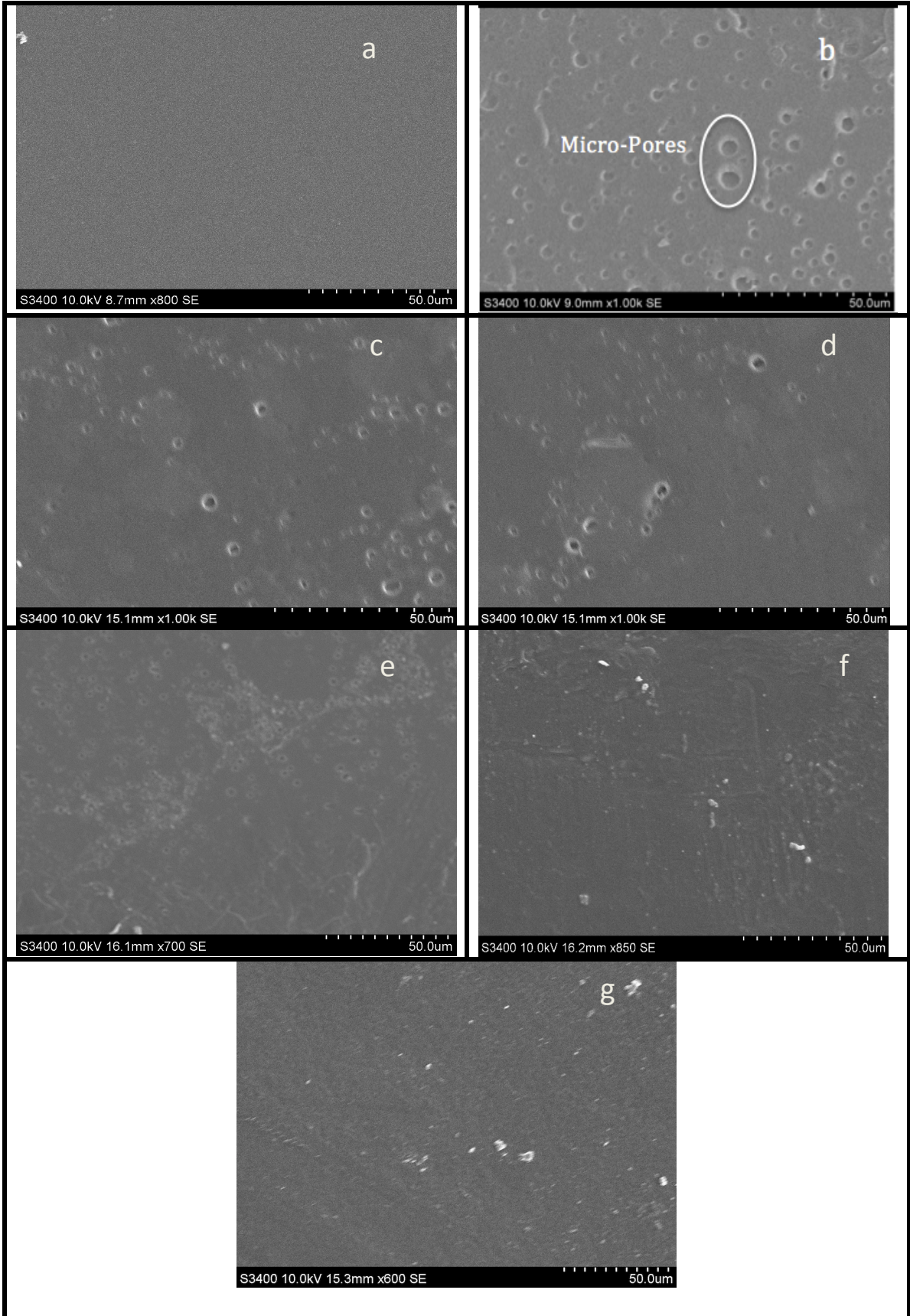


Figure 6.5 SEM images of (a) pristine PVA, (b) PVA with Pluronic F127, (c) PVA-GA-1, (d) PVA-GA-2, (e) PVA-GA-3, (f) PVA-GA-4 and (g) PVA-GA-5.

6.3.4 Atomic Force Microscopy (AFM)

Figures 6.6 & 6.7 illustrate the effect of Gum Arabic conjugation on the surface roughness of the PVA RO membranes utilizing AFM. The surface roughness decreased gradually after the conjugation of Gum Arabic. That apparent reduction of surface roughness might be explained with the aid of SEM images that have been discussed in the previous section. The many large pores that were formed with the infusion of Pluronic F127 made the surface rougher and induced a ridge-valley structure. Once Gum Arabic is conjugated, the pores were diminishing and the surface became denser and smoother, which reduced the surface roughness greatly.

Surface roughness has a crucial effect on biofouling mitigation [78]. The total surface area that microorganisms and biofoulants could adhere to increases as the membrane surface roughness increases. Besides, foulants tend to buildup on surfaces with ridge-valley pattern, which is a characteristic of rough surfaces [79]. Therefore, the surface roughness diminution with the conjugation of Gum Arabic is significant, because it is expected to have a vital role on biofouling mitigation.

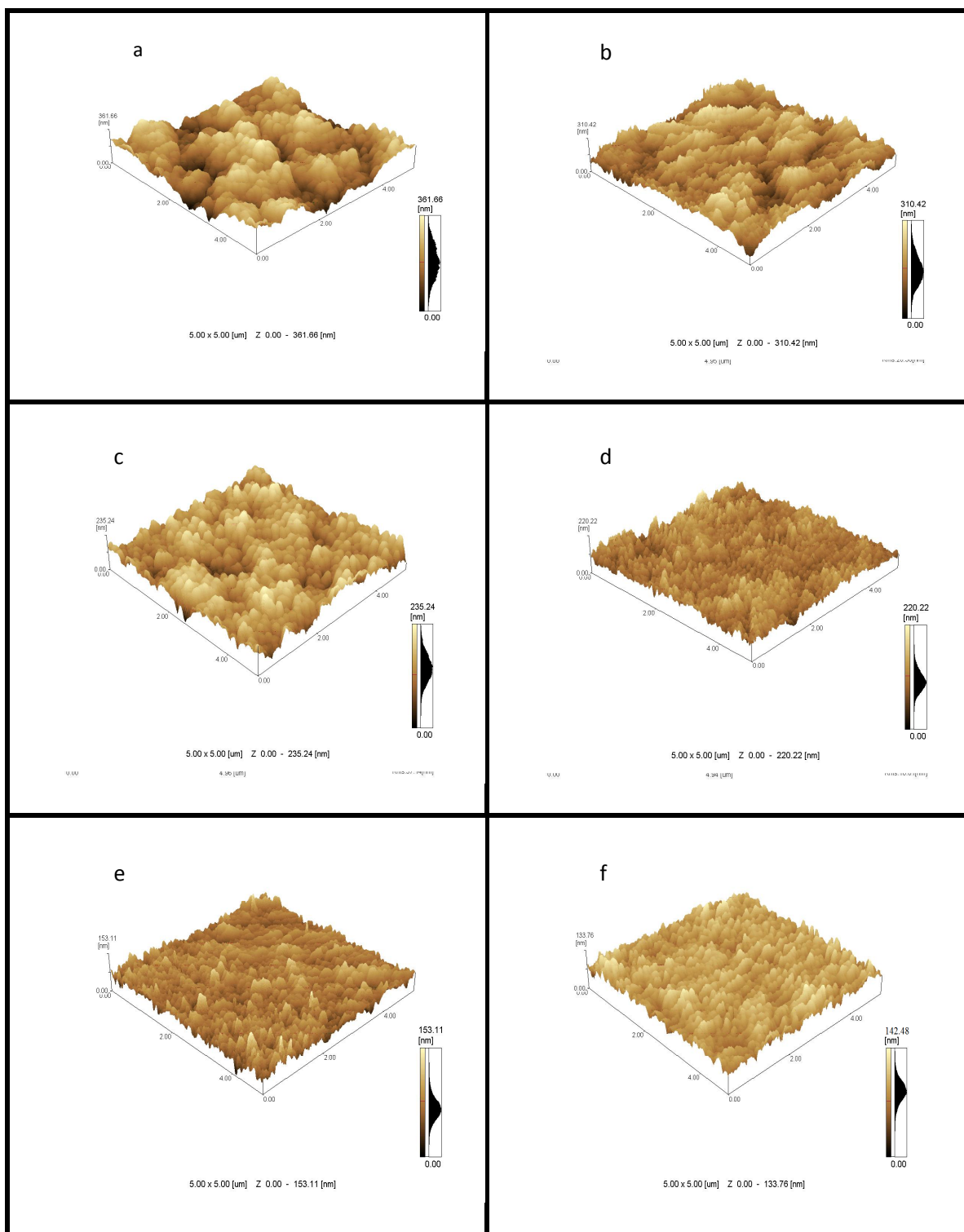


Figure 6.6 3-D AFM images of (a) PVA membranes with Pluronic F127, (b) PVA-GA-1, (c) PVA-GA-2, (d) PVA-GA-3, (e) PVA-GA-4 and (f) PVA-GA-5.

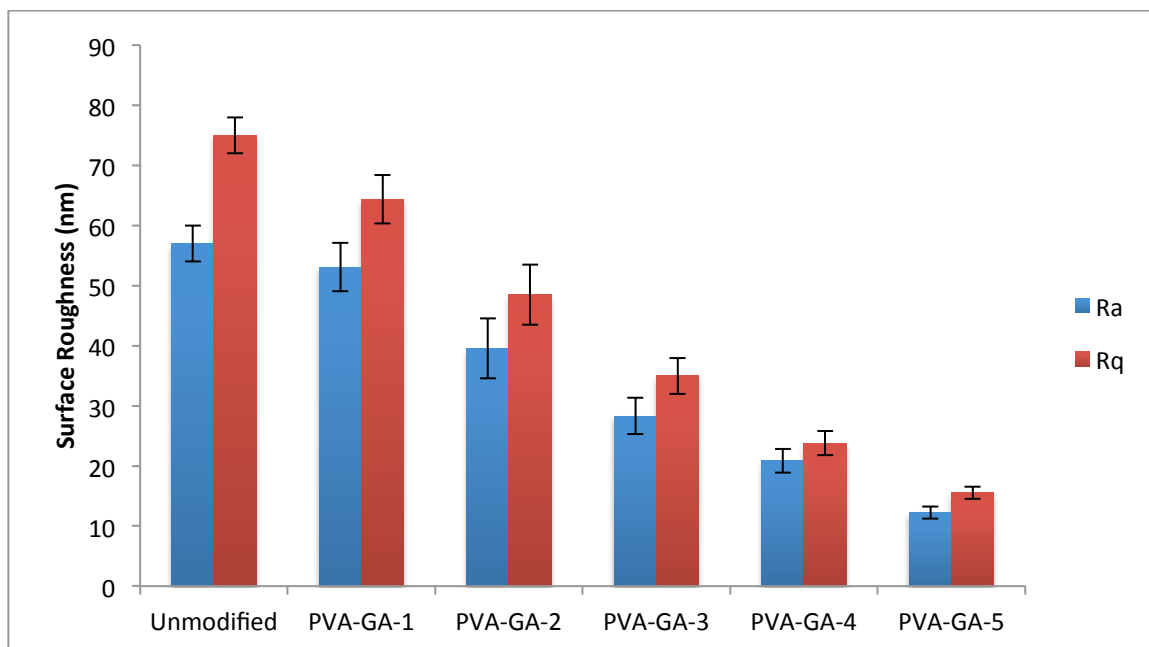


Figure 6.7 Effect of Gum Arabic conjugation on surface roughness of PVA membranes.

6.3.5 Contact Angle Analysis

Surface contact Angle measurement is a tool to quantify surface hydrophilicity/hydrophobicity. If the contact angle between a liquid droplet and a flat surface is less than 90° , the surface is considered hydrophilic [155].

6.3.5.1 Effect of mixing Pluronic F127 on hydrophilicity

Figure 6.8 shows the effect of Pluronic F127 inclusion into PVA membranes on the hydrophilicity of the membrane surface. The figure shows an apparent decrease in contact angle, which means an enhancement in surface hydrophilicity with the mixing of Pluronic F127. This improvement in hydrophilicity is attributed to the pores formation, which is believed to be a characteristic feature of Pluronic F127 [114, 156-158]. Porous

surfaces absorb water better. Moreover, Pluronic F127 molecules form micelles when fused into the casting solution. The hydrophobic PPO segments integrate closer to the center of the micelle, while the hydrophilic PEO segments project away from the center to form the external layers of the micelle [156, 158, 159, 192]. Therefore, the overall hydrophilicity is expected to improve, since the outer surfaces of the Pluronic F127 micelles are hydrophilic. Mixing 6 wt% of Pluronic F127 with PVA provided optimum hydrophilicity. The hydrophilicity started to decay with the inclusion of 8 wt% or more of Pluronic F127. The hydrophilicity reversal when additional amounts of Pluronic F127 are incorporated has been reported elsewhere [159]. The hydrophilic PEO segments of Pluronic F127 of the excess amounts start to convene themselves and attach to the hydrophilic membrane surface due to the hydrophilic/hydrophilic interactions. Therefore, the hydrophobic PPO segments form loops projected away from the surface facing the upstream [159]. Thus, the overall hydrophilicity of the membrane surface starts to decay after the initial improvement. Nevertheless, the modified membranes had better hydrophilicity compared to the pristine PVA membrane, even after the reversal of hydrophilicity.

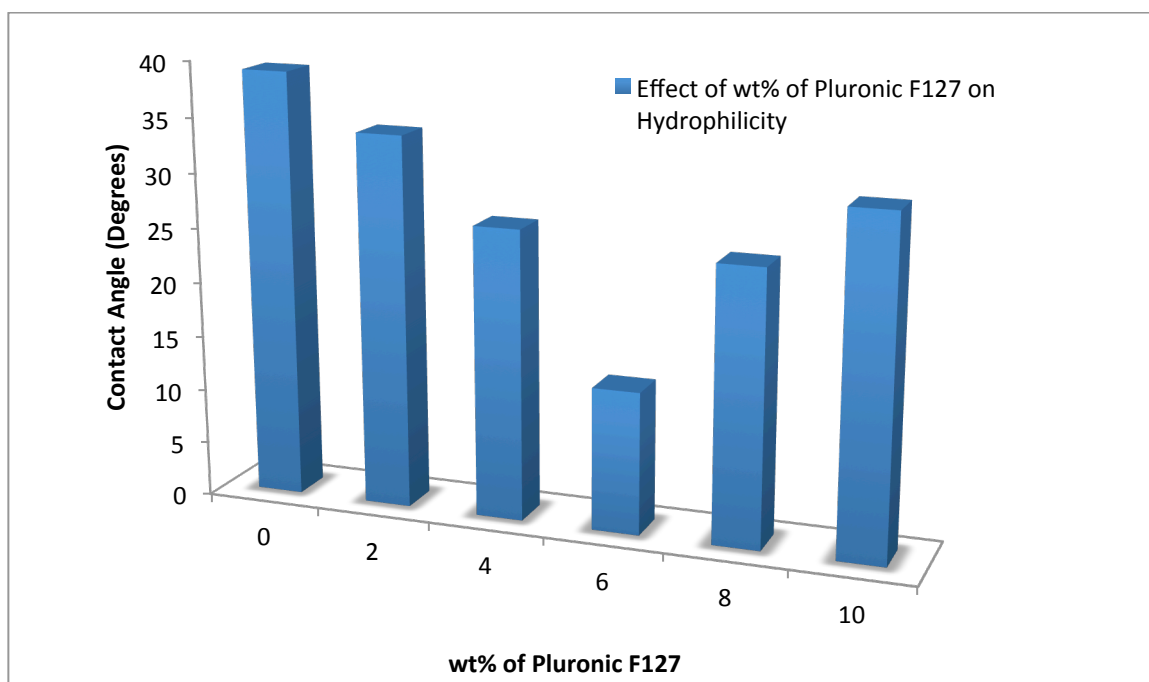


Figure 6.8 Effect of Mixing Pluronic F127 on the hydrophilicity of the PVA membrane.

6.3.5.2 Effect of conjugating Gum Arabic on Hydrophilicity

Figure 6.9 shows the effect of the conjugation of Gum Arabic on the hydrophilicity of the membrane's surface. The curve shows an improvement in the hydrophilicity of the membranes surfaces, as implied by the decrease in contact angle compared to the pure PVA membrane. The improvement in hydrophilicity is due to the hydrophilic nature of Gum Arabic that encompasses multiple $-OH$ groups. As the amount of Gum Arabic increases, the hydrophilicity improves, which is a direct consequence of the abundance of $-OH$ groups within the membrane from PVA and Gum Arabic [203].

Fabricating a hydrophilic membrane surface is one way to make the surface more biofouling resistant and to enhance permeability [41, 73]. When a surface becomes more hydrophilic, it forms a thin layer of water on top of the surface due to hydrogen bonding.

This water layer is important since it prevents or reduces the adsorption of biofoulants and it also enhances the water diffusion through the membrane [72].

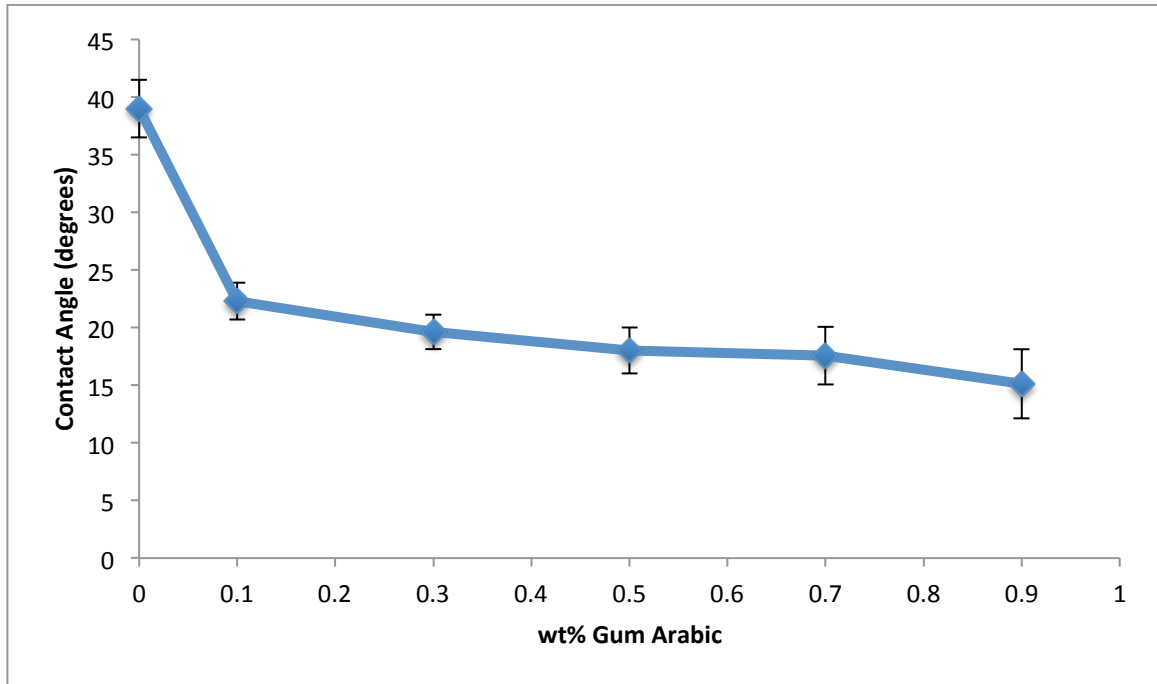


Figure 6.9 Effect of Mixing Gum Arabic on the hydrophilicity of the PVA membrane.

6.3.6 Mechanical Properties

Figures 6.10 & 6.11 show the stress-strain curves and the Young's modulus for the modified PVA RO membranes with different weight percentages of Gum Arabic. The stress-strain curves show that when the wt% of Gum Arabic increases the yield and tensile strengths of the modified membranes are greatly increased. Maximum yield strength of around 20 MPa has been reached when maximum loading of 0.9 wt% Gum Arabic was conjugated, i.e. PVA-GA-5. The ductility of the resultant membranes was around 160%, except for the maximum loading where the ductility became around 100%. Those ductility values are reasonably high. The modified membranes stiffness, as can be shown from Young's modulus values, has improved with the conjugation of Gum Arabic. When the maximum loading of Gum Arabic is incorporated, the stiffness of the membrane improved by 80%. That behavior could be explained by the fact that with the infusion of Gum Arabic, the crosslinking between PVA and the polysaccharides would toughen the polymer network even though the crystallinity has been reduced as mentioned earlier. This leads to an increase in tensile strength and a decrease in ductility [210]. These findings proved the mechanical stability of the fabricated modified PVA membranes. The fabricated membranes withstood the extremely high reverse osmosis pressure of 800 Psi without damage or rupture and without the use of a supportive layer or a substrate, which eliminates the many negative effects associated with the use of a substrate like internal concentration polarization that causes an increase in the applied RO pressure.

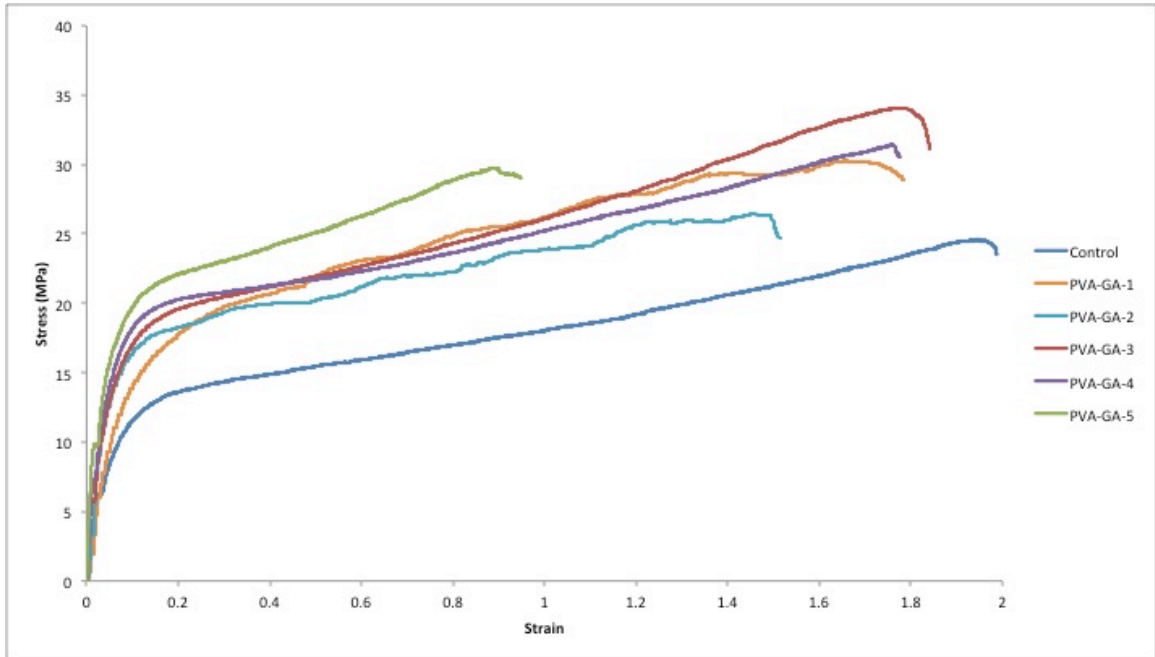


Figure 6.10 Stress-strain Curves for different Gum Arabic wt%.

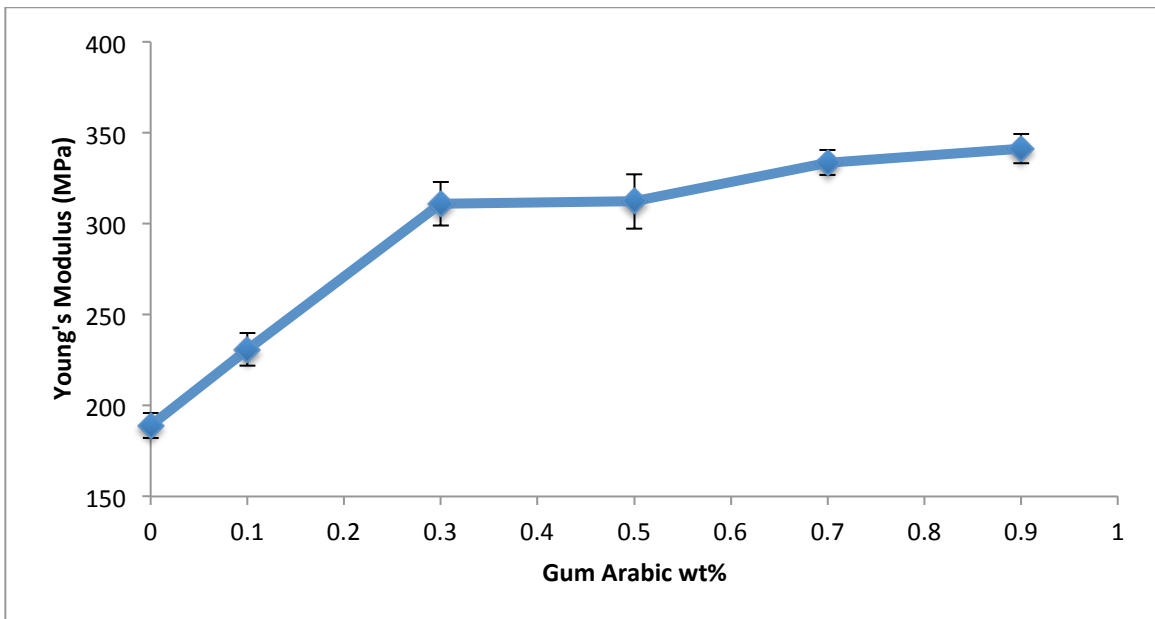


Figure 6.11 Effect of Gum Arabic wt% on Young's modulus of the membranes.

6.3.7 Permeate Flux and Salt Rejection

6.3.7.1 Separation performance of DGEBA crosslinked PVA membranes

Figure 6.12 shows the water permeation flux and the salt rejection percentages of the PVA crosslinked membranes with DGEBA. It is clear from the figure that as the amount of the crosslinker increased, the salt rejection improved, while the water permeation decreased. The reason behind this behavior is the crosslinking of PVA, as crosslinking polymer chains creates tighter and denser structures because of chains interweaving [88]. The resulting network structure will hinder the free passage of salt molecules as well as water molecules across the membrane, which enhances selectivity while reducing permeability. The purpose of PVA crosslinking is to overcome the swelling effect as well as to improve the selectivity of the membrane. Therefore, the optimal wt% of the crosslinker is the one that produces optimal salt rejection. Figure 6.12 shows that the DGEBA wt% of 0.16 created the membrane with the optimal salt rejection. This specific weight percentage will be infused into all of the PVA membranes for further modifications.

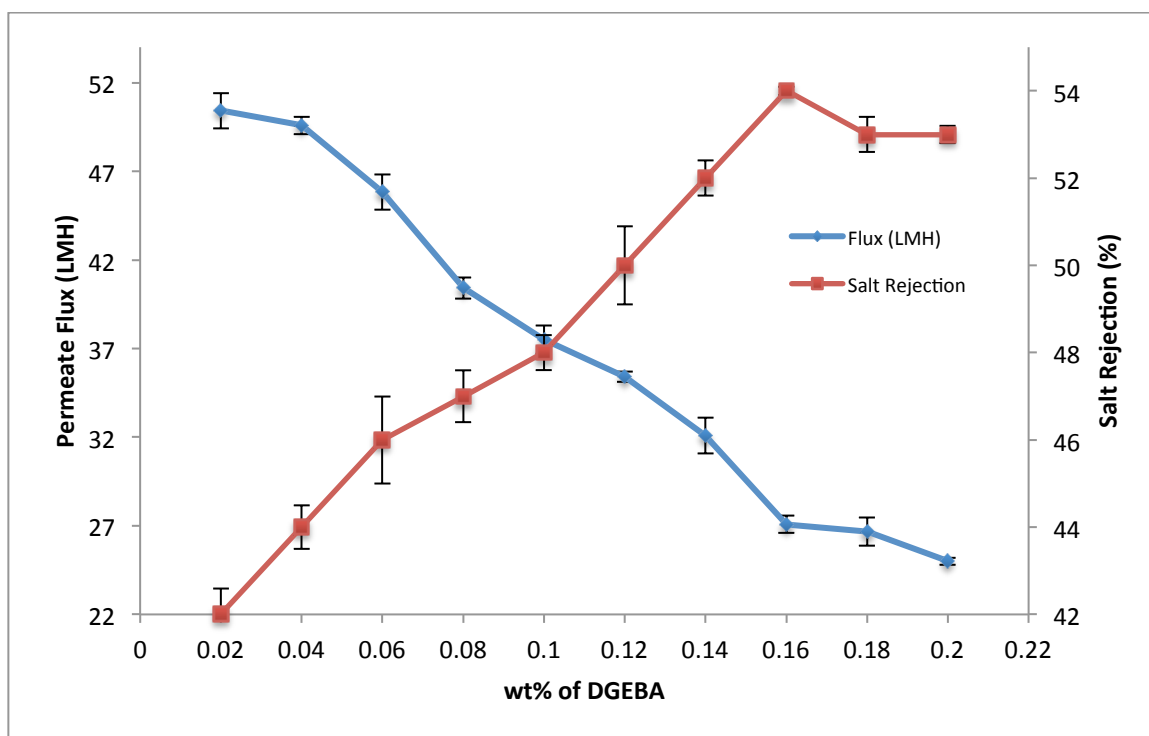


Figure 6.12 Effect of crosslinker wt% on the permeation and selectivity of the membrane.

6.3.7.2 Separation performance of PVA membranes incorporated with Pluronic F127

Figure 6.13 illustrates the effect of infusing Pluronic F127 into the crosslinked PVA membrane on the water flux after eight hours of operation. The addition of Pluronic F127 improved the permeation considerably, as shown from the figure. One reason for that enhancement is the hydrophilic nature of Pluronic F127 micelles, as has been discussed earlier; the other reason is evidently due to the pore formation, which is a characteristic feature of Pluronic F127 [114, 156-158, 172]. The salt rejection has improved as well until more than 6 wt% is added, after which the rejection started to decline. This could be due to the fact that forming more and more pores with bigger sizes will allow more salt

molecules to pass through, which negatively affects the selectivity. Hence, 6 wt% of Pluronic F127 was chosen as an optimal weight percentage and was integrated into subsequent membranes for further modifications.

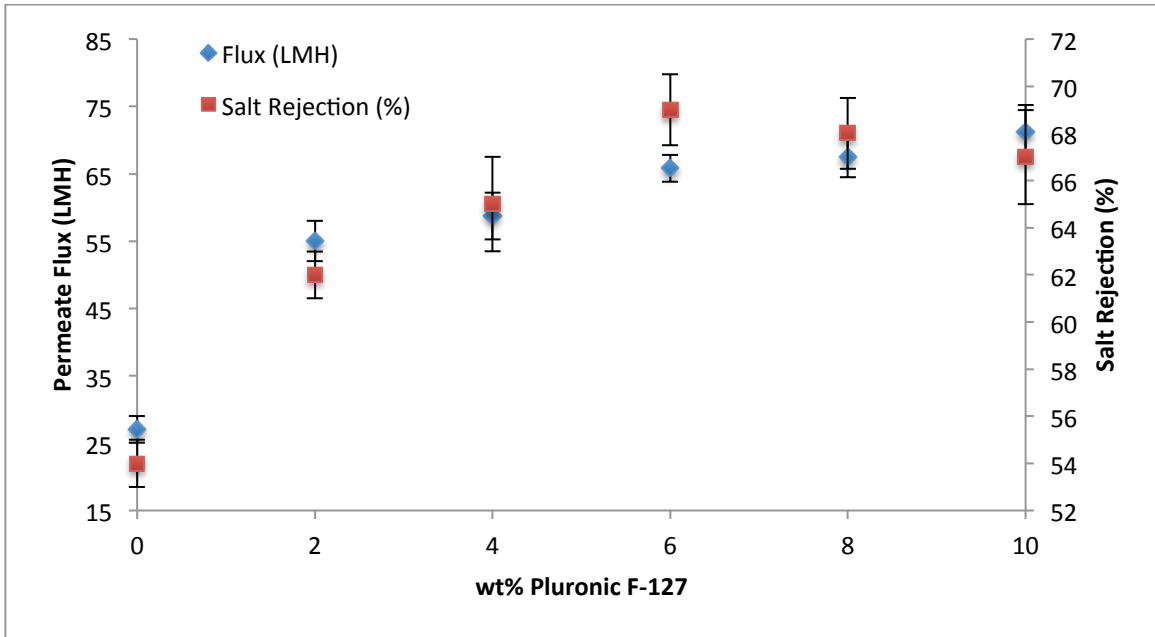


Figure 6.13 Effect of Pluronic F127 wt% on the permeation and selectivity of the membrane.

6.3.7.3 Effect of Gum Arabic conjugation on PVA membranes separation performance

Figure 6.14 shows the effect of the conjugation of different weight percentages of Gum Arabic on the permeate flux through the membrane and salt rejection. There was almost 50% improvement in permeate flux through the membrane when 0.3 wt%, PVA-GA-2, or more Gum Arabic is conjugated. The permeate flux enhancement is attributed to the increased hydrophilicity of the membrane surface. As reported earlier, improving the hydrophilicity of a membrane surface results in a better permeability [72]. Another way to explain the behavior is related to the stiffness of the membrane. Since RO testing is performed under a very high applied pressure, it is anticipated that the membrane and its internal pores will be deformed. Upon deformation, some of the pores will get jammed, which affects the overall permeation. Therefore, better membranes stiffness leads to better permeability. The membrane stiffness results, shown in Figure 6.11, presented a similar trend to the permeation results, shown in Figure 6.14. The stiffness enhancement with the conjugation of Gum Arabic is in a similar fashion compared to the permeation enhancement.

Figure 6.14, also, shows the effect of conjugating Gum Arabic on the selectivity of the synthesized membranes. It is clear that conjugating Gum Arabic with PVA enhanced the selectivity vastly compared to unmodified membranes. The selectivity improved from around 69% to 98% salt rejection with the addition of 0.7 wt% Gum Arabic, PVA-GA-4. This could be due to the hydrogen bonding between the numerous –OH groups Gum Arabic possesses and PVA polymer chains. Hydrogen bonding generates a network-like structure that hinders the passage of larger salt molecules [206]. This is a great finding as it is usually a compromise between permeability and selectivity; nonetheless, the

conjugation of Gum Arabic enhanced both.

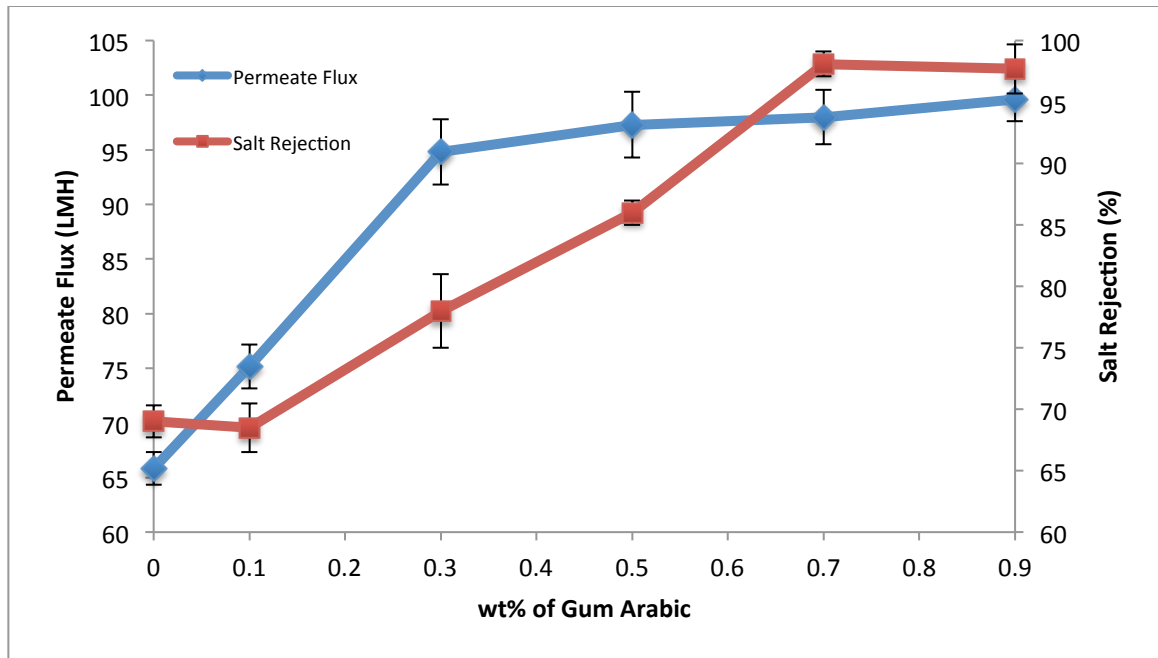


Figure 6.14 Effect of Gum Arabic wt% on the permeation and selectivity of the membrane.

6.3.8 Effect of Gum Arabic Conjugation on Membrane's Chlorine Resistance

Figure 6.15 illustrate the effect of Chlorination on the selectivity of the RO membranes comparing the PVA membranes conjugated with Gum Arabic with the unmodified ones. The unmodified membrane showed poor Chlorine resistance as the salt rejection decreased from 69 to 52.3%, a 24% decrease in salt rejection efficiency. This implies that the harsh environment caused by the presence of high concentration of Chlorine affected the membrane surface significantly. Upon conjugation with Gum Arabic, however, the

decline in salt rejection became very insignificant. The decrease in salt rejection was less than 3% for membrane PVA-GA-5, which is an 83% improvement of Chlorine resistance of the fabricated membrane. That enhancement of Chlorine resistance is an indication that the membrane surface is chemically stable. This is attributed to the intermolecular hydrogen bonding between the many –OH groups that PVA and Gum Arabic possess, which hinder the substitution of hydrogen with Chlorine on these –OH groups [69, 101].

Commercially available Polyamide (PA) RO membranes are severely affected by exposure to even lower levels of Chlorine than those used in the present study [179]. The decrease of salt rejection of the commercially available PA membrane is more than 25% in much less harsh conditions [179]. The synthesized PVA membranes conjugated with Gum Arabic in this research had a much better Chlorine resistance compared to commercial RO membranes. Chlorine resistance is a crucial membrane property as it reduces the necessity for the de-Chlorination process that is required to protect the membranes from the attack of Chlorine that is used for biofouling deterrence [181].

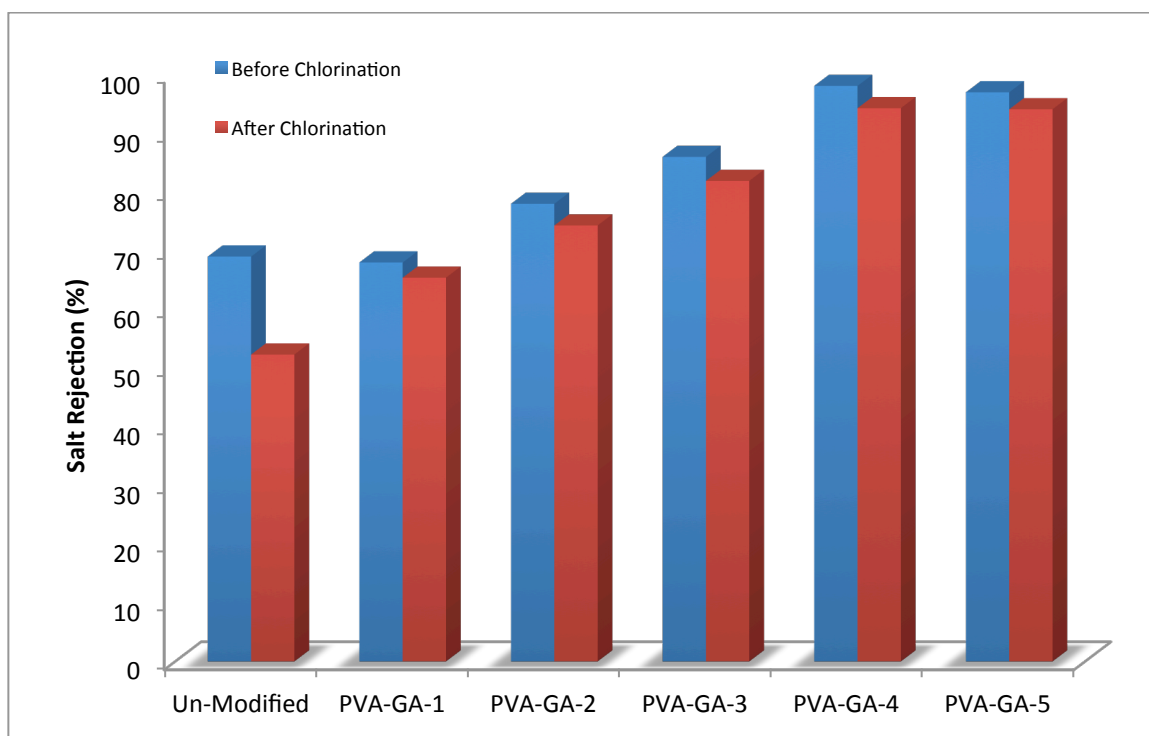


Figure 6.15 Effect of Gum Arabic conjugation on salt rejection before and after Chlorination.

6.3.9 Effect of Gum Arabic Conjugation on Membrane's Biofouling Resistance

The antibacterial activity of *E. coli*, implementing JIS L 1902–2002 methodology, was investigated to characterize the effect of Gum Arabic conjugation on biofouling resistance of the membranes. The conical flask that contained the unmodified membrane looked cluttered, which suggested bacterial growth, while flasks that contained the membranes conjugated with Gum Arabic, displayed a clear transparent solution. Figure 6.16 shows the optical density (OD) for the unmodified and modified membranes. The OD of the membranes conjugated with Gum Arabic indicated that there was a minimal

bacterial growth. It was concluded from the optical density analysis that the modified membranes effectively suppressed the bacterial growth. After the conjugation of Gum Arabic, most of the *E. coli* cells lost their cellular integrity and became more rigid indicating irreversible cell death and/or cell damage. The antibacterial property improved by more than 98% for PVA-GA-5 compared to the unmodified membrane. Three very important membrane surface characteristics that affect the antibacterial behavior of the membrane are hydrophilicity, surface roughness and surface charge. It has been reported that bacteria tend to adhere to more hydrophobic, positively charged and rougher surfaces [212]. This study illustrated that the conjugation of Gum Arabic improved the hydrophilicity and the surface roughness of the membranes. Hence, the improvement of antibacterial property could be explained by the improvement in hydrophilicity, which deterred the adhesion of bacteria that are mostly hydrophobic [213]. Furthermore, a smoother surface reduces the surface area that bacteria could be attached to [212]. Another explanation is that both the *E. coli* and Gum Arabic are negatively charged [203, 214, 215]. Due to electrostatic repulsion between the negatively charged polysaccharide and the *E. coli*, the membrane surface became expeller to the adhesion of *E. coli*.

Coupling this antibacterial property with the Chlorine resistance improvement is an outstanding outcome of this research as enhancing both extends the membrane life and preserves optimal salt rejection and permeability without the need of frequent cleaning.

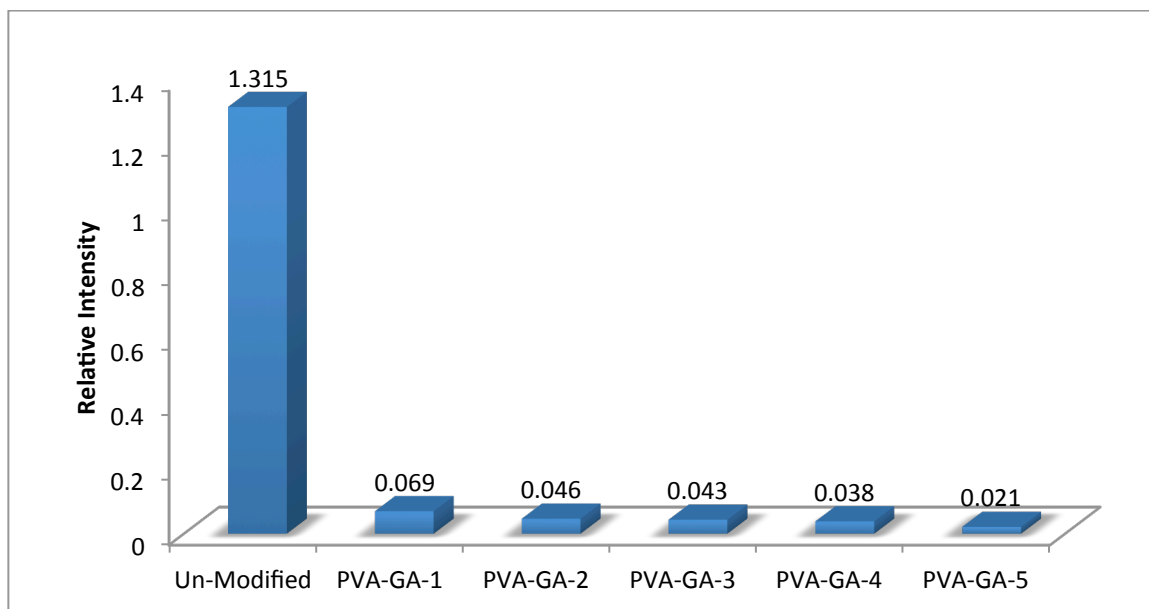


Figure 6.16 Relative amount and viability of *E. coli* cells adhering onto pristine and modified PVA membranes.

6.4 Conclusion

This research was undertaken to investigate the effect of conjugating Gum Arabic with crosslinked PVA/Pluronic F127 membranes on the overall reverse osmosis performance. The novelty of this work is that the PVA polymer matrix was utilized as an active RO layer without the use of any polymeric or ceramic substrate, which overcame many drawbacks associated with the use of substrates, such as internal concentration polarization.

Crosslinked PVA membranes conjugated with Gum Arabic were prepared using dissolution casting method. The conjugation with Gum Arabic and Pluronic F127 improved the overall RO performance of the membrane in terms of hydrophilicity,

surface roughness, water permeability, salt rejection, Chlorine resistance, biofouling resistance and mechanical strength. Figure 6.17 shows a target plot that determines which RO membrane has the optimal performance. The membrane properties and performance were ranked from level 1, the innermost loop on the target, to level 10, the outermost loop; level 10 indicates ideal properties. The target plot clearly illustrates that the conjugation of Gum Arabic improved the overall performance vastly. From the plot, the membrane PVA-GA-5 that contains 0.9 wt% Gum Arabic provided optimal salt rejection, Chlorine and biofouling resistance, mechanical strength, permeability, surface roughness and surface hydrophilicity. This research will serve as a base for future studies concerning the feasibility of the utilization of PVA and Gum Arabic as an active layer in RO plants in the near future.

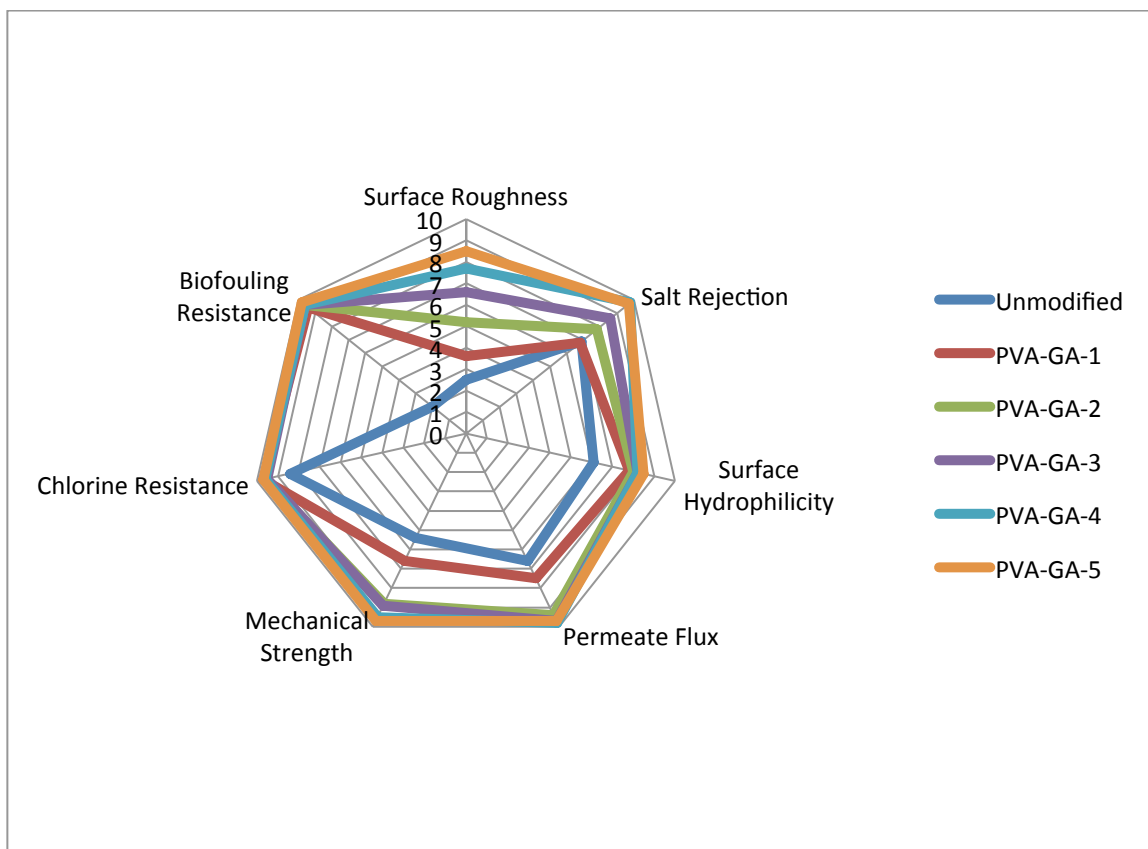


Figure 6.17 Target plot comparing RO performance properties for the unmodified PVA membranes and the membranes conjugated with Gum Arabic.

CHAPTER 7

High Performance and Chlorine Resistant PVA/DGEBA Crosslinked TFN-RO Polymer Membranes Infused with Pluronic F127/ZnO-NPs Using Natural Sea Salt for Desalination

7.1 Introduction

Global water crisis may become a peace threatening issue and can lead to conflict between nations with the passage of time. The demand of good quality drinking water is increasing due to the rapid growth of industry and population and a lack of wastewater management [5, 216]. The optimal available option to address the scarcity of clean water is to establish a desalination plant that removes salts and other impurities from saline water. There are many techniques available for desalination including multi-effect distillation (MED), multi-stage flashing (MSF), electrodialysis and reverse osmosis (RO). RO membrane plants are the most promising due to their energy efficiency, operational simplicity and low capital cost [15, 104, 217, 218].

A wide range of various synthetic polymers are explored for water purification processes [85, 103]. Membranes based on polyvinyl alcohol (PVA) are widely studied as a promising component for water treatment processes, which includes reverse osmosis, ultrafiltration, and nanofiltration [219]. The inherent hydrophilicity of PVA makes it an attractive polymer for membrane water treatment applications compared to other polymers as it also possesses good fouling resistance, film forming ability and chemical and physical stability [82]. Nonetheless, PVA membranes require physical or chemical modifications as it holds a low rate of salt rejection [220-223].

PVA is a polymer having –OH groups on its backbone. These groups are the source of hydrogen bonding and they can support polymer composite formation [224]. There are number of physical, chemical and thermal treatment methods for modifying PVA as supported in literature [29, 225-227]. Physical and chemical modification enhances mechanical stability, provides resistance to dissolution in water, and offers adhesive networks on PVA chains [228]. The large swelling capacity of PVA can be minimized by adequate crosslinking to ensure the retention and compaction under pressure [82, 88, 89].

Amphiphilic copolymer Pluronic F127 consists of highly hydrophilic poly (ethylene oxide) (PEO) and hydrophobic polypropylene oxide (PPO) arranged in ABA type triblock structure (PEO-PPO-PEO) [192]. Polyethylene oxide (PEO) is generally used for hydrophilic variation and enhancement of antifouling property of the membranes [229-231]. Poloxamers like Pluronic F127 are selected due to their pore formation ability and permeation enhancement, which influence the penetration rate of the solution in the membrane [157].

Thin film composite membranes formed by incorporating organic polymers with inorganic materials like zinc oxide, silica, zirconia, titania and alumina have shown improved thermal and mechanical properties and enhanced water permeability, salt rejection and fouling resistance compared to single polymer membranes [232-237]. Zinc oxide nanoparticles (ZnO-NPs) are widely used as additives in different products and considered as mature engineering materials in chemicals, ceramics and water purification, in particular for the removal of salts [238-240]. Infusion of ZnO-NPs in polymeric membrane enhances selectivity, chemical stability, heat resistibility and membrane

durability with additional benefits of good biocompatibility, strong antifungal and antibacterial properties [106].

In this research, crosslinked PVA membranes incorporated with Pluronic F127 and infused with ZnO-NPs for RO were fabricated. The newly synthesized membranes were then characterized and analyzed using various techniques like attenuated total reflection Fourier transform infrared spectroscopy (ATR-FTIR), contact angle measurements, X-ray diffraction (XRD), scanning electron microscopy (SEM), atomic force microscopy (AFM) and mechanical testing. The actual reverse osmosis performance of the membranes, including permeation testing, salt rejection and Chlorine resistance, was analyzed using a dead-end RO permeation unit.

7.2 Experimental procedure

7.2.1 Materials

Analytical grade PVA (Mw=89000), bisphenol A diglycidyl ether (DGEBA) (crosslinker), Pluronic F-127 (pore former), dimethyl sulphoxide (DMSO) (solvent) and sodium hypochlorite (NaClO) were obtained from Sigma Aldrich (USA). Zinc oxide nanoparticles (ZnO-NPs) with 99.7% purity were obtained from Inframat Advance Materials (USA). Commercially available natural sea salt collected from Pacific Ocean (USA) is used for RO process. All the chemicals were used without further purification.

7.2.2 Membrane Preparation

7.2.2.1 Preparation of single layer PVA/DGEBA crosslinked membrane

PVA (17.5wt %) was mixed with different weight % of DGEBA, as shown in Table 7.1, to prepare PVA/DGEBA membranes using dissolution casting methodology. The mixture was dissolved in DMSO (82.5wt %) solvent with continuous stirring of each solution for 2 h at 70°C. The clear, viscous and homogenous solutions of eleven concentrations of DGEBA from (0-0.2wt %) were labeled as PVA-DGEBA wt%.

7.2.2.2 Membrane Casting

The single layer PVA/DGEBA crosslinked solutions were spread slowly on Petri dishes and placed in an oven at 65°C for controlled evaporation of solvent keeping the membrane of uniform thickness. The solution was transferred to each Petri dish of the same diameter with equal quantity. The newly casted membranes had dense structure. The membranes were carefully removed from each Petri dish using sharp blades. Single layer PVA/DGEBA crosslinked membranes, shown in Figure 7.1 (step I), were evaluated for maximum salt rejection. From the results, PVA-0.16 was selected for further treatment with Pluronic F127 to enhance the permeation flux.

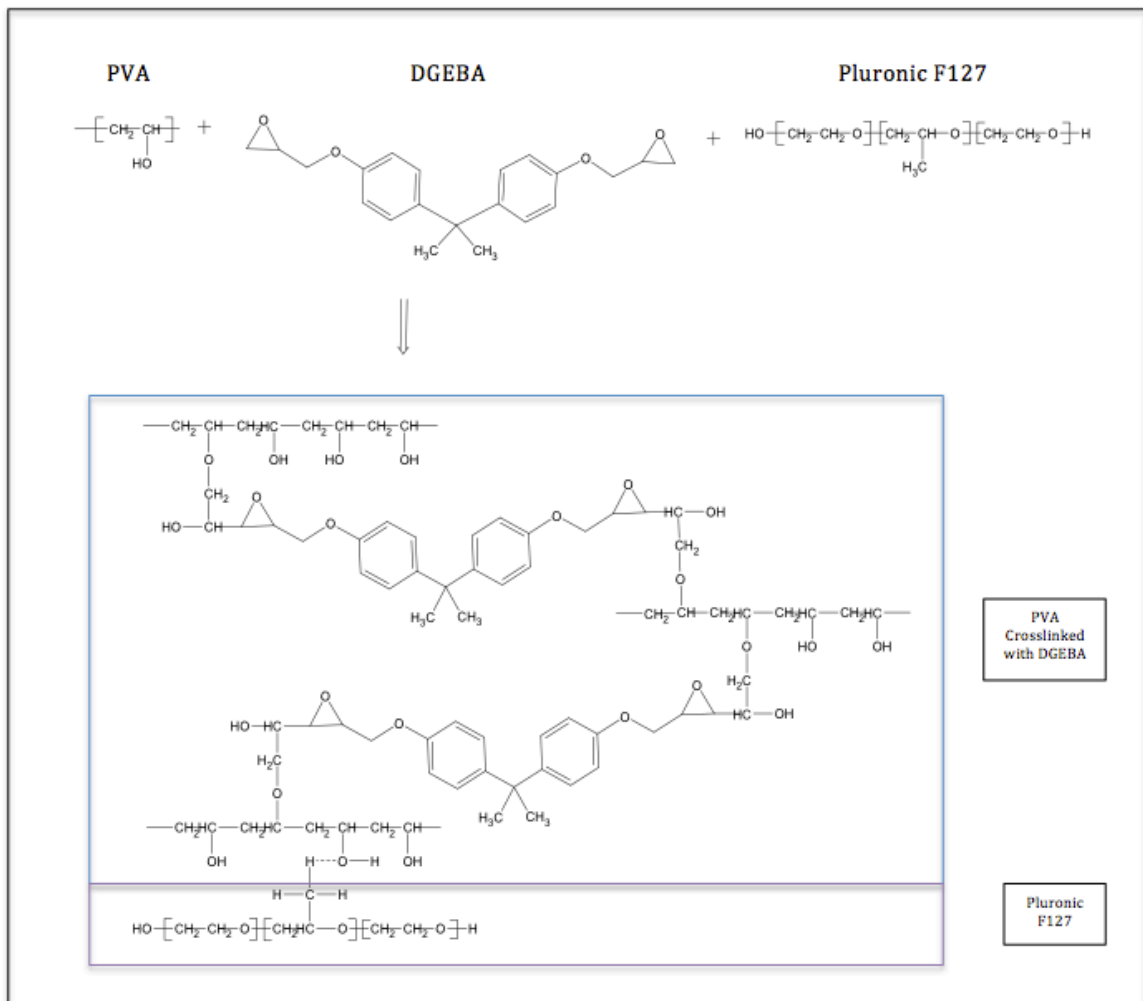


Figure 7.1 Schematic diagram of the crosslinking of PVA with DGEBA and the intermolecular hydrogen bonding with Pluronic F127.

7.2.2.3 Synthesis of thin film composite (PVA/DGEBA/PluronicF127) membrane

Several concentrations of Pluronic F127 (0-10wt%), shown in Table 7.1, were composited with the selected PVA-0.16 solution and magnetically stirred for 2 h at 70 °C

until homogeneous solutions (TFC labeled) were formed. Five films were casted on clean dried Petri dishes following the same procedure mentioned in the previous section. TFC3 membrane showed highest permeation flux and maximum salt rejection and was selected for further treatment. The membrane thickness (~ 0.1 mm) was measured by screw gauge. Figure 7.1 shows possible intermolecular interactions.

7.2.2.4 Infusion of ZnO-NPs in TFC membrane

ZnO-NPs with five different concentrations (0-0.1 wt%), as shown in Table 7.1, were infused with TFC3 membrane solution and sonicated for 2 h at 65 °C until finely dispersed solutions were formed. Membranes were casted on Petri dishes following the same procedure mentioned above and labeled as shown in Table 7.1.

Table 7.1 Composition and effect of PVA/DGEBA, Pluronic F127 and ZnO-NPs on average and root mean square roughness values (Rms and Ra) of the membranes.

Single layer crosslinked membrane		Thin-film composite membrane (TFC)		Thin-film nanocomposite membrane (TFN)		AFM- Roughness values		
Membrane Type	DGEBA Wt.%	Membrane Type *	Pluronic F127 Wt.%	Membrane Type**	ZnO-NPs Wt.%	Membrane Type	Rms	Ra
Pure PVA	0	TFC1	2	TFN1	0.02	PVA-0.16	108.6	120.1
PVA-0.02	0.02	TFC2	4	TFN2	0.04	TFN1	42.2	60.3
PVA-0.04	0.04	TFC3	6	TFN3	0.06	TFN2	38.1	59.4
PVA-0.06	0.06	TFC4	8	TFN4	0.08	TFN3	35.8	52.8
PVA-0.08	0.08	TFC5	10	TFN5	0.1	TFN4	32.6	49.1
PVA-0.1	0.1					TFN5	46.7	56.5
PVA-0.12	0.12							
PVA-0.14	0.14							
PVA-0.16	0.16							
PVA-0.18	0.18							
PVA-0.2	0.2							

* PVA-0.16

** TFC3

7.3 Membrane Characterization

7.3.1 Fourier Transform Infrared Spectroscopy

FTIR spectra of composite membranes were scanned by IR Prestige-21 (Shimadzu) using attenuated total reflectance (ATR) accessory equipped with zinc selenide (ZnSe) crystal. The air background of the instrument was run before each sample. The frequency range was from 4000-600 cm^{-1} at a resolution of 4.0 cm^{-1} and average of 120 scans per spectrum were reported.

7.3.2 Contact Angle Measurements

Goniometer (Digidrop, KSV Instruments) was used to evaluate sessile drop contact angles of single layer crosslinked (PVA-0.16), TFC3 and TFN (1-5) membranes. The equilibrium value was average of right and left angles. The reported data were the average of three measurements for each membrane sample.

7.3.3 Structural Investigation

The structure of all the prepared polymer blends was characterized by XRD analysis with an X'pert PRO diffractometer (PANalytical) using monochromatized $\text{CuK } \alpha_1$ radiation of wavelength 1.540 Å from a fixed source operated at voltage 40 kV and current 30 mA. The scanning range was from 4° to 80°.

7.3.4 Scanning Electron Microscopy

SEM micrographs of the membranes pure PVA, single layer crosslinked (PVA-0.16), TFC3 and TFN (1-5) were taken on S-3400N Hitachi (USA). The instrument was operated under low vacuum mode to analyze sample. For gold sputtering, samples were

prepared by using Denton Vacuum Sputtering Automatico Desk IV. This instrument was primarily utilized for SEM sample preparation.

7.3.5 Atomic Force Microscopy (AFM)

Atomic force microscopy (AFM) imaging was conducted using a Digital Instruments (Santa Barbara, CA) Dimension 3000 with a Nanoscope III controller. Topographical images were taken using standard tapping mode. In PFT-mode, a cantilever was oscillated sinusoidally at 350 kHz resonant frequency, and brief contacts with the sample surface at the down stroke of each cycle. A user-established set point force was set so that the sample surface was minimally deformed (on the order of a few nanometres) and used as feedback control. Scanned images were taken at 512 x 512 pixel resolution.

7.3.6 Mechanical Testing

The mechanical properties of the TFN (1-5) membranes, i.e. the stress strain curves, ultimate tensile strength, elongation at break and the Young's modulus, were primarily evaluated. Instron 5567 Tensile Testing Machine fitted with a 10 kN load cell was used to perform the load-extension experiments. Membranes were cut into strips with gauge length and width of 50 and 10 mm, respectively. The thickness of the membrane samples was measured using a micro-caliper and maintained at ~0.1 mm for all of the tested samples. All specimens were drawn at ambient temperature and the Young's modulus was calculated in triplicate using stress-strain curves, which were instantaneously recorded by a computer. A crosshead speed of 10 mm/min was maintained throughout the tensile experiments.

7.3.7 Reverse Osmosis Separation Performance Testing

The desalination performance of the freshly prepared, single layer crosslinked PVA-0.16, TFC3 and TFN (1-5) membranes was evaluated in terms of permeation flux and salt rejection % by using a dead-end filtration system made of stainless steel 316 (Model HP4750 Stirred Cell, Sterlitech Corp., Kent, WA), as shown in Figure 7.2.

The membrane sample was loaded in the stainless steel cell with an effective area of 14.6 cm² (2.26 in²). The feed solution was prepared using 3.28wt% of commercially available natural sea salt and the pressure was kept at 800 psi (55.2 bar). The membranes were tested in the RO cell while the permeation flux can be calculated by measuring the volume of the water penetrated through the membranes per effective area per unit time, and its unit was converted into m³/m²/day or gallon/ft²/day (gfd) in following Equation.

$$\text{Permeation Flux} = \frac{\text{Permeate unit (m}^3\text{)}}{\text{Membrane Area (m}^2\text{). Time (day)}}$$

The salinity of the permeate was determined by a salinity meter (TRACEABLE VWR, ISO 17025 Accredited). The reported RO experimental results were the average values obtained from at least three membrane samples prepared at different times, and the error bars showed the standard deviation.

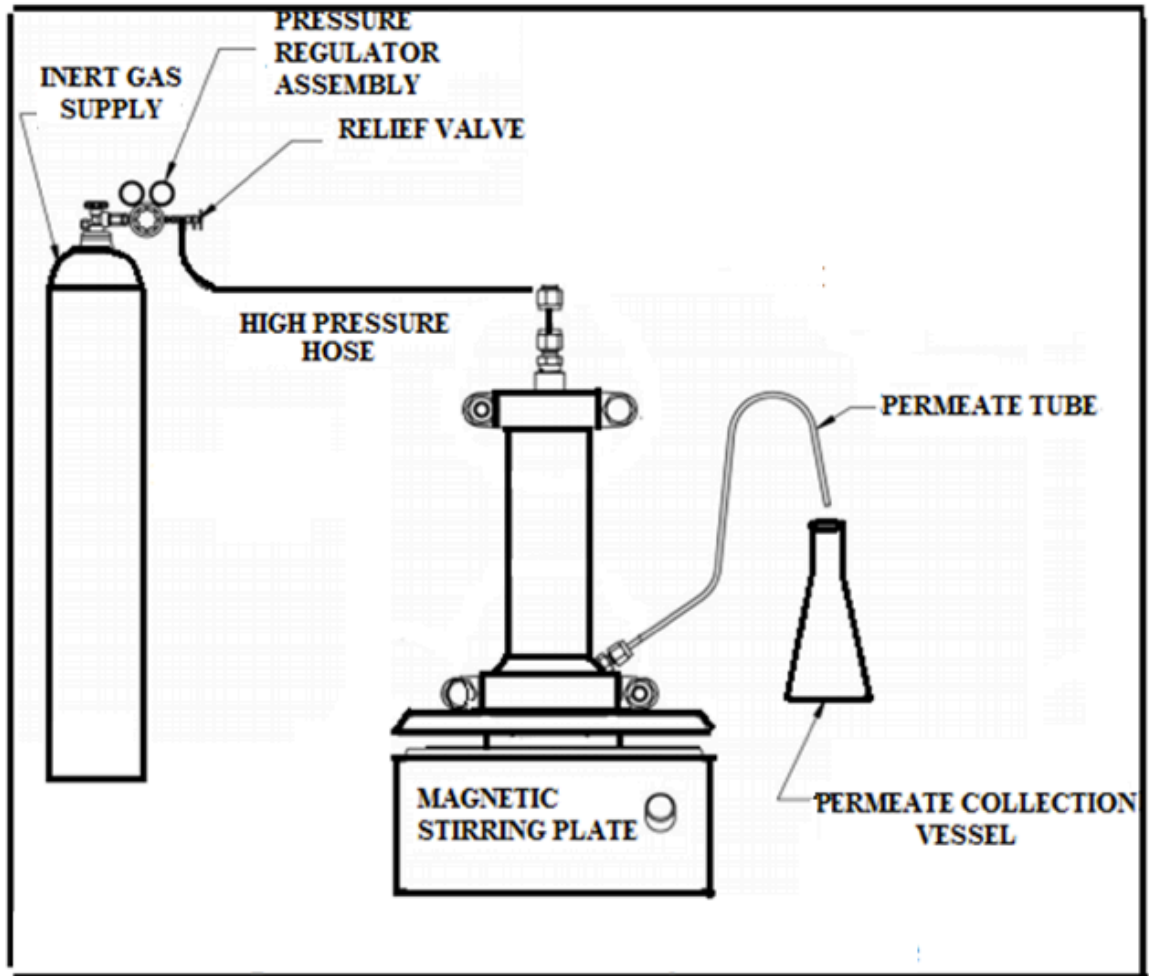


Figure 7.2. Dead-end filtration system for RO membranes.

7.3.8 Chlorine Resistance of The Prepared Membranes

It has been reported elsewhere that there is an equivalent resultant effect when comparing high concentration Chlorine exposure for a short period of time to low concentration Chlorine exposure for a longer period of time [104, 105]. Thus, it is more convenient to expose the membrane surface to a high concentration of Chlorine for a short period of time for Chlorine resistance testing in the lab. Chlorinated solution (2000 mg/L) was prepared by diluting a commercial NaClO solution (free Chlorine content of 10 wt%) with distilled water. The pH of the prepared hypochlorite solution was adjusted to 4.0 by HCl (0.1 M) to make it more oxidative and harsh environment [106]. To perform the Chlorination experiments, water flux and salt rejection performance of the membranes were evaluated using 2000 mg/L NaCl solution and after that, the membranes were taken out of the test cells, washed with distilled water and exposed to 2000 mg/L hypochlorite solution for 2 h at pH=4.0 and 25° C. After exposure, the Chlorinated membranes were washed thoroughly with distilled water and re-loaded in the test cells. The performance of the membranes was evaluated again with 2000 mg/L NaCl aqueous solution.

7.4 Results and Discussion

7.4.1 FTIR Analysis

Figure 7.3 shows the FTIR analysis carried out to confirm the proposed interactions among PVA, Pluronic F127 and ZnO-NPs in the presence of (DGEBA). The strong bands at 3303 and 2919 cm^{-1} are ascribed to hydrogen bonded -OH and -CH stretching vibrations, respectively, present in PVA and Pluronic F127 [151, 187]. The bands at 1236 and 1086 cm^{-1} are characteristics for C-O-C cyclic and acyclic groups of epoxy present in

DGEBA, respectively. The intensity of this peak remained the same due to the fixed concentration of DGEBA, while a weak band at 1600 cm^{-1} attributed to the aromaticity present in DGEBA. In addition, the band at 915 cm^{-1} confirmed the characteristic asymmetric vibration of epoxide ring [190, 191]. The band at 1138 cm^{-1} in all TFN spectra ascertained the existence of C-O bond in PVA and Pluronic 127. The band at 487 cm^{-1} confirmed the presence of ZnO-NPs [188]. This band has been shifted towards lower wavenumber of 484 cm^{-1} due to the H-bonding with PVA, as shown in Figure 7.1.

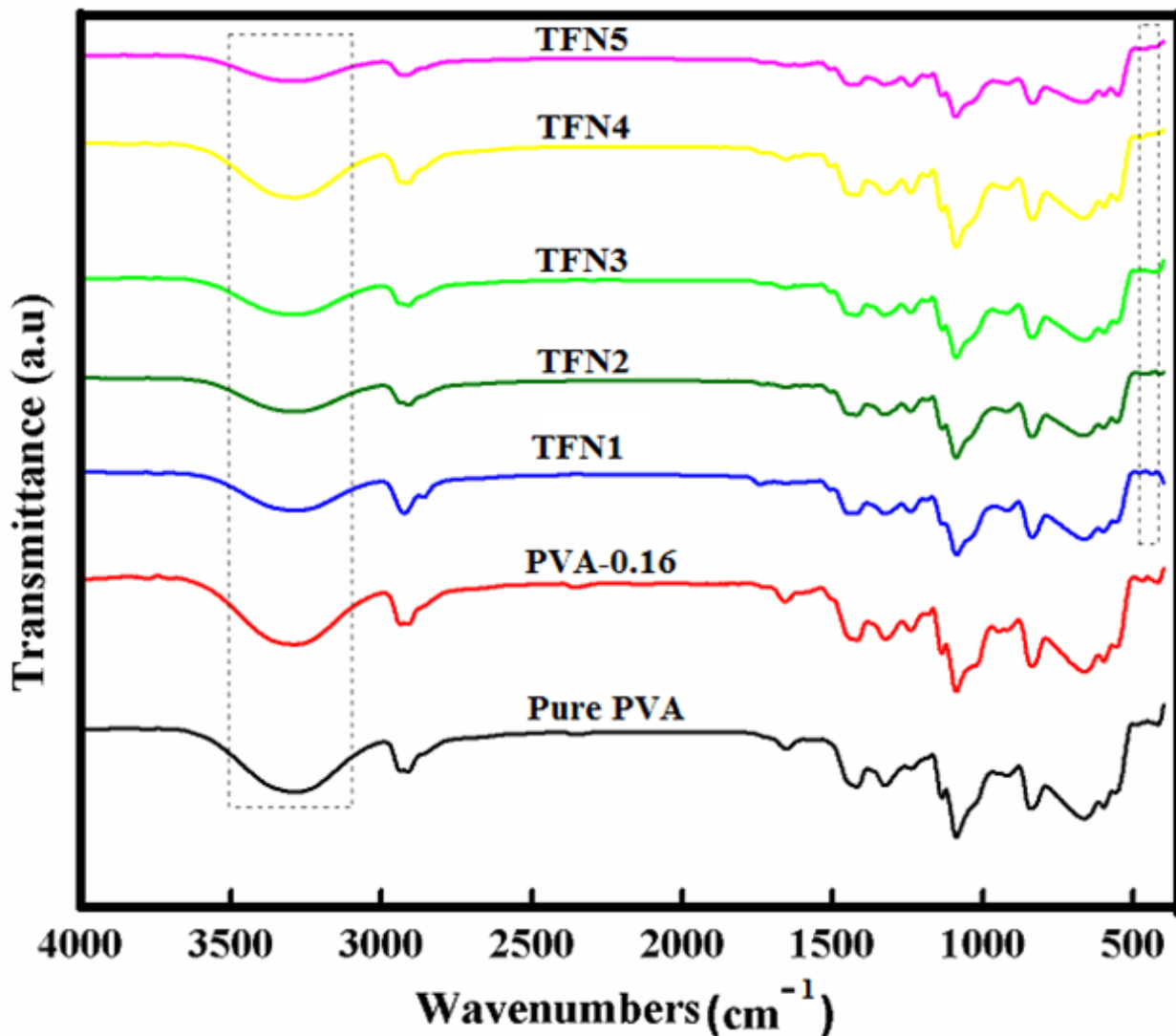


Figure 7.3 ATR-FTIR spectra of pure PVA, PVA-0.16 and TFN (1-5) membranes

7.4.2 Contact Angle Measurements

Figure 7.4 shows the contact angles of single layer crosslinked (PVA-0.16), TFC3 and TFN (1-5) membranes. The single layer crosslinked (PVA-0.16) membrane showed a relatively high contact angle of 70.8°. After the incorporation of Pluronic F-127, from 2 to 10 wt%, the contact angle of TFC3 membrane (6 wt%) decreased down to 57.1°. This decrease in the contact angle indicates an increase in hydrophilicity and a more

hydrophilic membrane surface typically produced better water permeability. The smaller contact angle also showed the increase in surface oxygen content [157]. Moreover, when ZnO-NPs loadings (0-0.1wt %) are added slightly to enhance hydrophilicity of the TFN (1-4) membranes as observed the decrease in contact angle from 52.5° and 48.8°. The reason could be due to the hydrophilic property of ZnO-NPs. But for TFN5, the contact angle again started to increase to 49.1°, which showed that the agglomeration of ZnO-NPs started blocking the pores in the membranes. Some of the nanoparticles tended to aggregate and could be partially exposed on the membrane surface at higher ZnO-NPs concentration. Thus, for TFN4 thin film nanocomposite membrane, surface hydrophilicity increased because of the sorption of water through the hydrophilic pores via capillary effects.

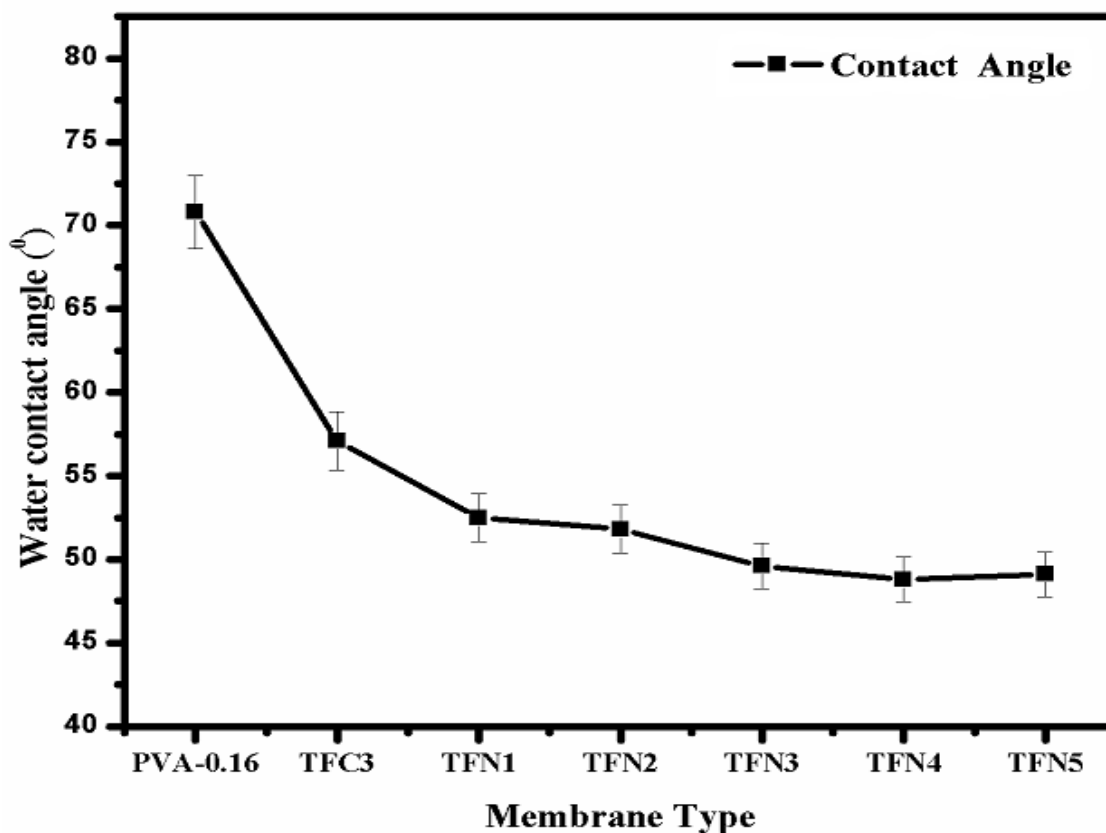


Figure 7.4 Contact angle of the prepared PVA-0.16, TFC3 and TFN (1-5) RO membranes

7.4.3 Structural Investigation

X-ray diffraction is used to find out the changes in microstructure of polymers and its composites. Figure 7.5 shows the diffraction pattern of pure PVA, PVA-0.16, TFC3 and TFN4. The XRD pattern of pure PVA (typical of crystalline PVA) membrane showed a strong peak at 19.35° ($10\bar{1}$), medium at 22.5° (101) and weak 40.5° (202) [241]. With the addition of crosslinker, the peak at 19.35° was broadened, which is acclaimed to be due to the presence of DGEBA that disrupt the semi-crystallinity of bonding scheme of PVA. It was observed that with the addition of ZnO-NPs in TFC3 membrane, the main diffraction peaks are present at 31.73° (100), 34.34° (002) and 36.42° (101) [242].

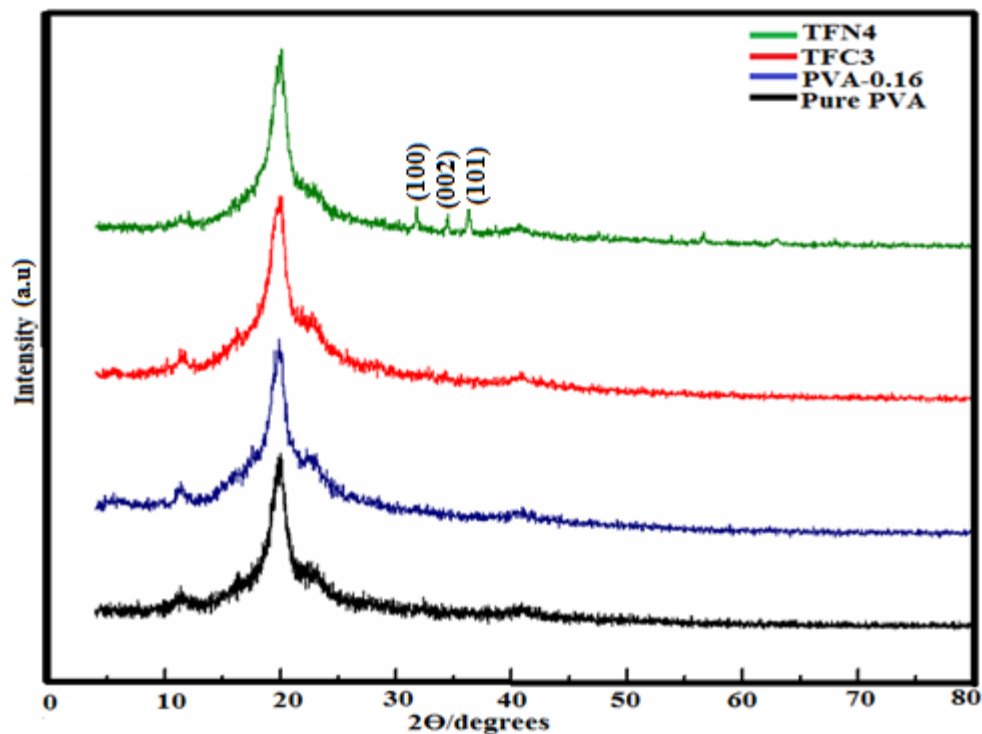


Figure 7.5 XRD patterns of pure PVA, PVA-0.16, TFC3 and TFN4 membranes

7.4.4 Scanning Electron Microscopy

The morphological studies of single layer crosslinked (PVA-0.16), TFC3 and multiple-layer TFN (1-5) membranes were carried out, as shown in Figure 7.6. It shows the morphology of all the membrane. The surface morphology of single layer crosslinked PVA-0.16 membrane is smoother and denser with no obvious porous structure. The additive (ZnO-NPs) is the influential factor for the final properties and structure of the membrane [243, 244]. SEM images inferred that the optimal concentration of Pluronic F127 (6 wt%) created pores in the membrane.

The micrograph images of TFN (1-5) membranes with different ZnO-NPs loadings (0-0.1wt %) are shown in Figure 7.6. They revealed that, the surface morphologies of the

membranes are significantly transmogrified with the infusion of ZnO-NPs. The interactions between ZnO-NPs and TFC3 disrupt the polymeric chains mobility [245]. It was observed that ZnO-NPs are evenly distributed in TFN (1-5) membranes but the pores started diminishing after optimal concentration of ZnO-NPs (0.08wt %), in which the defects of mottled surface are filled with agglomerates of ZnO-NPs, as shown in the SEM image. The nano pores (< 100 nm) are observed in TFN4 membranes.

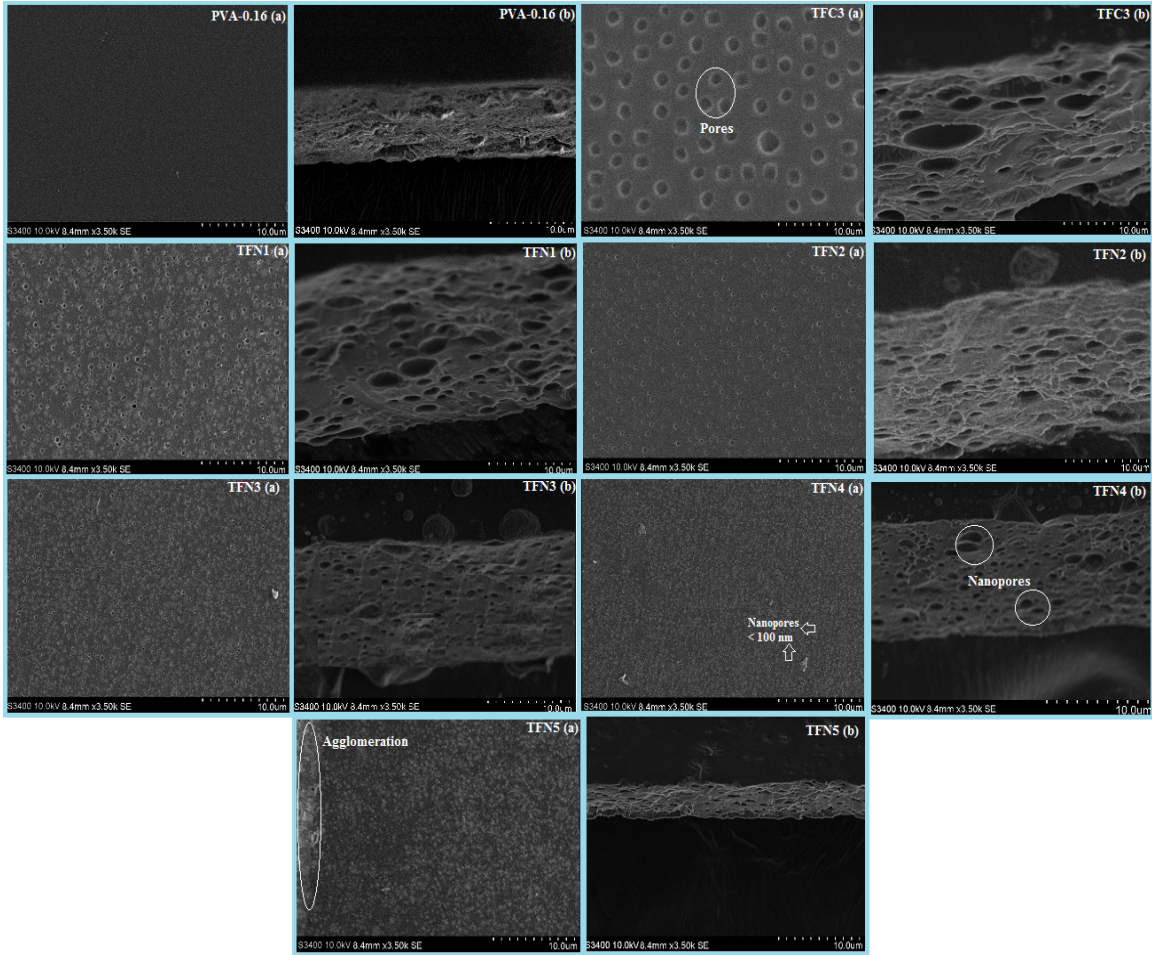


Figure 7.6 SEM micrographs of PVA-0.16, TFC3 and TFN 1-5 (a) top surface and (b) cross-section

7.4.5 Atomic Force Microscopy

Figure 7.7 shows surface topography of single layer crosslinked (PVA-0.16) and TFN (1-5) membranes. The PVA-0.16 membrane without Pluronic F127 and ZnO-NPs showed rough, ridge-valley structure [246, 247]. Upon ZnO-NPs infusion, the root mean square and average roughness (Rms and Ra) of the surface decreased with the increase in ZnO-NPs wt %, as given in Table 7.1. The decrease in surface roughness presented better condition for the adsorption on the membranes [108]. TFN (1-4) membranes showed that the surface roughness started decreasing with the increase in ZnO-NPs which optimize the extra-large pores caused by the Pluronic F127 content, as shown in SEM analysis. In TFN5, the surface roughness again increased. The small increase in surface roughness with the inclusion of larger amounts of ZnO-NPs could be due to the fact that the excess amounts will adhere to the surface and form the unwanted ridge-valley structure that increase the surface roughness. That effect could be seen from surface morphology images taken by SEM, which were discussed in the previous section.

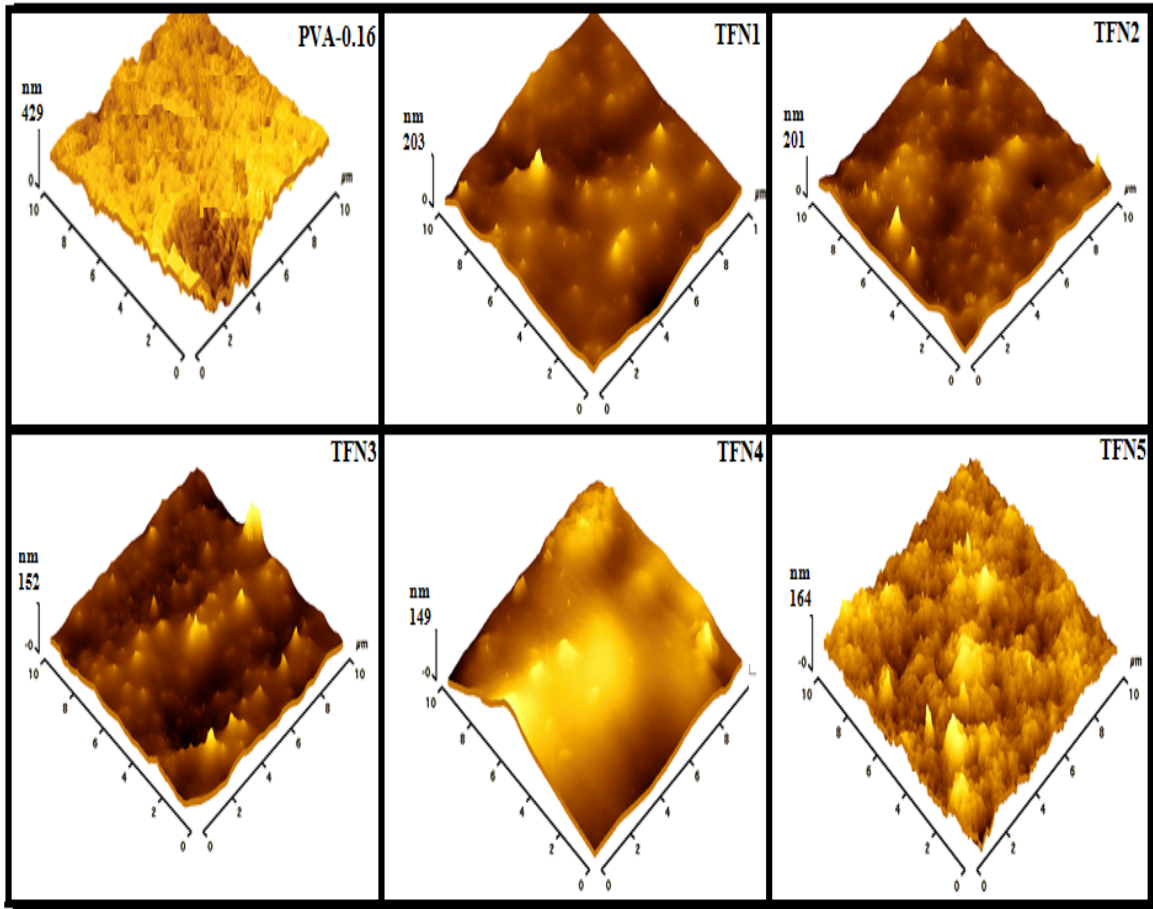


Figure 7.7 AFM images of single layer crosslinked PVA-0.16 and TFN (1-5) membrane

7.4.6 Mechanical Testing

The incorporation of ZnO-NPs into RO polymeric membranes can improve the mechanical properties due to the strong interfacial interactions between the organic polymer and the inorganic nanoparticles [69, 101, 105]. Figures 7.8 & 7.9 show the stress-strain curves and the Young's modulus, elongation at break ultimate tensile strength for TFN (1-5) membranes, respectively. TFN (1-5) membranes showed very high strength compared to the single layer crosslinked PVA-0.16 membrane. The yield strength is increased to almost double in TFN4. Overall, the mechanical properties of TFN (1-5) membranes have good mechanical stability. Mechanical strength is a crucial property in reverse osmosis processes, since the operating pressure is extremely high, of the order of 55 bar. It is observed that the tensile strength is increased gradually from 21.94 MPa in TFN1 to 41.97 MPa in TFN4. This is an outstanding finding, because the synthesized membranes are being utilized without substrates. Most of the RO membranes have a substrate layer for mechanical support. This layer may interfere undesirably with the reverse osmosis process.

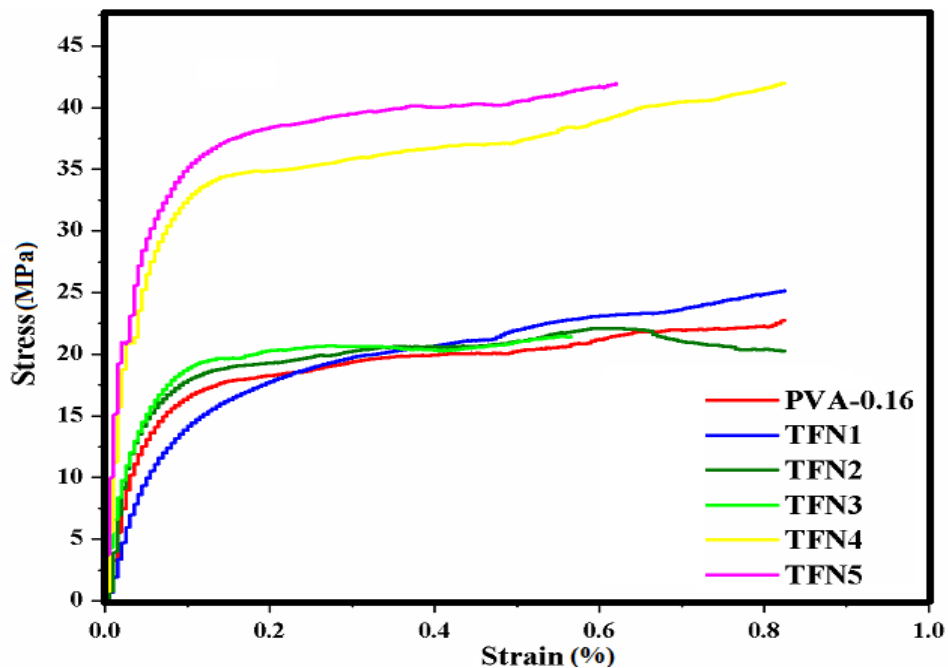


Figure 7.8 Stress-strain curves of PVA-0.16 and TFN (1-5) membranes

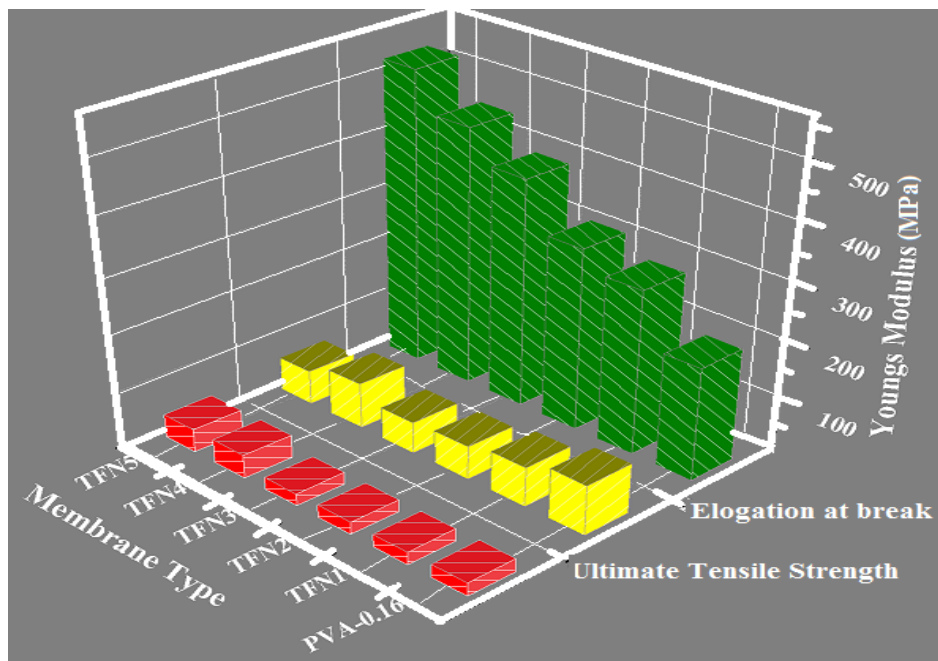


Figure 7.9 Young's modulus, Ultimate tensile strength and Elongation at break of PVA-0.16 and TFN (1-5) membranes.

7.4.7 Reverse Osmosis Separation Performance Testing

7.4.7.1 Effect of crosslinker on PVA membrane separation performance

Membranes were formed with and without varying concentration of DGEBA crosslinker (0-0.2wt %). Figure 7.10 shows the permeation flux and salt rejection of pure PVA and crosslinked membranes. It shows that increasing the amount of crosslinker resulted in continuous increase in salt rejection and demonstrates that the separation performance of pure PVA membrane is lower than crosslinked membranes.

With the lowest concentration of DGEBA (0.02wt%), the separation performance showed permeation flux of $1.21\text{m}^3/\text{m}^2/\text{day}$ and salt rejection of 42%. When employing single layer crosslinked PVA-0.16 membrane, the permeation flux declined to $0.66\text{m}^3/\text{m}^2/\text{day}$, while salt rejection increased up to 54%. When the crosslinker concentration increased up to 0.2wt%, there was no such visible difference found in the salt rejection and only a slight difference in permeation was observed as compared to PVA-0.16 membrane. Thus, that crosslinker concentration could be applied in the subsequent experiments. In PVA-0.2 the salt rejection slightly declined to 53 % but the permeation flux dropped to $0.59\text{m}^3/\text{m}^2/\text{day}$ endorsing the fact that the membrane is so dense and packed in structure that it hindered water to pass through. The single layer crosslinked PVA-0.16 membrane had the optimal concentration that yielded the best separation performance for better salt rejection.

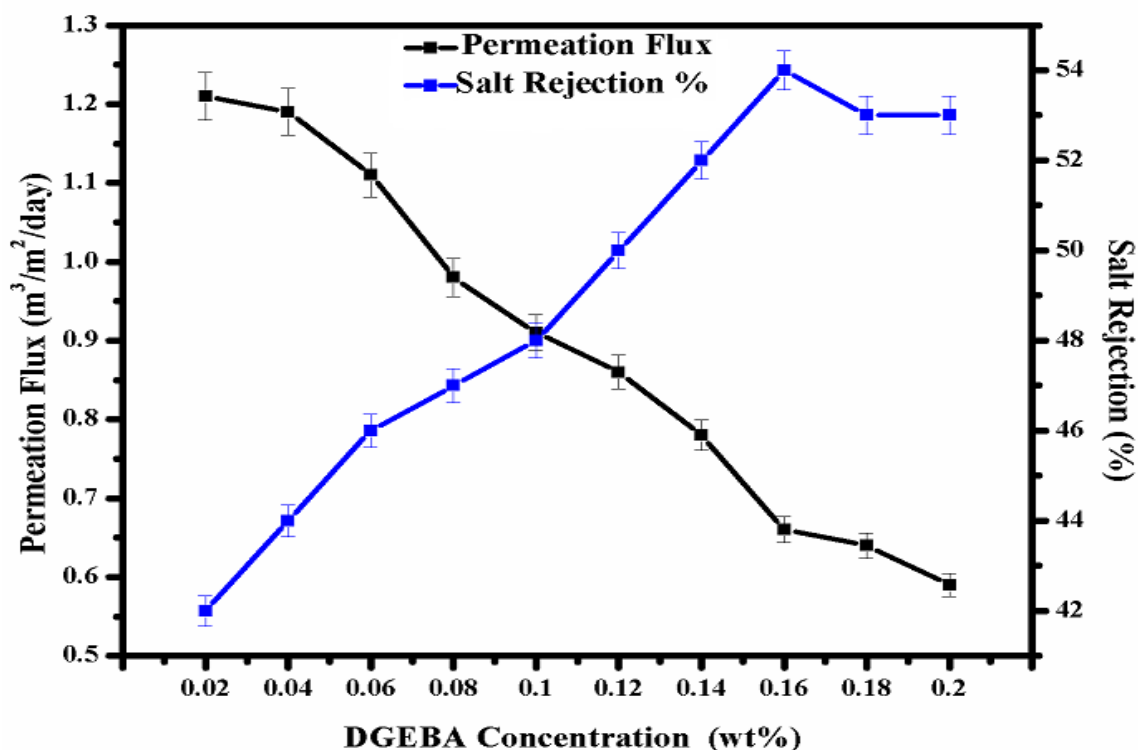


Figure 7.10 Effect of different concentration (0-0.2wt%) of crosslinker (DGEBA) on pure PVA membrane for separation performance.

7.4.7.2 Effect of Pluronic F127 loading on membrane separation performance

Figure 7.11 shows the effects of Pluronic F127 loading (0-10wt %) in single layer PVA-0.16 crosslinked membrane for RO desalination performance. The permeation flux increased continuously from $1.32 \text{ m}^3/\text{m}^2/\text{day}$ for TFC1 up to $1.71 \text{ m}^3/\text{m}^2/\text{day}$ for TFC5. The results indicated that the TFC3 had optimal performance due to the significant increase of the permeation flux, while maintaining the salt rejection. TFC3 (6wt%) showed more than double permeation flux ($1.58 \text{ m}^3/\text{m}^2/\text{day}$) compared to that of single layer PVA-0.16 crosslinked membrane. On the other hand, the salt rejection was 69.2%,

but kept nearly constant from TFC1-TFC3, but then showed a decrease to 68.4 and 67.6 % for TFC4 and TFC5 respectively.

The significant flux increase by the addition of Pluronic F127 is acclaimed to the Pluronic F127 particles that might change the bulk PVA membrane structure possibly by the formation of nano gaps at the interface, which could be responsible for the enhanced permeation flux. In addition, as shown by the contact angle measurements, the hydrophilicity of the TFC membranes have improved by the incorporation of hydrophilic side of Pluronic F127 particles. The tendency of pore formation is increased with Pluronic F127 and consequently the permeation flux enhanced.

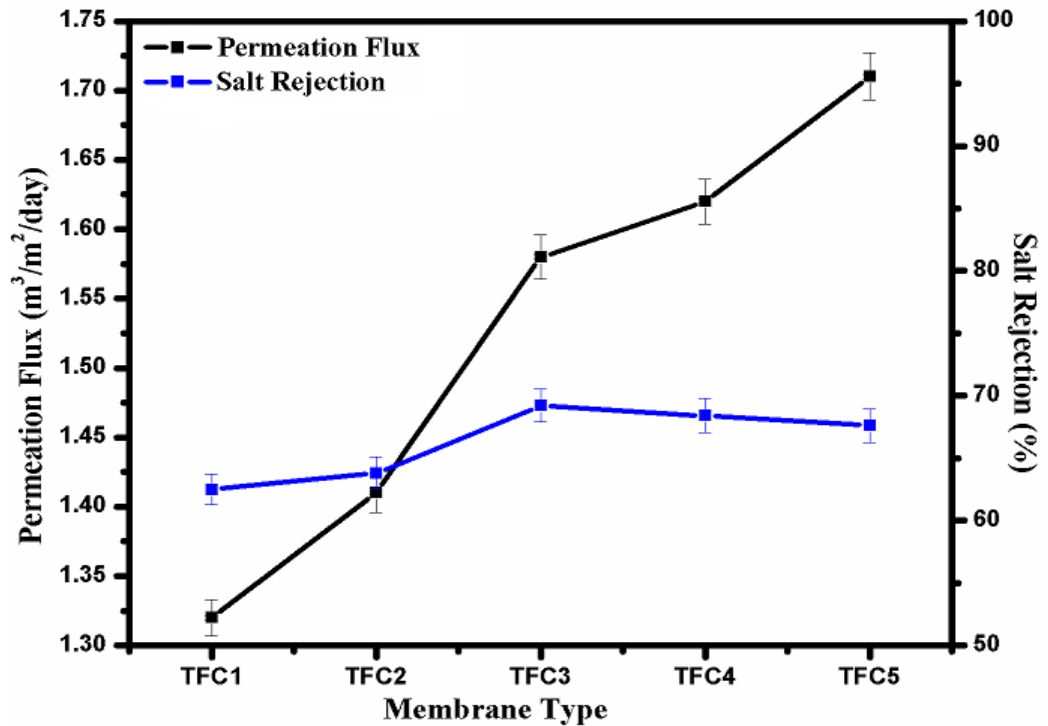


Figure 7.11 Effect of Pluronic F127 loading (0-10 wt%) on PVA-0.16 membrane for separation performance.

7.4.7.3 Effect of ZnO-NPs Loading on TFC membrane separation performance (TFN)

Figure 7.12 shows the effect of ZnO-NPs loading on TFC3 membrane, the permeation flux of TFN4 (0.08 wt% of ZnO-NPs) membrane is $1.96 \text{ m}^3/\text{m}^2/\text{day}$, which decreased in TFN5. The solution diffusion model can better elucidate the transport mechanism of the TFN membranes. It involves three steps: sorption at surface, diffusion under pressure into dense membrane and lastly the phenomena of desorption. The infusion of ZnO-NPs in TFC3 membrane can disrupt the packing of polymer chains by forming micro-porous defects between polymer interface and inorganic particles. The salt rejection increased from 69.2 for TFC3 to 98.7% for TFN4 membranes as a result of the incorporation of ZnO-NPs [241, 248]. The permeability of TFN (1-5) membrane increased with the increase in ZnO-NPs wt%. The PEO group in Pluronic F127 naturally acts as a driving force for water sorption and as a pore former in the membranes [69, 101, 242, 249]. TFN4 membrane, with optimal quantity of Pluronic F127 and ZnO-NPs, showed an increase in flux, and at the same time maintained high salt rejection. However, a slight decrease in permeation flux was observed at highest ZnO-NPs loading, TFN5 (0.1 wt%). The reason is probably acclaimed to the agglomeration of ZnO-NPs [250-253].

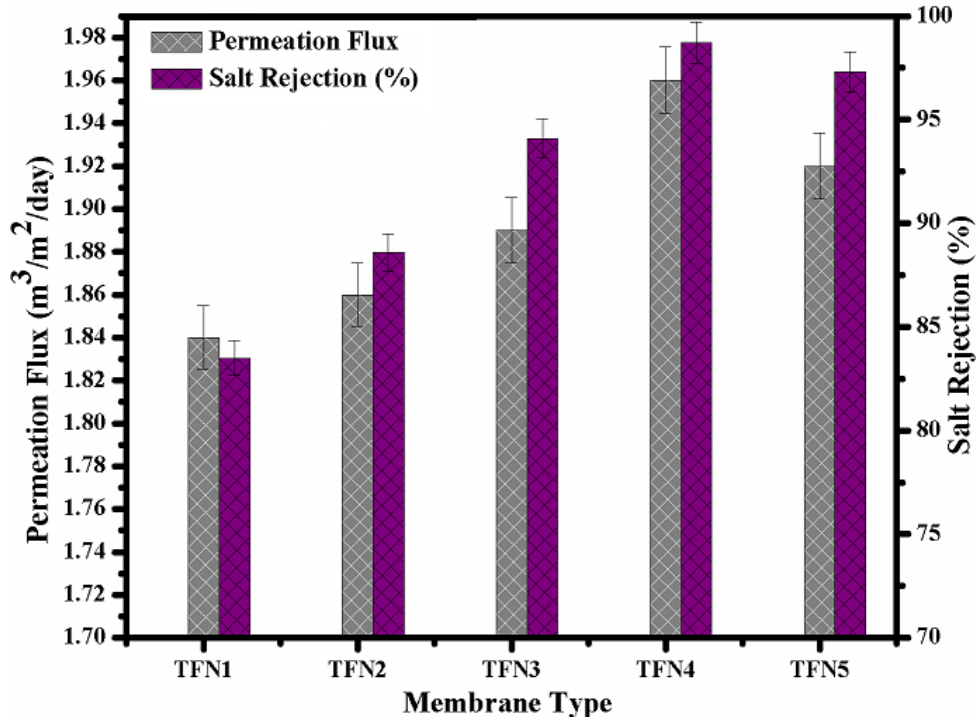


Figure 7.12 Effect of ZnO-NPs loading (0-0.1wt%) on TFC3 membrane for separation performance.

7.4.8 Chlorine Resistance of TFN-RO Membrane

The change in salt rejection before and after the Chlorine exposure is represented in Figure 7.13. Each of TFN (1-5) membranes is exposed to the sodium hypochlorite solution. The salt rejection of the PVA-0.16 membrane dropped from 54 to 41% after Chlorination. The significant performance decline for the single layer crosslinked PVA-0.16 membrane was caused by the severe conformational deformations of the polymeric chains. The orton-rearrangement and subsequent N-Chlorination and ring-Chlorination reactions could disrupt the intermolecular hydrogen bonds between the polymer chains in membrane and destroy the symmetry of PVA network leading to a transformation of crystalline regions to an amorphous sites [248]. The partial destruction of PVA layer

increased the free volume and flexibility of the polymer matrix, which caused free salt passage through the membrane [105]. Chlorine resistance of the TFN-RO membranes can be ascribed to the improved hydrophilicity and ZnO-NPs barrier is able to protect the polymeric thin layer [69]. Moreover, due to crosslinking and infusion of ZnO-NPs, the intermolecular hydrogen bonding was enhanced between the TFN membranes containing various functional groups. This impeded the substitution of hydrogen with Chlorine on the -OH groups of the PVA and increased the Chlorine resistance of the membrane [101].

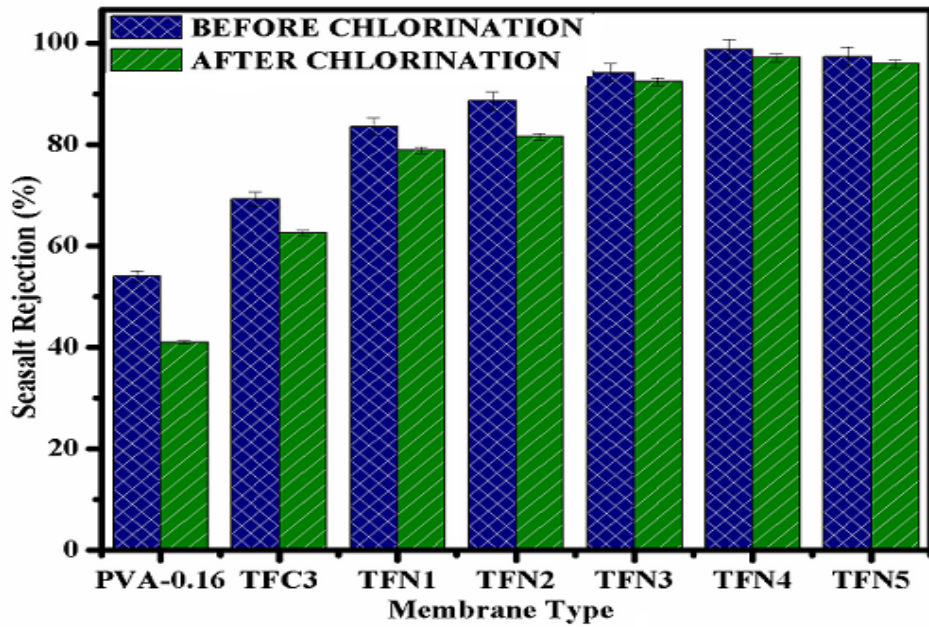


Figure 7.13 Chlorine resistance analysis before and after Chlorination for PVA-0.16, TFC3 and TFN (1-5).

7.5 Conclusion

TFN-RO membranes were prepared using dissolution casting method and ZnO-NPs were infused in the PVA single layer membrane by dispersion. The incorporation of Pluronic F127 and ZnO-NPs improved the performance of RO membrane in terms of water permeability, salt rejection and Chlorine resistance by improving hydrophilicity and surface roughness of TFN. TFN4 membrane containing 0.08 wt% ZnO-NPs exhibited superior RO performance including 1.96 m³/m²/day permeation flux, 98.7% NaCl rejection and improved Chlorine resistance.

CHAPTER 8

Hyperbranched Polyethyleneimine, A Polycation Induced Zwitterionic Membrane for Improved Fouling Resistance and High RO Performance

8.1 Introduction

Fouling is getting increased attention in different applications, ranging from biomedicine to membrane desalination processes. It refers to the unplanned accumulation of whole organisms (algae, plants, animals or microorganisms), biopolymers or unreacted surfactants on the wet structures of the membranes (reverse osmosis, micro, ultra filtration etc.). Reverse osmosis (RO) membranes are the most prevalent water purifying materials due to their high permeation rates and salt rejection as well as their excellent chemical, mechanical and thermal stability [5]. However, RO membranes fouling can lead to shortened membrane lifetime, reduction in permeation flux and decline in salt rejection [254]. This constraint is considered as a deadlock to improve the efficiency of RO process [255]. The fouling process can be reduced or delayed by periodic cleaning, pretreating the feed water, and surface modification of RO membranes [256, 257]. The first two methods are time-consuming and expensive as the periodic cleaning will shorten the membrane span life [258, 259]. Surface modifications like chemical bonding and physical adsorption are possible solutions to fouling problems [260].

RO membranes are sometimes classified into charged and neutral membranes based upon their inherent surface charge property. Broadly, applications of charged RO membranes are more than the neutral ones due to their fouling resistance. Anionic membranes generally attract positively charged species and are prepared mostly with carboxyl

containing groups. Thus, they often assure repulsion effect against the negatively charged substances, like colloids, anions, bacteria and so on [261, 262]. Similarly, cationic RO membranes often possess amino acids and their derivatives, which illustrate electrostatic repulsion on positively charged species. Moreover, anti-bacterial property of amino acid and its derivatives can enhance the RO system stability. Zwitterionic polymers (ZPs), which contain both anionic and cationic groups in the same unit are vital as an anti-fouling materials [263]. Due to the inter and intra-bonding between opposite charges within a zwitterion, “free water” hydration layers form and occupy the zwitterionic groups [264, 265]. The ionic solvation of these “free water” molecules, is much stronger than hydrogen bonded water molecules present in neutral hydrophilic polymers [266, 267]. This trait is the primary reason why zwitterionic molecules possess superior antifouling properties and excellent permeability compared to normal hydrophilic polymers. Zwitterionic-based materials can strongly cohere water molecules via electrostatically induced hydration. Therefore, zwitterionic-based materials are considered as the most promising candidates for the preparation of low fouling membrane surfaces [268, 269].

Hyperbranched polyethyleneimine (HPEI), an antifouling polymer, contains amine groups, which are widely used to modify the surface of RO membranes [270, 271]. By various methods of surface modification, HPEI can be retained onto the surfaces of base membranes and used as ligands or to provide more coupling sites for immobilization of different ligands [272, 273]. It owns a mixed charge property, which originates from negatively and positively charged moieties of different types of amino acid residues [274].

In this study, we focused on fabricating novel HPEI induced RO membranes by deposition of (HPEI) for antifouling RO membranes. Antifouling performance was observed for optimized zwitterionic coating with CTAB solution as a standard cationic surfactant foulant. HPEI-RO membranes are further characterized by contact angle measurement (θ), Fourier transform infrared spectroscopy (FTIR), scanning electron microscope (SEM), X-ray diffraction (XRD), atomic force microscope (AFM). The fouling resistance analysis of the optimized zwitterionic coatings under arduous fouling conditions was observed. The permeability and selectivity were studied using dead-end filtration unit.

8.2 Experimental

8.2.1 Materials

Analytical grade poly (vinyl alcohol) PVA ($M_w=89000$), maleic acid as a crosslinker ($C_4H_4O_4$; MA > 99%), Pluronic F-127 (pore former), hydrochloric acid (HCl) and hyperbranched polyethyleneimine (HPEI) were obtained from Sigma Aldrich (USA). Commercially available natural sea salt collected from Pacific Ocean (USA) was used for RO process. All the chemicals were used without further treatment.

8.2.2 Membranes Synthesis

8.2.2.1 Synthesis of PVA/MA crosslinked membranes

PVA (17.5wt %) was mixed with different wt % of maleic acid (Table 8.1) along with 1 mL of 2 M HCl (crosslinking catalyst) to prepare crosslinked solutions. The mixture was dissolved in distilled water (82.5wt %) with continuous stirring of each solution for 6 h at 80 °C. The clear, viscous and homogenous solutions of five concentrations of maleic acid

(0-0.1wt %) were dried at 60 °C and labeled as PVA/MA. The PVA/MA membranes were tested in RO assembly and the membrane with maximum salt rejection was selected. Then, different concentrations of Pluronic F-127 (0-5wt%), shown in Table 8.1 were composited with selected PVA/MA0.04 solution and magnetically stirred for 4 h at 80 °C until homogeneous solutions (labeled as PVA/MA/PluronicF127) were formed. The PVA/MA/PluronicF127 solutions were spread slowly on Petri dishes and placed in an oven at 60 °C for controlled evaporation of solvent keeping uniform thickness of the membrane. The solution was transferred to each Petri dish of the same diameter with equal quantity utilizing the dissolution casting methodology. The membranes were carefully removed from each Petri dish using sharp blades. PVA/MA/PluronicF127-4 (4 wt % of Pluronic F127) membrane showed highest permeation flux and maximum selectivity (salt rejection) and was selected for further treatment as a zwitterionic membrane.

8.2.2.2 *Membrane modification as zwitterion membrane*

HPEI was mixed in water at a pre-determined amount (1000-4000 ppm). The PVA/MA/PluronicF127 base was kept in a stationary test cell where the cylindrical cell behaved as a feed reservoir. Modification of membrane was conducted by charging the HPEI solution into the permeation chamber and the membrane surface contacted the solution for 4 h at ambient conditions, during which the polycation was deposited onto the PVA/MA/PluronicF127-4 membrane surface. Then the HPEI solution was taken out from the permeation cell and the membrane was properly rinsed with the deionized water. Throughout the membrane modification phenomenon, membranes were remained wet.

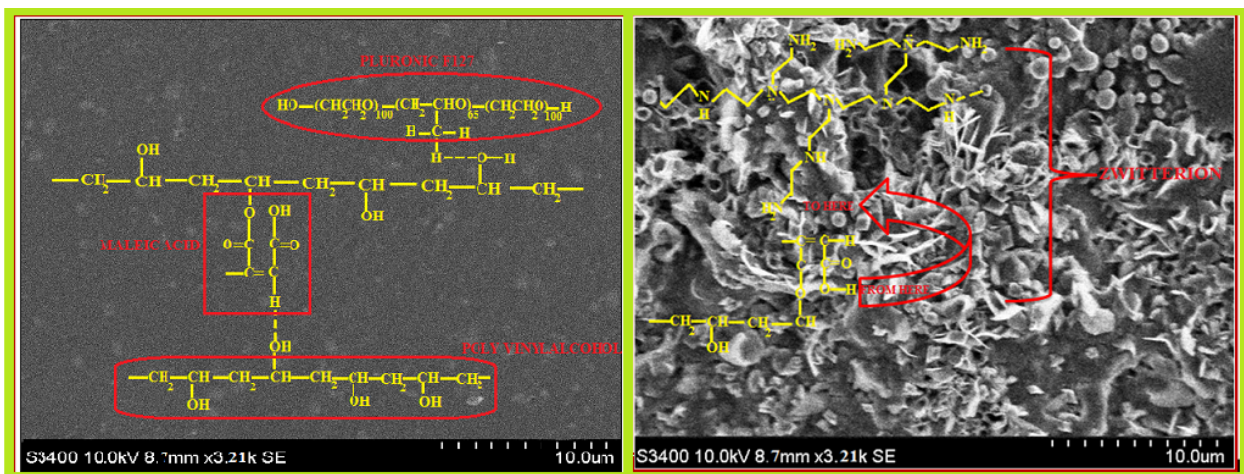


Figure 8.1 Schematic representation of Zwitterion membrane formation.

Table 8.1 Weight percentages of PVA/MA, Pluronic F127 and HPEI.

	Amount of loadings					
*Maleic acid (wt.%)	0	0.02	0.04	0.06	0.08	0.1
**Pluronic F127 (wt.%)	0	1	2	3	4	5
Hyperbranched Polyethyleneimine (HPEI) (ppm)	1000	2000	3000	4000		
*with 0.04wt.% of Maleic acid						
**with 0.04wt.% of maleic acid and Pluronic F127 4wt.%						

8.3 Membrane characterization

8.3.1 Fourier Transform Infrared Spectroscopy

An IR Prestige-21 (Shimadzu) using attenuated total reflectance (ATR) accessory equipped with zinc selenide (ZnSe) crystal was used to obtain FTIR spectra of the composite membrane samples. Before each sample scan, an air background of the instrument was run. The frequency range was from 4000-600 cm^{-1} at a resolution of 4.0 cm^{-1} and average of 120 scans per spectrum were reported.

8.3.2 Contact Angle Measurements

Goniometer (Digidrop, KSV Instruments) was used to evaluate sessile drop contact angles of single layer crosslinked (PVA-0.16), TFC3 and TFN (1-5) membranes. The equilibrium value was average of right and left angles. The reported data were the average of three measurements for each membrane sample.

8.3.3 Scanning Electron Microscopy

SEM micrographs of the membranes pure PVA, single layer crosslinked (PVA-0.16), TFC3 and TFN (1-5) were taken on S-3400N Hitachi (USA). The instrument was operated under low vacuum mode to analyze sample. For gold sputtering, samples were prepared by using DENTON VACUUM SPUTTERING AUTOMATICO DESK IV. Sputtering on the target will generate particulate vapor, which will condense into very thin, amorphous layers on available surfaces within the vacuum chamber. This instrument was primarily utilized for SEM sample preparation.

8.3.4 Atomic Force Microscopy (AFM)

Atomic force microscopy (AFM) imaging was conducted using a Digital Instruments (Santa Barbara, Ca) Dimension 3000 with a Nanoscope III controller. Topographical images were taken using standard tapping mode. In PFT-mode, a cantilever was oscillated sinusoidally at 350 kHz resonant frequency, and brief contacts with the sample surface at the down stroke of each cycle. A user-established set point force was established so that the sample surface was minimally deformed (on the order of a few nanometres) and used as feedback control. Scanned images were taken at 512 x 512 pixel resolution.

8.3.5 Mechanical Testing

The mechanical properties of the TFN (1-5) membranes, i.e. the stress strain curves, ultimate tensile strength, elongation at break and the Young's modulus, were primarily evaluated. Instron 5567 Tensile Testing Machine fitted with a 10 kN load cell was used to perform the load-extension experiments. Membranes were cut into strips with gauge length and width of 50 and 10 mm, respectively. The thickness of the membrane samples was measured using a micro-caliper and maintained at ~0.1 mm for all of the tested samples. All specimens were drawn at ambient temperature and the Young's modulus was calculated in triplicate using stress-strain curves, which were instantaneously recorded by a computer. A crosshead speed of 10 mm/min was maintained throughout the tensile experiments.

8.3.6 Biofouling Testing

The fouling tests for the membranes were conducted by adding different concentration (10, 50 and 100 ppm) of a cationic surfactant (CTAB) in the feed solution, and the

antifouling characteristic of the membrane was assessed by observing the permeation flux with respect to time.

8.3.7 Bacterial Adhesion Testing

The bacteria was kept warm in a solution of peptone and beef extract per liter and rotating at 100 ppm until it attained the immobile phase, with the amounts of $7-5.5 \times 10^8$ (CFU/mL) and $1.5-4 \times 10^9$ (CFU/mL) for *S. epidermidis* and *E. coli*, respectively. Samples of coated and uncoated control membranes were taken for analysis. These specimens were immersed at 38 °C in 1 mL of bacterial broth at 100 ppm. After 24 h of soaking, the samples were washed 4 times by 1 mL Phosphate-buffered saline (PBS). At the end, the samples were stained by Molecular Probes Live/Dead stain, which contained Syto-9 and Propidium Iodide to indicate dead cells as red and live cells as green [275].

8.4 Results and Discussion

8.4.1 Fourier Transform infrared spectroscopy

Figure 8.3 shows the FTIR analysis that was conducted to confirm the proposed interactions between PVA, Pluronic F127, and hyperbranched polyethyleneimine (HPEI) in the presence of constant amount of Maleic Acid (MA). The $-CH$ stretching was confirmed by the existence of band at 2914 cm^{-1} , which was moved towards lower wavenumber 2875 cm^{-1} due to the H-bonding with the addition of HPEI. The C-N band of HPEI was observed at 1183 cm^{-1} [276, 277]. The strong band at 3281 cm^{-1} was attributed to hydrogen bonded $-OH$ present in PVA and Pluronic 127 and also $-NH_2$ of HPEI [278]. A strong stretching band at

1643 cm^{-1} was ascribed to $-\text{C}=\text{C}-$ group of maleic acid [279]. The band at 1090 cm^{-1} in all spectra determined the existence of C-O band in PVA and Pluronic 127 [280, 281].

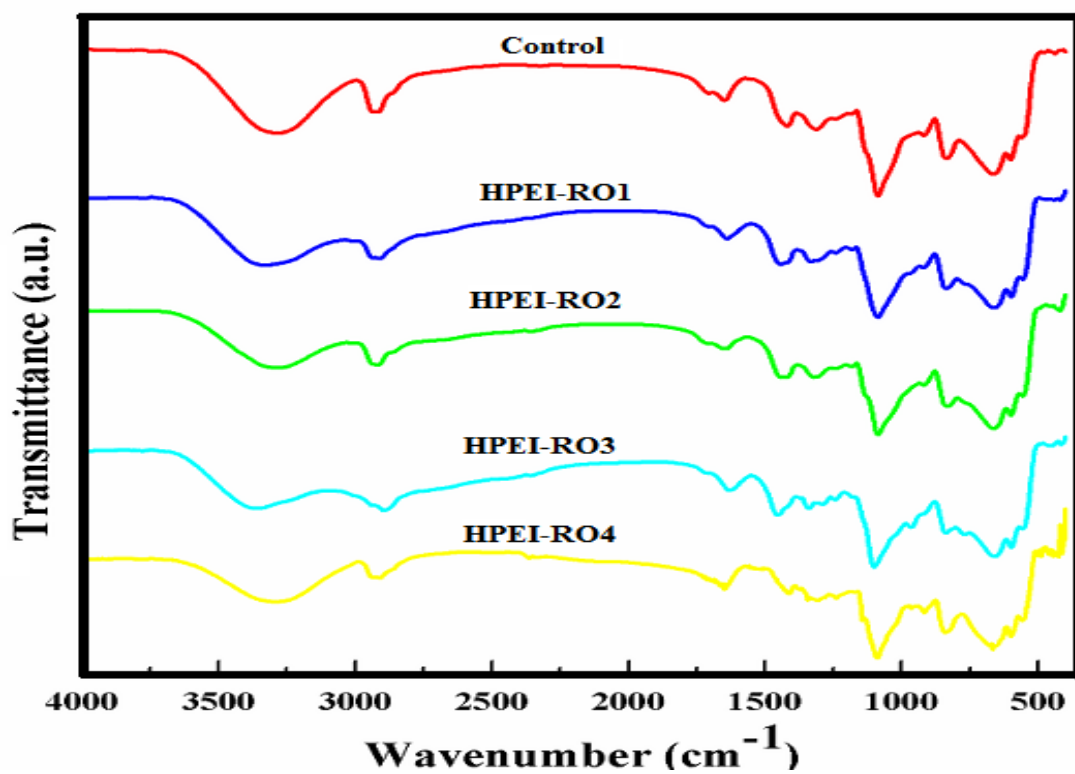


Figure 8.3 FTIR of control and HPEI-RO (1-4) membranes.

8.4.2 Contact Angle Measurements

Water contact angle was measured to determine the hydrophilic nature of the modified membranes. Figure 8.4 shows the water contact angle for the samples. Surface modification of membranes with HPEI decreased the water contact angle, which was due to the incorporation of hydrophilic groups. It was noted that after surface modification with HPEI, the water contact angle was reduced to 34.6° which was smaller than the controlled RO membrane.

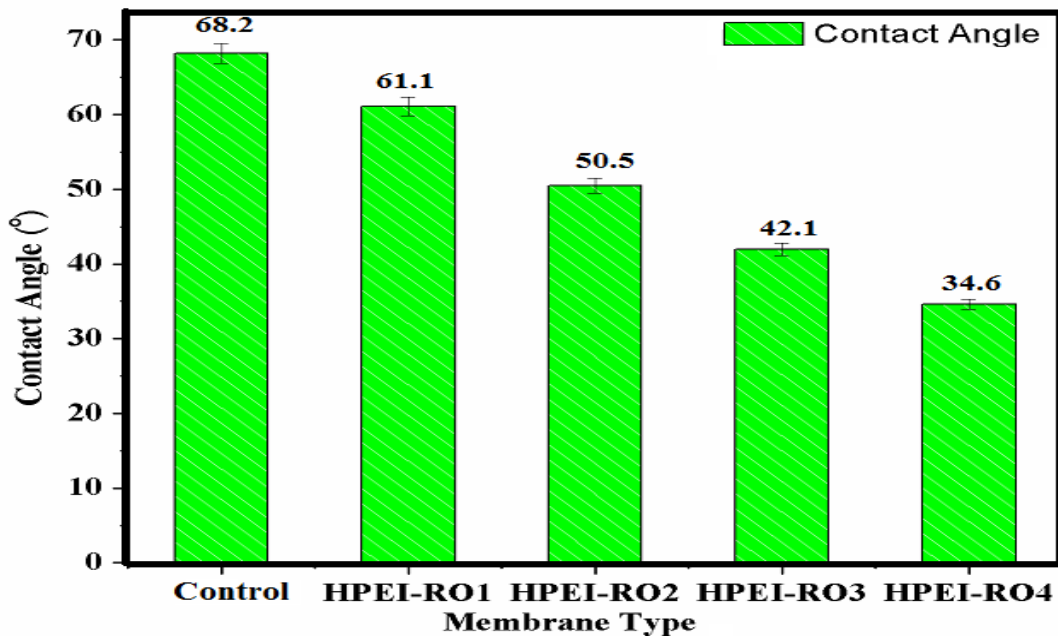


Figure 8.4 Contact angles of control and HPEI-RO (1-4) membranes.

8.4.3 Atomic force microscopy

Figure 8.5 displays the three-dimensional AFM images of control and HPEI-RO (1-4). It was observed that there was a conventional nodular structure, and the root mean square roughness (RMS) of HPEI-RO membranes decreased from 18.29 to 5.42 nm with increase in HPEI molar ratio from 1000 to 4000 ppm which might be due to the addition of HPEI, that had an ability to form chain conformation. The enhancement in inter- and intra-chain electrostatic attraction decreased the flexibility and rotational freedom of polymer chains, which resulted in a reduction in surface roughness [282]. The reduced surface roughness had also been discussed in literature in some other polymer modification membranes [283, 284]. This examination was mainly significant for the improvement of anti-fouling behavior of RO membranes as preceding literature had shown that the lower the roughness of a membrane surface, the lesser the adsorption of foulants [79].

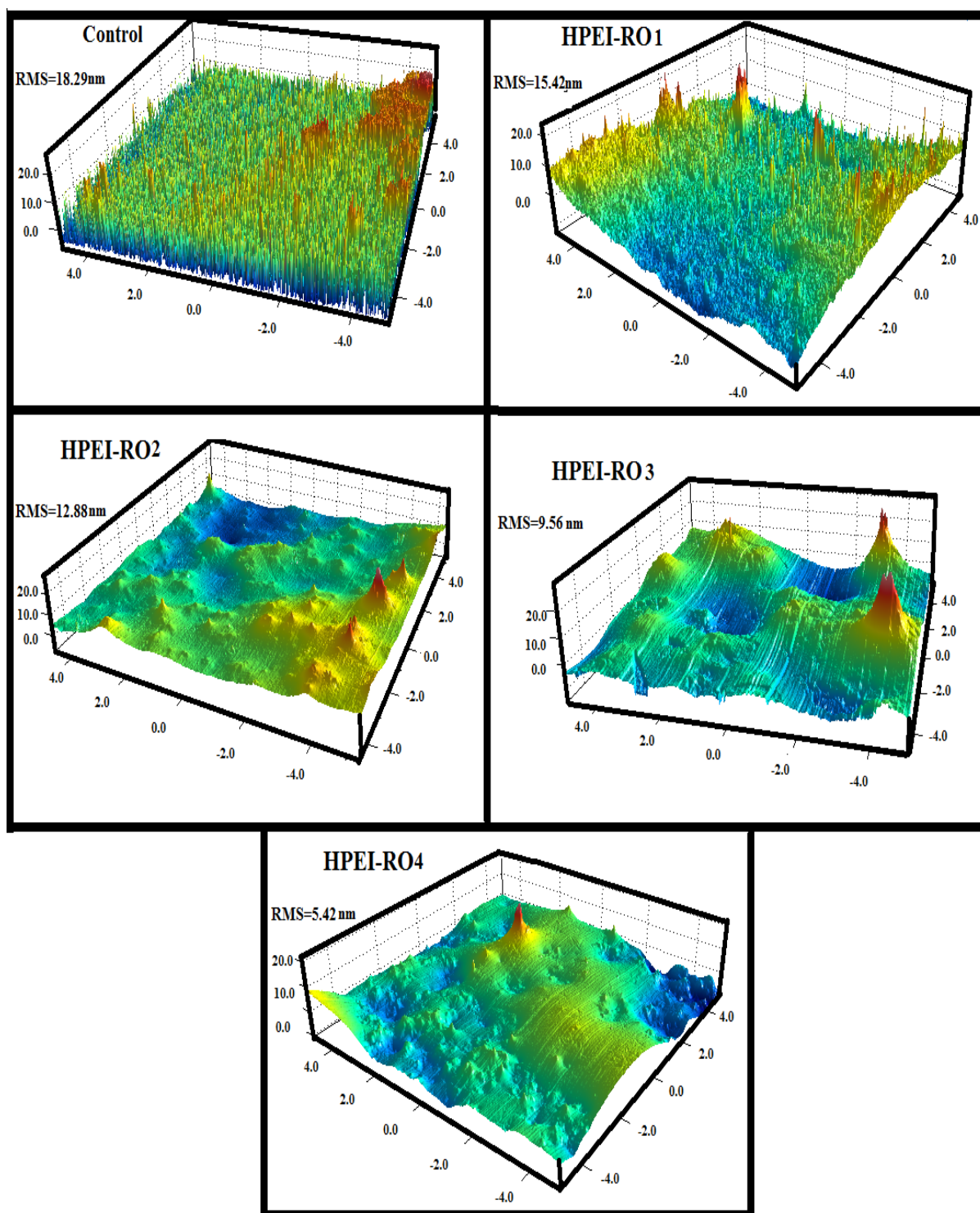


Figure 8.5 AFM images of control and HPEI-RO (1-4) membrane.

8.4.4 Scanning Electron Microscopy

The morphological studies of controlled, HPEI-RO (1-4) membranes were carried out, as shown in Figure 8.6. The control membrane was smoother and denser with no obvious porous structure. The HPEI is the influential factor for the final properties and structure of the membrane [285, 286]. SEM images inferred that Pluronic F127 created pores in the membrane. The figure revealed that the surface morphologies of the membranes were considerably transmogrified with the infusion of HPEI. The interaction of HPEI with PVA/Pluronic F127 disrupted the polymeric chains mobility [287]. The nano pores (< 100 nm) were observed in all HPEI-RO membranes. The observation suggested that the infusion of HPEI-RO as hybrid intermediate increased the compatibility between the interface layers.

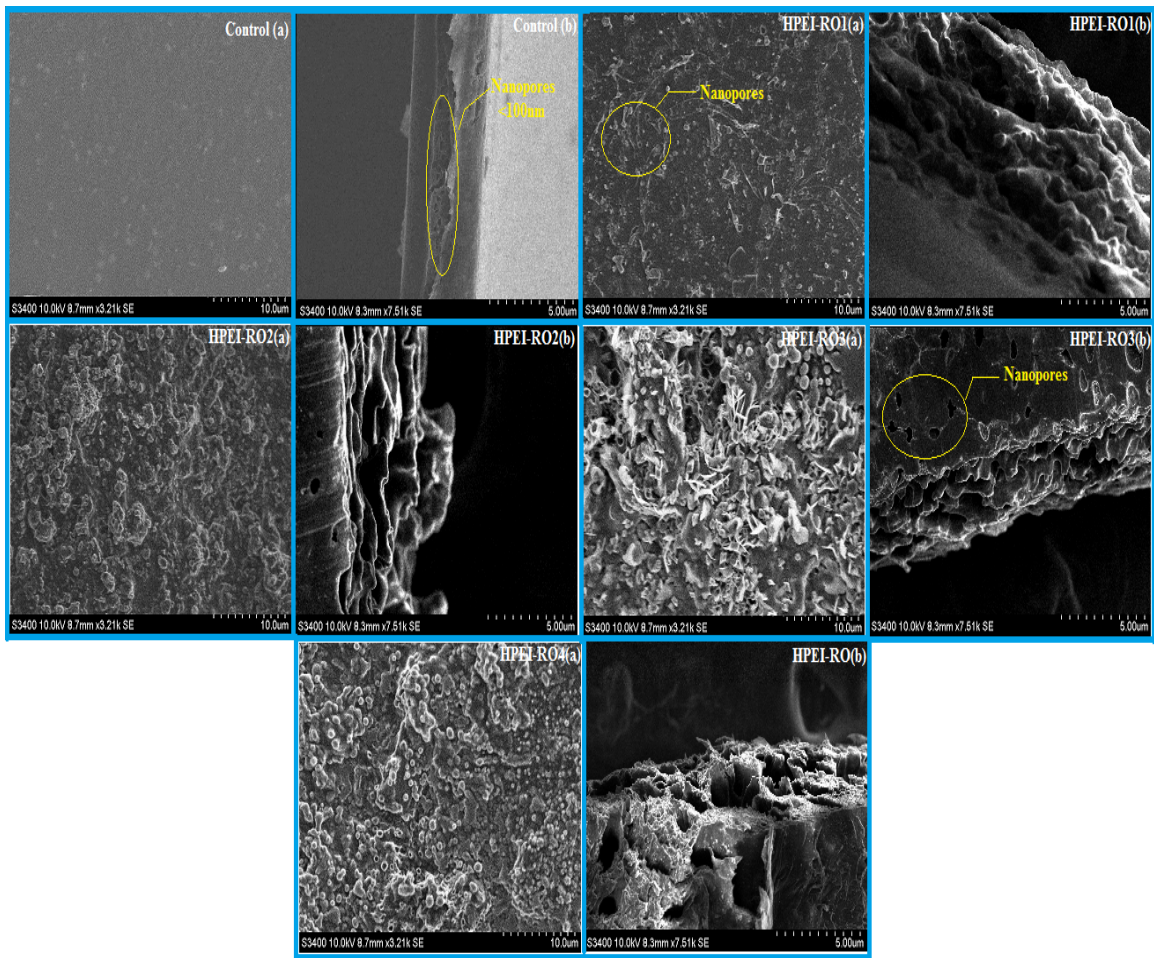


Figure 8.6 SEM micrographs of control and HPEI-RO(1-4) (a) top surface and (b) cross-section.

8.4.5 Membrane Fouling Resistance for HPEI-RO Membranes

Membrane fouling tests were carried out with salt (NaCl) solution using different concentration of CTAB (cationic surfactant) as a standard foulant. Figure 8.7 shows one set of membrane fouling experiment having CTAB (10, 50 and 100 ppm) concentrations. It was observed that in all of the samples with and without modification, the permeation flux started decreasing and after 6 h, the decline gradually approached a quasi-steady state. As shown from the figure, the zwitterionic membranes showed much improved water flux compared to the unmodified membranes. This implies that the zwitterionic membranes were truly biofouling resistant. The presence of foulants did not alter the performance of the modified membranes.

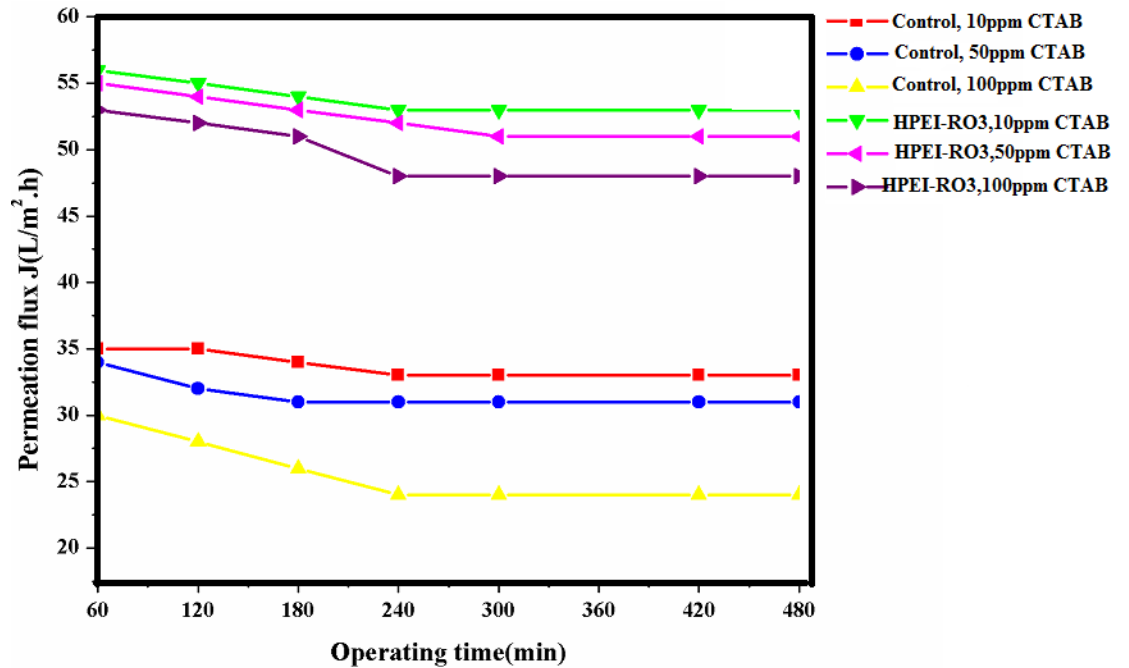


Figure 8.7 Permeation fluxes of control and HPEI-RO3 membranes during RO tests with NaCl solutions (3.28wt.%) containing different level of CTAB. The modified membranes were surface modified with 3000ppm HPEI.

8.4.6 Bacterial Adhesion test

The membrane resistance to bacterial adhesion was tested using two bacteria, *E. coli*, a Gram-negative bacterium and *S. epidermidis*, a Gram-positive bacterium. The two bacteria were cultured at each of its initial immobile phase and then the membranes were immersed the in the broth. The amount of *E. coli* in the broth was $4-1.5 \times 10^8$ (CFU/mL) and that of *S. epidermidis* was $7-5.5 \times 10^9$ (CFU/mL). The bacteria were stained by SYTO 9 and Propidium Iodide. The bacteria, dead or alive, stained by SYTO 9 were shown in green color. Only the dead bacteria were stained by Propidium iodide and were shown in red color. The stickiness was tested after the membranes had been immersed in broths for 4 h. It appeared that the zwitterionic moieties on the HPEI-RO membrane

could oppose the bacteria adhesion. Membrane HPEI-RO4 displayed a 97% improvement in antibacterial property compared to the unmodified membrane. Figure 8.9 shows the schematic representation of the zwitterionic membrane for anti-bacterial adhesion.

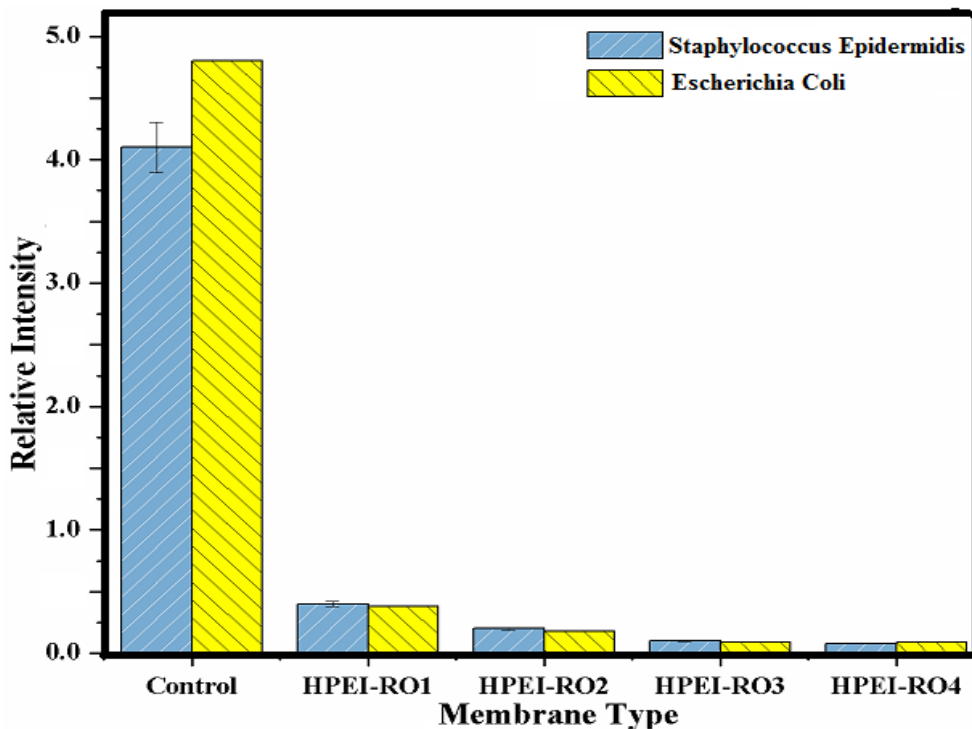


Figure 8.8 Relative amount and viability of S.epidermidis and E.coli adhering onto the control and HPEI-RO (1-4) membranes. S.epidermidis and E.coli had been cultured until initial stationary phase and membranes were kept in broths for 3h.

8.5 Conclusion

HPEI-RO membranes having zwitterions were effectively synthesized with HPEI and MA through surface modification and chemical crosslinking methods tested by dead end RO assembly. FTIR analysis confirmed the HPEI and MA functional group of the membranes. The AFM roughness value of all HPEI-RO membranes decreased with increasing HPEI content in zwitterionic membranes. Both water contact angle and RO performance test measurement demonstrated that HPEI-RO membranes have high permeation flux and could bind high amount of water molecules with zwitterions in membranes. In addition, the HPEI-RO3 exhibited the stability during desalination process and good fouling resistance property. As a result, this research offered a process for incorporating developed zwitterionic into RO membranes to attain high permeation flux selectivity, good stability fouling and bacterial resistance of the HPEI-RO membrane.

CHAPTER 9

CONCLUSIONS AND FUTURE WORK

9.1 Conclusions

Membrane-based RO desalination technology, like any other desalination technology, is not free from some serious challenges. The two major problems related to RO applications in desalination are membrane biofouling and Chlorine attack, which negatively affect the performance efficiency in RO industries. To promote the large-scale utilization of RO membrane technologies, it is crucial to overcome the challenges faced by current RO membranes.

The present research was designed to investigate novel PVA RO membranes with various fillers and combinations and their effectiveness as active RO separation layers with improved biofouling and Chlorine resistance. The uniqueness of this work was that the PVA polymer matrix was utilized as an active RO layer without the use of any polymeric or ceramic substrate. The utilization of the RO membranes without the use of a substrate reduces negative consequences, such as internal concentration polarization that causes an increase in the applied RO pressure. Although PVA possesses excellent separation and film forming properties, researchers tend not to use PVA as an active layer in RO applications because of PVA swelling effect and the membrane rupture under high pressure. Instead, they utilize PVA as a modifier. The results of this investigation showed that the fabricated RO membrane overcame those issues through appropriate crosslinking and through appropriate selection of fillers.

The crosslinked PVA RO membranes incorporated with various fillers were fabricated

using dissolution casting method. The fabricated membranes were then characterized and analyzed using various techniques like attenuated total reflection Fourier transform infrared spectroscopy (ATR-FTIR), contact angle measurements, X-ray diffraction (XRD), scanning electron microscope (SEM), atomic force microscope (AFM) and mechanical testing. The actual reverse osmosis performance of the membranes, including permeation testing, salt rejection and Chlorine resistance was examined using a reverse osmosis permeation unit.

This study showed that the incorporation of Pluronic F127 and MWCNTs into the PVA polymer matrix improved the overall RO performance of the membrane in terms of hydrophilicity, surface roughness, water permeability, salt rejection, Chlorine resistance and biofouling resistance. The membranes that contain 0.08 and 0.1 wt% MWCNTs provided optimal salt rejection, Chlorine and biofouling resistance and mechanical strength. Although the permeation of these two membranes is not the best, they relatively have an excellent water flux.

Furthermore, It has been shown that the conjugation of Vanillin and Pluronic F-127 improved the overall RO performance of the membrane in terms of hydrophilicity, surface roughness, salt rejection, Chlorine resistance, biofouling resistance and mechanical strength. Membranes PVA-V4 and PVA-V5 provided optimal salt rejection, Chlorine resistance, mechanical strength and surface hydrophilicity. Although the permeation of these two membranes is not the best, they relatively have an excellent water flux.

It has been shown that conjugating PVA with Gum Arabic and Pluronic F127 improved

the overall RO performance of the membrane in terms of hydrophilicity, surface roughness, water permeability, salt rejection, Chlorine resistance, biofouling resistance and mechanical strength. The membrane PVA-GA-5 that contains 0.9 wt% Gum Arabic provided optimal salt rejection, Chlorine and biofouling resistance, mechanical strength, permeability, surface roughness and surface hydrophilicity.

The incorporation of ZnO-NPs and Pluronic F-127 improved the performance of RO membrane, as well. The improvement was in terms of water permeability, salt rejection and Chlorine resistance by increasing hydrophilicity and affecting the roughness of the membrane. The membrane TFN4, containing 0.08 wt% ZnO-NPs, exhibited superior permeation flux, salt rejection and Chlorine resistance.

HPEI-RO membranes having zwitterions were effectively synthesized, as well. FTIR analysis confirmed the HPEI and MA functional group of the membranes. The AFM roughness value of all HPEI-RO membranes decreased with increasing HPEI content in zwitterionic membranes. Both water contact angle and RO performance test measurements demonstrated that HPEI-RO membranes had high permeation flux and could bind high amount of water molecules with zwitterions in membranes. In addition, the HPEI-RO3 exhibited the stability during desalination process and good fouling resistance property.

As a final conclusion, the outcomes of this study have shown a great promise for the proposed crosslinked PVA membrane as an active RO separation layer without a substrate. The results of this investigation showed that the fabricated RO membrane overcame PVA drawbacks through appropriate crosslinking and through appropriate

selection of fillers. The synthesized membranes had an improved RO performance and an enhanced Chlorine and biofouling resistance.

9.2 Future Work

The findings emerged from this research provide the following insights for future studies:

- The permeation experiments in this research have been performed utilizing a dead-end filtration unit, for lab testing purposes. In RO plants, the membranes are utilized in cross-flow configuration, where the feed solution flow direction is perpendicular to the membrane thickness. As an extension of this research, the permeability and selectivity of the membranes should be assessed in cross-flow configuration to mimic the industrial module.
- A further study could assess the effect of permeation experiment variables on the performance of the synthesized membranes. For instance, the feed solution temperature is an important factor that may alter the performance of the membrane. Even biofouling resistance could be affected by temperature, as higher temperatures accelerate the growth of microorganisms. Furthermore, the operating pressure is another variable that could affect the performance of the membrane.
- Long-term performance of the membrane needs to be investigated. Due to the limitation of the volume of the feed solution inside the dead-end filtration unit, the permeation experiments were limited. Employing a cross-flow filtration unit allows for long-term experimentation.
- A future study investigating probable interactions between the various fillers used in this research would be very interesting.

REFERENCES

1. Service, R.F., *Desalination freshens up*. Science, 2006. **313**(5790): p. 1088-1090.
2. Montgomery, M.A. and M. Elimelech, *Water and sanitation in developing countries: Including health in the equation*. Environmental Science & Technology, 2007. **41**(1): p. 17-24.
3. Oki, T. and S. Kanae, *Global hydrological cycles and world water resources*. Science, 2006. **313**(5790): p. 1068-1072.
4. McGinnis, R.L. and M. Elimelech, *Energy requirements of ammonia-carbon dioxide forward osmosis desalination*. Desalination, 2007. **207**(1-3): p. 370-382.
5. Shannon, M.A., et al., *Science and technology for water purification in the coming decades*. Nature, 2008. **452**(7185): p. 301-310.
6. Karagiannis, I.C. and P.G. Soldatos, *Water desalination cost literature: review and assessment*. Desalination, 2008. **223**(1-3): p. 448-456.
7. Zeng, Y., et al., *Significantly enhanced water flux in forward osmosis desalination with polymer-graphene composite hydrogels as a draw agent*. Rsc Advances, 2013. **3**(3): p. 887-894.
8. Bamaga, O.A., et al., *Hybrid FO/RO desalination system: Preliminary assessment of osmotic energy recovery and designs of new FO membrane module configurations*. Desalination, 2011. **268**(1-3): p. 163-169.
9. Saraf, A., K. Johnson, and M.L. Lind, *Poly(vinyl) alcohol coating of the support layer of reverse osmosis membranes to enhance performance in forward osmosis*. Desalination, 2014. **333**(1): p. 1-9.
10. Li, D., et al., *Forward osmosis desalination using polymer hydrogels as a draw agent: Influence of draw agent, feed solution and membrane on process performance*. Water Research, 2013. **47**(1): p. 209-215.

11. Chanukya, B.S., S. Patil, and N.K. Rastogi, *Influence of concentration polarization on flux behavior in forward osmosis during desalination using ammonium bicarbonate*. *Desalination*, 2013. **312**: p. 39-44.
12. Ghaffour, N., T.M. Missimer, and G.L. Amy, *Technical review and evaluation of the economics of water desalination: Current and future challenges for better water supply sustainability*. *Desalination*, 2013. **309**: p. 197-207.
13. Shiklomanov, I.A. *State Hydrological Institute (SHI, St. Petersburg) and United Nations Educational, Scientific and Cultural Organization (UNESCO, Paris), 1999; World Resources 2000-2001, People and Ecosystems: The Fraying Web of Life, World Resources Institute (WRI), Washington, DC, 2000; Paul Harrison and Fred Pearce, AAAS Atlas of Population 2001, American Association for the Advancement of Science, University of California Press, Berkeley.*
14. Zhou, Y. and R.S.J. Tol, *Evaluating the costs of desalination and water transport*. *Water Resources Research*, 2005. **41**(3).
15. Greenlee, L.F., et al., *Reverse osmosis desalination: Water sources, technology, and today's challenges*. *Water Research*, 2009. **43**(9): p. 2317-2348.
16. Al-Gholaikah, A., et al., *The world's first large seawater reverse osmosis desalination plant, at Jeddah, Kingdom of Saudi Arabia*. *Desalination*, 1978. **27**(3): p. 215-231.
17. Grellier, J., *Reverse Osmosis Desalination Plant in Spain*. 29 July 2010, Wikipedia.
18. Lee, K.P., T.C. Arnot, and D. Mattia, *A review of reverse osmosis membrane materials for desalination-Development to date and future potential*. *Journal of Membrane Science*, 2011. **370**(1-2): p. 1-22.
19. Fritzmann, C., et al., *State-of-the-art of reverse osmosis desalination*. *Desalination*, 2007. **216**(1-3): p. 1-76.
20. Li, D. and H.T. Wang, *Recent developments in reverse osmosis desalination membranes*. *Journal of Materials Chemistry*, 2010. **20**(22): p. 4551-4566.

21. Strathmann, H., L. Giorno, and E. Drioli, *Introduction to membrane science and technology*. 2011: Wiley-VCH Weinheim, Germany.
22. Kochkodan, V. and N. Hilal, *A comprehensive review on surface modified polymer membranes for biofouling mitigation*. *Desalination*, 2015. **356**: p. 187-207.
23. Lalia, B.S., et al., *A review on membrane fabrication: Structure, properties and performance relationship*. *Desalination*, 2013. **326**: p. 77-95.
24. Lau, W.J., et al., *A recent progress in thin film composite membrane: A review*. *Desalination*, 2012. **287**: p. 190-199.
25. Pendergast, M.M. and E.M.V. Hoek, *A review of water treatment membrane nanotechnologies*. *Energy & Environmental Science*, 2011. **4**(6): p. 1946-1971.
26. Sairam, M., et al., *Method for the preparation of cellulose acetate flat sheet composite membranes for forward osmosis-Desalination using MgSO₄ draw solution*. *Desalination*, 2011. **273**(2-3): p. 299-307.
27. Li, D., et al., *Composite polymer hydrogels as draw agents in forward osmosis and solar dewatering*. *Soft Matter*, 2011. **7**(21): p. 10048-10056.
28. A.K. Ghosh, R.C.B., S. Prabhakar and P.K.Tewari, *Composite Polyamide Reverse Osmosis (RO) Membranes – Recent Developments and Future Directions*. *BARC Newsletter*, 2011. **321**(July-August): p. 43-51.
29. C.E.Reid, E.J.B., *Water and Ion Flow Across Cellulosic Membranes*. *journal of applied polymer science*, 1959. **1**(2): p. 133-143.
30. Loeb, S. and S. Sourirajan, *Sea Water Demineralization by Means of an Osmotic Membrane*, in *Saline water conversion II*. 1963, American Chemical Society. : Washington, DC. p. 117-132.
31. Loeb, S., *The Loeb-Sourirajan Membrane: How It Came About*, in *Synthetic Membranes*:. 1981, AMERICAN CHEMICAL SOCIETY. p. 1-9.

32. Sudak, R.G., *Reverse Osmosis*, in *Handbook of Industrial Membrane Technology*, M.C. Porter, Editor. 1990, Noyes Publication: New Jersey. p. 260-306.
33. W.M. King, P.A.C., L.W. Schoellenback, C.R. Cannon, *High retention reverse osmosis desalination membranes from cellulose acetate*, in *Membranes from cellulose and cellulose derivatives*, A.F. Turbak, Editor. 1970, Interscience Publishers: New York.
34. Beasley, J.K., *The evaluation and selection of polymeric materials for reverse osmosis membranes*. *Desalination*, 1977. **22**(1-3): p. 181-189.
35. Kirsh, Y.E. and Y.M. Popkov, *New Trends In The Development Of Polymer Materials For Reverse Osmotic Membranes*. *Uspekhi Khimii*, 1988. **57**(6): p. 1001-1009.
36. Congjie, G., *Development and extension of seawater desalination by reverse osmosis*. *Chinese Journal of Oceanology and Limnology*, 2003. **21**(1): p. 40-45.
37. Cadotte, J.E., et al., *New Thin-Film Composite Seawater Reverse-Osmosis Membrane*. *Desalination*, 1980. **32**(1-3): p. 25-31.
38. Wijmans, J.G. and R.W. Baker, *The solution-diffusion model: a review*. *Journal of Membrane Science*, 1995. **107**(1-2): p. 1-21.
39. Paul, D.R., *Reformulation of the solution-diffusion theory of reverse osmosis*. *Journal of Membrane Science*, 2004. **241**(2): p. 371-386.
40. Matin, A., *Enhancing the Biofouling Resistance of Reverse Osmosis Membranes by a Novel Surface Modification Technique*, in *Mechanical Engineering Department*. 2012, King Fahd University of Petroleum and Minerals: Saudi Arabia.
41. Fane, A.G. and C.J.D. Fell, *A Review of Fouling and Fouling Control in Ultrafiltration*. *Desalination*, 1987. **62**: p. 117-136.
42. Goosen, M.F.A., et al., *Fouling of reverse osmosis and ultrafiltration membranes: A critical review*. *Separation Science and Technology*, 2004. **39**(10): p. 2261-2297.

43. Misdan, N., W.J. Lau, and A.F. Ismail, *Seawater Reverse Osmosis (SWRO) desalination by thin-film composite membrane-Current development, challenges and future prospects*. Desalination, 2012. **287**: p. 228-237.
44. Fujiwara, N. and H. Matsuyama, *Elimination of biological fouling in seawater reverse osmosis desalination plants*. Desalination, 2008. **227**(1-3): p. 295-305.
45. Flemming, H.C., *Reverse osmosis membrane biofouling*. Experimental Thermal and Fluid Science, 1997. **14**(4): p. 382-391.
46. Bartman, A.R., et al., *Mineral scale monitoring for reverse osmosis desalination via real-time membrane surface image analysis*. Desalination, 2011. **273**(1): p. 64-71.
47. Reverter, J.A., S. Talo, and J. Alday, *Las Palmas III - the success story of brine staging*. Desalination, 2001. **138**(1-3): p. 207-217.
48. Flemming, H.C., et al., *Biofouling—the Achilles heel of membrane processes*. Desalination, 1997. **113**(2–3): p. 215-225.
49. Hong, S.K. and M. Elimelech, *Chemical and physical aspects of natural organic matter (NOM) fouling of nanofiltration membranes*. Journal of Membrane Science, 1997. **132**(2): p. 159-181.
50. Belfer, S., et al., *Surface modification of commercial composite polyamide reverse osmosis membranes*. Journal of Membrane Science, 1998. **139**(2): p. 175-181.
51. Matin, A., et al., *Biofouling in reverse osmosis membranes for seawater desalination: Phenomena and prevention*. Desalination, 2011. **281**: p. 1-16.
52. Baker, J.S. and L.Y. Dudley, *Biofouling in membrane systems - A review*. Desalination, 1998. **118**(1-3): p. 81-89.
53. Flemming, H.C., *Biofouling in water systems - cases, causes and countermeasures*. Applied Microbiology and Biotechnology, 2002. **59**(6): p. 629-640.

54. Abd El Aleem, F.A., K.A. Al-Sugair, and M.I. Alahmad, *Biofouling problems in membrane processes for water desalination and reuse in Saudi Arabia*. International Biodeterioration & Biodegradation, 1998. **41**(1): p. 19-23.
55. Kim, D., et al., *Biocide application for controlling biofouling of SWRO membranes - an overview*. Desalination, 2009. **238**(1-3): p. 43-52.
56. De Beer, D. and P. Stoodley, *Microbial Biofilms*. Prokaryotes: A Handbook on the Biology of Bacteria, Vol 1, Third Edition: Symbiotic Associations, Biotechnology, Applied Microbiology, ed. M. Dworkin, et al. 2006, New York: Springer. 904-937.
57. Sadr Ghayeni, S.B., et al., *Adhesion of waste water bacteria to reverse osmosis membranes*. Journal of Membrane Science, 1998. **138**(1): p. 29-42.
58. Ramsey, M.M. and M. Whiteley, *Pseudomonas aeruginosa attachment and biofilm development in dynamic environments*. Molecular Microbiology, 2004. **53**(4): p. 1075-1087.
59. Sommariva, C., et al., *Relationship between biofouling and recovery ratio: the theoretical approach and one experimental case*. Desalination, 2007. **204**(1-3): p. 175-180.
60. Schneider, R.P., et al., *Dynamics of organic carbon and of bacterial populations in a conventional pretreatment train of a reverse osmosis unit experiencing severe biofouling*. Journal of Membrane Science, 2005. **266**(1-2): p. 18-29.
61. Herzberg, M. and M. Elimelech, *Biofouling of reverse osmosis membranes: Role of biofilm-enhanced osmotic pressure*. Journal of Membrane Science, 2007. **295**(1-2): p. 11-20.
62. Vrouwenvelder, J.S., et al., *Biofouling of spiral-wound nanofiltration and reverse osmosis membranes: A feed spacer problem*. Water Research, 2009. **43**(3): p. 583-594.
63. Monroe, D., *Looking for chinks in the armor of bacterial biofilms*. Plos Biology, 2007. **5**(11): p. 2458-2461.

64. Ridgway, H.F., *Microbial Adhesion and Biofouling of Reverse Osmosis Membranes*, in *Reverse Osmosis Technology: Applications for High-Purity Water Production*, B.S. Parekh, Editor. 1988, Marcel Dekker: New York, Basel. p. 429-481.
65. Ridgway, H.F.a.S., J, *Biofouling of Reverse Osmosis Membranes*, in *Biofouling and Biocorrosion in Industrial Water Systems*, H.C.a.G. Flemming, G. G., Editor. 1990, Springer-Verlag. p. 81-111.
66. Ramon, G.Z., B.J. Feinberg, and E.M.V. Hoek, *Membrane-based production of salinity-gradient power*. *Energy & Environmental Science*, 2011. **4**(11): p. 4423-4434.
67. Konagaya, S., H. Kuzumoto, and O. Watanabe, *New reverse osmosis membrane materials with higher resistance to chlorine*. *Journal of Applied Polymer Science*, 2000. **75**(11): p. 1357-1364.
68. Tessaro, I.C., J.B.A. da Silva, and K. Wada, *Investigation of some aspects related to the degradation of polyamide membranes: aqueous chlorine oxidation catalyzed by aluminum and sodium laurel sulfate oxidation during cleaning*. *Desalination*, 2005. **181**(1-3): p. 275-282.
69. Liu, M., et al., *Improving fouling resistance and chlorine stability of aromatic polyamide thin-film composite RO membrane by surface grafting of polyvinyl alcohol (PVA)*. *Desalination*, 2015. **367**: p. 11-20.
70. Kawaguchi, T. and H. Tamura, *Chlorine-resistant membrane for reverse osmosis. I. Correlation between chemical structures and chlorine resistance of polyamides*. *Journal of applied polymer science*, 1984. **29**(11): p. 3359-3367.
71. Rana, D. and T. Matsuura, *Surface Modifications for Antifouling Membranes*. *Chemical Reviews*, 2010. **110**(4): p. 2448-2471.
72. Kochkodan, V., *Reduction of Membrane Fouling by Polymer Surface Modification*, in *Membrane Modification : Technology and Applications*, N. Hilal, Khayet, M. and Wright, C. J., Editor. 2012, CRC Press, ProQuest ebrary: London, GBR. p. 41-76.

73. Hilal, N., et al., *Methods employed for control of fouling in MF and UF membranes: A comprehensive review*. Separation Science and Technology, 2005. **40**(10): p. 1957-2005.
74. Al-Amoudi, A. and R.W. Lovitt, *Fouling strategies and the cleaning system of NF membranes and factors affecting cleaning efficiency*. Journal of Membrane Science, 2007. **303**(1-2): p. 6-28.
75. Van der Bruggen, B., M. Manttari, and M. Nystrom, *Drawbacks of applying nanofiltration and how to avoid them: A review*. Separation and Purification Technology, 2008. **63**(2): p. 251-263.
76. Ulbricht, M., *Advanced functional polymer membranes*. Polymer, 2006. **47**(7): p. 2217-2262.
77. Kato, K., et al., *Polymer surface with graft chains*. Progress in Polymer Science, 2003. **28**(2): p. 209-259.
78. Elimelech, M., et al., *Role of membrane surface morphology in colloidal fouling of cellulose acetate and composite aromatic polyamide reverse osmosis membranes*. Journal of Membrane Science, 1997. **127**(1): p. 101-109.
79. Vrijenhoek, E.M., S. Hong, and M. Elimelech, *Influence of membrane surface properties on initial rate of colloidal fouling of reverse osmosis and nanofiltration membranes*. Journal of membrane science, 2001. **188**(1): p. 115-128.
80. Kang, G.-d. and Y.-m. Cao, *Development of antifouling reverse osmosis membranes for water treatment: A review*. Water Research, 2012. **46**(3): p. 584-600.
81. Liu, M., et al., *Enhancing the permselectivity of thin-film composite poly(vinyl alcohol) (PVA) nanofiltration membrane by incorporating poly(sodium-p-styrene-sulfonate) (PSSNa)*. Journal of Membrane Science, 2014. **463**: p. 173-182.
82. Bolto, B., et al., *Crosslinked poly(vinyl alcohol) membranes*. Progress in Polymer Science, 2009. **34**(9): p. 969-981.

83. Liu, Y., et al., *High-flux microfiltration filters based on electrospun polyvinylalcohol nanofibrous membranes*. *Polymer*, 2013. **54**(2): p. 548-556.
84. You, H., et al., *Low pressure high flux thin film nanofibrous composite membranes prepared by electrospaying technique combined with solution treatment*. *Journal of Membrane Science*, 2012. **394–395**: p. 241-247.
85. Bezuidenhout, D., et al., *Reverse osmosis membranes prepared from potassium peroxydisulphate-modified poly(vinyl alcohol)*. *Desalination*, 1998. **116**(1): p. 35-43.
86. Hu, S.Y., et al., *Composite membranes comprising of polyvinylamine-poly(vinyl alcohol) incorporated with carbon nanotubes for dehydration of ethylene glycol by pervaporation*. *Journal of Membrane Science*, 2012. **417–418**: p. 34-44.
87. Yee, K.F., et al., *Novel MWCNT-buckypaper/polyvinyl alcohol asymmetric membrane for dehydration of etherification reaction mixture: Fabrication, characterisation and application*. *Journal of Membrane Science*, 2014. **453**: p. 546-555.
88. Gohil, J.M. and P. Ray, *Polyvinyl alcohol as the barrier layer in thin film composite nanofiltration membranes: Preparation, characterization, and performance evaluation*. *Journal of Colloid and Interface Science*, 2009. **338**(1): p. 121-127.
89. Katz, M.G. and T. Wydeven, *Selective permeability of PVA membranes. II. Heat-treated membranes*. *Journal of Applied Polymer Science*, 1982. **27**(1): p. 79-87.
90. Huang, R.Y.M., et al., *Pervaporation separation of acetic acid-water mixtures using modified membranes. I. Blended polyacrylic acid (PAA)-nylon 6 membranes*. *Journal of Applied Polymer Science*, 1988. **35**(5): p. 1191-1200.
91. Cha, W.-I., S.-H. Hyon, and Y. Ikada, *Microstructure of poly(vinyl alcohol) hydrogels investigated with differential scanning calorimetry*. *Die Makromolekulare Chemie*, 1993. **194**(9): p. 2433-2441.
92. Gebben, B., et al., *Intramolecular crosslinking of poly(vinyl alcohol)*. *Polymer*, 1985. **26**(11): p. 1737-1740.

93. Macho, V., et al., *Modified poly(vinyl alcohol) as a dispersant in suspension polymerization of vinyl chloride: 3. Acetalized poly(vinyl alcohol)*. *Polymer*, 1994. **35**(26): p. 5773-5777.
94. Huang, R.Y.M. and J.W. Rhim, *Modification of poly(vinyl alcohol) using maleic acid and its application to the separation of acetic acid-water mixtures by the pervaporation technique*. *Polymer International*, 1993. **30**(1): p. 129-135.
95. Korsmeyer, R.W. and N.A. Peppas, *Effect of the morphology of hydrophilic polymeric matrices on the diffusion and release of water soluble drugs*. *Journal of Membrane Science*, 1981. **9**(3): p. 211-227.
96. Giménez, V., A. Mantecón, and V. Cádiz, *Crosslinking of poly(vinyl alcohol) using dianhydrides as hardeners*. *Journal of Applied Polymer Science*, 1996. **59**(3): p. 425-431.
97. Hachisuka, H. and K. Ikeda, *Composite reverse osmosis membrane having a separation layer with polyvinyl alcohol coating and method of reverse osmotic treatment of water using the same*. 2001, Google Patents.
98. Kim, I.-C. and K.-H. Lee, *Dyeing process wastewater treatment using fouling resistant nanofiltration and reverse osmosis membranes*. *Desalination*, 2006. **192**(1): p. 246-251.
99. Rana, H.H., et al., *Low fouling and improved chlorine resistant thin film composite reverse osmosis membranes by cerium(IV)/polyvinyl alcohol mediated surface modification*. *Desalination*, 2015. **357**: p. 93-103.
100. Rajaeian, B., et al., *Improved separation and antifouling performance of PVA thin film nanocomposite membranes incorporated with carboxylated TiO₂ nanoparticles*. *Journal of Membrane Science*, 2015. **485**: p. 48-59.
101. Bano, S., et al., *Chlorine resistant binary complexed NaAlg/PVA composite membrane for nanofiltration*. *Separation and Purification Technology*, 2014. **137**: p. 21-27.

102. Nikkola, J., et al., *Surface modification of thin film composite RO membrane for enhanced anti-biofouling performance*. Journal of Membrane Science, 2013. **444**: p. 192-200.
103. Muhammed, A., M. El-Hashash, and R. Guirguis, *Polyvinyl alcohol-cellulose acetate composite reverses osmosis membranes: I. Synthesis and characterization*. Hydrology: Current Research, 2012. **2012**.
104. Petersen, R.J., *Composite reverse osmosis and nanofiltration membranes*. Journal of Membrane Science, 1993. **83**(1): p. 81-150.
105. Liu, M., et al., *Thin-film composite polyamide reverse osmosis membranes with improved acid stability and chlorine resistance by coating N-isopropylacrylamide-co-acrylamide copolymers*. Desalination, 2011. **270**(1-3): p. 248-257.
106. Augustine, M.S., et al., *Excellent UV absorption in spin-coated thin films of oleic acid modified zinc oxide nanorods embedded in Polyvinyl alcohol*. Journal of Physics and Chemistry of Solids, 2012. **73**(3): p. 396-401.
107. Institute, C.L.S., *Performance Standards For Antimicrobial Disk Susceptibility Tests*. 2006, Clinical Laboratory Standards Institute: Wayne, PA.
108. Sabir, A., et al., *Novel polymer matrix composite membrane doped with fumed silica particles for reverse osmosis desalination*. Desalination, 2015. **368**(0): p. 159-170.
109. Fang, T.-H. and W.-J. Chang, *Effects of AFM-based nanomachining process on aluminum surface*. Journal of Physics and Chemistry of Solids, 2003. **64**(6): p. 913-918.
110. Subramani, A. and J.G. Jacangelo, *Emerging desalination technologies for water treatment: A critical review*. Water Research, 2015. **75**: p. 164-187.
111. Puguán, J.M.C., et al., *Low internal concentration polarization in forward osmosis membranes with hydrophilic crosslinked PVA nanofibers as porous support layer*. Desalination, 2014. **336**: p. 24-31.

112. Malaeb, L. and G.M. Ayoub, *Reverse osmosis technology for water treatment: State of the art review*. Desalination, 2011. **267**(1): p. 1-8.
113. Kim, H.K., H.J. Chung, and T.G. Park, *Biodegradable polymeric microspheres with "open/closed" pores for sustained release of human growth hormone*. Journal of Controlled Release, 2006. **112**(2): p. 167-174.
114. Lv, C.L., et al., *Enhanced permeation performance of cellulose acetate ultrafiltration membrane by incorporation of Pluronic F127*. Journal of Membrane Science, 2007. **294**(1-2): p. 68-74.
115. Amanda, A., et al., *Semicrystalline poly(vinyl alcohol) ultrafiltration membranes for bioseparations*. Journal of Membrane Science, 2000. **176**(1): p. 87-95.
116. Iwasaki, Y., A. Yamasaki, and K. Ishihara, *Platelet compatible blood filtration fabrics using a phosphorylcholine polymer having high surface mobility*. Biomaterials, 2003. **24**(20): p. 3599-3604.
117. Ishihara, K., H. Hanyuda, and N. Nakabayashi, *Synthesis of phospholipid polymers having a urethane bond in the side chain as coating material on segmented polyurethane and their platelet adhesion-resistant properties*. Biomaterials, 1995. **16**(11): p. 873-879.
118. Yajima, S., et al., *Ion-sensor property and blood compatibility of neutral-carrier-type poly(vinyl chloride) membranes coated by phosphorylcholine polymers*. Analytica Chimica Acta, 2002. **463**(1): p. 31-37.
119. Spitalsky, Z., et al., *Carbon nanotube-polymer composites: Chemistry, processing, mechanical and electrical properties*. Progress in Polymer Science, 2010. **35**(3): p. 357-401.
120. Bose, S., R.A. Khare, and P. Moldenaers, *Assessing the strengths and weaknesses of various types of pre-treatments of carbon nanotubes on the properties of polymer/carbon nanotubes composites: A critical review*. Polymer, 2010. **51**(5): p. 975-993.
121. Andrews, R. and M.C. Weisenberger, *Carbon nanotube polymer composites*. Current Opinion in Solid State and Materials Science, 2004. **8**(1): p. 31-37.

122. De Volder, M.F.L., et al., *Carbon Nanotubes: Present and Future Commercial Applications*. Science, 2013. **339**(6119): p. 535-539.
123. Khalid, A., et al., *Preparation and properties of nanocomposite polysulfone/multi-walled carbon nanotubes membranes for desalination*. Desalination, 2015. **367**(0): p. 134-144.
124. Choi, J.-H., J. Jegal, and W.-N. Kim, *Fabrication and characterization of multi-walled carbon nanotubes/polymer blend membranes*. Journal of Membrane Science, 2006. **284**(1-2): p. 406-415.
125. Celik, E., et al., *Carbon nanotube blended polyethersulfone membranes for fouling control in water treatment*. Water Research, 2011. **45**(1): p. 274-282.
126. Medina-Gonzalez, Y. and J.-C. Remigy, *Sonication-assisted preparation of pristine MWCNT-polysulfone conductive microporous membranes*. Materials Letters, 2011. **65**(2): p. 229-232.
127. Wu, H., B. Tang, and P. Wu, *Novel ultrafiltration membranes prepared from a multi-walled carbon nanotubes/polymer composite*. Journal of Membrane Science, 2010. **362**(1-2): p. 374-383.
128. Shawky, H.A., et al., *Synthesis and characterization of a carbon nanotube/polymer nanocomposite membrane for water treatment*. Desalination, 2011. **272**(1-3): p. 46-50.
129. Peng, F., et al., *Novel nanocomposite pervaporation membranes composed of poly(vinyl alcohol) and chitosan-wrapped carbon nanotube*. Journal of Membrane Science, 2007. **300**(1-2): p. 13-19.
130. Kang, D.-Y., et al., *Single-Walled Aluminosilicate Nanotube/Poly(vinyl alcohol) Nanocomposite Membranes*. ACS Applied Materials & Interfaces, 2012. **4**(2): p. 965-976.
131. Li, X., et al., *Desalination of dye solution utilizing PVA/INDF hollow fiber composite membrane modified with TiO₂ nanoparticles*. Journal of Membrane Science, 2014. **471**: p. 118-129.

132. Deng, L. and M.-B. Hagg, *Carbon nanotube reinforced PVAm/PVA blend FSC nanocomposite membrane for CO₂/CH₄ separation*. International Journal of Greenhouse Gas Control, 2014. **26**: p. 127-134.
133. Flynn, E.J., et al., *Pervaporation performance enhancement through the incorporation of mesoporous silica spheres into PVA membranes*. Separation and Purification Technology, 2013. **118**(0): p. 73-80.
134. Sun, L.K., L.F. Liu, and F.L. Yang, *The Antifouling Properties of PVA/PVAm Modified Polyester Membrane*. Procedia Engineering, 2012. **44**(0): p. 1426-1427.
135. Pourjafar, S., A. Rahimpour, and M. Jahanshahi, *Synthesis and characterization of PVA/PES thin film composite nanofiltration membrane modified with TiO₂ nanoparticles for better performance and surface properties*. Journal of Industrial and Engineering Chemistry, 2012. **18**(4): p. 1398-1405.
136. Barona, G.N.B., M. Choi, and B. Jung, *High permeate flux of PVA/PSf thin film composite nanofiltration membrane with aluminosilicate single-walled nanotubes*. Journal of Colloid and Interface Science, 2012. **386**: p. 189-197.
137. Maiti, J., et al., *PVA nano composite membrane for DMFC application*. Solid State Ionics, 2011. **201**(1): p. 21-26.
138. Wu, S., et al., *Effects of poly (vinyl alcohol) (PVA) content on preparation of novel thiol-functionalized mesoporous PVA/SiO₂ composite nanofiber membranes and their application for adsorption of heavy metal ions from aqueous solution*. Polymer, 2010. **51**(26): p. 6203-6211.
139. Li, N., et al., *Preparation and properties of PVDF/PVA hollow fiber membranes*. Desalination, 2010. **250**(2): p. 530-537.
140. Yang, C.-C. and Y.-J. Lee, *Preparation of the acidic PVA/MMT nanocomposite polymer membrane for the direct methanol fuel cell (DMFC)*. Thin Solid Films, 2009. **517**(17): p. 4735-4740.
141. Zhang, L.-Z., et al., *Synthesis and characterization of a PVA/LiCl blend membrane for air dehumidification*. Journal of Membrane Science, 2008. **308**(1-2): p. 198-206.

142. Shang, Y. and Y. Peng, *UF membrane of PVA modified with TDI*. Desalination, 2008. **221**(1–3): p. 324-330.
143. Yang, C.-C., *Synthesis and characterization of the cross-linked PVA/TiO₂ composite polymer membrane for alkaline DMFC*. Journal of Membrane Science, 2007. **288**(1–2): p. 51-60.
144. Shang, Y. and Y. Peng, *Research of a PVA composite ultrafiltration membrane used in oil-in-water*. Desalination, 2007. **204**(1–3): p. 322-327.
145. Guo, R., et al., *Novel PVA–silica nanocomposite membrane for pervaporative dehydration of ethylene glycol aqueous solution*. Polymer, 2007. **48**(10): p. 2939-2945.
146. Peters, T., et al., *Thin high flux ceramic-supported PVA membranes*. Desalination, 2006. **200**(1–3): p. 37-39.
147. Qui, Y.R. and Q.X. Zhang, *Preparation and properties of metal-PVA composite hydrophilic ultrafiltration membranes*. Journal of Central South University of Technology, 2003. **10**(2): p. 117-121.
148. Billard, P. and M. Kind, *Performance of PVA- and zeolite-membranes in selective drying processes*. Chemical Engineering and Processing: Process Intensification, 2003. **42**(1): p. 23-28.
149. Jian, S. and S. Xiao Ming, *Crosslinked PVA-PS thin-film composite membrane for reverse osmosis*. Desalination, 1987. **62**(0): p. 395-403.
150. Ying, W., *Desalination by the use of dynamically formed PVA membranes*. Desalination, 1983. **46**(1–3): p. 335-342.
151. Islam, A. and T. Yasin, *Controlled delivery of drug from pH sensitive chitosan/poly (vinyl alcohol) blend*. Carbohydrate Polymers, 2012. **88**(3): p. 1055-1060.
152. Cherdoud-Chihani, A., M. Mouzali, and M.J.M. Abadie, *Study of crosslinking acid copolymer/DGEBA systems by FTIR*. Journal of Applied Polymer Science, 2003. **87**(13): p. 2033-2051.

153. Fischer, J. and H. Ritter, *Oligomeric epoxide–amine adducts based on 2-amino-N-isopropylacetamide and α -amino- ϵ -caprolactam: Solubility in presence of cyclodextrin and curing properties*. Beilstein Journal of Organic Chemistry, 2013. **9**: p. 2803-2811.
154. Cunha, C., et al., *Hybrid composites made of multiwalled carbon nanotubes functionalized with Fe₃O₄ nanoparticles for tissue engineering applications*. Nanotechnology, 2012. **23**(46): p. 465102.
155. Kwok, D.Y. and A.W. Neumann, *Contact angle measurement and contact angle interpretation*. Advances in Colloid and Interface Science, 1999. **81**(3): p. 167-249.
156. Zhao, W., et al., *Fabrication of antifouling polyethersulfone ultrafiltration membranes using Pluronic F127 as both surface modifier and pore-forming agent*. Journal of Membrane Science, 2008. **318**(1-2): p. 405-412.
157. Liu, B.C., et al., *Low-cost antifouling PVC ultrafiltration membrane fabrication with Pluronic F 127: Effect of additives on properties and performance*. Desalination, 2012. **307**: p. 26-33.
158. Loh, C.H. and R. Wang, *Effects of Additives and Coagulant Temperature on Fabrication of High Performance PVDF/Pluronic F127 Blend Hollow Fiber Membranes via Nonsolvent Induced Phase Separation*. Chinese Journal of Chemical Engineering, 2012. **20**(1): p. 71-79.
159. Govender, S., et al., *A robust approach to studying the adsorption of Pluronic F108 on nonporous membranes*. Journal of Colloid and Interface Science, 2005. **282**(2): p. 306-313.
160. Wang, X., et al., *High Flux Filtration Medium Based on Nanofibrous Substrate with Hydrophilic Nanocomposite Coating*. Environmental Science & Technology, 2005. **39**(19): p. 7684-7691.
161. Vedala, H., et al., *Effect of PVA functionalization on hydrophilicity of Y-junction single wall carbon nanotubes*. Applied Surface Science, 2006. **252**(22): p. 7987-7992.

162. Kulanthaisami, S., D. Mangalaraj, and S.K. Narayandass, *Conduction studies on polyvinyl alcohol films*. European Polymer Journal, 1995. **31**(10): p. 969-975.
163. Kozlov, M., et al., *Adsorption of Poly(vinyl alcohol) onto Hydrophobic Substrates. A General Approach for Hydrophilizing and Chemically Activating Surfaces*. Macromolecules, 2003. **36**(16): p. 6054-6059.
164. Granite, M., et al., *Interactions between block copolymers and single-walled carbon nanotubes in aqueous solutions: a small-angle neutron scattering study*. Langmuir, 2010. **27**(2): p. 751-759.
165. Wang, X., et al., *Pluronic F108 coating decreases the lung fibrosis potential of multiwall carbon nanotubes by reducing lysosomal injury*. Nano letters, 2012. **12**(6): p. 3050-3061.
166. Wan, J., et al., *In situ decoration of carbon nanotubes with nearly monodisperse magnetite nanoparticles in liquid polyols*. Journal of Materials Chemistry, 2007. **17**(12): p. 1188-1192.
167. Loh, C.H., et al., *Fabrication of high performance polyethersulfone UF hollow fiber membranes using amphiphilic Pluronic block copolymers as pore-forming additives*. Journal of Membrane Science, 2011. **380**(1-2): p. 114-123.
168. Susanto, H. and M. Ulbricht, *Characteristics, performance and stability of polyethersulfone ultrafiltration membranes prepared by phase separation method using different macromolecular additives*. Journal of Membrane Science, 2009. **327**(1-2): p. 125-135.
169. Zhang, H.L., et al., *Electrospun PLGA/multi-walled carbon nanotubes/wool keratin composite membranes: morphological, mechanical, and thermal properties, and their bioactivities in vitro*. Journal of Polymer Research, 2014. **21**(1).
170. Saeed, K. and S.-Y. Park, *Preparation of multiwalled carbon nanotube/nylon-6 nanocomposites by in situ polymerization*. Journal of Applied Polymer Science, 2007. **106**(6): p. 3729-3735.

171. Chen, D., et al., *Electrospinning Fabrication of High Strength and Toughness Polyimide Nanofiber Membranes Containing Multiwalled Carbon Nanotubes*. The Journal of Physical Chemistry B, 2009. **113**(29): p. 9741-9748.
172. Raslan R., M.A.W., *Polysulfone/Pluronic F127 Blend Ultrafiltration membranes: Preparation and Characterization*. Journal of Applied Sciences, 2010. **10**(21): p. 2628-2632.
173. Van Wagner, E.M., et al., *Effect of crossflow testing conditions, including feed pH and continuous feed filtration, on commercial reverse osmosis membrane performance*. Journal of Membrane Science, 2009. **345**(1–2): p. 97-109.
174. Song, R., D. Yang, and L. He, *Preparation of semi-aromatic polyamide (PA)/multi-wall carbon nanotube (MWCNT) composites and its dynamic mechanical properties*. Journal of Materials Science, 2008. **43**(4): p. 1205-1213.
175. Li, W.H., et al., *Preparation and shear properties of carbon nanotubes/poly (butyl methacrylate) hybrid material*. Polymer Composites, 2008. **29**(9): p. 972-977.
176. Lee, S.Y., et al., *Silver nanoparticles immobilized on thin film composite polyamide membrane: characterization, nanofiltration, antifouling properties*. Polymers for Advanced Technologies, 2007. **18**(7): p. 562-568.
177. Park, J., et al., *Enhancement of chlorine resistance in carbon nanotube based nanocomposite reverse osmosis membranes*. Desalination and Water Treatment, 2010. **15**(1-3): p. 198-204.
178. Inukai, S., et al., *High-performance multi-functional reverse osmosis membranes obtained by carbon nanotube-polyamide nanocomposite*. Scientific Reports, 2015. **5**:13562 p. 1-10.
179. Knoell, T., *Chlorine's impact on the performance and properties of polyamide membranes*. Ultrapure Water, 2006. **23**(3): p. 24-31.
180. Park, H.B., et al., *Highly Chlorine-Tolerant Polymers for Desalination*. Angewandte Chemie International Edition, 2008. **47**(32): p. 6019-6024.

181. Zhang, Y., et al., *Highly chlorine-resistant multilayer reverse osmosis membranes based on sulfonated poly(arylene ether sulfone) and poly(vinyl alcohol)*. Desalination, 2014. **336**: p. 58-63.
182. Ponnusamy, K., et al., *Anti-biofouling property of vanillin on *Aeromonas hydrophila* initial biofilm on various membrane surfaces*. World Journal of Microbiology and Biotechnology, 2013. **29**(9): p. 1695-1703.
183. Ngarmsak, M., et al., *Antimicrobial activity of vanillin against spoilage microorganisms in stored fresh-cut mangoes*. Journal of Food Protection, 2006. **69**(7): p. 1724-1727.
184. Nam, A., et al., *Reduction of biofouling using vanillin as a quorum sensing inhibitory agent in membrane bioreactors for wastewater treatment*. MEMBRANE WATER TREATMENT, 2015. **6**(3): p. 189-203.
185. Kappachery, S., et al., *Vanillin, a potential agent to prevent biofouling of reverse osmosis membrane*. Biofouling, 2010. **26**(6): p. 667-672.
186. Anis, S.F., B.S. Lalia, and R. Hashaikeh, *Controlling swelling behavior of poly (vinyl) alcohol via networked cellulose and its application as a reverse osmosis membrane*. Desalination, 2014. **336**: p. 138-145.
187. Bolden, N.W., V. Rangari, and S. Jeelani. *Synthesis of drug loaded iron oxide nanoparticles*. in *ICCM-17 17th International Conference on Composite Materials*. 2009.
188. Sharma, A. and P.S. Kumar, *Synthesis and Characterization of CeO-ZnO Nanocomposites*. Nanoscience and Nanotechnology, 2012. **2**(3): p. 82-85.
189. Thomas, P., et al., *FTIR study of the thermal degradation of poly (vinyl alcohol)*. Journal of thermal analysis and calorimetry, 2001. **64**(2): p. 501-508.
190. Mehta, R., et al., *Synthesis and characterization of a biocompatible monotyrosine-based polymer and its interaction with DNA*. Journal of Materials Chemistry B, 2014. **2**(37): p. 6236-6248.

191. Cherdoud-Chihani, A., M. Mouzali, and M. Abadie, *Study of crosslinking acid copolymer/DGEBA systems by FTIR*. Journal of applied polymer science, 2003. **87**(13): p. 2033-2051.
192. Li, Y.-Y., et al., *Pluronic F127 nanomicelles engineered with nuclear localized functionality for targeted drug delivery*. Materials Science and Engineering: C, 2013. **33**(5): p. 2698-2707.
193. Lee, Y., et al., *Reduction of inflammatory responses and enhancement of extracellular matrix formation by vanillin-incorporated poly (lactic-co-glycolic acid) scaffolds*. Tissue Engineering Part A, 2012. **18**(19-20): p. 1967-1978.
194. Tai, A., et al., *Evaluation of antioxidant activity of vanillin by using multiple antioxidant assays*. Biochimica et Biophysica Acta (BBA) - General Subjects, 2011. **1810**(2): p. 170-177.
195. Zhang, Z.-H., et al., *Enhancing mechanical properties of chitosan films via modification with vanillin*. International Journal of Biological Macromolecules, 2015. **81**: p. 638-643.
196. Kayaci, F. and T. Uyar, *Solid Inclusion Complexes of Vanillin with Cyclodextrins: Their Formation, Characterization, and High-Temperature Stability*. Journal of Agricultural and Food Chemistry, 2011. **59**(21): p. 11772-11778.
197. Li, X., S. Deng, and H. Fu, *Adsorption and inhibition effect of vanillin on cold rolled steel in 3.0 M H3PO4*. Progress in Organic Coatings, 2010. **67**(4): p. 420-426.
198. Peña, B., et al., *Characterization of Polysulfone and Polysulfone/Vanillin Microcapsules by 1H NMR Spectroscopy, Solid-State 13C CP/MAS-NMR Spectroscopy, and N2 Adsorption-Desorption Analyses*. ACS Applied Materials & Interfaces, 2011. **3**(11): p. 4420-4430.
199. Drioli, E. and L. Giorno, *Comprehensive membrane science and engineering*. Vol. 1. 2010: Newnes.
200. Perera, D.H.N., et al., *Room-temperature development of thin film composite reverse osmosis membranes from cellulose acetate with antibacterial properties*. Journal of Membrane Science, 2014. **453**: p. 212-220.

201. Quevedo, N., et al., *Reverse osmosis pretreatment alternatives: Demonstration plant in the seawater desalination plant in Carboneras, Spain*. *Desalination*, 2011. **265**(1-3): p. 229-236.
202. Roque, A.C.A., et al., *Biocompatible and bioactive gum Arabic coated iron oxide magnetic nanoparticles*. *Journal of Biotechnology*, 2009. **144**(4): p. 313-320.
203. Tsai, R.-Y., et al., *Chitosan/pectin/gum Arabic polyelectrolyte complex: Process-dependent appearance, microstructure analysis and its application*. *Carbohydrate Polymers*, 2014. **101**: p. 752-759.
204. Shahgholian, N. and G. Rajabzadeh, *Fabrication and characterization of curcumin-loaded albumin/gum arabic coacervate*. *Food Hydrocolloids*, 2015: p. In Press.
205. Kong, H., et al., *Synthesis and antioxidant properties of gum arabic-stabilized selenium nanoparticles*. *International Journal of Biological Macromolecules*, 2014. **65**: p. 155-162.
206. Juby, K., et al., *Silver nanoparticle-loaded PVA/gum acacia hydrogel: Synthesis, characterization and antibacterial study*. *Carbohydrate polymers*, 2012. **89**(3): p. 906-913.
207. Hu, Q., et al., *Antimicrobial eugenol nanoemulsion prepared by gum arabic and lecithin and evaluation of drying technologies*. *International Journal of Biological Macromolecules*, 2016. **87**: p. 130-140.
208. Chang, Y., L. McLandsborough, and D.J. McClements, *Antimicrobial delivery systems based on electrostatic complexes of cationic ϵ -polylysine and anionic gum arabic*. *Food Hydrocolloids*, 2014. **35**: p. 137-143.
209. Tan, C., et al., *Polysaccharide-based nanoparticles by chitosan and gum arabic polyelectrolyte complexation as carriers for curcumin*. *Food Hydrocolloids*, 2016. **57**: p. 236-245.
210. Li, C., et al., *Physical and structural properties of peanut protein isolate-gum Arabic films prepared by various glycation time*. *Food Hydrocolloids*, 2015. **43**: p. 322-328.

211. Cai, L., et al., *Physicochemical responses and quality changes of red sea bream (*Pagrosomus major*) to gum arabic coating enriched with ergothioneine treatment during refrigerated storage*. Food Chemistry, 2014. **160**: p. 82-89.
212. Padil, V.V.T., et al., *Synthesis, fabrication and antibacterial properties of a plasma modified electrospun membrane consisting of gum Kondagogu, dodeceny succinic anhydride and poly (vinyl alcohol)*. Surface and Coatings Technology, 2015. **271**: p. 32-38.
213. Hartley, M.G., et al., *Adhesive and hydrophobic properties of *Escherichia coli* from the rectal mucosa of patients with ulcerative colitis*. Gut, 1993. **34**(1): p. 63-67.
214. Gottenbos, B., et al., *Antimicrobial effects of positively charged surfaces on adhering Gram-positive and Gram-negative bacteria*. Journal of Antimicrobial Chemotherapy, 2001. **48**(1): p. 7-13.
215. Ikeda, S., T. Funami, and G. Zhang, *Visualizing surface active hydrocolloids by atomic force microscopy*. Carbohydrate Polymers, 2005. **62**(2): p. 192-196.
216. Elimelech, M. and W.A. Phillip, *The Future of Seawater Desalination: Energy, Technology, and the Environment*. Science, 2011. **333**(6043): p. 712-717.
217. Marcovecchio, M.G., et al., *Optimization of hybrid desalination processes including multi stage flash and reverse osmosis systems*. Desalination, 2005. **182**(1-3): p. 111-122.
218. Peyki, A., A. Rahimpour, and M. Jahanshahi, *Preparation and characterization of thin film composite reverse osmosis membranes incorporated with hydrophilic SiO₂ nanoparticles*. Desalination, 2015. **368**: p. 152-158.
219. Lang, K., et al., *A study on the preparation of polyvinyl alcohol thin-film composite membranes and reverse osmosis testing*. Desalination, 1996. **104**(3): p. 185-196.
220. Yang, J.M., et al., *Evaluation of chitosan/PVA blended hydrogel membranes*. Journal of Membrane Science, 2004. **236**(1-2): p. 39-51.

221. Ma, X., et al., *Enhancing the antifouling property of polyethersulfone ultrafiltration membranes through surface adsorption-crosslinking of poly(vinyl alcohol)*. Journal of Membrane Science, 2007. **300**(1–2): p. 71-78.
222. Koops, G., et al., *Selectivity as a function of membrane thickness: gas separation and pervaporation*. Journal of applied polymer science, 1994. **53**(12): p. 1639-1651.
223. Katz, M.G. and T. Wydeven, *Selective permeability of PVA membranes. I. Radiation-crosslinked membranes*. Journal of Applied Polymer Science, 1981. **26**(9): p. 2935-2946.
224. Chandrakala, H.N., et al., *Polyvinyl alcohol/carbon coated zinc oxide nanocomposites: Electrical, optical, structural and morphological characteristics*. Journal of Alloys and Compounds, 2013. **580**: p. 392-400.
225. Hickey, A.S. and N.A. Peppas, *Mesh size and diffusive characteristics of semicrystalline poly (vinyl alcohol) membranes prepared by freezing/thawing techniques*. Journal of membrane science, 1995. **107**(3): p. 229-237.
226. Katz, M.G. and T. Wydeven, *Selective permeability of PVA membranes. II. Heat-treated membranes*. Journal of Applied Polymer Science, 1982. **27**(1): p. 79-87.
227. Hasimi, A., et al., *Transport of water in polyvinyl alcohol films: Effect of thermal treatment and chemical crosslinking*. European Polymer Journal, 2008. **44**(12): p. 4098-4107.
228. Arena, J.T., et al., *Surface modification of thin film composite membrane support layers with polydopamine: enabling use of reverse osmosis membranes in pressure retarded osmosis*. Journal of Membrane Science, 2011. **375**(1): p. 55-62.
229. Wagner, V.E., J.T. Koberstein, and J.D. Bryers, *Protein and bacterial fouling characteristics of peptide and antibody decorated surfaces of PEG-poly (acrylic acid) co-polymers*. Biomaterials, 2004. **25**(12): p. 2247-2263.
230. Li, L., et al., *Protein adsorption on oligo (ethylene glycol)-terminated alkanethiolate self-assembled monolayers: the molecular basis for nonfouling behavior*. The Journal of Physical Chemistry B, 2005. **109**(7): p. 2934-2941.

231. Ostuni, E., et al., *A survey of structure-property relationships of surfaces that resist the adsorption of protein*. Langmuir, 2001. **17**(18): p. 5605-5620.
232. Yang, Y., et al., *The influence of nano-sized TiO₂ fillers on the morphologies and properties of PSF UF membrane*. Journal of Membrane Science, 2007. **288**(1): p. 231-238.
233. Wara, N.M., L.F. Francis, and B.V. Velamakanni, *Addition of alumina to cellulose acetate membranes*. Journal of Membrane Science, 1995. **104**(1): p. 43-49.
234. Castro, R.P., H.G. Monbouquette, and Y. Cohen, *Shear-induced permeability changes in a polymer grafted silica membrane*. Journal of Membrane Science, 2000. **179**(1): p. 207-220.
235. Lin, D.-J., et al., *Effect of salt additive on the formation of microporous poly(vinylidene fluoride) membranes by phase inversion from LiClO₄/water/DMF/PVDF system*. Polymer, 2003. **44**(2): p. 413-422.
236. Zavastin, D., et al., *Preparation, characterization and applicability of cellulose acetate-polyurethane blend membrane in separation techniques*. Colloids and Surfaces A: Physicochemical and Engineering Aspects, 2010. **370**(1): p. 120-128.
237. Razmjou, A., J. Mansouri, and V. Chen, *The effects of mechanical and chemical modification of TiO₂ nanoparticles on the surface chemistry, structure and fouling performance of PES ultrafiltration membranes*. Journal of Membrane Science, 2011. **378**(1): p. 73-84.
238. Istadi, I., et al., *Active Acid Catalyst of Sulphated Zinc Oxide for Transesterification of Soybean Oil with Methanol to Biodiesel*. Procedia Environmental Sciences, 2015. **23**: p. 385-393.
239. Kothari, A. and T.K. Chaudhuri, *One-step deposition of ZnO morphologies from single aqueous chemical bath prepared from reverse osmosis processed water*. Materials Letters, 2014. **137**: p. 366-368.
240. Sudhagar, S., et al., *Targeting and sensing cancer cells with ZnO nanoprobe in vitro*. Biotechnology letters, 2011. **33**(9): p. 1891-1896.

241. Zou, L., et al., *Surface hydrophilic modification of RO membranes by plasma polymerization for low organic fouling*. Journal of Membrane Science, 2011. **369**(1-2): p. 420-428.
242. Mazid, M., *Mechanisms of transport through reverse osmosis membranes*. Separation Science and Technology, 1984. **19**(6-7): p. 357-373.
243. Barth, C., et al., *Asymmetric polysulfone and polyethersulfone membranes: effects of thermodynamic conditions during formation on their performance*. Journal of Membrane Science, 2000. **169**(2): p. 287-299.
244. Matsuura, T., *Synthetic membranes and membrane separation processes*. 1993: CRC press.
245. Arthanareeswaran, G., T.S. Devi, and M. Raajenthiren, *Effect of silica particles on cellulose acetate blend ultrafiltration membranes: Part I*. Separation and Purification Technology, 2008. **64**(1): p. 38-47.
246. Sabir, A., et al., *Conjugation of silica nanoparticles with cellulose acetate/polyethylene glycol 300 membrane for reverse osmosis using MgSO₄ solution*. Carbohydrate Polymers, 2016. **136**: p. 551-559.
247. Sabir, A., et al., *Fabrication of tethered carbon nanotubes in cellulose acetate/polyethylene glycol-400 composite membranes for reverse osmosis*. Carbohydrate Polymers, 2015. **132**: p. 589-597.
248. Pendergast, M.M. and E.M. Hoek, *A review of water treatment membrane nanotechnologies*. Energy & Environmental Science, 2011. **4**(6): p. 1946-1971.
249. Arthanareeswaran, G., D. Mohan, and M. Raajenthiren, *Preparation, characterization and performance studies of ultrafiltration membranes with polymeric additive*. Journal of Membrane Science, 2010. **350**(1): p. 130-138.
250. Saleh, T.A. and V.K. Gupta, *Synthesis and characterization of alumina nanoparticles polyamide membrane with enhanced flux rejection performance*. Separation and purification technology, 2012. **89**: p. 245-251.

251. Li, J.H., et al., *Effects of ZnO nanoparticles on the mechanical and antibacterial properties of polyurethane coatings*. Progress in Organic Coatings, 2009. **64**(4): p. 504-509.
252. Lee, J., et al., *Properties of nano-ZnO/poly(vinyl alcohol)/poly(ethylene oxide) composite thin films*. Current Applied Physics, 2008. **8**(1): p. 42-47.
253. Vicentini, D.S., A. Smania, and M.C. Laranjeira, *Chitosan/poly (vinyl alcohol) films containing ZnO nanoparticles and plasticizers*. Materials Science and Engineering: C, 2010. **30**(4): p. 503-508.
254. Callow, J.A. and M.E. Callow, *Trends in the development of environmentally friendly fouling-resistant marine coatings*. Nature communications, 2011. **2**: p. 244.
255. Song, Z. and Z. Xu, *Ultimate Osmosis Engineered by the Pore Geometry and Functionalization of Carbon Nanostructures*. Scientific reports, 2015. **5**.
256. Kurihara, M. and Y. Himeshima, *The major developments of the evolving reverse osmosis membranes and ultrafiltration membranes*. Polymer journal, 1991. **23**(5): p. 513-520.
257. Heiranian, M., A.B. Farimani, and N.R. Aluru, *Water desalination with a single-layer MoS₂ nanopore*. Nature communications, 2015. **6**.
258. Huang, J., et al., *A novel composite conductive microfiltration membrane and its anti-fouling performance with an external electric field in membrane bioreactors*. Scientific reports, 2015. **5**.
259. Inukai, S., et al., *High-performance multi-functional reverse osmosis membranes obtained by carbon nanotube· polyamide nanocomposite*. Scientific reports, 2015. **5**.
260. Prince, J., et al., *Self-cleaning Metal Organic Framework (MOF) based ultra filtration membranes-A solution to bio-fouling in membrane separation processes*. Scientific reports, 2014. **4**.

261. Raval, H.D., P.S. Rana, and S. Maiti, *A novel high-flux, thin-film composite reverse osmosis membrane modified by chitosan for advanced water treatment*. RSC Advances, 2015. **5**(9): p. 6687-6694.
262. Shafi, H.Z., et al., *Surface modification of reverse osmosis membranes with zwitterionic coatings: A potential strategy for control of biofouling*. Surface and Coatings Technology, 2015. **279**: p. 171-179.
263. Chu, F., et al., *Zwitterion-coated graphene-oxide-doped composite membranes for proton exchange membrane applications*. Journal of Membrane Science, 2015. **496**: p. 31-38.
264. Shih, Y.-J. and Y. Chang, *Tunable blood compatibility of polysulfobetaine from controllable molecular-weight dependence of zwitterionic nonfouling nature in aqueous solution*. Langmuir, 2010. **26**(22): p. 17286-17294.
265. Azari, S. and L. Zou, *Fouling resistant zwitterionic surface modification of reverse osmosis membranes using amino acid l-cysteine*. Desalination, 2013. **324**: p. 79-86.
266. Chen, S., et al., *Surface hydration: principles and applications toward low-fouling/nonfouling biomaterials*. Polymer, 2010. **51**(23): p. 5283-5293.
267. Ni, L., et al., *Water and salt transport properties of zwitterionic polymers film*. Journal of Membrane Science, 2015. **491**: p. 73-81.
268. Higaki, Y., et al., *Versatile inhibition of marine organism settlement by zwitterionic polymer brushes*. Polymer Journal, 2015.
269. Chan, W.-F., et al., *Zwitterion functionalized carbon nanotube/polyamide nanocomposite membranes for water desalination*. ACS Nano, 2013. **7**(6): p. 5308-5319.
270. Ba, C., J. Langer, and J. Economy, *Chemical modification of P84 copolyimide membranes by polyethylenimine for nanofiltration*. Journal of Membrane Science, 2009. **327**(1): p. 49-58.

271. Sun, Z., et al., *Fabrication and application of silicalite-1 and TS-1 hollow fibers with polyethylene imine (PEI) fibers as substrates*. Journal of Industrial and Engineering Chemistry, 2012. **18**(1): p. 92-97.
272. Zhang, R., et al., *A novel positively charged composite nanofiltration membrane prepared by bio-inspired adhesion of polydopamine and surface grafting of poly (ethylene imine)*. Journal of Membrane Science, 2014. **470**: p. 9-17.
273. Sahiner, N., *Preparation of poly (ethylene imine) particles for versatile applications*. Colloids and Surfaces A: Physicochemical and Engineering Aspects, 2013. **433**: p. 212-218.
274. Meng, H., et al., *Improving anti-protein-fouling property of polyacrylonitrile ultrafiltration membrane by grafting sulfobetaine zwitterions*. Journal of Chemistry, 2014. **2014**.
275. Chang, Y., et al., *A highly stable nonbiofouling surface with well-packed grafted zwitterionic polysulfobetaine for plasma protein repulsion*. Langmuir, 2008. **24**(10): p. 5453-5458.
276. Zhang, X., et al., *Biocompatible fluorescent organic nanoparticles derived from glucose and polyethylenimine*. Colloids and Surfaces B: Biointerfaces, 2014. **123**: p. 747-752.
277. Chen, L., et al., *Multi-armed poly (L-glutamic acid)-graft-oligoethylenimine copolymers as efficient nonviral gene delivery vectors*. The journal of gene medicine, 2010. **12**(1): p. 64-76.
278. Wang, F., et al., *Characterization of a polyamine microsphere and its adsorption for protein*. International journal of molecular sciences, 2012. **14**(1): p. 17-29.
279. Max, J.-J. and C. Chapados, *Infrared spectroscopy of aqueous carboxylic acids: Comparison between different acids and their salts*. The Journal of Physical Chemistry A, 2004. **108**(16): p. 3324-3337.
280. Nagpal, M., S.K. Singh, and D. Mishra, *Synthesis characterization and in vitro drug release from acrylamide and sodium alginate based superporous hydrogel devices*. International journal of pharmaceutical investigation, 2013. **3**(3): p. 131.

281. Ebrahimi, H.A., et al., *Repaglinide-loaded solid lipid nanoparticles: effect of using different surfactants/stabilizers on physicochemical properties of nanoparticles*. DARU Journal of Pharmaceutical Sciences, 2015. **23**(1): p. 1.
282. Lowe, A.B. and C.L. McCormick, *Synthesis and solution properties of zwitterionic polymers*. Chemical reviews, 2002. **102**(11): p. 4177-4190.
283. Khayet, M., *Membrane surface modification and characterization by X-ray photoelectron spectroscopy, atomic force microscopy and contact angle measurements*. Applied surface science, 2004. **238**(1): p. 269-272.
284. Wandera, D., S.R. Wickramasinghe, and S.M. Husson, *Modification and characterization of ultrafiltration membranes for treatment of produced water*. Journal of Membrane Science, 2011. **373**(1): p. 178-188.
285. Chakrabarty, B., A. Ghoshal, and M. Purkait, *Effect of molecular weight of PEG on membrane morphology and transport properties*. Journal of Membrane Science, 2008. **309**(1): p. 209-221.
286. Chen, Z., et al., *Preparation and performance of cellulose acetate/polyethyleneimine blend microfiltration membranes and their applications*. Journal of membrane science, 2004. **235**(1): p. 73-86.
287. Wang, Y.-q., et al., *Remarkable reduction of irreversible fouling and improvement of the permeation properties of poly (ether sulfone) ultrafiltration membranes by blending with pluronic F127*. Langmuir, 2005. **21**(25): p. 11856-11862.

VITA

Wail Sulaiman Falath

Wail Falath was born on January 19, 1985 in Jeddah, Saudi Arabia. He obtained his Bachelor of Science (BSc) degree in Mechanical Engineering at King Fahd University of Petroleum and Minerals (KFUPM) with Honors in June 2007. In July 2007, he was admitted to the Graduate program at KFUPM to pursue his Masters degree (MSc) in Mechanical Engineering. During that time, he was a lecturer at the school with several teaching and research duties. In July 2010, he was awarded the Master of Science degree (MSc) in Mechanical Engineering. In August 2010, he was admitted to the Doctor of Philosophy program (PhD) of the School of Polymers, Textiles and Fibers Engineering at Georgia Institute of Technology under the guidance of Dr. Karl Jacob. Wail will be completing his PhD in Summer 2016. Upon graduation, Wail will start his career as an assistant professor at KFUPM.